Nanocomposites for Theranostic Applications

A Thesis

Submitted in partial fulfilment for the award of degree of

Doctor of Philosophy

By

Amaresh Kumar Sahoo

Centre for Nanotechnology

Indian Institute of Technology Guwahati

Assam, India,

September 2014

Dedicated to My Parents and beloved Grandmother

DECLARATION

I, hereby, declare that the work embodied in this thesis entitled "**Nanocomposites for Theranostic Applications**" is the result of investigations carried out by me in the Centre for Nanotechnology, Indian Institute of Technology Guwahati, under the supervision of Prof. Siddhartha Sankar Ghosh & Prof. Arun Chattopadhyay for the award of Doctor of Philosophy. In keeping up with the general scientific traditions, wherever the work described is based upon the findings of other investigators, due acknowledgements have been made. This work has not been submitted elsewhere for any degree, diploma of any institute or university to the best of my knowledge and belief.

Centre for Nanotechnology

Indian Institute of Technology Guwahati

Assam, India,

September 2014

Amaresh Kumar Sahoo

Roll No. 09615301

INDIAN INSTITUTE OF TECHNOLOGY GUWAHATI

CERTIFICATE

This is to certify that the thesis "**Nanocomposites for Theranostic Applications"** being submitted to the Indian Institute of Technology Guwahati by **Amaresh Kumar Sahoo** for the award of the degree of **Doctor of Philosophy** in **Nanotechnology,** is absolutely a bonafide record of research work carried out by him. The contents of this thesis have not been submitted to any other university or institute for the award of any degree or diploma.

Prof. Siddhartha Sankar Ghosh (Supervisor)

Prof. Arun Chattopadhyay (Supervisor)

Acknowledgement

An unspeakable joy and happiness cover my mind in order to express my deepest appreciation to all those who helped me a lot during this entire PhD life and provided the opportunity to submit my PhD thesis.

Foremost, I would like to express my sincere gratitude to my advisors Prof. Siddhartha Sankar Ghosh and Prof. Arun Chattopadhyay, for their continuous support, strong motivation, immense patience, and vast knowledge which blessed my PhD life. Their valuable suggestions and noble thoughts inspired me a lot. I consider it as a great opportunity to do my doctoral programme under their supervision and to learn from their research expertise. Most importantly the freedom I got to work independently as well as group instigated me to express my thoughts and made my life most pleasurable during the entire endeavour. They always made themselves available to clarify my doubts resolve my problems despite of their busy schedules. I shall always remain indebted to them for their generous care and concern throughout this period. Thank you Sirs, for all your help and support not only in to overcome the difficulties during experiments but also in writing in papers and thesis.

Besides my advisors, I would like to express my sincere gratefulness the rest of my doctorate committee members Dr. Biplab Bose, Prof. Lingaraj Sahoo, Dr. Debasis Manna and Dr. Chandan K. Jana for their time to time evaluation of my works, insightful comments, and critical questions. Their suggestions and encouragement assist me significantly to understand and envisage the problem more comprehensively and execute them more accurately.

I am really thankful to Centre for Nanotechnology, Department of Biotechnology, Department of Chemistry and Central Instrumentation facilities, IIT-Guwahati for providing me the world class research infrastructure, offering the facilities of sophisticated instruments, and advantages of using them. I owe my gratitude to our scientific officers Dr. Pranjoli Das, Mr. Kaustubh Acharyya and Mr. Indrajit Talukdar for their constant help with instruments and friendly support. I also thankful to our office staff Mr. Paran Jyoti Dutta for his persistent livelihood.

Next, I would like to take this opportunity to acknowledge my friend Dr. Pallab Sanpui, because of him only I got the chance here and could able to finish my PhD. His unconditional assistance aided me to overcome several difficulties I faced personally and professionally during this period. I am also grateful to Dr. Madhuchanda Banerjee for her care and assistance at beginning of my research life. I feel happy to share the lab with my friend Dr. Shilpa Sharma. I am thankful of having sincere lab mate Dr. Amit Jaiswal. I am quite happy of getting a bubbly junior Upashi for her endless pleasing talk and immense care for lab mates. I am extremely lucky of having junior like Sunil and Bandhan from them I learnt lot of minute things. I am thankful to Depanjalee for helping me in correction of my thesis. I feel delighted to work with my group members and friends Dr. Subhojit, Dr. Raihana, Dr. Subhamoy, Dr. Nidhi, Rumi, Palash, and Rama. I am fortunate to have other members Dr. Sonit Kumar Gogoi, Dr. Jashmini Deka, Dr. Krishna Kanti Dey, Dr.

Sadhucharan Mallick , Dr. Vinod Yata, Dr. Kohila, Dr. Chockalingam, Archita, Satya, Anushree, shilaj, Sabyasachi, Uday, Sharmila, Asif, Neha, Kafeel, Sreelatha and Srestha. I also thank Dr. Agile Mathew, Dr. Francis, Ashish, Ravi, Jitendra, Santosh, Subbarao, Amit Singh, Nilanjan, Shyam.

Furthermore, I would also like to acknowledge with much appreciation of some of my close friends Bramhachari Goutam, Dr. Dijen, Dr. Ritobrata, Nimai, Uttam for their help and enjoyments. I am really thankful to Munmun for her endless care, help and encouragement during my entire PhD life.

I am extremely indebted to each of my family members. Words fail me to express my appreciation to my grandmother and her role in my life because of her unconditional love, affection and help I was able to finish my graduation. The dream of become a good human being is fostered within me due to her only. I grateful to my parents, uncles, unties and their hard works and selfless supports to fulfil my dream. My brothers and sisters are always making me happy and delighted. I like to chat with my cute nephew Munku.

At last not the least 'God almighty', for his blessings. I would like to appreciate the advices and thoughts that I got and inculcated within me from the great philosopher and pious monks of Ramakrishna Mission Calcutta students' Home which influences my entire life. Their dedication and honesty towards works inspire me and my views.

Amaresh Kumar Sahoo

CONTENTS

Chapter 2: Quick and Simple Estimation of Bacteria Using a Fluorescent Paracetamol Dimer-Au nanoparticle Composite

Chapter 3: Plasmid DNA linearization in the antibacterial Action of a new Fluorescent Ag Nanoparticle-Paracetamol Dimer composite

Chapter 5: Simultaneous RGB Emitting Au Nanoclusters in Chitosan Nanoparticles for Anticancer Gene Theranostic

Chapter 6: Single Cycle PCR Based Synthesis of Highly Fluorescent Au Nanoclusters for Gene Expression

Chapter 7: Conclusion and Future Outlook

ABSTRACT

Nanomaterials have immense potential to improve healthcare by designing simple, low cost biosensors, generation of the novel therapeutics and delivery of the therapeutics with enhanced efficacy by suitable cargo. My PhD thesis works are focused on synthesizing and engineering nanomaterials, having dual characteristics of diagnostic and therapy i.e. theranostics, in order to address important issues of healthcare.

The thesis is divided into seven chapters. Chapter 1 - Introduction and Review of Literature - describes the scholastic insights of the reports available in the literature related to the present work and involving synthesis and characterization of the different nanomaterials suitable for biomedical applications. Also, the context of the present thesis vis-à-vis current technological challenge in nanobiotechnology is elaborated. In Chapter 2, synthesis of a novel fluorescent Au NP- composite has been reported, based on reaction of reaction of paracetamol (p-hyrdoxy acetanilide) - a well-known anti-pyretic and analgesic molecule, generally considered as safe for human consumption- and HAuCl4. The Au NP-PD composite employed in detection of both Gram positive and Gram negative bacteria. Next aim was to develop a novel antibacterial agent effective against common bacterial strains. The Ag NPs has been found to be highly bactericidal against both Gram positive and Gram negative bacteria. Hence, the synthesis of Ag NP-PD composite by reaction of the $AgNO_3$ and paracetamol was reported in Chapter 3. Interestingly, enhancement in the reactive oxygen species (ROS) generation was observed in presence of the composite. It is proposed that the ROS generation led to oxidation of the dimer to N-acetyl p-benzoquinone imine (NAPQI). The generated NAPQI acted as a DNA gyrase inhibitor causing bacterial cell death following linearization of DNA. The above findings opened up the hope that the paracetamol dimer along with suitable ROS generator would be a potential cancer therapeutic agent. Thus, in Chapter 4, the cytotoxic effect of PD along with the ‘few atoms’ silver nanoparticles of size less than 2 nm, commonly called as silver nanoclusters (NCs), is reported. To perform targeted delivery folic acid was conjugated with the chitosan and carried out the cytotoxicity study for different types of cancer cells. Next, one step simple aqueous synthesis of the Au NCs by using the biopolymer chitosan as template is reported in Chapter 5. The chitosan Au NC composite was converted into polymeric nanoparticles and used for the suitable

bioimaging agents. In order to convert these fluorescent NPs as theranostic NPs, suicide gene (CD-UPRT) was loaded and delivered in cervical cancer cells (HeLa) for induction of cell death. In Chapter 6, a simple way of synthesis of highly fluorescent Au NCs was devised by exploiting the polymerase chain reaction (PCR) condition and amplified DNA as template was reported. As the Au NC was found to be non-cytotoxic, therefore, the method offers exceptional promises for synthesizing highly fluorescent Au NCs and concurrently estimating DNA amplification, which can be applied for designing devices.

Chapter 7 summarizes overall thesis works and describes future prospects. In brief, the present thesis is aimed at synthesizing nanomaterials, which are useful for the biomedical applications. Some of the methods developed during the pursuit of the thesis have important future implications in bacterial estimation and annihilation, fluorescence based imaging and killing of cancer cells and quantitative estimation of gene expression.

Keywords: Nanoparticles, Paracetamol dimer, Bacterial estimation, Antibacterial activity, Nanoclusters, Targeted drug delivery, Suicide gene therapy, DNA- nanoclusters,

List of Abbreviations

Ag NC	Silver Nanocluster	**MIC**	Minimum Inhibitory Concentration
Ag NP	Silver Nanoparticle	**MTT**	3-(4,5-dimethylthiazol-2-yl)-2,5-diphenyltetrazolium bromide
AO	Acridine Orange	**NAPQI**	N-acetyl p-benzoquinone imine
Au NC	Gold Nanocluster	**NCs**	Nanoclusters
Au NP	Gold Nanoparticle	**OD**	Optical Density
BSA	Bovine Serum Albumin	**PCR**	Polymerase Chain Reaction
CD-UPRT	Cytosine Deaminase Uracil Phosphoribosyl Transferase	**PD**	Paracetamol Dimer
CFU	Colony Forming Unit	**pDNA**	Plasmid DNA
CS	Chitosan	**pHA**	p-hyrdoxy acetanilide
HeLa	Cervical Cancer Cell	**QY**	Quantum Yield
E.coli	Escherichia coli	**Q-dots**	Quantum Dots
EDC	1-Ethyl-3-(3-dimethylaminopropyl) carbodiimide	**ROS**	Reactive Oxygen Species
FA	Folic Acid	**SAED**	Selected Area Electron Diffraction
FR	Folic Acid Receptor	**SEM**	Scanning Electron Microscope
FACS	Fluorescence Activated Cells Sorter	**TEM**	Transmission Electron Microscope
FESEM	Field Effect Scanning Electron Microscope	**TPP**	Sodium Tri-Polyphosphate

FTIR	Fourier Transformed Infra-Red	**XRD**	X-ray Diffraction
MALDI-TOF	Matrix Assisted Laser Desorption Ionization Time of Flight		
MBC	Minimum Bactericidal Concentration	**XTT**	(2,3-Bis-(2-Methoxy-4-Nitro-5-Sulfophenyl)-2H-Tetrazolium-5-Carboxanilide)
5-FU	5-fluorouracil		

Chapter 1

Introduction and Review of Literature

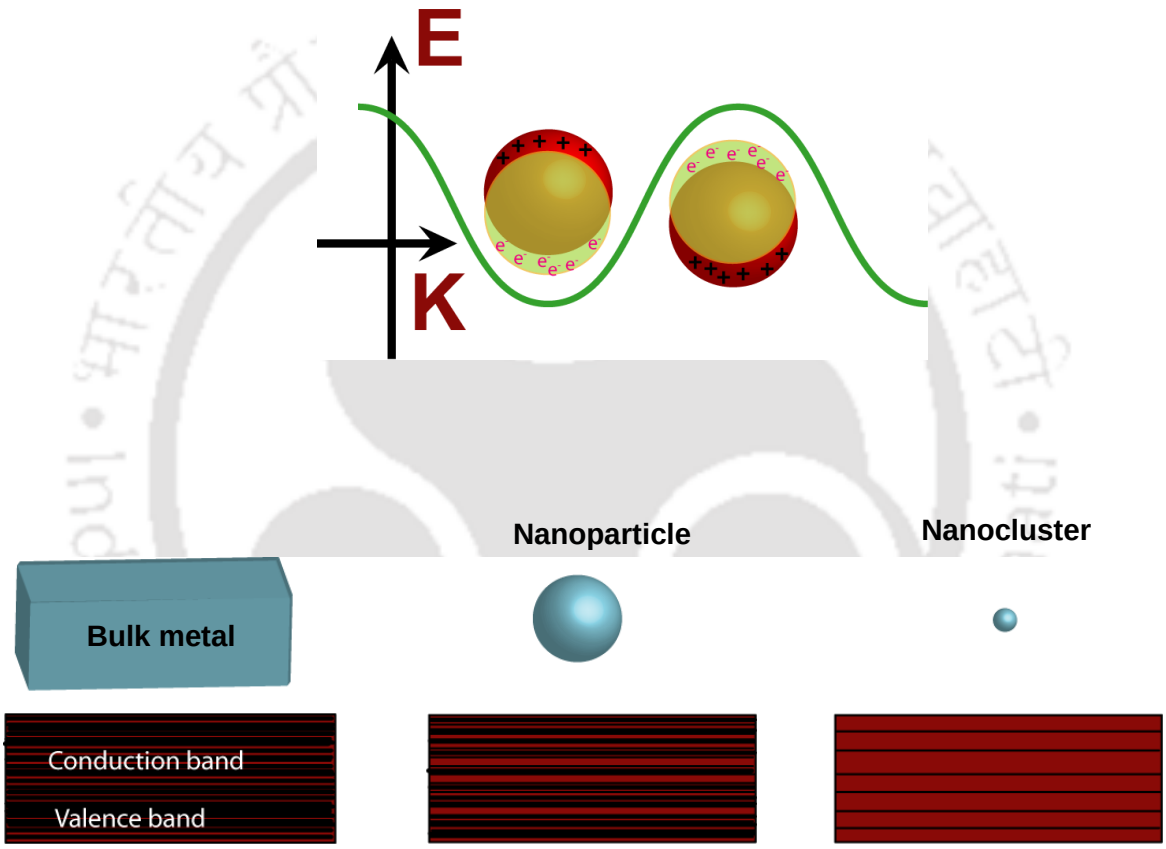

Chapter 1:

Introduction and Review of Literature

1.1. Introduction

'Nanotechnology' involves manipulation of matters with dimensions in nanometer range (1 nm= 10^{-9} m), which evolves unique characteristics. The high surface to volume ratio of the nanoscale material possesses various physical, chemical, electronic, and biological properties vastly different from their bulk counterparts, thereby, expanding their horizon of applications in both basic research as well as in applied fields.[1-3] Exploring the size constraint atomistic domains of different materials provide a unique opportunity to study and design the basic building blocks of matter. Essentially, the dimension of nanoscale materials is in the domain of biomacromolecules such as, DNA and proteins. Hence, understanding and engineering of such sophisticated nanomaterials can be tuned with desired properties to address various issues related to human life.[4]

The idea of nanotechnology was endorsed by the Nobel laureate physicist Richard Feynman through his visionary lecture on 'There's plenty of room at the bottom' in 1959.[5] For last few decades, nanotechnology progressed with great speed through merging of various disciplines under a common roof. In conjunction with the on-going pursuit of basic research, significant effort is laid to develop products, which are useful in wide range of applications. Essentially, it offers huge opportunities in the field of healthcare by offering novel materials and techniques having potential to change the landscape of this field. This integration of nanotechnology in the healthcare in the area of diagnosis and therapy is termed as the nanomedicine. Currently, in a broad view of obtaining high through put, the attention is shifted towards engineering materials having dual characteristic of diagnosis and therapy i.e. theranostics[6-7] to address several issues in real life models.

There are two fundamentals approaches, which can be used to synthesize nano-sized materials. One is 'top down' approach, as the name indicates; reaching the desired level from the top i.e. bulk. Top down approach involves slicing or successive cutting of a bulk material to get nano sized material. The most common tools, which are used to

reduce the size of the materials, are electron beam and laser. On the other hand, building up of nano-sized materials by successive arrangement of atoms or molecules, is called 'bottom up' approach. This means, creation of material from its constituent components or atoms in a spontaneous and natural manner by providing favourable environment. This is the most powerful method to synthesize nano materials now-a-days.

1.2. Nanoparticles (NPs)

Presently, a myriad of NPs are available in the field of nanotechnology having different characteristics and purposes. Based on the starting materials, NPs can be broadly categorized into the following classes such as metal and metal oxide NPs, semiconductor NPs generally known as quantum dots (Q-dots), carbon dots (C-dots), liposomes, dendrimers, fullerenes and polymer NPs. However, the present thesis primarily focuses on the synthesis of metal NPs, polymeric NPs and their composites for the theranostic applications.

1.2.1. Metal nanoparticles

The evolution of human society is strongly associated with extensive use of the metals. However, synthesis of metal NPs has been initiated since last few decades only. Basically, metal nanoparticles are nothing but a group of atoms organized in a systematic fashion. By comparing the size of atoms (Angstrom = 10^{-10} m) with the NP (nanometer = 10^{-9} m) it can be easily estimated that NP (1-100 nm) comprises of 10 to 10^3 atoms.

1.2.1.1. Synthesis of the metal nanoparticles

The most commonly used method of synthesis of metal NPs is the chemical reduction. The reduction of metals ions, however, relies on the reduction potential of the individual metals. Generally, metals are electropositive, and have high tendency of donating electrons depending on their ionization energies.[8] Due to the high electropositive nature it is likely to exist as an ion in the solution phase rather than metallic state (0) and hence acts as a strong reducing agent. Consider, for example, all alkali (Group 1, in Periodic Table), alkaline earth metals (Group 2, in Periodic Table) and some of the d-block elements. Among them, metals such as lithium ($Li^+|Li$= −3.05 V), sodium ($Na^+|Na$= −2.71 V), iron ($Fe^{2+}|Fe$= −0.44 V), cobalt ($Co^{2+}|Co$= −0.27 V) and nickel ($Ni^{2+}|Ni$= −0.25 V) cannot exist in the metallic state as they are readily oxidized by oxygen or water ($O_2|OH^-$= 0.40 V). Hence, it is difficult to synthesize metal NPs from these metals under

standard atmospheric conditions; however, metal oxide NPs can be synthesized from some of these metals.

On the other hand, there are some metals (mainly transition metals, d-block elements), which do not obey this rule; they are gold ($Au^{3+}|Au$=1.5 V), platinum ($Pt^{2}+|Pt$=1.2 V), palladium ($Pd^{2+}|Pd$=0.83 V), silver ($Ag^{+}|Ag$=0.80 V) and copper (Cu^{2+} |Cu = 0.337 V) etc. The reduction potential favours these metals to exist in metallic state and thus, it is rather easy to form NPs. Generally, these metals do not participate in any kind of chemical reactions (e.g., oxidation) so usually known as the noble metals.[9]

Now, another vital point is the thermodynamics of the metal NP, which states that its high surface energy accounts for high reactivity. To produce stable NPs, it is essential to terminate the particle growth reaction by providing some suitable agents during the process of reduction, generally known as stabilizing agents, which explicitly dissipates the high surface energy and helps in formation of stable NPs. Nucleophiles serve as suitable stabilizing agents as surface of the NPs is electron deprived in nature (electrophilic). Furthermore, colloidal solution of the NPs tends to agglomerate owing to Van der Waals interactions, which are also restricted by the stabilizing agents providing uniform surface charge to NPs based on Columbic repulsion and/or steric hindrance.

1.2.1.2. Unique optical properties of metals NPs

The size and shape dependent optical properties are the most exciting features of the noble metal NPs which are neither similar with those of the individual constituent atoms nor those of the bulk. This unique property of NPs arises due to the surface plasmon resonances (SPR).[10] When the dimensions of the metals are reduced- having the diameter comparable with the electron mean free path (50 nm) – the electromagnetic wave perturbs the coherent oscillation of the free electrons of the conduction band with respect to the much heavier ionic core of a spherical nanoparticle i.e. nuclei, inducing dipole oscillation. The oscillation or perturbation of the electron cloud is prominent at the metal- dielectric interface. If the frequency of the dipole oscillation matches with the frequency of the interacting electromagnetic wave at that wavelength the metal NPs show a strong absorption band due to constructive interference which is known as the surface plasmon resonance (SPR).[11] Importantly, the SPR absorption of a fairly diluted colloidal solution of NPs can be measured using a UV–Vis absorption spectrometer. The surface plasma frequency lies in the visible part of the spectrum for gold, copper and silver, and thereby

colloidal solution of these metal NPs display exquisite colours. However, for most of the metals, the SPR lies either in the UV or IR range of the spectrum and hence NPs do not display any colour.

In 1908, German physicist Gustav Mie offered an exact electrodynamic explanation of the SPR, by applying the Maxwell's electromagnetic equations with appropriate boundary condition.[10] Optical properties of metal NPs ($R << \lambda$), interacting with external electromagnetic fields, are dependent on their sizes, free electron density and dielectric constant of both surrounding medium and NPs. He addressed the exact solution of interaction of light with spherical metallic NPs immersed in a continuous homogeneous medium. According to the "Mie theory", the extinction coefficient explicitly depends on the electric dipole for the smaller NPs (2 -20 nm for gold) due to uniform surface polarization, which results in a sharp peak of the surface plasmon resonance. However, for larger NPs (> 20 nm), the light cannot induce polarization homogeneously due to retardation effects of the electromagnetic field across the particle leading to quadrupole mode of oscillation rather than dipole oscillation, which results in bathochromic peak shifting and broadening. The dielectric constant of both metal and the surrounding environment are involved in the calculation of "Mie theory" so the solvent polarity in which the NPs are immersed attributes in the variation in the SPR frequency too. The position of the plasmon peak shifts to longer wavelengths with increasing dielectric constant of the solvent.

Importantly, shape of the NPs is also another parameter which attributes to the SPR as well. The change of surface geometry causes a shift in the electric field density on the surface. As a consequence, multiple resonance peaks may appear due to unequal longitudinal and transverse dipole polarization of electrons across the NP. Generally, the longitudinal plasmon resonance peak appears as red-shifted and broadened than the peak of transverse resonance. The optical behaviour of these anisotropic NPs can be described by using discrete dipole approximation (DDA) theory.[11]

1.2.2. Gold nanoparticles (Au NPs)

For centuries, gold has fascinated mankind due to its everlasting intrinsic lustre and is considered as a precious metal. Moreover, ancient documents symbolized gold as the sun and silver as the moon due to their own colour.[8] The human body contains ~ 0.35 μg of gold (0) per gram of dry tissue weight and blood gold concentrations in healthy humans have been found to be around 0.001 ppm.[8] Metallic gold, Au (0) is extremely inert and generally considered as biocompatible and safe. Importantly, metallic gold can be easily excreted through urine and feces.

Literature suggests that long ago colloidal solution of gold NPs (Au NPs) was employed by artists as an alternative of paint due to their exquisite colours, which originate from their interaction with visible light i.e., surface plasmon resonance (SPR). However, scientists began reviewing their properties in more detail only in the 1850s. The Au NPs display a single SPR absorption peak in the visible range of 520 nm to 550 nm. With increasing particle size the corresponding SPR peak is red shifted and the width of the spectrum correlates with the size distribution of the NPs. In addition, the variation in shape also results in variation of optical response. The opto-electronics properties of Au NPs open up new prospects in various fields for use in high technology applications.

1.2.2.1. Applications of Au NPs as sensors

The rapid development of various synthetic methods for Au NPs and their functionalization have helped open up a new regime in the development of novel bio and chemo sensors, based on the change in colour of their colloidal solution in presence of specific analytes including ions, DNA, pesticide, proteins, and even cells.[12-13] The colorimetric assays primarily rely on the change in the SPR signal due to agglomeration or alteration in the environment of the Au NPs, which can be probed by simple visualization or otherwise by using UV-vis spectroscopy. This method gains edge over other methods due to the low cost, simplicity and the sensitivity. In addition, the high conductivity of Au NPs allows them to be used in the design of electrochemical biosensors.[14] The Au NPs serve as effective interface between the electrode and analytes, where redox reactions occur, and subsequently transmit the electrical signal in case of electrochemical biosensors.

1.2.1.2. Therapeutic applications of Au NPs

Intense research is going on with respect to Au NP based photothermal therapy which employs absorptions of light by NPs to achieve the selective heating of the local environment ultimately leading to disruption of the cell's membrane.[15] Electrons of NPs make transitions from the ground state to the excited state when interacts with light. The electronic excitation energy subsequently relaxes through nonradioactive decay which results in the increase in the kinetic energy leading to heating of the local environment around the NPs. Another alternative therapeutic approach which has been recently explored in the field of medical science is photodynamic therapy. This involves activation of photosensitizers (drugs) which undergo an energy state transition from ground state to a higher energy triplet state upon exposure of a specific wavelength of light.[16-17] The activated triplet state interacts with molecular oxygen, generating singlet oxygen and/or free radicals. These are highly reactive and able to damage DNA and other macromolecules which eventually lead to cell death. Use of Au NP offers huge potential in these aforementioned methods since it absorbs light in the range of visible to near-infrared (NIR) based on its size and shape.

1.2.3. Silver nanoparticles (Ag NPs)

Along with gold another precious metal which has been used widely for long time is silver. Silver ions and silver-based compounds have been used as anti-microbial agents for treatment of wounds and infections for more than 100 years. However, the synthesis and the application of the Ag NPs have been explored for last few decades. The amount of silver present in the human blood is < 0.1 µg/L. The overdose of silver is toxic for our body in contrast to gold. Chronic exposure leads to enhanced melanin production in skin resulting in a condition known as argyria.[8]

1.2.3.1. Applications of Ag NPs

Apart from SPR suitable for the colorimetric assay, Ag NPs possess numerous remarkable properties such as high electrical and thermal conductivity, surface-enhanced Raman scattering (SERS), catalytic activity and nonlinear optical behaviour. SERS involves utilization of the enhanced Raman signal from Raman-active molecules adsorbed on Ag NPs, through amplification of electromagnetic fields, generated by the excitation of surface plasmons of Ag NPs.[18] This sensitive method allows for the development of optical sensors having faster response times and lower detection limits. In

addition, the Ag NPs can act as good catalyst in various chemical reactions. The catalytic power of the Ag NPs, however, relies on the size and morphology of the NPs, which increases with decreasing the size.[19]

1.2.3.2. Biomedical applications of Ag NPs

The Ag NPs exhibit broad spectrum bactericidal[20] and fungicidal activities[21]; hence, it offers huge promises such as anti-microbial coating agents of surgical instruments, contraceptive devices and bone prostheses.[22] Besides, Ag NPs containing dressing materials offer superior wound healing properties for the treatment of various injuries, including burns, which are now commercially available (e.g. Acticoat^{TM}).[23] Recent reports recognized that it can be used as anti-cell proliferative and anti-inflammatory agents. The Ag NPs and its combination with photosensitizers increase generation of reactive species in several folds than only drugs which renders huge prospective in the killing of pathogenic microorganisms and even cancer cells.[24-25] It is also useful in waste water treatment for large scale production of drinking water. **Table 1.1** shows possible biomedical uses of the silver NPs and the silver based materials, which are being currently used in the field of healthcare.[26]

Table 1.1 Uses of silver in medicine. Figure has been reprinted with permission from the reference 26. Copyright by *Trends in Biotechnology* 2010.

Product	Company	Description	Clinical uses
Acticoat™	Smith & Nephew	Nano crystalline silver wound dressing	Dressing for a range of wounds including burns and ulcers; prevents bacterial infection and improves wound healing.
Silverline ᴿ	Spiegelberg	Polyurethane ventricular catheter impregnated with NS	Neurosurgical drain of CSF for hydrocephalus. Also can be adapted for use as shunts. Antibacterial silver NP coating prevents catheter-associated infections.
SilvaSorbᴿ	Medline Industries and AcryMed	Antibacterial products: hand gels, wound dressings, cavity filler	Wound dressings and cavity filler prevent bacterial infection. Hand gels used to disinfect skin in clinical and personal hygiene purposes.
ON-Q SilverSoaker™	I-Flow Corporation	Silver-NP-coated catheter for drug delivery	Delivery of medication (e.g. local anaesthetics or analgesics) per-, peri- or post-operatively for pain management or for antibiotic treatment.

1.3. Fluorescent metal nanoclusters

Now, an important question that needs to be addressed here is: what will happen if the particle size is reduced further, such that < 2 nm, where 'each atoms count'[27] In this particular size regime, the metal NPs does not exhibit the SPR i.e. optical, electronic, and chemical properties of these small NPs differ vividly from the plasmonic counterpart.

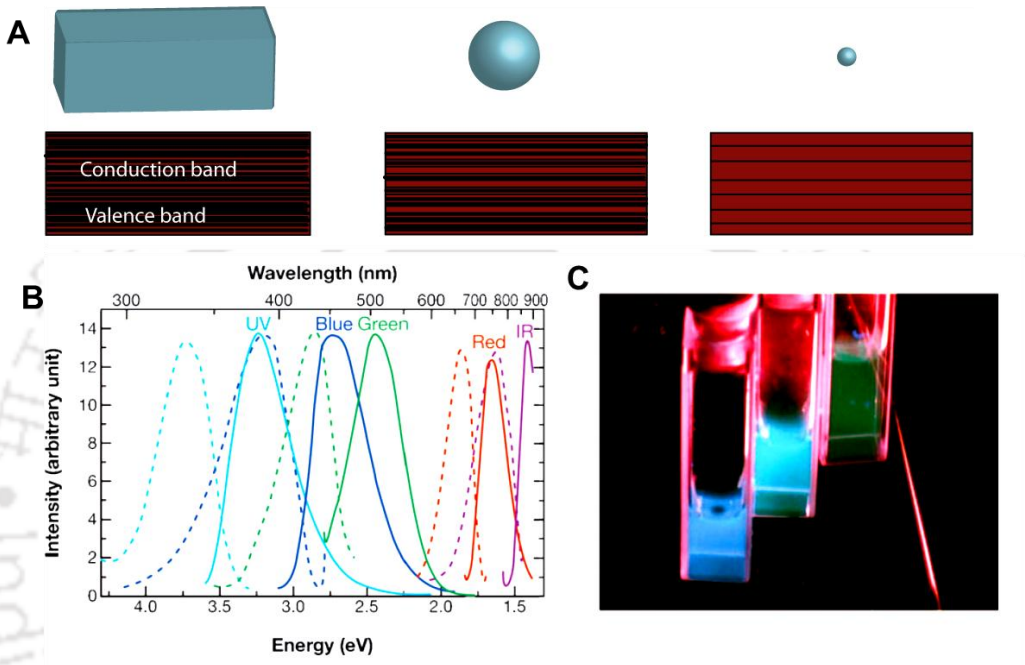

Figure 1.1 (**a**) Schematic representation of relative size and the nature of the band structure of the metal, NP and the fluorescent metal cluster. The continuous energy band of the bulk metal changes to increasingly more discrete energy levels with decreasing its size i.e. the density of the electronic states decreases. In the size range of nanocluster it transforms to completely discrete energy states (**b**) Excitation (dashed) and emission (solid) spectra of different Au nanoclusters. Excitation and emission maxima shift to longer wavelength with increasing the size of the cluster due to lower-energy emission. (**c**) Emission from the three different Au-nanocluster solutions (from left to right) under long-wavelength ultraviolet (UV)-lamp irradiation (366 nm). Figure has been reprinted with permission from the reference 27. Copyright by *American Physical Society* 2004.

When the particle size becomes comparable with the Fermi wavelength of an electron (i.e., de Broglie's wavelength of an electron at the Fermi energy, ~0.5 nm for gold and silver) the continuous energy band structure split into discrete electronic states, hence the metal NPs behaves as molecular species, and exhibits strong size tunable fluorescence emission. This type of small NPs is termed as fluorescent metal nanoclusters as depicted in **Figure 1.1.**

Likewise, single atoms, free electrons of nanocluster make electronic shells around central positive core formed by the nuclei of corresponding atoms. The electrons are also delocalized over the electronic shells surrounding the nuclei and follow the Pauli Exclusion Principle to fill the newly formed orbitals. These newly formed orbitals are known Jellium orbitals; however, the magic number of the Jellium orbitals varies from atomic orbitals due to difference in the surface potential between clusters and atoms.[28] The electrons of the atoms interact by Coulomb (r^{-1}) potential whereas electrons of cluster follow the harmonic (r^2) potential. Hence, in this model the angular momentum is not controlled by the principal quantum number like atoms. The magic number (N^0) in the n^{th} shell of atoms is governed by

$$N^0 = \frac{2}{3}n(n+\frac{1}{2})(n+1)$$

N^0 = 2, 10, 28 …which correspond to 1s, 2s, 2p, 3s, 3p, 3d… electronic shells while the magic number (N^0) of the cluster can be obtained by

$$N^0 = \frac{1}{3}(n+1)(n+2)(n+3)$$

That indicates N^0 = 2, 8, 20, 40… corresponding to 1s, 1p, 1d, 2s, 1f, 2p… electronic shells.

The energy involved in each discrete level is $E_{Fermi}/N^{1/3}$, where E_{Fermi} is the Fermi energy of bulk metal and N is the number of atoms. It indicates that the emission properties of the metal clusters strongly depends on the size of the cluster in the order of $N^{1/3}$ so that as the diameter of the cluster increases the emission energy decreases, which means the emission wavelength shifts to higher wavelength. Other than the size, free-electron density on the cluster also shows similar role in the electronic transitions of the nanocluster. Thus, along with the size of the nanocluster, the surface properties such as

the ligand to metal charge transfer (LMCT) are also responsible for the variation in the excitation and emission wavelength of clusters without compromising the structure of metal core.[27]

1.4. Polymeric nanoparticles and their importance

Polymeric NP mediated drug delivery offers unique opportunity over the delivery of the free drugs as their critical size and the physicochemical properties facilitate interaction with the cell membrane and also promote their penetration across the physiological barriers.[29-30] Besides, they increase specificity, water solubility and blood circulation half-life of the drugs, which are the immediate problems faced during use of most of the frontline drug molecules that demands higher doses and frequencies. In addition, these NPs are amenable to surface functionalization or modification to achieve desired characteristics such as probing of stimuli responsive (both physical and chemical) controlled delivery of the therapeutics. In the presence of particular stimuli such as temperature, pH or ionic strengths, the carriers may degrade or diffuse to release the encapsulated drugs at the target sites and intended time.[31] These nano carrier mediated drug delivery has already shown significant efficacy in treatment of various diseases including cancers and their mechanism of circulation in human bodies has been extensively investigated. In fact, the exclusive surface modification allows them to precisely localize into the specific organelle within cytoplasmic or nucleus. Several such engineered drug delivery carriers are in clinical practice so far for example liposomal doxorubicin and albumin conjugate paclitaxel. [32]

Design of nano carriers influenced by various factors including the physicochemical properties of the drug as well as the polymer characteristics such as either it is hydrophilic or hydrophobic, the route of administration and its metabolism. The essential properties that one nanocarrier should possess are that its constituents polymers must be chemically inert, nontoxic, biodegradable and inexpensive. There are several such polymers including natural and synthetic, available in the field of the drug delivery. The most commonly used natural polymers are polysaccharides (dextran and cellulose), chitosan (CS), sodium alginate and biopolymers such as lipids, proteins (BSA, lysozyme) and nucleic acids. The synthetic polymers are polylactic acid (PLA), poly-lactate-co-glycolic acid (PLGA), poly-vinyl pyrrolidone (PVP), poly-vinyl alcohol (PVA) poly acrylamide,

and poly-ethylene glycol (PEG). These wide ranges of polymers had offered significant level of success of delivering a variety of payloads into the cells.[33]

Among them, cationic polymer chitosan (CS), made up of liner chain of D-glucosamine (deacetylated unit) and N-acetyl-D-glucosamine (acetylated unit) covalently linked by β-(1-4)-linkage, offers huge promises in the synthesis of the nanocarriers (NCs) as its positive surface charge allows easy interaction with the negatively charged plasma membrane. It is inexpensive, biodegradable and generally considered as non-immunogenic.[34-35] Chitosan is primarily obtained by deacetylation of naturally occurring biopolymers chitin. The water solubility of CS depends on the degree of deacetylation and pH i.e., protonation of free amino groups. It is highly soluble in the acidic solution (pH <6.3) and easy to form CS NPs by addition of any ion gelatine agent like sodium tripolyphosphate (TPP), offering the feasibility of internalization inside the cells. These properties of the CS have prompted its worldwide research activities as drug and gene delivery vehicles.

1.5. Major challenges and opportunities

1.5.1. Drug resistance

Starting with the discovery of penicillin in 1928 by Alexander Fleming, antibiotics have been employed as effective medicine for infectious diseases including bacterial infections. However, for the last few decades, increasing number of multidrug resistant (MDR) or extensively drug resistant (XDR) bacteria demand effective alternative of the conventional antibacterial therapy. Mutation in some of the vital gene(s) is a factor responsible for the acquisition of drug resistance, which poses a great threat as it can achieve much larger dimensions due to wide and rapid dissemination.[36] This has led to an intensified search for newer materials and/or methods at low cost and with higher activity.

To address these concomitant issues in a comprehensive and timely manner certain strategies can be followed such as (1) development of the simple and sensitive methods for early detection of the bacterial infection, which would provide information about the type and the intensity of the infection, before applying any therapy, (2) another approach that can be implied to combat against resistant strains is to improve the potential of existing therapeutic agents. As first line of choices, modifying them in such a way that it obliterates the possibility of development of resistance by targeting the genetic materials

(i.e., DNA), which would undoubtedly provide some extraordinary potential of killing by minimizing the progress of mutations, and (3) use of the conventional drugs along with some non-conventional agents, which are being recently incorporated in the field of medical science, known as 'combination antimicrobial therapy' to kill the emerging drug resistant strains.

1.5.2. Detection of bacteria

Currently, a variety of approaches and tools have been developed to detect the bacterial infection based on the advanced biochemical techniques such as PCR, immunological assays, micro array and enzyme assays.[37-38] Nevertheless, these methods are lacking certain shortcomings such as these are either not always feasible due to complex instrumental settings or are very specific to a particular type of strain along with the issue of high cost. Hence, there is a necessity to devise a simple and fast method of detection as well as estimation of bacteria, which is vital in 'point of care' diagnosis and prognosis with lower cost. Over last few decades nanotechnology has provided ample opportunities to develop new diagnostic tools which are very sensitive and have faster response time in detection of pathogens including bacteria.[39] For example, *Mycobacterium tuberculosis* (TB) bacteria was targeted by highly magnetic NPs and subsequently detected by nuclear magnetic resonance (NMR).[40] Reports suggest that by using antibody-conjugated NPs it can specifically identify variety of bacteria including *Escherichia coli* O157:H7. Latest progresses in this field has evolved as 'lab on a chip' – which primarily relies on colorimetric or fluorescence assays- and are suitable for multiplex analysis with heightened sensitivity.[41-42]

1.5.3. Antibacterial activity of nanoscale materials

Apart from this, nanotechnology offers immense potential to formulate novel therapeutic materials that can be either used itself as potent antibacterial agent or as non-conventional component in the 'combination therapy'. In this pursuit, the Ag NPs and their composite(s) offer significant potential.[43-44] It is worth mentioning that the uses of silver in wound care have had a long history. In that case, ionic silver is responsible for its antimicrobial activity. However, the effective concentration of silver required for antimicrobial activity is far less when in the form of Ag NPs than the Ag^{+} ions. Size, shape and surface charge are the important parameters that decide the bactericidal efficacy of the Ag NPs. For example, NPs of size less than 10 nm diameters are more

effective antibacterial agents. Reports indicate that the NPs get attached to the sulfur containing protein of bacterial cell wall, leading to increase permeability of the cell membrane, causing cell death. In addition, Ag^{+} ions provided by the active surface of Ag NPs have been reported to induce generations of ROS in bacterial cells. However, the minimum inhibitory concentration (MIC) and minimum bactericidal concentration (MBC) were still quite high 22.64 μg/mL and 28.3 μg/ mL.[45]

This high concentration of the Ag NPs is cytotoxic to mammalian cells which demands lower dose of silver in case of direct use of NPs as antibacterial agent. Therefore, there have been constant efforts from several laboratories - including ours - in order to reduce the effective concentration of the silver. The subsequent studies primarily focused on the synthesis of Ag NPs using biocompatible agents which are essentially antimicrobial also. For example, previous study from our lab had used biocompatible polymer chitosan which is eventually anti-microbial; hence, the composite had better bactericidal activity than its constituent components, such as Ag NPs and chitosan. It was demonstrated that the positively charged chitosan helped in attachment with the negatively charged bacterial cell walls, and as a consequence it showed superior bactericidal activity. The MIC and MBC values of Ag NPs were significantly reduced to 2.2 μg/mL and 2.6 μg/mL respectively.[46] To move forward in this line of interest, three component nanocomposite was made of silver-chitosan-iodine, where the catalytic production of iodine atoms from the composite led to generation of ROS augmented the antibacterial potential of the composite. This managed dramatic reduction of the effective concentration of the silver.[47] However, apart from this direct 'particle specific effect' there are some researchers who believe that active surface of the Ag NPs serves as source of the Ag^{+}, possibly through influence of oxygen availability, particle size, shape, and/or type of surface stabilizing agents, which is the main toxicant (**Figure 1.2**).[48]

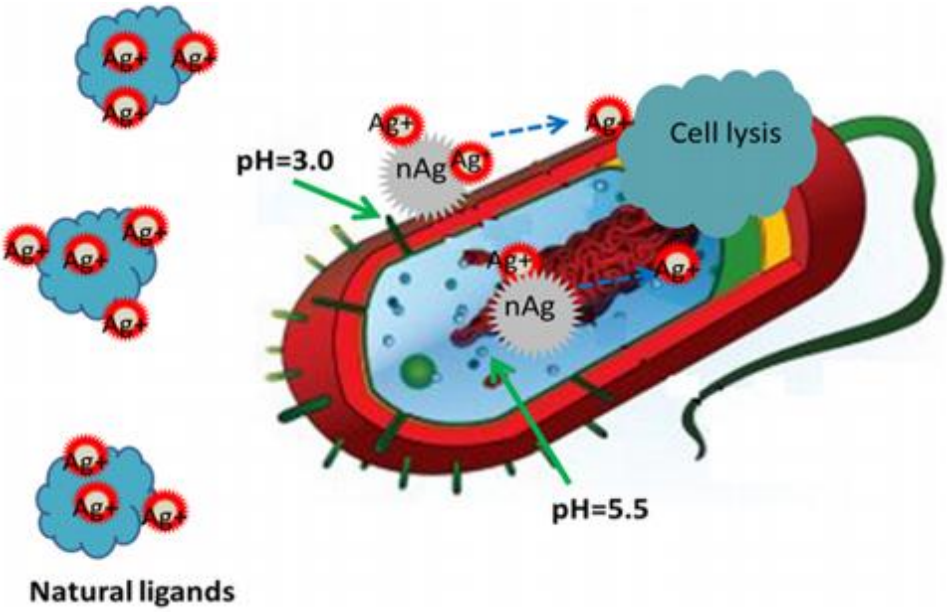

Figure 1.2 Schematic of Ag NPs, Ag+ and cell interactions. Ag NPs may serve as a vehicle to deliver Ag+ more effectively (being less susceptible to binding and reduced bioavailability by common natural ligands) to the bacteria cytoplasm and membrane. Figure has been reprinted with permission from the reference 48. *Nano Letters* 2012.

Hence, there is some sort of ambiguity that still remains in the mode of action of the silver NPs which needs to be addressed. Additionally, the challenge lies on the selection of suitable antibacterial agents, which in combination with Ag NPs would not only increase the antibacterial potency by using minimum amount of silver, but also pose no additional danger to the human health and the environment.

1.5.4. Targeting DNA for bactericidal action

Due to accumulation of random mutations (point mutations) and horizontal gene transfer, disease causing microbes become resilient toward conventional antibiotics. Thus, development of novel nanomaterials which can target DNA would definitely improve the curative power of the therapeutic materials along with the likelihood of the development of the resistant strains. One of the viable options is to introduce some of the enzyme inhibitors that would directly or indirectly target DNA in the antibacterial action. One of such inhibitor is topoisomerases II or DNA gyrase inhibitors that would serve as novel antibacterial agent when it is used along with some other antibacterial agents. The mode

of action of the DNA gyrase is illustrated in **figure 1.4**. It shows the inhibitor, which is specific to its sub unit B, acts as restriction enzyme. It linearizes the circular DNA like plasmid DNA. Therefore, it is to be deemed that synthesis of novel silver based composite along with some DNA gyrase inhibitors will not only reduce the effective concentration of silver but also cut down the possibility of the accumulation of the drug resistant genes.

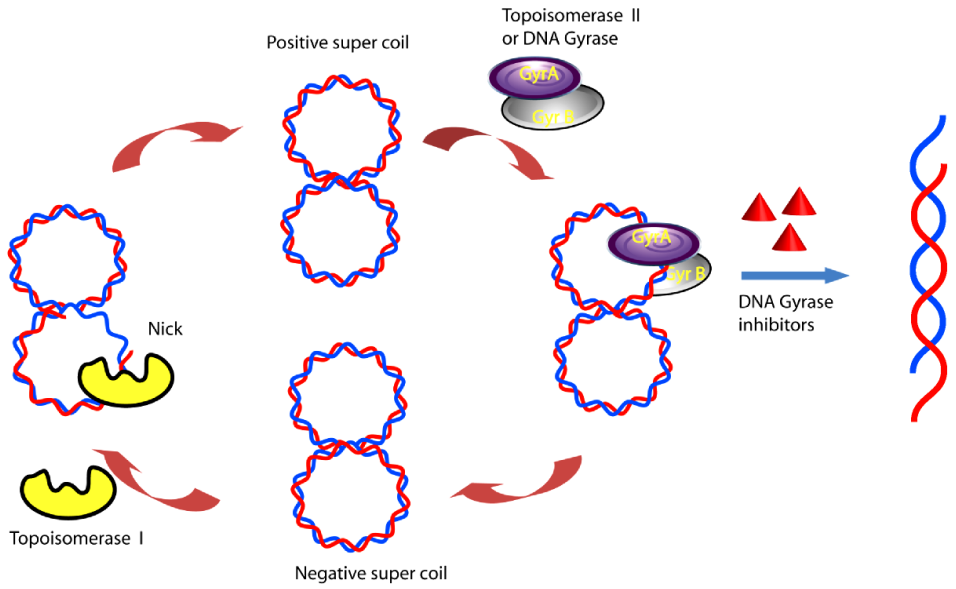

Figure 1.3 Schematic representation of the mode of action of the DNA gyrase in presence of its inhibitors.

1.6. Cancer therapy

Science and the technology have been developed significantly; still cancer is posing a huge threat of mortality all over the world. This devastating and the perilous disease is killing thousands of innocent lives every day. As per the statistics, the world's population is expected to be 7.5 billion by 2020 new cancer cases shall be diagnosed which is alarming for all of us. Moreover, the one-fifth of the world cancer patients are from India, the number of cancer cases in the Indian sub-continent is growing due to poor to moderate living standards and the lack of awareness.[49]

Cancer can be caused by either internal factors like inherited mutations, hormones, and immune conditions or environmental factors such as tobacco, radiation, food habits, and

other agents. These factors are known as carcinogens, which disturb the normal functions of the cells and are responsible for generation of the cancer.[50] Cancers occur when cells cease to obey the laws of cell division. In normal condition, cells divide to make new cells in order to replace damaged or old cells. The daughter cells produced by cell division possess same genetic information as it was in the parent cells. However, under certain circumstances carcinogens are able to interact with genetic material i.e. DNA of the normal cells, causing mutations of the some of the important genes. The mutations lead to alteration of the normal cell cycle process and induce uncontrolled cell proliferation and growth which appears as tumour. These tumour cells, under certain circumstances generate toxic products, invade nearby tissues and spread to other parts of the body, which is known as the malignant tumours or cancer. The process of the movement of the cancer cells from one part of the body to another part and the induction of the cancer at that part is known as metastasis or secondary cancer.

The most commonly used methods of killing of cancer cells cell are the surgery, chemotherapy and radiotherapy. However, methods of chemo and radio therapy possess some inherent limitation such as they generate resistant cells which are even more tolerant against all kind of therapeutics. Moreover, the tumour vasculature fenestrations differ depending on various factors such as cancer type, stage of disease and site in the body which offer huge discrepancy in the cancer therapy. Thus, developments of novel therapeutic approaches to combat cancer are essential. In this scenario, nanotechnology offers huge possibilities, in order to develop new therapeutic agents and otherwise delivery of the existing therapeutics by nanocarriers, which exhibit high efficacy owing to their favourable size and tunable physicochemical properties. This provides the plausibility of precise localization of the drug molecules and consequently increases the therapeutic index, which is an important problem, faced by conventional drugs, as it is hard to access the cancer cells due to their intricate cellular organization in comparison to normal cells.

Ag NP and its composite(s) gain considerable attention as novel cancer therapeutics, since it has the ability to cause programmed cell death (i.e., apoptosis) of the mammalian cells. Recent studies have manifested that it destabilizes the plasma membrane integrity and induces reactive oxygen species (ROS) production causing mitochondria dependent apoptosis.[51] Further, the higher doses of Ag NPs are cytotoxic towards normal cells. This inherent demerit limits its direct use as cancer therapeutic agents. Various reports from

several laboratories - including ours - have demonstrated that nanocarrier mediated delivery of Ag NPs could reduce the effective concentration of silver.[52-53]

1.6.1. Passive targeting

Treatment of cancer relies on the basic understanding of the tumour architecture and the properties of cancer cells that make them different from normal cells and even from person to person. Rapid and uncontrolled angiogenesis results in leaky blood vessels that is large gaps (200 nm) between adjacent endothelial cells and the poor lymphatic drainage.[54-55] In addition, the corona of tumour mass possesses less number of blood vessels resulting in poor oxygenation and blood circulation which eventually reduce the amount of drug uptake. These inherent characterises of the tumour cells lead to maximum resistant towards any kind of therapy. In this regard, the critical size of the NPs let them accumulate exclusively at tumour site by taking advantage of the leaky blood vessels of tumour cells, which is commonly known as passive targeting. This also increases blood circulation half-life and bioavailability of the drugs within a therapeutic frame.

1.6.2. Active targeting

Conjugation of specific ligand(s) on the surface of the NPs provides significant level of selectivity by active targeting. This method extensively increases the effective localization of drugs at pre-determined target in therapeutic concentration, while restricting its availability to non-target normal cells, thus minimizing toxic effects and maximizing therapeutic index of the drugs. Tumour cells, however, over-express receptors for some of the essential molecules such as glucose and vitamins, which promotes their growth and differentiations. Interactions of the ligands with their receptors are very specific which facilitate the receptor-mediated endocytosis of the ligands; hence, if one could conjugate any additional therapeutic entity with the ligand that will also help in the endocytosis of the therapeutics.[2, 56] Based on this natural phenomenon a great repertoire of the drug molecules have been delivered exclusively into the cancer cells. For example, some of the initial approaches employed the transferrin receptor (TfR) for delivery of the drug conjugated NPs. Another widely employed delivery system is the folate receptor (FR) mediated delivery of NPs for the cancer targeting as there are several cancer cell lines which over-express receptor for folic acid.[57-58] In addition, the cancer markers and recombinant antibodies also extensively are used as potential targeting elements to trigger cellular uptake through receptor mediated endocytosis of NPs.

1.7. Key areas and scopes

With the knowledge of the present scenario gained from the literature survey in the field of nanobiotechnology, particularly in the areas of the synthesis and engineering of the nanoscale materials for healthcare, the scope of the thesis had been identified as summarized below.

- Development of the novel biocompatible nanocomposite with conventional drug for detection of the bacterial contamination.
- Development of the novel drug based nanocomposite suitable for killing of antibiotic resistance bacteria by targeting DNA.
- Design of the biopolymer based nanocarriers for targeted cancer therapy in cell culture model.
- Development of suitable theranostic NP, based on the fluorescent metal nanocluster, which would be suitable for cancer therapy and for studying the detailed mechanism of the cell death.
- Devise a fluorescent based simple method to measure the gene expression of cancer cells for future application.

Significance and the salient features of the present study

The salient features of the present dissertation are as below:

- ❖ Non-biocidal Au NP composite was synthesized and characterized from a convention drug paracetamol, which is extensively use as an antipyretic and analgesic agent and generally considered as a safe drug due to easy clearance from the body. In this this process paracetamol was converted to paracetamol dimer (PD), which had emission at 450 nm when excited by UV light. The fluorescence intensity decreased in presence of the bacteria suitable for the detection of the both Gram positive and Gram negative bacteria with a sensitivity of the 100 CFU/mL.
- ❖ Ag NPs were synthesized from paracetamol to study their antibacterial effects. The reaction generated PD acted as stabilizing agent for the NPs. The composite was found to be potent bactericidal agent with minimum concentration of silver for both Gram positive and Gram negative bacteria.

The results suggested that the composite strongly interacted with the bacterial cell walls leading to cell bursting.

- ❖ It was found that the ROS generation led to oxidation of the PD to N-acetyl p-benzoquinone imine (NAPQI). The generated NAPQI acted as a DNA gyrase inhibitor, causing bacterial cell death, following linearization of DNA.
- ❖ Further, interest was driven to explore the anti-cancer effect of PD along with the 'few atoms' silver NPs of size less than 2 nm. For this, chitosan based nanocarriers were developed and chemically conjugated with the folic acid for targeted delivery of the PD.
- ❖ Two different cancer cell lines, one with folic acid receptor over-expressed (HeLa) and other one with folic acid receptor down regulated (MCF-7) elucidated the relative effect of the PD, after nanocarrier mediated delivery along with the Ag NCs. Detailed mechanism of the cell death was also illustrated.
- ❖ A simple, first aqueous synthesis of the highly fluorescent Au NCs was developed from biopolymer chitosan, which was further converted to polymer NPs (Au NC-CS NPs) and used as novel fluorescent dye in microscopy and FACS analysis.
- ❖ Further, positively charged Au NC-Cs NPs were employed to deliver the suicide gene (CD-UPRT) to the cancer cells and the mechanism of the cell death established.
- ❖ PCR based single step synthesis of periodic Au NC on DNA was developed and was used, to measure gene expression based of the relative fluorescence of the NCs.

1.9. References

1. M. C. Roco, *Journal of Nanoparticle Research*, 2011, **13**, 427–445.
2. O. C. Farokhzad and R. Langer, *ACS Nano*, 2009, **3**, 16–20.
3. S. E. McNeil, *Journal of Leukocyte Biology*, 2005, **78**, 585–594.
4. R. Langer, Cancer nanotechnology: small, but heading for the big time, *Nature Review*, 2007,**6**, 174
5. D. Son, J. Lee, S. Qiao, R. Ghaffari, J. Kim, J. E. Lee, C. Song, S. J. Kim, D. J. Lee, S. W. Jun, S. Yang, M. Park, J. Shin, K. Do, M. Lee, K. Kang, C. S. Hwang, N. Lu, T. Hyeon, and D.-H. Kim, *Nature Nanotechnology*, 2014, **9**, 397–404.
6. N. Bhattarai, *Journal of Nanomedicine & Nanotechnology*, 2012, **03**.
7. T., Christopher, Reading Feynman Into Nanotechnology: A Text for a New Science, Techné 12:3 Fall 2008
8. T. Pradeep and Anshup, *Thin Solid Films*, 2009, **517**, 6441–6478.
9. A. Abedini, A. Daud, M. Abdul Hamid, N. Kamil Othman, and E. Saion, *Nanoscale Research Letters*, 2013, **8**, 474.
10. S. K. Ghosh and T. Pal, *Chemical Reviews*, 2007, **107**, 4797–4862.
11. S. Eustis and M. A. El-Sayed, *Chemical Society Reviews*, 2006, **35**, 209.
12. A. S. Thakor, J. Jokerst, C. Zavaleta, T. F. Massoud, and S. S. Gambhir, *Nano Letters*, 2011, **11**, 4029–4036.
13. P. Liu, X. Yang, S. Sun, Q. Wang, K. Wang, J. Huang, J. Liu, and L. He, *Analytical Chemistry*, 2013, **85**, 7689–7695.
14. E. Hutter and D. Maysinger, *Trends in Pharmacological Sciences*, 2013, **34**, 497–507.
15. I. Salas-García, F. Fanjul-Vélez, N. Ortega-Quijano, and J. L. Arce-Diego, eds. L. D. Lilge and R. Sroka, 2013, p. 88030N.
16. M. K. Khaing Oo, Y. Yang, Y. Hu, M. Gomez, H. Du, and H. Wang, *ACS Nano*, 2012, **6**, 1939–1947.
17. T. Stuchinskaya, M. Moreno, M. J. Cook, D. R. Edwards, and D. A. Russell, *Photochemical & Photobiological Sciences*, 2011, **10**, 822.
18. G. Herrera, A. Padilla, and S. Hernandez-Rivera, *Nanomaterials*, 2013, **3**, 158–172.
19. A. Salehi-Khojin, H.-R. M. Jhong, B. A. Rosen, W. Zhu, S. Ma, P. J. A. Kenis, and R. I. Masel, *The Journal of Physical Chemistry C*, 2013, **117**, 1627–1632.

20. L. Yu, Y. Zhang, B. Zhang, and J. Liu, *Scientific Reports*, 2014, **4**.
21. A. Panáček, M. Kolář, R. Večeřová, R. Prucek, J. Soukupová, V. Kryštof, P. Hamal, R. Zbořil, and L. Kvítek, *Biomaterials*, 2009, **30**, 6333–6340.
22. B. Reidy, A. Haase, A. Luch, K. Dawson, and I. Lynch, *Materials*, 2013, **6**, 2295–2350.
23. Q. H. Tran, V. Q. Nguyen, and A.-T. Le, *Advances in Natural Sciences: Nanoscience and Nanotechnology*, 2013, **4**, 033001.
24. S. Mukherjee, D. Chowdhury, R. Kotcherlakota, S. Patra, V. B, M. P. Bhadra, B. Sreedhar, and C. R. Patra, *Theranostics*, 2014, **4**, 316–335.
25. A. Salehi-Khojin, H.-R. M. Jhong, B. A. Rosen, W. Zhu, S. Ma, P. J. A. Kenis, and R. I. Masel, *The Journal of Physical Chemistry C*, 2013, **117**, 1627–1632.
26. L. Yu, Y. Zhang, B. Zhang, and J. Liu, *Scientific Reports*, 2014, **4**.
27. J. Zheng, P. R. Nicovich, and R. M. Dickson, *Annual Review of Physical Chemistry*, 2007, **58**, 409–431.
28. J. Zheng, C. Zhang, and R. Dickson, *Physical Review Letters*, 2004, **93**.
29. E. Hutter and D. Maysinger, *Trends in Pharmacological Sciences*, 2013, **34**, 497–507.
30. I. Salas-García, F. Fanjul-Vélez, N. Ortega-Quijano, and J. L. Arce-Diego, eds. L. D. Lilge and R. Sroka, 2013, p. 88030N.
31. M. K. Khaing Oo, Y. Yang, Y. Hu, M. Gomez, H. Du, and H. Wang, *ACS Nano*, 2012, **6**, 1939–1947.
32. J. M. Chan, P. M. Valencia, L. Zhang, R. Langer, and O. C. Farokhzad, *Methods Mol. Biol.*, 2010, **624**, 163–175.
33. A. Kumari, S. K. Yadav, and S. C. Yadav, *Colloids and Surfaces B: Biointerfaces*, 2010, **75**, 1–18.
34. L. E. van Vlerken and M. M. Amiji, *Expert Opinion on Drug Delivery*, 2006, **3**, 205–216.
35. S. Svenson and R. K. Prud'homme, Eds., *Multifunctional Nanoparticles for Drug Delivery Applications*, Springer US, Boston, MA, 2012.
36. H. Nikaido, *Annu. Rev. Biochem.*, 2009, **78**, 119–146.
37. Y. Yamamoto, *Clinical and Vaccine Immunology*, 2002, **9**, 508–514.
38. J. B. Delehanty and F. S. Ligler, *Analytical Chemistry*, 2002, **74**, 5681–5687.
39. G. Longo, L. Alonso-Sarduy, L. M. Rio, A. Bizzini, A. Trampuz, J. Notz, G. Dietler, and S. Kasas, *Nature Nanotechnology*, 2013, **8**, 522–526.

40. A. McNally, *Nature Nanotechnology*, 2013, **8**, 315–316.
41. A. L. Chun, *Nature Nanotechnology*, 2009, **4**, 698–699.
42. Y. Wan, Y. Sun, P. Qi, P. Wang, and D. Zhang, *Biosens Bioelectron*, 2014, **55**, 289–293.
43. S. Mohanty, P. Jena, R. Mehta, R. Pati, B. Banerjee, S. Patil, and A. Sonawane, *Antimicrobial Agents and Chemotherapy*, 2013, **57**, 3688–3698.
44. X. Yuan, M. I. Setyawati, A. S. Tan, C. N. Ong, D. T. Leong, and J. Xie, *NPG Asia Materials*, 2013, **5**, e39.
45. S. K. Gogoi, P. Gopinath, A. Paul, A. Ramesh, S. S. Ghosh, and A. Chattopadhyay, *Langmuir*, 2006, **22**, 9322–9328.
46. P. Sanpui, A. Murugadoss, P. Prasad, S. Ghosh, and A. Chattopadhyay, *International Journal of Food Microbiology*, 2008, **124**, 142–146.
47. M. Banerjee, S. Mallick, A. Paul, A. Chattopadhyay, and S. S. Ghosh, *Langmuir*, 2010, **26**, 5901–5908.
48. Z. Xiu, Q. Zhang, H. L. Puppala, V. L. Colvin, and P. J. J. Alvarez, *Nano Letters*, 2012, **12**, 4271–4275.
49. I. Ali, W. A. Wani and K. Saleem, *Cancer Therapy* 2011, **8**,56-70
50. J. G. Senapathy, P Umadevi, P.S. Kannika, *Asian Pacific J Cancer Prev*, 2011, **12**, 1107-1115.
51. L. Yildirimer, N. T. K. Thanh, M. Loizidou, and A. M. Seifalian, *Nano Today*, 2011, **6**, 585–607.
52. P. Sanpui, A. Chattopadhyay, and S. S. Ghosh, *ACS Applied Materials & Interfaces*, 2011, **3**, 218–228.
53. P. V. AshaRani, G. Low Kah Mun, M. P. Hande, and S. Valiyaveettil, *ACS Nano*, 2009, **3**, 279–290.
54. N. Bertrand, J. Wu, X. Xu, N. Kamaly, and O. C. Farokhzad, *Advanced Drug Delivery Reviews*, 2014, **66**, 2–25.
55. S. Bamrungsap, Z. Zhao, T. Chen, L. Wang, C. Li, T. Fu, W. Tan, *Nanomedicine.* 2012; **7,** 1253-1271.
56. E. Ruoslahti, S. N. Bhatia, and M. J. Sailor, *The Journal of Cell Biology*, 2010, **188**, 759–768.

57. X. Zhao, H. Li, and R. J. Lee, *Expert Opin Drug Deliv*, 2008, **5**, 309–319.

58. Z. M. Qian, H. Li, H. Sun, and K. Ho, *Pharmacol. Rev.*, 2002, **54**, 561–587.

Chapter 2

Quick and Simple Estimation of Bacteria Using a Fluorescent Paracetamol Dimer-Au nanoparticle Composite

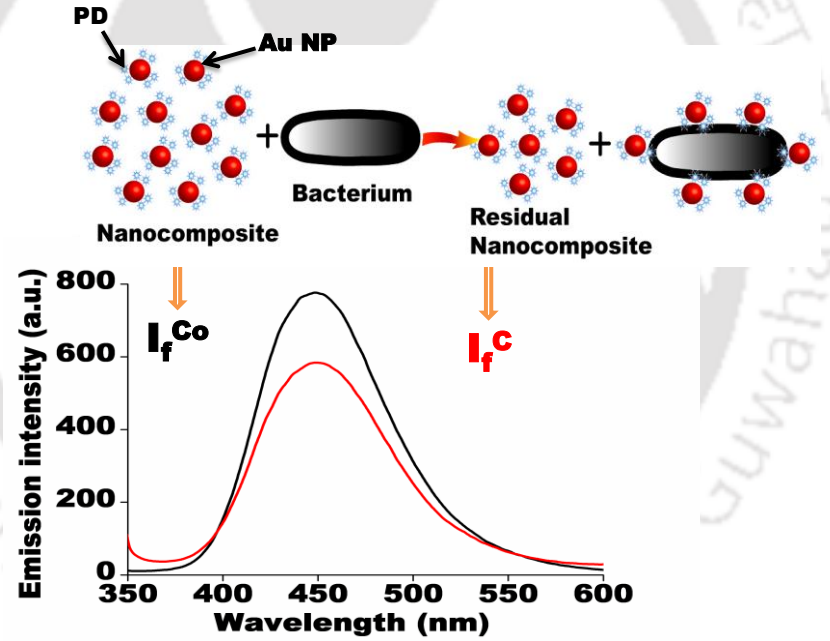

A. K. Sahoo, S. Sharma, A. Chattopadhyay and S. S. Ghosh, **2012**. ***Nanoscale,*** 4, 1688-1694.

Chapter 2:

Quick and Simple Estimation of Bacteria Using a Fluorescent Paracetamol Dimer-Au nanoparticle Composite

2.1. Introduction

In the last few decades, bacterial contamination in food, water and health care leading to life threatening diseases has become a serious problem.[1-8] Besides, the increasing risk of bioterrorism attacks[9-10] demands fast, simple and reliable methods of quick detection and quantification of bacterial population during early stage of contamination to protect public health and environment. Plating and colony counting is a conventional method to enumerate the bacterial cell number in the test samples.[11-13] Undoubtedly, this culture based method is accurate and reliable but is time consuming (more than 24 h), laborious and prone to errors. In addition, there are several highly specific and sensitive molecular biology based methods available like PCR[14-16], microarrays[17-18], monoclonal antibody and/or enzyme based immunological assays[19-21] which require considerably less time (only several hours) than culture based methods. However, such methods employing sophisticated instruments and expensive reagents are costly and require significant training and skills. In view of the above background, low cost method for instant and sensitive detection of pathogens remains a challenge. Recently, nanotechnology based biosensors have been developed for pathogen detection with high sensitivity.[22-26] Functionalized nanoparticles (NPs) [27-29] and quantum dots (QDs) [30-31] have been studied as probes to identify specific and even single microorganism [32-35] among a heterogeneous population. Though the nanomaterial based strategies are very specific and ultra-sensitive, but cannot detect numerous classes/species of micro-organisms simultaneously, this is important for a general contamination test. To address these coexisting issues, fluorescence based methods - an ideal background free method- are involved researchers due to its rapid response time, easy operation and sensitivity.

In this regard, not much research has been done on detection of multiple pathogens using a single probe. Thus, with the aim to detect multiple bacterial by single probe, a well-known drug paracetamol (acetaminophen) i.e. p-hydroxyacetanilide (pHA)

has been opted to synthesize nanocomposites. Paracetamol is extensively use as an antipyretic and analgesic agent and generally consider as a safe drug.

2.2. Outline of the research work

1. A simple method of bacteria detection was proposed by using a highly fluorescent nano composite comprising of paracetamol dimer (PD)-gold nanoparticles (Au NPs) in aqueous media at physiological condition (PBS buffer, pH 7.4). The method requires minimum efforts of sample preparation and precaution.
2. The composite was synthesized by reaction of $HAuCl_4$ with paracetamol (p-hydroxyacetanilide, pHA) at basic condition and elevated temperature followed by a series of the characterizations such as UV-Vis spectroscopy, Fluorescence spectroscopy, transmission electron microscopy, mass spectroscopy and FT-IR analysis.
3. The gradual fluorescence quenching of the composite with the presence of bacteria offers the plausibility to enumerate the number of bacteria present in the test sample.
4. The sensitivity of the method was found to be 100 CFU/mL based on our experiments with three Gram- positive and three Gram-negative bacterial strains.
5. In addition, the composite interacted differently with Gram-positive and Gram-negative bacteria making it possible to differentiate between the two without using antibodies or radioactive markers.
6. Importantly, the composite comprised of non-antibacterial components (PD and Au NPs) that did not cause any harm to bacteria, making it a suitable fluorescent probe for detection and enumeration of bacteria at a broad range of bacterial concentrations.

2.3. Experimental section

2.3.1. Chemicals and growth media

$HAuCl_4$ (17 wt% solution of $HAuCl_4$ in dilute HCl; 99.99 %) was obtained from Sigma-Aldrich Chemicals, U.S.A. Luria-Beterni broth (LB), Nutrient broth (NB), Brain-Heart Infusion (BHI), and de Man Rogosa and Sharpe (MRS) growth media were purchased from HiMedia, Mumbai, India. Paracetamol was procured from Merck India Pvt. Ltd, Mumbai, India and used as received.

2.3.2. Synthesis of paracetamol dimer (PD)-Au NP composite

The composite (PD-Au NP) was synthesized by mixing 1 ×10 $^{-2}$ M of paracetamol (pHA) and 500 µl of 0.3 M NaOH (pH 10.0) in a conical flask containing 100 ml deionozed water heating at 90 ^{0}C under constant stirring. After 10 min, 0.5 ml of freshly prepared 10 mM $HAuCl_4$ solution was added drop by drop. The appearance of red color immediately after addition of gold salt indicated formation of AuNPs. For complete reduction of gold, heating was continued for another 30 min.

2.3.3. Culture of the bacterial strains

The six bacterial strains used in the present investigation include three Gram-positive: *Pediococcus acidilactici* CFR K7, *Bacillus cereus* MTCC1305, *Enterococcus faecalis* MTCC 439 and three Gram-negative: *Escherichia coli* MTCC 433, *Enterobacter aerogenes* MTCC 2822, *Pseudomonas aeruginosa* MTCC 2488 strains. The *Pediococcus acidilactici* CFR K7 was propagated in static condition at 37 °C in MRS. The *Enterococcus faecalis* MTCC 439 was grown in BHI at 37 °C at 220 rpm for 12 h, and the same conditions were kept to grow all other strains in NB medium. The recombinant GFP-expressing *E. coli* cells (DH5α) were grown in LB media according to our previous study. [36]

2.3.3. Fluorescence measurements

All fluorescence experiments were carried out using a fluorescence spectrophotometer (LS55, Perkin Elmer). For bacteria detection, the bacterial cultures were grown in the respective media for 12 h and cells were harvested from 1.0 mL aliquot of culture broth by centrifugation at 6000 rpm for 5 min. The cell pellets were washed twice with PBS to remove the residual media components and were resuspended in same buffer. To start the experiments, serial dilutions of 10, 100, 1000, 10000 and 100000 times were made (separately) and the absorbance of each sample was taken at 595 nm in a UV-Vis spectrophotometer. 80 µl of each sample was spread on agar plates and incubated at 37 °C overnight to obtain the colonies. The number of colonies obtained was related to the absorbance of each sample. This was done for all six strains. For all further experiments, the number of bacteria was kept fixed by adjusting the absorbance at 595 nm. The composite was incubated with different dilutions of bacteria in a ratio of 20:1 (v/v) and the changes in the emission intensity of the composite were recorded.

2.3.4. TEM analysis

For TEM analysis, 7.0 µL aliquot of the as-synthesized PD-Au NPs composite was drop-cast on a carbon-coated copper grid followed by air-drying. The grids were then analyzed under TEM (JEM-2100, JEOL, Japan), operating at a maximum accelerating voltage of 200 keV. The interaction of nanocomposite with bacteria was also studied with the same instrument. For this, overnight grown bacterial culture was first incubated with the composite for 1 hr at 37 ^{0}C, centrifuged and then washed with PBS to avoid interference of residual media with resolution of the images. Then, 7µL of the bacterial suspension was deposited on a carbon coated copper grid, air dried, and analyzed under TEM as described above.

2.3.5. X-ray diffraction (XRD) analysis

For XRD measurements, the composite was evaporated on a microscope glass slide followed by recording of diffraction using a Bruker Advance D8 XRD machine Cu Kα source at 1.54 Å wavelength).

2.3.6. Mass spectroscopy

Electro spray mass spectrometry ESI (-) MS of the composite was performed using LC-MS/MS- operation system, Q-Tof Premier^{TM} after filtering the as synthesized composite through a 0.2µm filter.

2.4. Results and discussion

2.4.1. Synthesis and characterization of PD-Au NP composite

The PD-Au NP composite was synthesized using 1 ×10 $^{-2}$ M paracetamol and 10 mM $HAuCl_4$ in basic condition at high temperature. The UV-Vis spectrum showed a sharp plasmon peak of Au NPs at 525 nm (**Figure 2.1a**). The TEM images showed that the synthesized NPs were monodisperse and mainly spherical in shape (**Figure 2.1b**). The average size of the NPs was found to be 7.0 $\pm$ 0.5 nm (inset **Figure 2.1b**). The high resolution electron microscope (HRTEM) image showed distinct lattice planes (**Figure 2.1c**) of Au NPs. The selected area electron diffraction patterns (SAED) of single NP demonstrated that the synthesized NPs were polycrystalline (inset of the **Figure 2.1c**). The energy-dispersive X-ray spectroscopy (EDX) was also performed in the same instrument which indicated that the NPs were composed exclusively of gold (refer to

Appendix **Figure A1.1a**). The additional carbon, oxygen and nitrogen peaks were due to PD that stabilized Au NPs and Cu signal was due to TEM grid. Further, the X-ray diffraction pattern of the composite showed 2θ values at 38.30°, 44.24° and 65.20° which correspond to the (111), (200) and (220) lattice planes respectively of the face center cubic (fcc) Au(0) (**Figure 2.1 d**). The additional peaks observed in the diffraction pattern were due to crystalline pHA and its dimer [37].

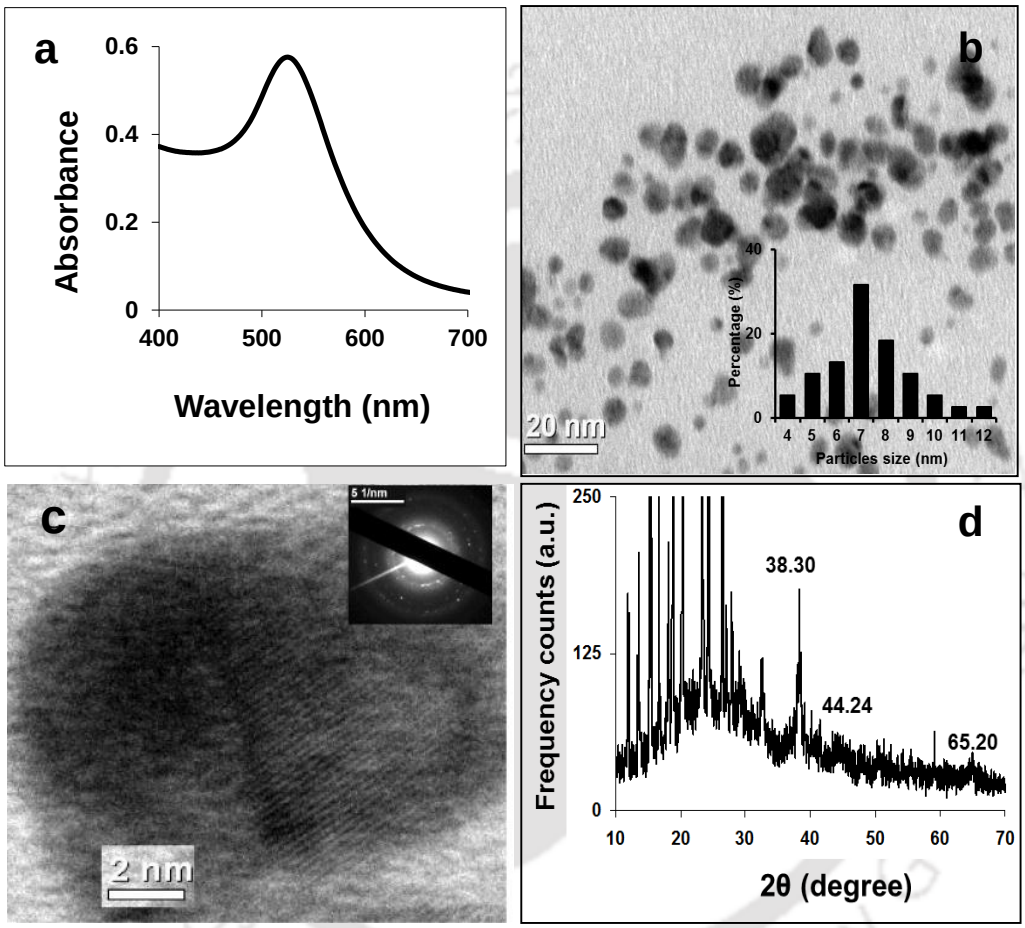

Figure 2.1. (**a**) UV-Vis spectrum of Au NPs at 525 nm. (**b**) TEM image of the composite inset is particle size distribution. (**c**) HRTEM of single NP; inset is SAED of single NP. (**d**) Powder XRD of the composite.

The Electro spray mass spectrometry (ESI-MS) of the composite in the negative mode revealed most abundant peak at 299 (M-1) that corresponds to deprotonated paracetamol dimer (PD) and peak at 150 (m-1) corresponding to unreacted paracetamol (**Figure 2.2a**). It should be mentioned here that the amount of unreacted paracetamol was less as compared to its dimer. Due to the presence of PD, the composite showed a strong blue

emission peak at 435 nm (**Figure 2.2b**) when excited at 320 nm, as characteristic emission of the paracetamol dimer (5, 5'-bis (acetyl amino)-2, 2'-dihydroxybiphenyl) [38-39].

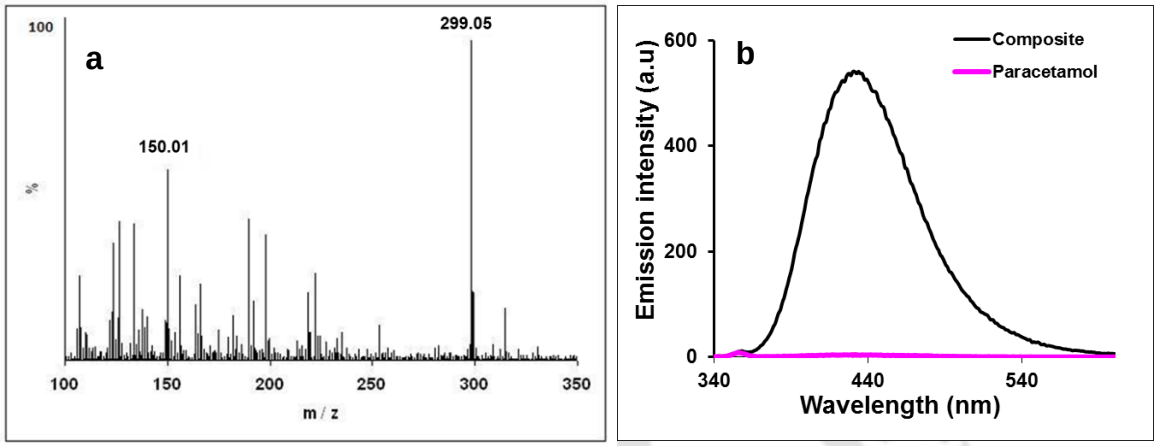

Figure 2.2 (**a**) Mass spectra of composite showing the peak correspond to PD. (**b**) Emission spectra of the composite showing the peak at 435 nm when excited with 320 nm.

2.4.2. Estimation of bacteria using PD-Au NPs composite

The fluorescence of the composite was dependent on the pH of the solution. The optimum pH at which it exhibited maximum emission intensity was 7.50 (refer to Appendix **Figure A1.1b**), which interestingly is very close to the physiological pH. In addition, it was found that the fluorescence intensity of the composite was quenched in the presence of bacteria (both Gram-positive and Gram-negative) in the medium. The emission intensity of the composite (at 435 nm) decreased gradually with increasing concentration of bacteria (**Figure 2.3**) making it a suitable fluorescent probe for detection of bacteria.

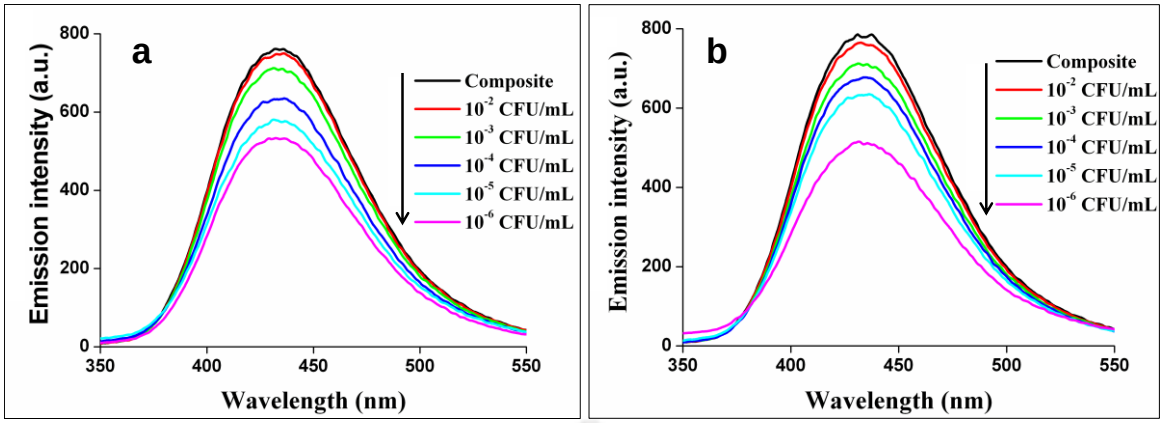

Figure 2.3 Decrease in fluorescence intensity (at 435 nm) of PD-Au NPs composite with increase in bacterial cell number, where excitation was fixed at 320 nm (**a**) *Enterococcus faecalis* MTCC439 (Gram-positive). (**b**) *Escherichia coli* MTCC433 (Gram-negative).

To verify whether the observed changes in emission intensity after addition of bacterial cells were due to non-covalent interaction of bacteria and composite or due to nonspecific molecular crowding of bacteria on nanoparticles or aggregation of nanoparticles, the composite was incubated with bacteria for 15 min at 37 ^{0}C. The cells were precipitated and the emission intensity of supernatant was measured. Results showed that the fluorescence of the supernatants was reduced significantly as compared to the control sample (only composite without bacteria) indicating interaction of the composite with bacterial cells**.**

Moreover, the quenching of the fluorescence of the composite (fluorophore) with increasing bacterial concentration provided an opportunity to quantitate bacterial number using a well-known relationship between the intensity of fluorescence and the concentration of the fluorescent species.[40-41] According to this relation, the steady state fluorescence intensity I^{c}_{f} of a fluorophore of concentration C (mol/L) at the wavelength (λ_{em}) is directly proportional to the steady state fluorescence intensity per absorbed photon F_{λ} (λ_{em}) and the total number of photons absorbed at the excitation wavelength (λ_{ex}). Rewriting the total number of photons by the absorbance intensity I_0 at wavelength (λ_{ex}) the fluorescence intensity can be expressed as

$$I^{c}_{f} = \kappa F_{\lambda} I_0 \{1 - e^{-2.3C \varepsilon l}\} \quad (1)$$

Here κ is the proportionality constant; ε is the molar extinction coefficient ($Lmol^{-1}cm^{-1}$) at the excitation wavelength (λ_{ex}) and l is the optical path length (cm). If sample is excited at

fixed wavelength keeping all the optical parameters unaltered, the above equation can be simplified as

$$I_f^C = B\{1 - e^{-2.3C\varepsilon l}\} \quad (2)$$

Where $B = \kappa F_\lambda I_0$.

The above simplified relation was applied to our experimental results. For the pure sample (without the quencher i.e bacteria), when the fluorophore (composite) concentration was Co the eq. 2 can be written as

$$I_f^{Co} = B\{1 - e^{-2.3\,Co\,\varepsilon l}\} \quad (3)$$

In the presence of bacterial cells (quencher in our experiment), the effective fluorophore concentration was decreased to C = (Co – zN) due to interaction with the bacterial cell surface. Here, N is the number of bacteria (CFU/mL) and 'z' is a factor relating the number of bacteria (CFU/mL) to the concentration of the composite (mol/L) to which they are attached. So eq.3 can be written as

$$I_f^C = B\{1 - e^{-2.3\,(Co-zN)\,\varepsilon l}\} \quad (4)$$

Eq.3 and eq.4 were combined, approximated and taking logarithm with base 10 on both sides as

$$\log_{10}(I_f^{Co} / I_f^{Co} - I_f^C) = \log_{10} K - \log_{10} N \quad (5)$$

Where $K = (Co / ze^{-2.3Co\,\varepsilon l})$

From eq.5 it was clear that K was a constant whose value depended on initial concentration and absorbance at the excitation wavelength (λ_{ex}) of the fluorophore. Interestingly, when the logarithm of fluorescence of pure composite divided by residual fluorescence after quenching by the bacteria ($I_f^{Co} / I_f^{Co} - I_f^C$) was plotted against the logarithm of number of bacterial cells (N), a linear relationship was obtained. All the six strains including Gram-positive (*Pediococcus acidilactici* CFR K7, *Bacillus cereus* MTCC 1305 and *Enterococcus faecalis* MTCC 439) and Gram-negative (*Escherichia coli* MTCC 433, *Enterobacter aerogenes* MTCC 2822 and *Pseudomonas aeruginosa* MTCC 2488) followed the linear relationship (**Figure 2.4**) demonstrating generality and non-specificity of the method.

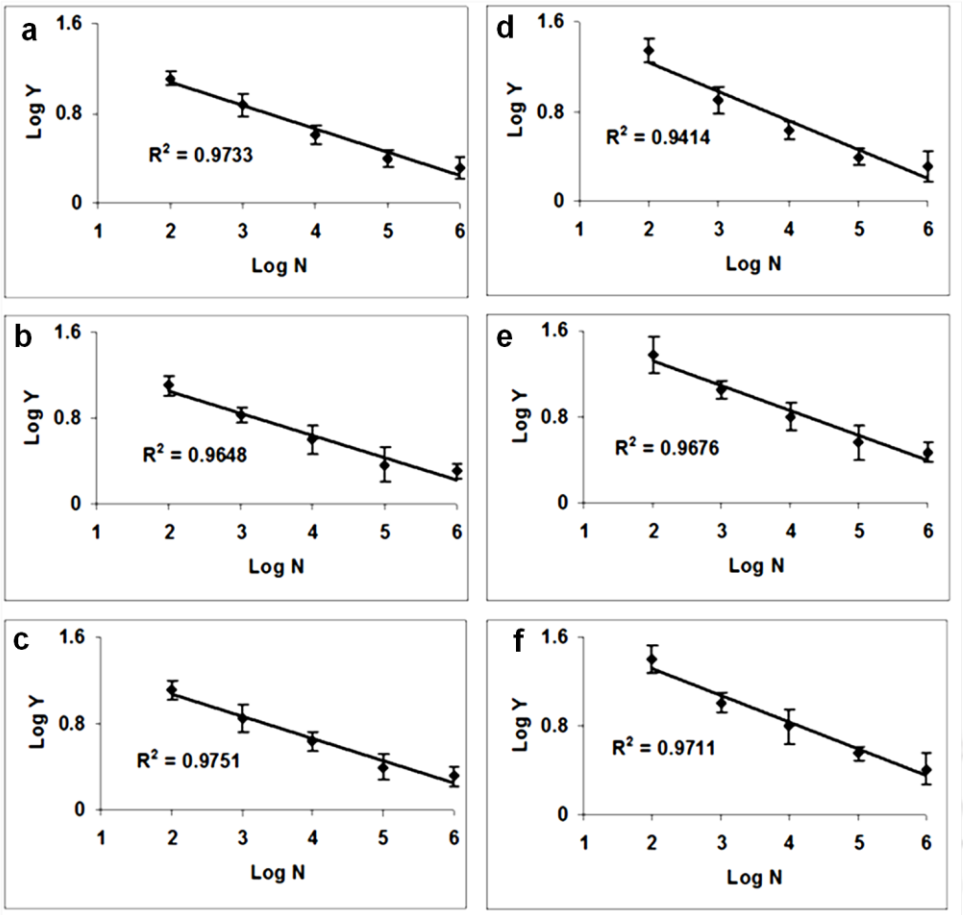

Figure 2.4 Decrease in fluorescence intensity of PD-Au NPs composite at 435 nm as a function of bacterial cell number, where Y= (I_f^{Co} / I_f^{Co} - I_f^{C}) and N is the number of bacteria (CFU/ mL). (**a**) *Pediococcus acidilactici* CFR K7; (**b**) *Bacillus cereus* MTCC1305 and (**c**) *Enterococcus faecalis* MTCC439 are Gram Positive Bacteria. (**d**) *Escherichia coli* MTCC433 ;(**e**) *Enterobacter aerogenes* MTCC2822 and (**f**) *Pseudomonas aeruginosa* MTCC2488 are Gram Negative Bacteria. The data represents mean ± S.D. of three experimental results.

The results showed that the Gram-positive bacterial strains viz. *P. acidilactici* CFR K7, *B .cereus* MTCC 1305 and *En. faecalis* showed higher slope values of -0.208, -0.203 and -0.204 respectively as compared to the Gram-negative strains of *E. coli* MTCC 433 , *En. aerogenes* MTCC 2822 and *Ps. aeruginosa* MTCC 2488 which had slope values of -0.259, -0.232 and -0.243 respectively. The average slope for Gram-positive strains was -0.205 and that of Gram-negative was -0.245. This clearly demonstrates that the Gram-positive strains interacted more strongly with the composite as compared to Gram-negative. The possible reason for difference in interaction is their different cell wall composition. The major component of the outer layer of Gram-positive cell wall is

peptidoglycan and that of Gram-negative cell wall are phospholipids and lipopolysaccharide.[43-44] The bacterial interaction is influenced by the surface charge and hydrophobicity of its cell wall composition. The bacterial cells have net negative charge on their surface at physiological environment though the magnitude may vary from stain to strain [45], which could be a possible reason for variation in slope value of Gram-positive and Gram-negative strains. It should be mentioned here that our method can detect bacteria upto 100 CFU/mL by simply incubating the composite with bacteria for few minutes. High sensitivity, simplicity and quick detection makes our composite an attractive alternative to conventional methods of bacteria detection.

2.4.3. Probing GFP fluorescence of recombinant *E. coli*

Further, to confirm the above observations, we took the green fluorescent protein (GFP) expressing recombinant E. coli, which has an intrinsic emission peak at 510 nm when preferentially excited at 400 nm due to presence of GFP. It was found that as the concentration of bacteria increased from 10^2 CFU/mL to 10^6 CFU/ mL, the emission intensity of PD decreased and as expected, the intensity of GFP emission (at 510 nm) increased **(Figure 2.5a)** due to increase in number of cells. The slope value of this strain was calculated from the above relation and found to be -0.265 **(Figure 2.5b)**. In the next step, different concentrations of the composite were incubated with constant number (10^6 CFU/mL) of cells of recombinant GFP expressing E. coli. It was found that the emission intensity of GFP decreased with increase in composite concentration **(Figure 5c-d).** This was possibly due to spectral overlapping of absorption of Au NPs (at 525 nm) due to localized surface plasmon resonance (LSPR) [46] and the emission of GFP (at 510 nm) that confirmed interaction of composite with bacteria.

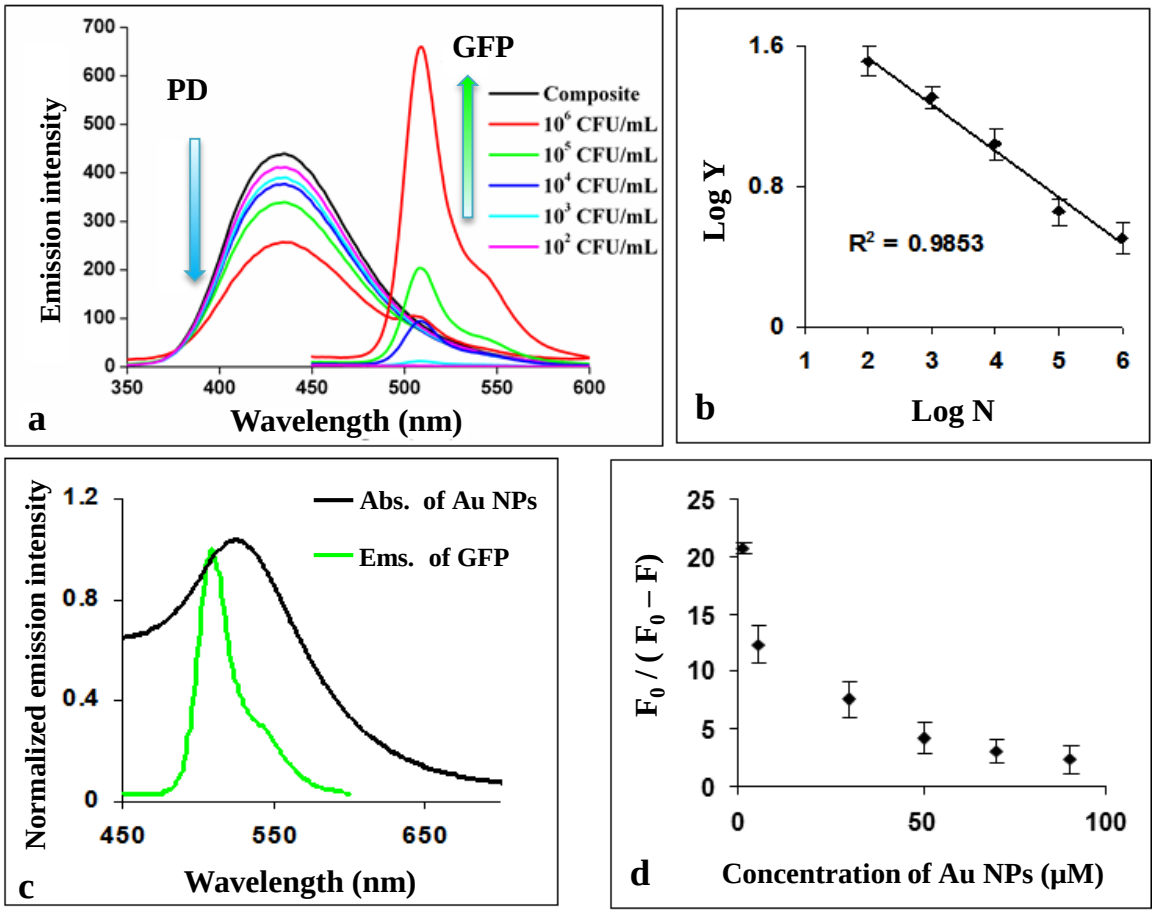

Figure 2.5 (**a**) Emission intensity of GFP (at 510 nm) when excited at 400 nm was increased when bacterial cell number increased from 102 to 106 CFU/mL whereas the emission intensity of PD (at 435 nm) was decreased. (**b**) Decrease in fluorescence intensity at 435 nm of the PD-Au NPs composite as a function of bacterial cell number, where Y= (I_f^{Co} / I_f^{Co}- I_f^{C}) and N is the number of bacteria (CFU/ mL). (**c**) Normalized spectra showing spectral overlapping of PD-Au NPs absorbance at 525 nm and emission of GFP at 510 nm. (**d**) Relative fluorescence quenching of GFP at 510 nm when excited at 400 nm with gradual increase of PD-Au NPs (µM), where F_0 is fluorescence intensity of GFP expressing E. coli and F is fluorescence intensity of same bacteria after addition of composite. The data represents mean ± S.D. of three experimental results.

2.4.4. TEM analysis

Further to confirm the interaction of the composite with bacterial cells, TEM study was done. The TEM image of composite treated GFP expressing recombinant E. coli showed that Au NPs attached to the bacterial cell surface **(Figure 2.6a)** in contrast to the untreated control cell **(Figure 2.6b)**. Interestingly, treatment with the composite did not cause any visual damage or destruction of cell surface.

2.4.5. Non-antibacterial effect of the composite

An important point that should be taken care of during development of a new sensing method is that the probe should not be harmful. In the present study, the composite comprised of PD, Au NPs and very less amount of unreacted paracetamol (that additionally stabilized Au NPs). Several studies have established that Au NPs are non-antibacterial and biocompatible [47-48]. Besides, there are no reports available till date on the adverse effects of PD on bacteria though there are reports on the toxic effects of overdose of paracetamol on mammalian cells [39-40, 49]. So, to address the bacteria viability issue, bacterial growth study was done at concentration of the composite (0.49 mM pHA and 5.0 µM Au) used in bacterial estimation experiments. The study showed that the composite did not exert any antibacterial activity against both Gram-positive and Gram-negative strains at the dose used in the experiments as well as high dose **(Figure 2.6 c-d)**. It should be mentioned here that Ag NP-PD nanocomposite is antibacterial in contrast to PD-Au NP as reported recently from our lab[50].

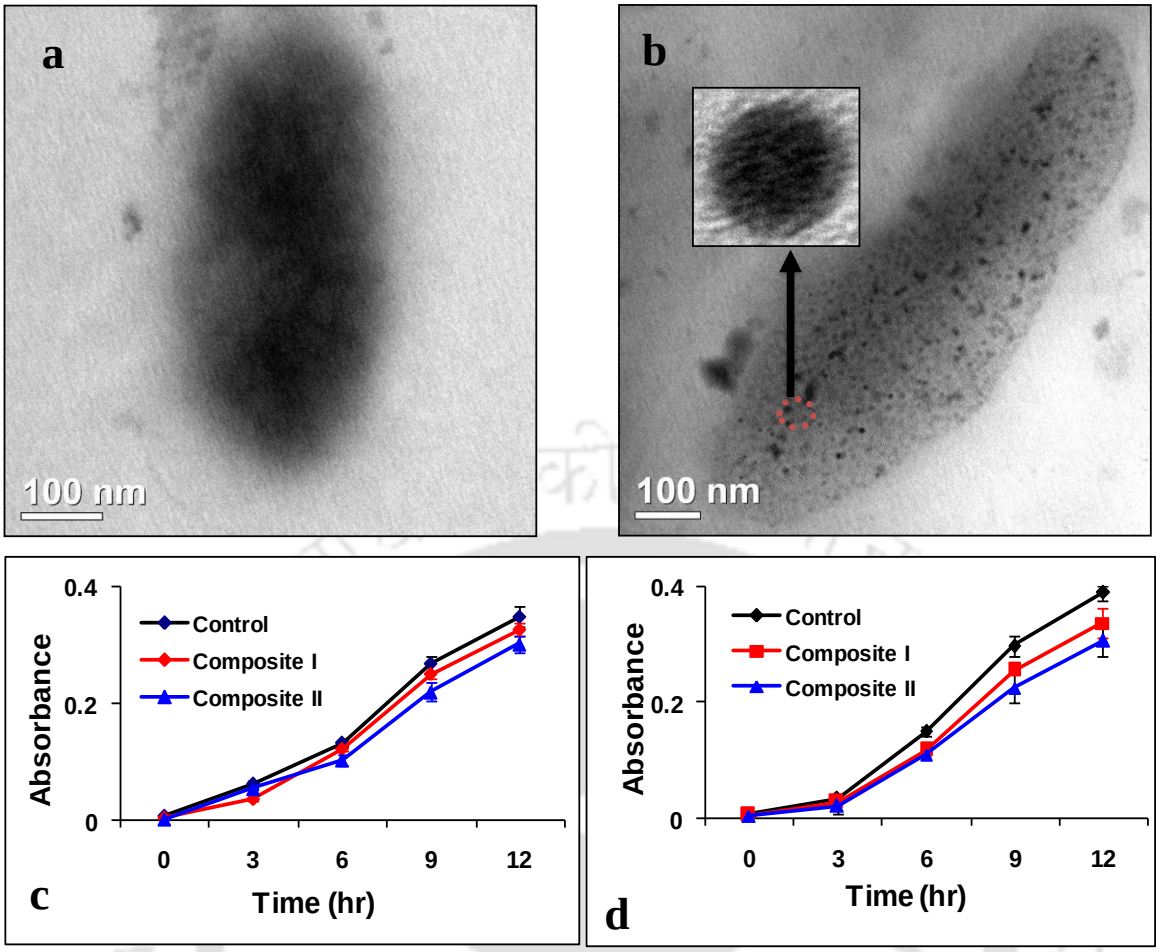

Figure 2.6 (**a**) Untreated bacterial cell (Control). (**b**) TEM image of composite treated cell, inset is TEM image of single NP. Growth curve of (**c**) Enterococcus faecalis MTCC439 (Gram-positive) and (**d**) Escherichia coli MTCC433 (Gram-negative) bacteria in presence of composite.

2.4.6. Statistical analysis

In a scientific study, every experiment is associated with certain degree of error depending on the test conditions and parameters, so the statistical significance of an experiment is very much important; if the likelihood of an event out comes (results) are statistically significant then only we can confidently say that the results did not happen by chance. To check the reliability of our test results, we have done well known chi-square (χ^2) test to find out the statistical significance of our proposed method.

For chi-square (χ^2) test, overnight culture of GFP expressing recombinant E .coli was suitably diluted and spread on previously prepared 1.5 % LB-agar plate containing 100 µg/mL ampicillin. After incubation for 12 h at 37 °C, the colonies were counted and

compared with the bacterial cell number from the standard curve of *E. coli* (Figure 4B) mentioned before. The chi square test was performed and value was found to be 11.79 with the degree of freedom (df) 6, which corresponds to the $0.1 < p < 0.05$, as calculated from the chi square test table (Supporting Information, Table S1). This means that ≥ 90% test results were true. Based on the statistical test, we concluded that there was no statistically significant difference between observed (number of colonies) and expected (values obtained from standard curve of fluorescence quenching experiments) frequency of bacterial cells which conclusively established the accuracy and relevance of this method.

2.5. Conclusion

In brief, a fluorescent PD-Au NP composite was synthesized using a conventional drug paracetamol. The composite exhibited maximum emission peak at physiological pH and remained stable for more than a week. The fluorescence intensity of the composite decreased with increasing bacterial concentration which provided an efficient means to find out the bacterial number in the test sample. Using this method, three Gram positive and Gram negative bacteria were successfully detected with sensitivity of 100 CFU/ ml. The difference in interaction of the composite with Gram-positive and Gram-negative bacteria and corresponding difference in quenching of the fluorescence of the composite made it possible to distinguish between the two. The composite was not antibacterial and the chi-square test showed statistical significance of this method. Ease of operation, quick and non-specific detection with high sensitivity over broad range of bacterial concentrations in a short span of time, makes this method an attractive alternative over conventional methods of bacteria detection.

2.6. References

1. E. Scott, S. F. Bloomfield, Lett. Appl. Microbiol. 1993, **16,** 173-177.
2. S. Pedley, J. Bartram, G. Rees, A. Dufour, J. A. Cotruvo, Pathogenic Mycobacteria in Water; World Health Organization: London, 2004.
3. M. E. Brecher, S. N. Hay, Clinical Microbiology Reviews 2005, **18,** 195-204.
4. A. Crepet, I. Albert, C. Dervin, F. Carlin, Applied and Environmental Microbiology 2006, **73,** 250-258.
5. K. Mølbak, N. Højlyng, S. Jepsen, K. Gaarslev, Epidemiol. Infect. 2009, **102,** 309-316.
6. A. B. Christie, Proc.Nutr.Sco. 1972, **31,** 33-37.
7. J. Runner, Am. J. Infec. Control, 2007, **35,** 527-530.
8. T. V. Inglesby, et al. J. Am. Med. Assoc. 2002, **287,** 2236-2252.
9. D. B .Jernigan, et.al. Emerg. Infect. Dis. 2002, **8,** 1019-1028.
10. M. W. LeChevallier, R. J.Seidler, T. M. Evans, Appl. Environ. Microbiol. 1980, **40,** 922–930.
11. M. W. Jennison, J. Bact., 1937, **33,** 462-477
12. M. Allen, Int. J. Food Microbiol. 2004, **92,** 265-274.
13. I. R. McDonald, E. M. Kenna, J. C. Murrell, Appl. Environ. Microbiol., 1995, **61**, 116-121.
14. R. F. Wang, W. W. Cao, C. E. Cerniglia, Appl. Environ. Microbiol., 1996, **62**,1242-1247.
15. P. Belgrader, Science 1999, **284,** 449-450.
16. J. B. Delehanty, F. S. Ligler, Anal. Chem. 2002, **74,** 5681-5687.
17. J. Peplies, F. O. Glockner, R. Amann, Appl. Environ. Microbiol. 2003, **69,** 1397-1407.
18. A.-M. Svennerholm, J. Holmgren, Current Microbiology 1978, **1,** 19-23.
19. I. Abdel-Hamid, Analytica Chimica Acta 1999, **399,** 99-108.
20. M. Blake, K. Johnston, G. Russelljones, E. Gotschlich, Anal. Biochem. 1984, **136,** 175-179.
21. O. Lazcka, F. J. D. Campo, F. X. Muñoz, Biosensors and Bioelectronics 2007, **22,** 1205-1217.
22. H. Gu, P.-L. Ho, K. W. T. Tsang, L. Wang, B. Xu, J. Am. Chem. Soc. 2003, **125,** 15702-15703.

23. H. Gu, K. Xu, C. Xu, B. Xu, Chem. Commun. 2006, **9,** 941-949.
24. L. Wang, W. Zhao, M. B. O'Donoghu, W. Tan, Bioconjugate Chem. 2007, **18,** 297-301.
25. U. H. F. Bunz, V. M. Rotello, Angew. Chem. Int. Ed. 2010, **49,** 3268 – 3279
26. C. Kaittanis, S. A. Naser, J. M. Perez, Nano Lett. 2007, **7,** 380-383.
27. J. Yan, M. C. Estévez, J. E. Smith, K. Wang, X. He, L. Wang, W. Tan, Nano Today 2007, **2,** 44-50.
28. Y. F. Huang, Y. F. Wang, X. P. Yan, Environ. Sci. Technol. 2010, **44,** 7908-7913.
29. M. A. Hahn, J. S. Tabb, T. D. Krauss, Anal. Chem. 2005, **77,** 4861-4869.
30. L. Yang, Y. Li, Analyst 2006, **131,** 394-401.
31. M. D. Disney, J. Zheng, T. M. Swager, P. H. Seeberger, J. Am. Chem. Soc. 2004, **126,** 13343-13346.
32. S. Dwarakanath, J. G. Bruno, A. Shastry, T. Phillips, A. John, A. Kumar, L. D. Stephenson, Biochem. Biophy.s Res. Commun. 2004, **325,** 739-743.
33. Chen, Z.; Li, G.; Zhang, L.; Jiang, J.; Li, Z.; Peng, Z.; Deng, L. Anal Bioanal Chem 2008, **392,** 1185-1188.
34. G. Naja, P. Bouvrette, S. Hrapovic, J. H. T. Luong, Analyst 2007, **132,** 679-686.
35. T. P. Burg, M. Godin, S. M. Knudsen, W. Shen, G. Carlson, J. S. Foster, K. Babcock, S. R. Manalis, Nature 2007, **446,** 1066-1069.
36. S. K. Gogoi, P. Gopinath, A. Paul, A. Ramesh, S. S. Ghosh, A. Chattopadhyay, Langmuir 2006, **22,** 9322-9328.
37. S .Das, A. K. Sahoo, S. S. Ghosh, A. Chattopadhyay, Langmuir, 2010, **26,** 15714–15717.
38. J. V. Steveninck, J. F. Koster, T. M.A. Dubbelman, Biochem. J. 1989, **259,** 633-637.
39. W. Clegg, S. J. Teat, K. V. R. Prasad, R. I. Ristic, D. B. Sheen, E. A. Shepherd, J. N. Sherwood, R. M. Vrcelj, Acta Crystallogr C Cryst Struct Commun 1998, **54,** 1881-1882.
40. B. Valeur, In Molecular Fluorescence; Wiley-VCH: Weinheim, Germany, 2002; pp 50-51.
41. B. R. Panda, A. K. Singh, A .Ramesh,; A. Chattopadhyay, Langmuir 2008, **24,** 11995-12000.
42. L .S. Young, W. J. Martin, R.D. Meyer, R. Weinstein, E.T. Anderson, Ann Intern Med. 1977, **86,** 456-71.

43. U. Sleytr, Prog. Surf. Sci. 2001, **68,** 231-278.

44. S. J. Dickson, M. Koohmaraie, Appl. Envion. Microbiol. 1989, **55,** 832-836.
45. K. L. Kelly, E. Coronado, L. L. Zhao, G. C. Schatz, J. Phys. Chem. B 2003, **107,** 668-677.
46. R. Shukla, V. Bansal, M. Chaudhary, A. Basu, R. R. Bhonde, M. Sastry, Langmuir 2005, **21,** 10644-10654.
47. Z. Krpetić, F. Porta, E. Caneva, V. Dal Santo, G. Scarì, Langmuir 2010, **26,** 14799-14805.
48. U. S. Ruepp, P. R. Tonge; J. Shaw, N. Wallis, F. Pognan, Toxicol. Sci. 2002, **65,**135-150.
49. E. Dybing, J. A. Holme, W. P. Gordon, E. J. Soderlund, D. C. Dahlin, S. D. Nelson, Mutat. Res. 1984, **138**, 21-32.
50. A. K. Sahoo, M. Palashuddin Sk, S. S. Ghosh, A. Chattopadhyay, Nanoscale 2011, DOI: 10.1039/c1nr10389j.
51. R.A. Fisher, Statistical Methods for Research Workers, Edinburg: Oliver and Boyd,1958, p112-113

Chapter 3

Plasmid DNA linearization in the antibacterial Action of a new Fluorescent Ag Nanoparticle-Paracetamol Dimer composite

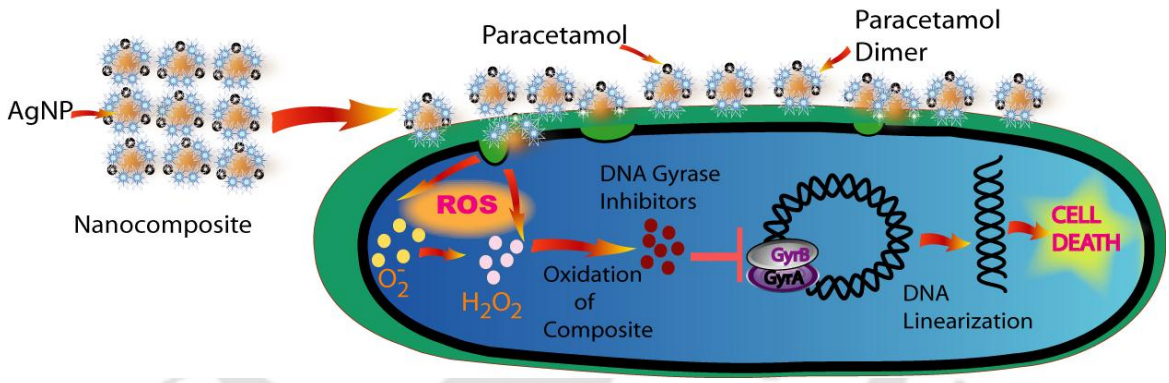

A. K. Sahoo, Md P. Sk, S. S. Ghosh and A. Chattopadhyay, **2011**. ***Nanoscale***, 3, 4226-4233..

Chapter 3:

Plasmid DNA linearization in the antibacterial Action of a new Fluorescent Ag Nanoparticle-Paracetamol Dimer composite

3.1. Introduction

Chemistry arguably offers a great repertoire of compounds and protocols in developing newer drugs and pharmaceutically important molecules in modern healthcare. The need for developing viable alternatives to conventional antibiotics, in this regard, has been an area of increasing concern due to the ever-increasing prevalence of antibiotic resistant bacteria.[1-3] Moreover, the hunt for potential alternatives has recently been underscored by the discovery of a new antibiotic resistance mechanism (conferred by New Delhi metallo-β-lactamase 1, NDM-1) of multi-drug resistant (MDR) bacteria, currently prevalent in India, Pakistan and the United Kingdom. It is deemed to have the potential to become a serious threat to public health worldwide, if left unattended.[4] Herein an opportunity lies with the 'combinational antimicrobial therapy', a new regimen specially developed for emerging MDR or extensively drug resistant (XDR) bacterial strains. Among the available options, Ag nanoparticles (NPs) have been demonstrated to have advantages over conventional antibiotics with the unlikelihood of the bacteria developing resistance to the NPs. In addition, Ag NPs work against a broad spectrum of bacteria. However, apparent cytotoxicity of Ag NPs to mammalian cells demands their use at lower doses, [5] which could be achieved by using them in composites with antimicrobial and biocompatible polymers or other agents. [6-7] The Ag NPs cause perforation of the bacterial cell wall making them unviable. They do not necessarily affect the DNA or proteins of the bacteria. [8-10] It is also known that when the NPs are used in the form of a composite, the antimicrobial properties of the host (a polymer) or stabilizing molecule would also work in tandem with the NPs in order to provide increased efficacy. For example, it has been established that in a chitosan-Ag NP composite, the positively charged chitosan helps in attachment to the negatively charged cell surface of the bacterium and the Ag NPs make pores in the cell wall, thereby making the bacterium unviable at lower individual component concentrations. However, the challenge remains with the lowering

of the concentration of Ag NPs. One of the ways in which this can be achieved is by identifying a suitable component, which would not only increase the bactericidal potency but also pose no additional danger to the human health and the environment. Additionally, it would imply immense therapeutic importance if any of the components could affect the bacterial DNA, via its linearization, resulting in the inhibition of bacterial growth as well as survival. Interestingly, not much investigation has been directed in this regard.

Para-hydroxyacetanilide (pHA), commonly known as paracetamol (acetaminophen), is used as an over-the-counter low cost anti-pyretic and analgesic and it is relatively safe to use at low concentrations, although excess administration causes elevation of cellular oxidative stress, [11-13] leading to its oxidation. Oxidation of pHA in mammalian cells primarily produces two metabolites - pHA dimer (5, 5'-bis (acetyl amino)-2, 2'-dihydroxybiphenyl, PD) and/or N-acetyl p-benzoquinone imine (NAPQI). [14-15] NAPQI is known to inhibit topoisomerase II resulting in enzyme-mediated double-stranded DNA breakage and thus affecting DNA replication.[16-17] On the other hand, there is no report on the perilous effects of the dimer in the mammalian cells. Importantly, glutathione detoxifies NAPQI and thereby prevents DNA breakage in mammalian cells under normal conditions, rendering the use of NAPQI rather safe. In vitro studies have revealed that NAPQI also inhibits DNA gyrase and topoisomerase IV, which are the only topoisomerase II type enzymes present in bacteria.[18] This indicates that an ideal way of developing antimicrobial drug could be the inhibition of DNA gyrase by taking recourse to NAPQI either as a part of the drug or being produced inside bacterial cells from the drug in use. Hence, advantage of the second way in developing a new antimicrobial composite was chosen for subsequent studies.

3.2. Outline of the research work

1. A highly fluorescent composite of Ag NPs and PD was synthesized by reaction of pHA with $AgNO_3$. The formation of the composite was confirmed by UV-Vis spectroscopy, fluorescence spectroscopy, and TEM analysis.
2. The composite exhibited high antimicrobial activity against a wide range of bacterial (Gram-positive as well as Gram-negative) populations at relatively low concentrations of Ag which were nontoxic to mammalian cells.

3. Additionally, green fluorescent protein (GFP) expressing recombinant E. coli was used in order to elucidate the details of mechanism of antibacterial activity of the composite.
4. The TEM analysis revealed that the composite was strongly interacted with the bacterial cell was leading to the damage to it.
5. By probing the fluorescence of the GFP via fluorescence microscopy and fluorescence spectroscopy study the number of the viable bacteria after treatment with the composite was determined, indicating the potential eradication of the bacterial population.
6. Essentially, the results showed that the oxidative stress (ROS) generated by the nanocomposite, in addition to the perforation of the bacterial cell walls led to possible oxidation of the composite producing NAPQI, which might have subsequently inhibited DNA gyrase causing increased linearization of DNA.

3.3. Experimental section

3.3.1. Growth media and chemicals

Luria-bertani (LB), nutrient broth (NB), brain –heart infusion (BHI) and man rogosa and sharpe (MRS) bacterial growth medium were purchased from HiMedia, Mumbai, India. Paracetamol, silver nitrate ($AgNO_3$) and sodium borohydride ($NaBH_4$) were procured from Merck India, Ltd and were used as received. High-purity molecular biology grade chemicals and reagents used for agarose gel electrophoresis were obtained from Sigma-Aldrich chemical Pvt. Ltd., Kolkata, India and were used as received.

3.3.2. Bacterial strains

Ec. faecalis MTCC439 and *P. acidilactici* CFR K7 were grown in BHI and MRS media respectively at 37 ^{0}C. All other wild type bacterial strains used in the present investigation were cultured at the same physiological condition in NB medium.

3.3.3. GFP construct

The recombinant GFP-expressing *E. coli* cells (DH5α) were generated by cloning the GFP gene into an ampicillin-resistant pUC-derived plasmid vector as described previously [19] and was grown in LB medium.

3.3.4. Synthesis of the Ag NPs

The composite was synthesized by reaction of 1.0×10^{-4} M freshly prepared $AgNO_3$ with 2.0×10^{-2} M of pHA (pKa = 9.5) under alkaline condition (pH=10.0) and at 90 ^{o}C. In about 30 min of constant heating, the color of the solution turned yellow indicating the formation of Ag NPs in the medium. The pH of the medium was adjusted before adding to the bacterial medium.

3.3.5. Isolation of PD

In order to isolate the fluorescent PD, the nanocomposite was synthesized in large quantity by reacting 11.3 mg of $AgNO_3$ with 1.5 g of pHA using the procedure described above. The mixture was then subjected to centrifugation for 15 min at 26,000 rpm, 8 ^{0}C, washed with water followed by repeating the process twice and the supernatant was collected. The organic mixture was extracted from the aqueous solution (supernatant) to ethyl acetate (EtOAc) followed by reduction of volume to ca.5 mL in rotary vacuum evaporator. Then the PD was purified from this concentrated solution (in EtOAC) by column chromatography (using Silica gel 60-120 mesh). The R_f value of PD was found to be 0.51 (in 100% EtOAc).

3.3.6. Analytical measurements

UV-vis spectra were recorded by a Perkin-Elmer lambda 45 spectrophotometer (Perkin-Elmer, Fremont, CA). Fluorescence spectra were recorded by a Perkin-Elmer fluorescence spectrophotometer (model: LS 55).

3.3.6. Transmission electron microscopy (TEM)

The composite was analyzed using a high resolution transmission electron microscope (TEM; JEM 2100; Jeol, Peabody, MA, USA) operating at a maximum accelerating voltage of 200 KeV. Also, bacteria treated with the composite were analyzed using TEM. For this, 5 µL of each type of sample was drop-coated onto a carbon coated copper TEM grid followed by air drying. Selected area electron diffraction (SAED) and energy-dispersive X-ray (EDX) spectroscopy were pursued using the same instrument and on the same samples.

3.3.7. X-ray diffraction (XRD) studies

For XRD measurements, the as-synthesized sample was evaporated on microscope glass slide followed by recording of diffraction using a Bruker Advance D8 XRD machine (with Cu α source at 1.54 Å).

3.3.8. FTIR spectroscopy

The FTIR spectrum of isolated PD was recorded in a Perkin Elmer-Spectrum One FTIR spectrometer, in the range of 4000–400 cm^{-1}. The dried PD and other samples were mixed with KBr to make pellets required for the measurements.

3.3.9. NMR and mass spectroscopy

The ^{1}H NMR (400MHz, MeOD-d_4) and ^{13}C NMR (100 MHz, DMSO-d_6) spectra of the dried PD and other samples were measured using a Varian FT-400 (400 MHz) spectrometer with Me_4Si as internal standard and the chemical shifts were recorded on the scale of parts per million (ppm). Electro spray mass spectrometry (ESI-MS) of the composite was performed using a WATER LC-MS/MS- operation system of Q-Tof Premier^{TM} .

3.3.10. Fluorescence microscopy

The bactericidal activity of the composite on GFP- expressing E. coli cells was observed under a fluorescence microscope (Axioskop 2 MAT, Karl Zeiss). Individual aliquots of treated and untreated (30 µL) bacterial cultures were placed on microscope slides at different time points and air-dried before recording the images. A band pass (445-495 nm) filer was used in the excitation light source, while the observation filter had a long pass filter for wavelengths above 515 nm.

3.3.11. Oxidative stress measurement

Oxidative stress assay in bacterial cells was performed by using the established nitroblue tetrazolium (NBT) reduction method.[7] Bacterial suspensions (10^6 cfu/mL, of overnight grown culture) of both Gram positive and Gram negative ones were incubated in 0.1 mL of Hanks' balanced salt solution (HBSS), with composite (at minimum inhibitory concentration, MIC), Ag NPs, pHA and the dimer at 37 ^{0}C for 0, 30, 60, 90 and 120 min, respectively. Then 0.5 mL of 1.0 mg/mL NBT was added to each of the solutions and incubated for 30 min at 37 ^{0}C. The reaction was stopped by addition of 0.1 mL of 0.1 M

HCl, and the mixture was centrifuged at 5000 rpm for 10 min to separate cells from the supernatants. The bacterial pellets were treated with 0.3 mL of DMSO to extract the reduced NBT followed by addition of 0.7 mL of HBSS for dilution. Absorption of Formazan blue obtained from cells was measured at 575 nm using a UV-vis spectrophotometer.

3.3.12. Probing linearization of the plasmid DNA

The DNA cleavage and re-ligation reactions were monitored by using E. coli DNA gyrase enzyme (BioLabs). The cleavage re-ligation equilibrium was established by incubating 30 µL of topoisomerase I product with reaction mixture containing 35 mM Tris-HCL, 24 mM KCl, 4 mM $MgCl_2$, 2 mM DTT, 1.75 mM ATP, 5 mM Spermidine, 0.1 mg/ml BSA, and 6.5 % glycerol at 37 ^{0}C for 1 h. Further, to probe the details of mechanism of in vivo DNA linearization, the composite was treated with diluted H_2O_2 (7.5mM). The different concentrations of the oxidized product were then used to treat the isolated plasmid DNA (4 µg) in the presence of DNA gyrase. Gel electrophoresis was performed with the treated DNA along with control samples.

3.3.13. Cytotoxicity assay

Cytotoxicity of the nanocomposite to mammalian cells was addressed by pursuing viability studies of HT29 cells by dual staining with acridine orange and ethidium bromide in the presence of the composite at minimum inhibitory concentration (MIC) and minimum bactericidal concentrations (MBC). The cells were treated for 24 and 48 h prior to view under a fluorescence microscope. Live cells appeared green due to uptake of acridine orange and the dead cells stained red with ethidium bromide.

3.4. Results and discussion

3.4.1. Synthesis of the Ag NP-Paracetamol Dimer Composite

An alkaline solution of pHA and $AgNO_3$ turned yellow after heating at 90 ^{0}C for 30 min. UV-vis spectrum of the solution exhibited a peak at 409 nm, indicating the formation of Ag NPs (**Figure 3.1ai**). An additional peak occurring at 320 nm indicated the possible formation of a dimer of pHA[20-23] in the process (**Figure 3.1aii**). The **Figure 3.1b** represents TEM image of as prepared composite showing the formation of individual NPs in the process. The average particle size of the Ag NPs so formed was measured to be 4.0

± 0.5 nm (**Figure 3.1c**). The corresponding HRTEM images also recorded indicating the lattice fringes of Ag NPs (**Figure 3.2a**). The presence of Ag NPs was further confirmed by EDX spectroscopy and XRD analysis of the composite as depicted in **Figure 3.2b**. SAED patterns indicated the formation of polycrystalline NPs of Ag (**Figure 3.2c**). The XRD patterns of the composite consisted of three peaks occurring at 38.3^0, 44.4^0 and 64.5^0 corresponding to diffraction from (111), (200) and (220) planes respectively of Ag (0) (**Figure 3.2d**). Interestingly, when the aqueous solution of the composite was excited at 320 nm, a blue emission at 435 nm was observed (**Figure 3.1d**). This could be attributed to the characteristic emission of the PD.[20-23]

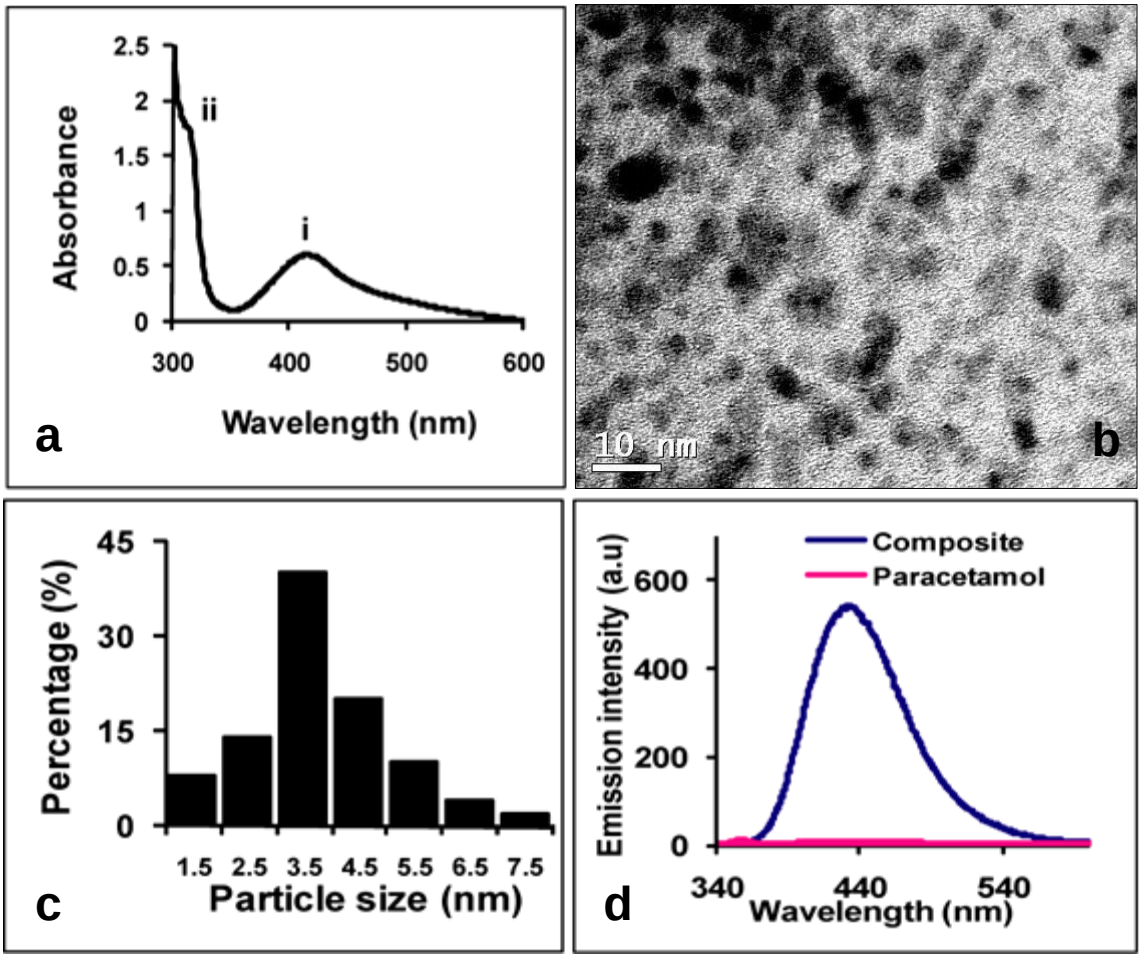

Figure 3.1 (**a**) Absorption spectrum of the solution containing the product of reaction involving $AgNO_3$ and pHA under alkaline conditions. (**b**) TEM image of the composite. (**c**) Particle size distribution as calculated from the TEM image. (**d**) Fluorescence emission spectrum of the solution with excitation wavelength being fixed at 320 nm.

The formation of PD was further confirmed by FTIR, ^{1}H NMR, ^{13}C NMR spectroscopy and ESI (-) mass spectrometry (Appendix **Figure A 3.1 and 3.2**). The peaks in the FTIR spectrum (**Figure 3.3a**) occurring at 3431 cm^{-1}, 3337 cm^{-1} and 1662 cm^{-1} correspond to –OH, –NH and C=O (-$NHCOCH_3$) stretching vibration of PD respectively. **Figure A3.1a** and **Figure A3.1b** represent the ^{1}H NMR (400 MHz, MeOD-d_4) and ^{13}C NMR (100 MHz, DMSO-d_6) spectra of purified PD respectively. The peaks at δ = 7.42-7.36 (m, 4H), 6.89 (d, J=8.8 Hz, 2H), 2.10 (s, 6H, 2×COCH3) in ^{1}H NMR spectrum and peaks at δ=169.23, 151.04, 131.20, 126.18, 123.53, 120.72, 116.15, 24.10 in ^{13}C NMR spectrum showed that the dimer was formed as a result of covalent bond formation between two ortho carbon atoms (with respect to OH group) of two pHA molecules .[24]

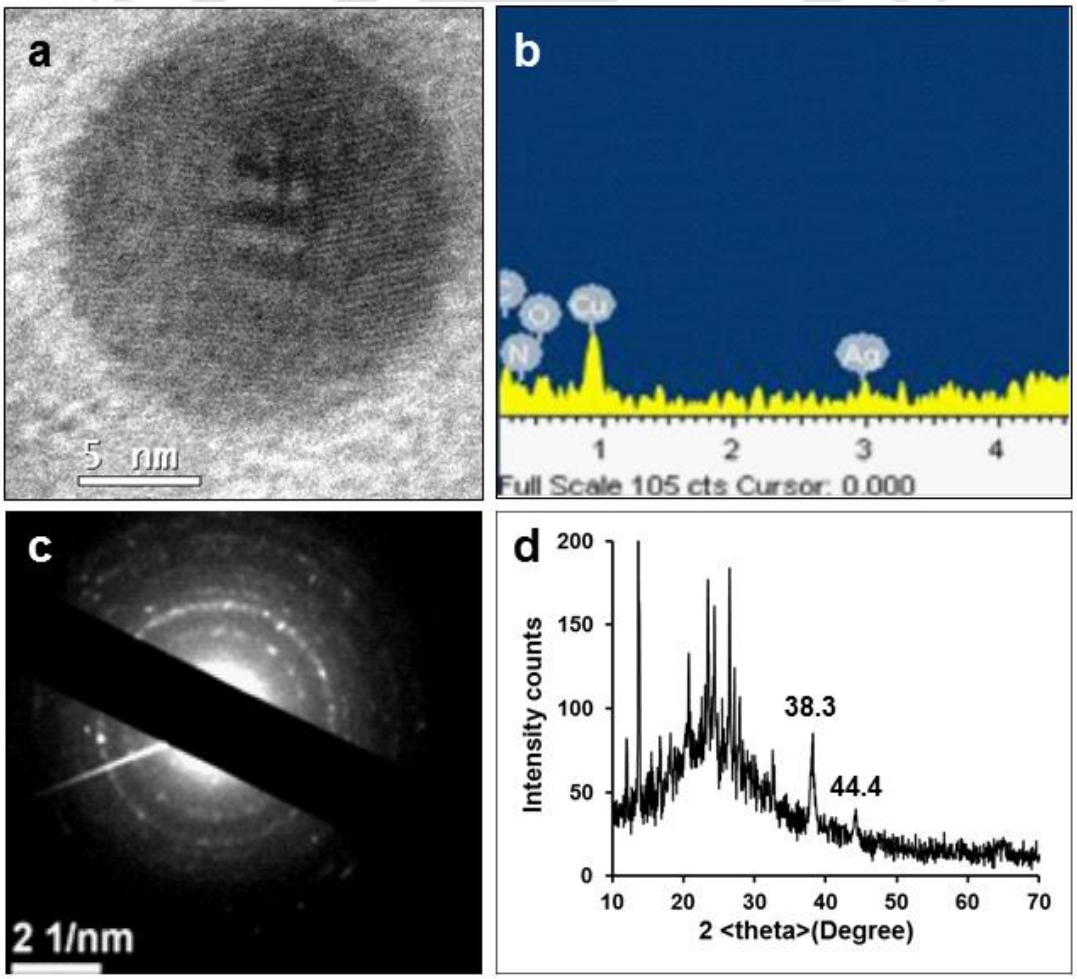

Figure 3.2 (**a**) HRTEM image of the Ag NPs (**b**) EDX spectrum of the composite showing the presence of Ag (0). (**c**) SAED of the Ag NP (**d**) Powder X- ray diffraction of the composite.

The Ag NPs synthesized in the present study were separated by centrifugation at 15,000 rpm and subsequently redispersed in water in order to investigate whether PD was attached to the NPs. The fluorescence emission **(Figure 3.3a)** as well as the UV-vis spectrum of the redispersed solution remained unchanged indicating that PD was attached to Ag NPs in the composite. The product yielded an ESI (-) mass spectrum with a prominent peak of deprotonated PD at 299 $(M-H)^-$ along with molecular peak at 300 (M) and peaks of corresponding fragmented ions of PD.[25] The peak assigned to the unreacted deprotonated pHA at 150 $(m-H)^-$ was also present **(Figure 3.3b)**.Thus it can be concluded that the reaction of pHA with $AgNO_3$ under the present experimental condition resulted in a composite primarily consisting of small Ag NPs and PD along with the presence of pHA. It may be mentioned here that the composite was observed to be stable for weeks as probed by UV-vis as well as fluorescence spectroscopy.

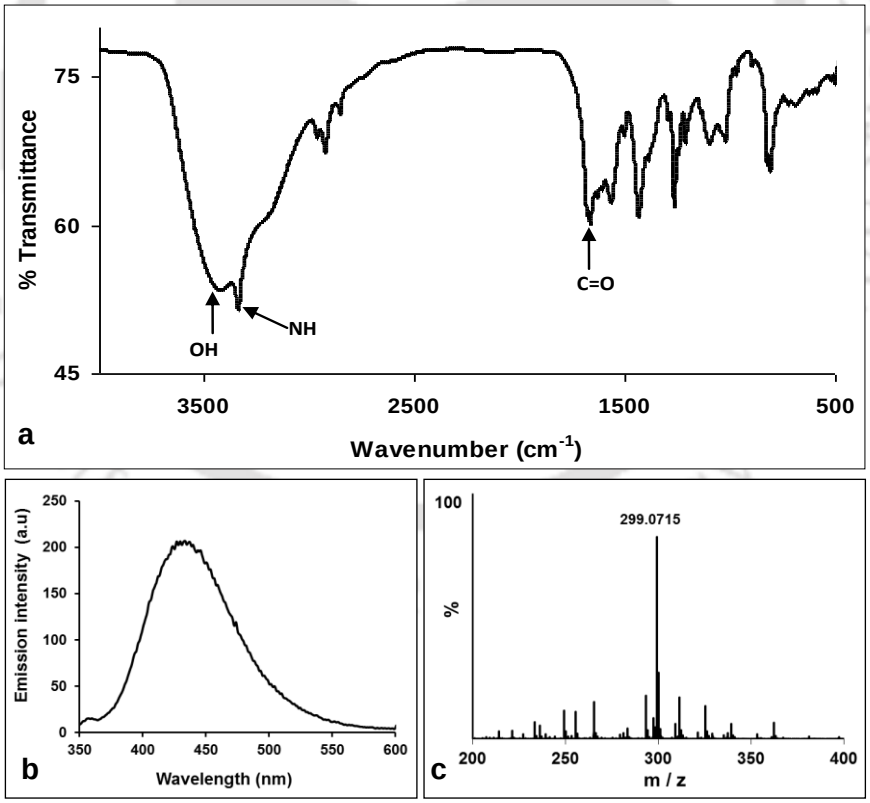

Figure 3.3 (**a**) FTIR spectrum of the PD, (**b**) Emission spectrum of the composite after centrifugation, showing the characteristics emission peak of PD at 435 nm. (**c**) Mass spectrum of the composite.

3.4.2. Antibacterial activity

The time-dependent growth of GFP expressing *E. coli* bacteria, in the presence of the composite and other controls were followed by measuring optical density (OD) at 595 nm in order to study the antibacterial efficacy of the composite. As is evident from Figure 2 bacterial growth was arrested in the presence of the composite. The minimum concentration of the composite at which GFP expressing E. coli bacterial growth in LB medium containing 100 µg/mL of ampicillin was measurably inhibited (i.e. no turbidity was observed) after 12 h incubation at 37 ^{0}C was taken to be the minimum inhibitory concentration (MIC). The cultures which were not turbid were reinoculated in the same physiological conditions into fresh media. The minimum bactericidal concentration (MBC) of the composite was taken to be the minimum concentration of composite that prevented growth of the bacterial cells following reinoculation for 12 h. The MIC of the composite was found to contain 2.87 ± 0.50 µg/mL Ag NPs and 0.37 ± 0.07 mg/mL pHA. On the other hand MBC was found to consist of 3.37 ± 0.50 µg/mL Ag NPs and 0.44 ± 0.07 mg/mL pHA. It must be mentioned here that the pHA concentration referred herein corresponds to the amount of compound used in the original reaction vessel and thus refers to both the dimer and the monomer. Interestingly, the concentration of Ag NP required here (MBC) was an order of magnitude less than that required if only Ag NPs were used. The test for antibacterial activity was further extended to other Gram negative (E. Coli MTCC433, Pseudomonas aeruginosa MTCC2488, Enterobacter aerogenes MTCC2822) as well as Gram positive (Bacillus cereus MTCC1305, Pediococcus acidilactici CFR K7, Enterococcus faecalis MTCC439) bacteria. The corresponding MIC and MBC values **(Table 3.1)** revealed the superior bactericidal activity of the composite in comparison to Ag NPs, pHA at their respective individual concentrations present in the composite. In addition, when pure PD, isolated from the composite by column chromatography, was used as control for the experiments, it was revealed that dimer alone was not effective in the killing of the bacteria, results of which are shown in **Figure 3.4**.

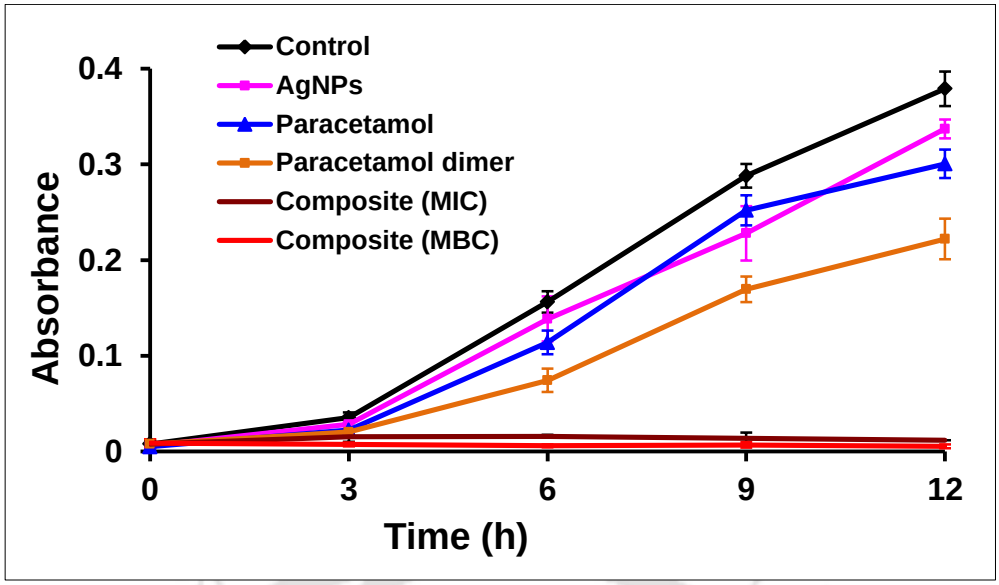

Figure 3.4 The growth curve of GFP expressing E. coli bacteria in the presence of the composite and other agents as mentioned in the legends. Data are represented as Mean ± S.D. of three individual experiments.

A critical issue to be addressed, with respect to the development of new antimicrobial agent, is the cytotoxicity of the new compound to mammalian cells. In the present case, this was pursued by viability assay of HT29 cells in the presence of the composite (at MIC and MBC of GFP expressing recombinant *E. coli*) using AO/EB dual staining. The results indicated that the composite was not cytotoxic to the cells at both MIC and MBC values (refer to Appendix, **Figure A3.2**). Thus, it can be inferred that composite exhibited strong antimicrobial properties, and at the same time being non-cytotoxic to mammalian cells.

Table 3.1 Antibacterial efficacy of the composite against Gram-positive and Gram- negative bacteria. Data are represented as Mean ± S.D. of three individual experiments. The concentration of Ag NPs means that Ag presents in the composite. Further the concentration of pHA refer to here was the concentration of pHA plus PD produced in the reaction medium, expressed in terms of initial pHA concentration (used for reaction).

Bacteria	**MIC**		**MBC**	
Gram Negative	AgNPs **(µg/ml)**	pHA **(mg/ml)**	AgNPs **(µg/ml)**	pHA **(mg/ml)**
E. coli MTCC433	2.95±0.50	0.39±0.07	3.78±0.50	0.50±0.07
Ps. aeruginosa MTCC2488	3.37±0.70	0.45±0.09	3.78±0.80	0.50±0.11
En. aerogenes MTCC2822	3.37±0.60	0.45±0.08	4.16±0.50	0.55±0.07
GFP- *E. coli* (recombinant)	2.87±0.50	0.37±0.07	3.37±0.50	0.44±0.07
Gram Positive				
B. cereus MTCC1305	2.51±0.91	0.33±0.12	2.95±0.80	0.39±0.10
En. faecalis MTCC439	2.95±0.70	0.39±0.09	3.37±0.70	0.45±0.09
P. acidilactici CFR K7	2.51±0.60	0.33±0.08	2.95±0.91	0.39±0.10

3.4.3. Understanding the bactericidal action

A prerequisite for the development of a new drug or antimicrobial agent is to understand the mechanism of its operation. This would not only reveal the details of its mode of action but also help in developing newer and improved therapeutic materials for increased efficiency at minimum cytotoxic and environmental risks. Fluorescence spectroscopic experiments with GFP expressing *E. coli* bacteria indicated that there was an increase in emission intensity in case of control (untreated), and in the presence of Ag NPs or pHA only (of the same concentration as in the composite) due to multiplication of bacteria with time (refer to Appendix, **Figure A3.3**). However, there was no increase in fluorescence with time in case of treated sample (at MIC) indicating no bacterial growth. The observed

emission intensity in this case was due to bacterial cells used as inoculum. The interaction with composite might have caused leaking of GFP from these cells causing the total emission intensity to remain unchanged with time. This was further confirmed by the fluorescence microscopic observation **(Figure 3.4)** which revealed that the bacteria in the media were obliterated with time in the presence of the composite (at MIC), while there was substantial increase in their number in the presence of pHA or Ag NPs only.

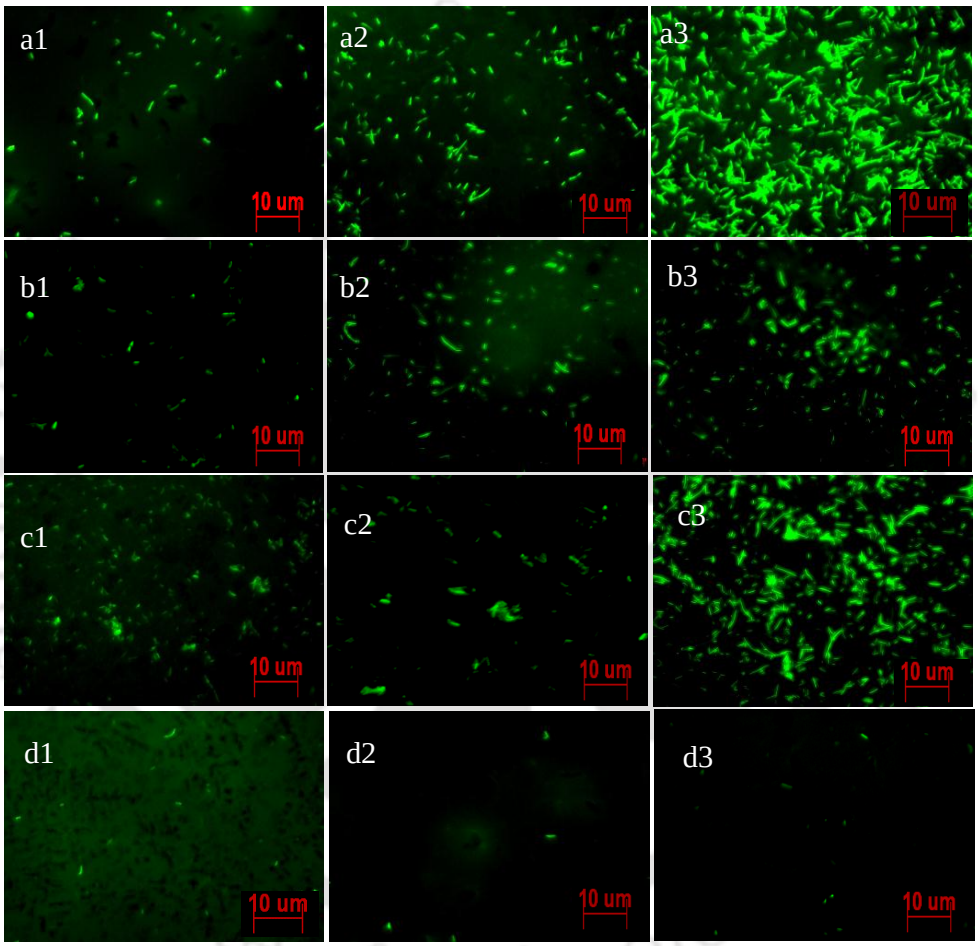

Figure 3.4 Fluorescence microscopic images of GFP expressing E.coli grown under different experimental conditions. Series (**a**), (**b**), (**c**) and (**d**) refer to control, Ag NPs, pHA and the composite (at MIC) treated samples respectively; while 1, 2, 3 refer to the samples observed at 3 h, 6 h and 12 h of growth respectively.

TEM measurements of the cells incubated with the composite for different times indicated that the NPs were attached to the bacteria before damaging the cells. In Figure 3, a healthy cell (at incomplete cell division state) could be observed after 1 h in the presence of growth medium only **(Figure 3.4i)**. On the other hand, treatment with the composite at MIC led to attachment of the NPs to the cells by 30 min **(Figure 3.4ii)**; while by 1 h the cells were burst-open **(Figure 3.4iii and iv)**. Essentially, the results indicated that the composite attached efficiently to the bacterium and the cell disintegrated with time.

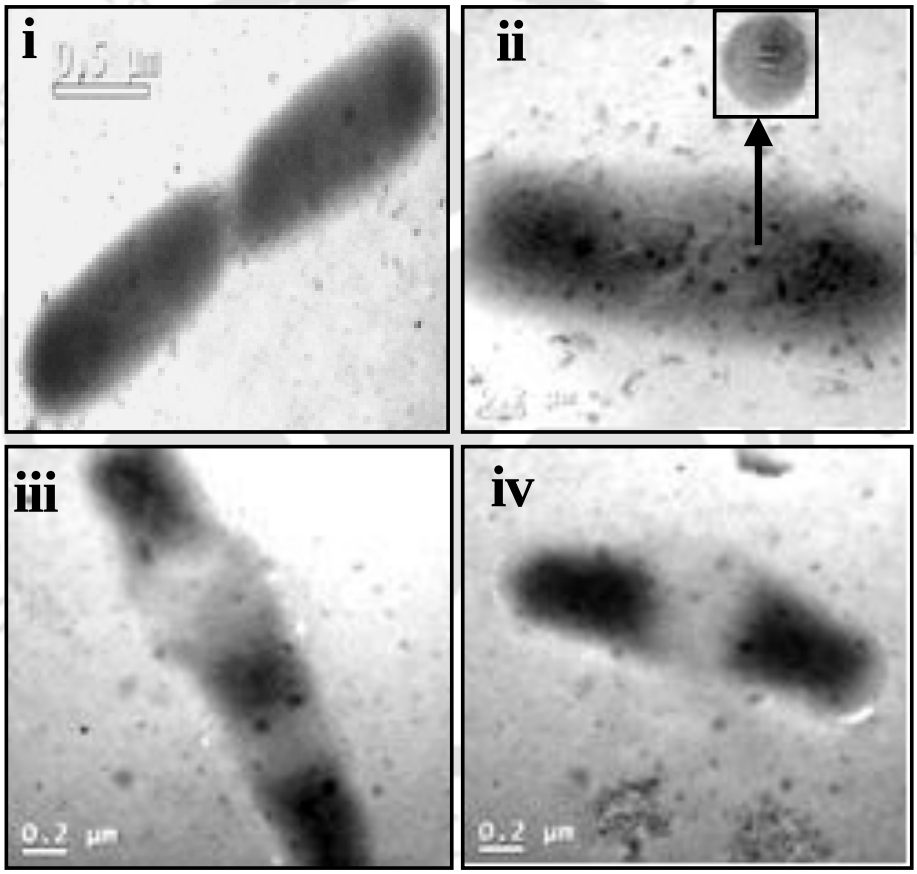

Figure 3.4 TEM micrographs showing interactions between Ag NPs and the bacterium with deposits of NPs being seen on cell surface. **(**i) Untreated bacterial cells (in dividing state) after 1 h of growth, (ii) composite treated cells after 30 min and after 1 h (iii and iv) of treatment.

3.4.4. Linearization of plasmid DNA

In order to probe the effect of the composite at the cellular level, bacterial cells were incubated with the suitable amount of the composite (below the MIC) for 3 h and 6 h respectively, followed by extraction of plasmid DNA and the running of agarose gel electrophoresis. Linear form of plasmid DNA appeared from the composite treated bacterial cells at both the time points (**Figure 3.5**). It may be mentioned here that the formation of linear plasmid DNA was confirmed by comparing its analogous migration profile with the single-digested (performed by using restriction endonuclease) linear form of the same plasmid DNA (refer to Electronic Supplementary Information, Figure S10).

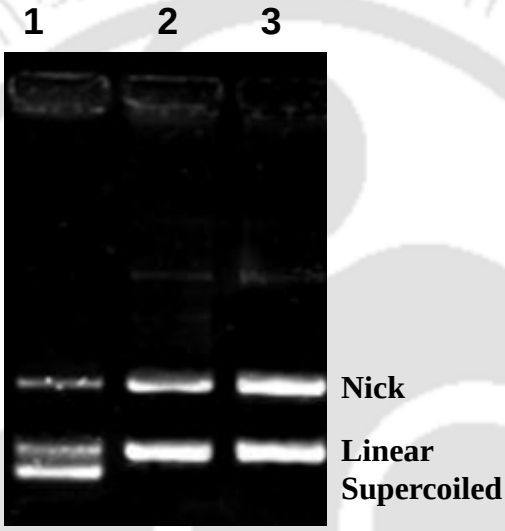

Figure 3.5 In-vivo plasmid DNA linearization experiment. Lane 1 is for control DNA; Lane 2 and 3 are for DNA isolated from bacterial cells treated with the composite for 3 h and 6 h respectively.

It is known that DNA gyrase (i.e. topoisomerase II) removes the knots and tangles of DNA during the DNA replication and transcription.[17] DNA gyrase first linearizes the DNA by breaking its both strands, captures another segment of the same DNA molecule and then reseals it after passing through the double strand break. Thus, the presence of DNA gyrase inhibitor(s) that blocks the sealing mechanism of the DNA strands leads to DNA linearization.[27-29] Therefore; it was assumed from the DNA-linearization results that the composite could be an inhibitor of DNA gyrase. To investigate the role of the composite as a DNA gyrase inhibitor, linearization of plasmid DNA in vitro was studied. This was pursued by incubating plasmid DNA, isolated from non-treated bacteria, with different concentrations of the composite (0.45 µg pHA and 3.45 ng Ag NPs, 0.75 µg

pHA and 5.75 ng Ag NPs, 1.05 µg pHA and 8.05 ng Ag NPs respectively in 20 µL reaction mixtures in the presence of DNA gyrase. It must again be mentioned here that the pHA concentration mentioned here corresponds to the amount of compound used in the original reaction mixture and thus refers to both the dimer and the monomer concentration together in the units of concentration of pHA. Interestingly, gel electrophoresis results revealed that there was no linearization of the plasmid DNA in the presence of the composite alone (**Figure 3.6**). This indicated that the composite by itself was not responsible for linearization of the DNA, and hence it is not a gyrase inhibitor in its native (monomer/dimer of pHA and Ag NPs) form.

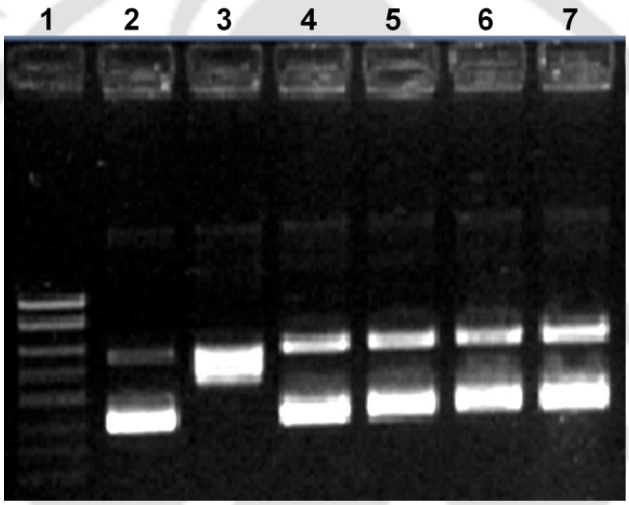

Figure 3.6 In-vitro plasmid DNA linearization experiment was performed by incubating the plasmid DNA with different concentration of composite in presence of DNA gyrase. Lane 1 is the marker (M), Lanes 2 is the control, lane 3 is for topoisomerase I treated sample, lane 4 DNA gyrase treated sample, Lane: 5 -7 is for DNA gyrase treated sample with three different concentration of composite containing (0.45 µg pHA and 3.45 ng Ag NPs), (0.75 µg pHA and 5.75ng Ag NPs) and (1.05 µg pHA and 8.0 ng Ag NPs) respectively.

3.4.5. Oxidative stress

The differential response of the composite in linearizing plasmid DNA in vivo and in vitro could be due to the difference in the physiological environment, especially with respect to the oxidative stress. The induction of oxidative stress in microbial as well as mammalian cells, as a consequence of increase intracellular ROS production, by engineered nanomaterials has been reported extensively [5,7, 30]. On the other hand, the cellular oxidative stress might lead to the oxidation of PD producing NAPQI which is, as discussed earlier, a potent inhibitor of DNA gyrase. To verify this hypothesis for the linearization of plasmid DNA in the present study, the cellular oxidative stress in the composite treated bacteria was further investigated using the standard NBT assay. The results are shown in **Figure 3.7**. As is clear from the figure, high levels of ROS were generated in the presence of the composite than that in the presence of either of Ag NPs, pHA or the dimer. This provides a clue that the ROS generated in the cells by the composite might have been directly or indirectly responsible for the observed linearization of DNA.

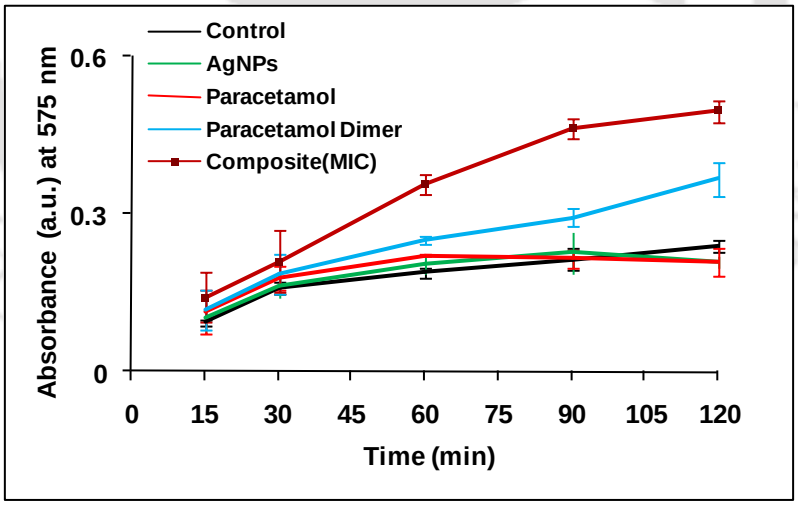

Figure 3.7 Effect of the composite and its individual components on the intracellular ROS generation of GFP expressing E. coli bacteria. Data are represented as Mean ± S.D. of three individual experiments.

3.4.6. *In-vitro* plasmid DNA linearization

The proposed hypothesis of DNA linearization by the composite in the present study was further validated by mimicking the "oxidative environment" in vitro. The composite was first treated with diluted H_2O_2 (7.5 mM), followed by addition of different concentrations of the so-treated solution (reaction solution) to isolated plasmid DNA in the presence of DNA gyrase. Surprisingly, DNA linearization was observed with increased concentration of the composite (**Figure 3.8a**). The band intensity of linear DNA was about ten times (**Figure 3.8b**) more in case of the highest concentration of the composite (containing 1.05 µg pHA and 8.05 ng Ag NPs) as compared to lower concentrations. The concentration of pHA referred here is the combined concentration of pHA and PD as mentioned before. This is interesting as the same amount of composite, without H_2O_2-treatment, could not linearize the plasmid DNA in presence of DNA gyrase (**Figure 3.6**). Furthermore, the bright blue fluorescence of PD present in the composite can be seen clearly in the agarose gel (**Figure 3.8a**) when visualized under UV illumination[31]. Additionally, careful observation of the agarose gel (**Figure 3.8a**) demonstrates the presence of NAPQI fluorescence [16] below the PD fluorescence (at the bottom of the gel) in the lanes corresponding to H_2O_2-treated composite. The formation of NAPQI upon treatment with H_2O_2 was further supported by the ESI (-) mass spectroscopy of H_2O_2-treated PD (refer to appendix, **Figure A3.4**) that revealed a prominent peak of tautomeric NAPQI. It may be emphasized here that previous experiments involving the study of the effect of Ag NPs on the recombinant GFP-expressing E. coli bacteria revealed that the NPs did not cause any linearization of DNA.[19] Also, there was no observable DNA damage nor any abnormality was present in the DNA migration profile. This means the presence of only Ag NPs might not have affected the DNA gyrase of E. coli. Thus even if the presence of Ag NPs increased the production of ROS in the bacterial cells it might not have caused inhibition of activity of DNA gyrase. On the other hand, it is plausible that ROS led to the oxidation of the composite generating NAPQI, which is a specific DNA gyrase inhibitor. NAPQI inhibits DNA sealing function of DNA gyrase causing DNA linearization. Further, our observations with experiments in vitro also suggested that the presence of the composite alone did not lead to linearization of DNA. On the other hand, it was found that the composite in the presence of H_2O_2 could produce NAPQI. Hence it can be concluded from the available evidences herein that the composite induced oxidative stress to the cells. The ROS thus generated might have produced NAPQI from the composite which acted as a DNA gyrase inhibitor.

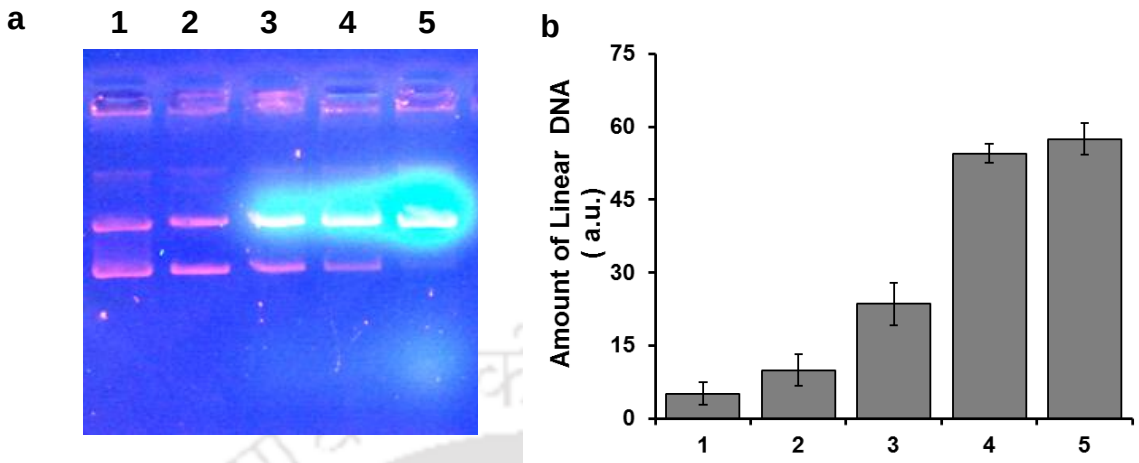

Figure 3.8 (**a**) Plasmid DNA cleavage reaction was carried out with E.coli DNA gyarse in the presence of various concentration of oxidized product of the composite. Lane 1 control DNA**,** Lane 2 DNA gyrase alone, Lanes 3-5 DNA gyrase incubated with different concentrations of oxidized product of the composite (0.45 µg pHA and 3.45 ng Ag NPs), (0.75 µg pHA and 5.75 ng Ag NPs) and (1.05 µg pHA and 8.05 ng Ag NPs) in 20 µL reaction volume respectively. (**b**) Bar graph was drawn based on relative band intensities which were determined by image J software.

3.4.7. Proposed mechanism of bactericidal action

Based on the results presented above, an overall picture of the activity of the composite on the bacterial cells is depicted schematically in Figure 7. Reaction of Ag^{+} with pHA under alkaline condition produced the fluorescent dimer (PD) which stabilized the Ag NPs produced concurrently. Also, unreacted pHA was present in the composite as an additional stabilizer. The composite was effective in killing a broad range of bacteria involving both the NPs and the dimer, each one possibly playing a role complementary to the other. As far as the mechanism of action is concerned, it is proposed that the composite was attached to the bacterial cell wall leading to possible perforation of the wall. Earlier studies also indicated that bacterial cell wall gets perforated in the presence of Ag NPs.[25] The composite then possibly entered the bacterial cell and raised the intracellular ROS level. Previous reports have elucidated that Ag NPs participate in elevation of oxidative stress along with membrane damage by releasing Ag^{+} ions.[7, 26, 32, 33]

Hence, Ag NPs in conjunction with the dimer (PD), in the present study, possibly induced oxidative stress in the bacterial cells. The oxidative species such as superoxide anion (O_2^-), hydrogen peroxide (H_2O_2), and the highly reactive hydroxyl radicals (·OH), which might have been generated in the cells, converted the dimer to NAPQI which, in turn, inhibited DNA gyrase enzyme leading to DNA linearization. *In vitro* experiments with the H_2O_2-oxidized composite leading to linearization of DNA further supported this proposal.

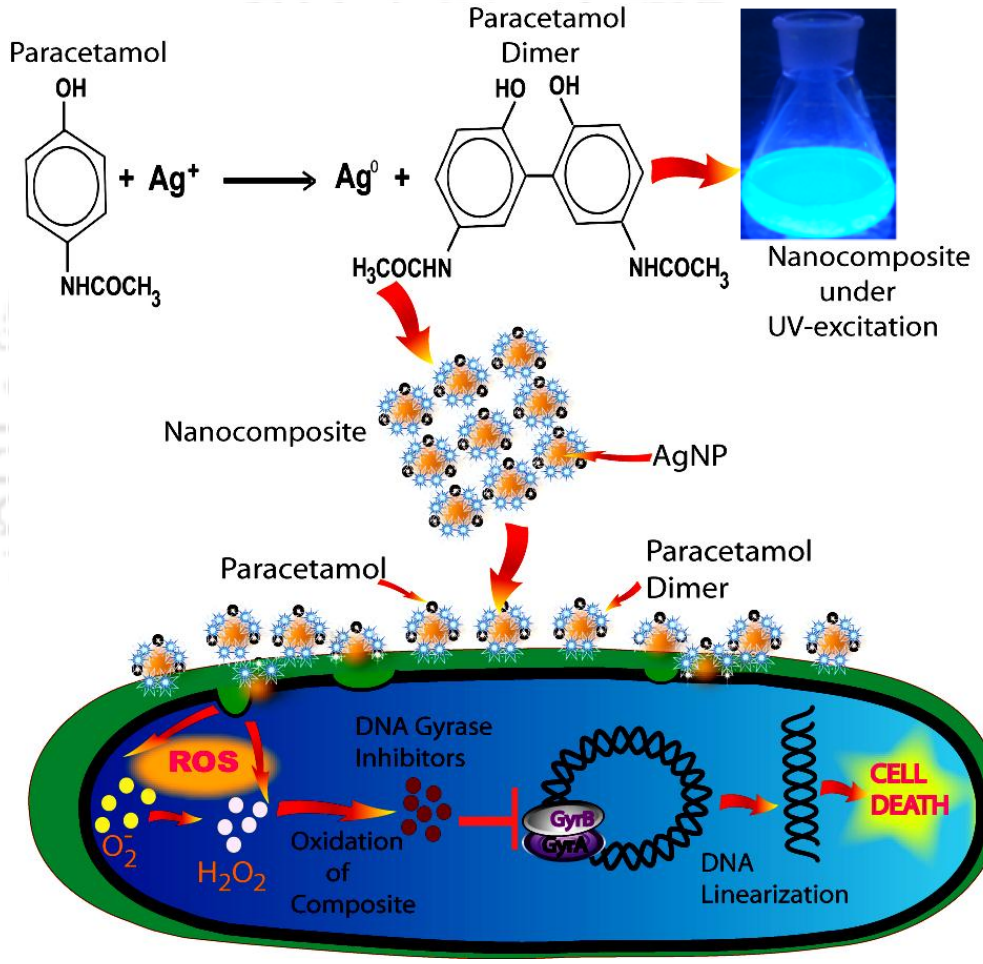

Figure 3.9 A schematic representation of mechanism of antimicrobial activity of the nanocomposite, which was generated by the reaction of $AgNO_3$ with paracetamol.

3.5. Conclusion

In brief, a new composite consisting of Ag NPs and PD (along with the presence of pHA) has been synthesized. The composite is fluorescent and highly antimicrobial against a wide range of Gram positive and Gram negative bacteria, at low concentrations of Ag NPs. The composite contributed to the increased ROS production subsequent to possible cell perforation by Ag NPs. The ROS provided the oxidizing environment for the generation of DNA gyrase – inhibitor NAPQI from PD which might have been responsible for DNA linearization. The antimicrobial dose used here was also non-toxic towards animal cells (HT 29) and thus provides an eminent opportunity of using this composite without unduly compromising the health of the patient. This is, to the best of my knowledge, the first report where an antimicrobial nanocomposite has been demonstrated to cause DNA-linearization that has important consequences in the development of antimicrobial drugs. That the antimicrobial action of the composite involved the conversion of PD to DNA gyrase –inhibitor NAPQI, triggered by enhanced ROS generation, is reminiscent of a "prodrug/sucide gene therapy" used for cancer treatment.

3.6. References

1. F. C. Tenover, Am. J. Infect. Control, 2006, **34**, S3–S10.
2. J. Josephson, Environ. Sci. Technol., 2006, **40**, 6531–6534.
3. M. Rai, A. Yadav, A. Gade, Biotech. Adv., 2009, **27**, 76-83.
4. K. K. Kumarasamy, M. A. Toleman, T. R. Walsh, J. Bagaria, F. Butt, R. Balakrishnan, U. Chaudhary, M. Doumith, C. G. Giske, S. Irfan, P. Krishnan, A. V. Kumar, S. Maharjan, S. Mushtaq, T. Noorie, D. L. Paterson, A. Pearson, C. Perry, R. Pike, B. Rao, U. Ray, J. B. Sarma, M. Sharma, E. Sheridan, M. A. Thirunarayan, J. Turton, S. Upadhyay, M. Warner, W. Welfare, D. M. Livermore, and N. Woodford, Lancet Infect. Dis., 2010, **10**, 597-602.
5. P. V. Asharani, G. L. K. Mun, M.P. Hande, S. Valiyaveettil, ACS Nano, 2009, **3**, 279-290.
6. P. Sanpui, A. Murugados, D. P. V. Prasad, S. S. Ghosh, A. Chattopadhyay, Int. J. Food Microbiol., 2008, **124**,142-146.
7. M. Banerjee, S. Mallick, A. Paul, A. Chattopadhyay, S. S. Ghosh, Langmuir, 2010, **26**, 5901-5908.
8. J.R. Morones, J.L. Elechiguerra, A.Camacho, K. Holt, J.B. Kouri, J.T. Ramírez, M.J. Yacaman, **Nanotechnology, 2005, 16, 2346-2353.**
9. I. Sondi, B. Salopek-Sondi, J. Colloid Interface Sci., 2004, **275**, 177–182.
10. B.L. Coppel, W.M.Greimner, P.L. Iversen, Toxicol. Appl. Pharmacol., 1995, **133**, 53-63.
11. L. F. Prescott, Am. J. Ther., 2000, **7**, 143-147.
12. U. S. Ruepp, P. R. Tonge, J. Shaw, N. Wallis, F. Pognan, J. Toxicol. Sci., 2002, **65**, 135-150.
13. E. Dybing, J. A. Holme, W. P. Gordon, E. J. Soderlund, D. C. Dahlin, S. D. Nelson, Mutat. Res., 1984, **138**, 21-32.
14. J. D. Gibson, N. R. Pumford, V. M. Samokyszyn, J. A. Hinson, Chem. Res.Toxicol., 1996, **9**, 580-585.
15. K. J. Reszka, B.A. Wagner, C.P. Burns, B.E. Britigan, Arch. Biochem. Biophys., 2004, **427**, 16–29.
16. O. Mirochnitchenko, M. Weisbrot-Lefkowitz, K. Reuhl, L. Chen, C. Yang, M. Inouye , J. Biol. Chem., 1999, **274**, 10349-10355.

17. M. Chatterji, S. Unniraman, S. Mahadevan, V. J. Nagaraja, Antimicrob. Chemother., 2001, **48**, 479-485.
18. M. Couturier, M. E. Bahassi, L. V. Melderen, Trends. Microbiol., 1998, **6**, 269-275.
19. S. K. Gogoi, P. Gopinath, A. Paul, A. Ramesh, S.S. Ghosh, A. Chattopadhyay, Langmuir, 2006, **22**, 9322-9328.
20. W. Clegg, J. S. Teat, K.V.R Prasad, R.I. Ristic, S.J. Teat, D.B. Sheen, E.A. Shephered, J.N. Sherwood, R.M. Vrcelj, Acta Cryst., 1998, **C54**, 1881-1882.
21. J.L. Vilchez, R. Blanc, R. Avidad, A. Navalon, J. Pharm. Biomed. Anal., 1995 , **13**, 1119 -1125
22. D. C. Hiremath, C. V. Hiremath, S. T. Nandibewoor, E-J. Chem., 2006, **3**, 13-24,
23. Q.L. Feng, J. Wu, G.Q. Chen, F.Z. Cui, T.M. Kim, J.O. Kim, J. Biomed. Mater. Res., 2000, **52**, 662–668.
24. J. V. Steveninck, F. Jn. Koster, M. A. R. T. Dubbman, Biochem. J., 1989, **259**, 633-637.
25. D.W. Potter, D.W. Miller, J. A. Hinson, J. Biol. Chem., 1985, **260**, 12174-12180.
26. K. Darlica, X. Zhao, Microbiol. Mol. Biol. Rev., 1997, **61**, 377–392.
27. R. J. Reece and A. Maxwell, Crit. Rev. Biochem. Mol. Biol., 1991, **26,** 335-375.
28. R. J. Lewis, F. T. F. Tsai, D. B. Wigley, Bioessays, 1996, **18**, 661-671.
29. S. B. Farr, T. Kogoma, Microbiol. Rev., 1991, **55**, 561-585.
30. P. Sanpui, A. Chattopadhyay, S. S. Ghosh, ACS Appl. Mater. Interfaces, 2011, **3**, 218-28.
31. The electrophoresis migration pattern proved that the composite was negatively charged in the TAE-running buffer (pH=7.2) and did not attach with DNA; on the contrary it was lagging behind the DNA, even though the PD has low molecular weight compared to DNA. The observed migration profile could be due to non-covalent interaction of the dimer with the Ag NPs, which resulted in apparent higher effective mass than plasmid DNA.
32. O. Choi, T. Cleuenger, B. Deng, R. Surampalli, L. Ross, Z. Hu, Water Res., 2008, **42,** 3066-3074.
33. T. Amimoto, T. Matsura, S.Y. Koyama, T. Nakanishi, K. Yamada, G. Kajiyama, Free Radic. Biol. Med., 1995, **19**, 169-176.

Chapter 4

Fluorescent Ag nanoclusters Loaded FA-CS NPs for Targeted Drug Delivery into the Cancer cells

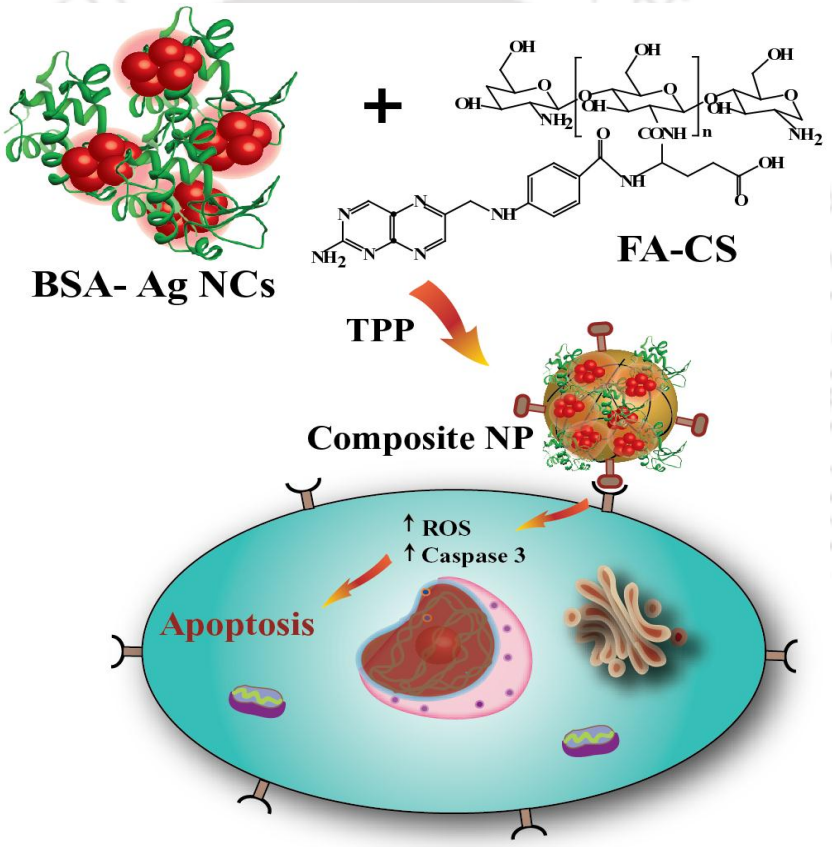

Chapter 4:

Fluorescent Ag nanoclusters Loaded FA-CS NPs for Targeted Drug Delivery into the Cancer cells

4.1. Introduction

The latest developments in medical science is still stranded to prevail the challenge of complete cure of cancers along with poor survival outcome of conventional and existing therapies.[1-3]Moreover, most of the frontline chemotherapeutic drugs have various limitations such as non-specificity,[4] poor water solubility,[5] and shorter blood circulation half-life[6] which demands higher doses and frequencies of the drug . To address these coexisting issues, nanotechnology offers huge promises, in order to develop new therapeutic modalities and delivery of the existing therapeutics by using suitable nanocarriers.[7-8] The Ag NPs and its composite(s) gain considerable attentions as novel cancer therapeutics as it causes programmed cell death (i.e., apoptosis) into the mammalian cells.[9-11] Recent studies have manifested that it destabilizes the integrity of the plasma membrane and induces reactive oxygen species (ROS), causing mitochondria dependent apoptosis.[9] Eventually, the higher dose of the Ag NPs is cytotoxic towards the normal cells. This inherent demerit limits its direct use as cancer therapeutic agents because of the unavoidable association of cancer cells with normal cells. Various reports from several laboratories including us have demonstrated that nanocarrier mediated delivery of Ag NPs could reduce the effective concentration of silver[10, 12-13].The nano carrier offers likelihood of size explicit 'passive targeting' and/or cell specific ligand-receptors interaction mediated 'active targeting' - which improves the bioavailability of the therapeutics at the 'programmed' sites and as a consequence lower the effective concentration of drug. Active targeting gains edge over the passive targeting due to its high level of selectivity and specificity.[14-15] Generally, cancer cells over expresses the receptors for growth factors such as glucose and vitamins (e.g. folic acid) to promote its growth and differentiation.[13] Thus, by targeting this specific ligand-receptors interaction one could easily deliver the Ag NPs into predetermined sites. Another aspect is the size of the Ag NPs, smaller the size better is the activity of apoptosis mediated cell death. For instance, Ag NPs particularly size less than 10 nm were always found to have enhanced

activities than its bigger counterparts.[16-17] In this pursuit, the cytotoxic effect of 'few atoms' silver nanoparticles size less than 2 nm, termed as silver nanoclusters, offers huge promises.[18] Owing to its critical size, metal nanoclusters do not support the surface plasmon resonance (SPR) which is a general signature of the metal NPs. On the other hand, the continuous energy band of the metal clusters discretise, hence exhibits bright fluorescence emission.[19] Apart from this, it possesses the large Stokes-shifted emission and high photostability which is the inherent limitation of organic fluorophores and thus offers the advantages of using it as multi-coloured dye for *in vivo* imaging.[20-21]

4.2. Outline of the research work

1. Florescent silver nanoclusters (Ag NCs) was synthesized by using bovine serum albumin (BSA) which was further converted into targeted composite NPs by using folic acid (FA) conjugated chitosan.
2. The formation of the Ag NCs and the composite NPs were validated by TEM, fluorescence spectroscopy and UV-Vis spectroscopy.
3. Two different cancer cells lines HeLa which over expresses receptors for folic acid and A 549 down regulates its expression took as model to study the differential uptakes of folic acid conjugated composite NPs.
4. To facilitate receptor-mediated endocytosis these fluorescent composite NPs were employed to deliver - paracetamol dimer (PD) -to the cancer cells to study the synergistic effect of Ag NCs and the PD.
5. Recently, our group has reported the synthesis of nano composites of paracetamol dimer (PD) by the reaction of silver as well as gold salt with paracetamol which is a commonly used anti pyretic and analgesic agent.
6. Interests were involved to explore the anti-cancer activity of the PD as there are no reports available till date on adversary activity of PD towards mammalian cells, except the plausibility of the non-covalent interaction with macrophage migration inhibitory factor (MIF).
7. These fluorescent composite NPs (Ag NCs- FA-CS NPs) were employed to deliver the PD into HeLa cells (human cervical carcinoma) and A549 cells with the anticipation that PD may convert into NAPQI-potential gyrase inhibitors in-combination with Ag NCs to find out the synergistic effect in cancer therapy.
8. Details mode of cell death was illustrated by performing various biochemical assays.

4.3. Materials and Methods

4.3.1. Chemicals

Paracetamol, silver nitrate ($AgNO_3$) and sodium borohydride ($NaBH_4$) were purchased from Merck India, Ltd. The 1-(3-Dimethylaminopropyl)- 3-ethylcarbodiimide hydrochloride (EDC), anhydrous dimethyl sulfoxide (DMSO), N-Hydroxysuccinimide (NHS), chitosan (viscosity averaged molecular weight, Mv,672 kDa and degree of deacetylation >75%), folic acid, sodium tripolyphosphate (TPP) were procured from Sigma- Aldrich and used as received.

4.3.2. Conjugation of the folic acid and chitosan

Chitosan (CS) was conjugated with folic acid (FA) via formation of the amide bond.[27] For that, the folic acid was first activated by EDC and N-Hydroxysuccinimide, in 20 mL anhydrous DMSO (molar ratio of FA, EDC and NHS was 1:1:0.5) and stirred at room temperature for 2 h. Into this 0.5% (w/v) chitosan in acetic acid solution (0.1% v/v, pH 4.5) was added and stirred at room temperature in the dark for 24 h to complete reaction. The conjugated product of FA-CS was collected by adjusting the pH of the solution to 9.0 by addition of NaOH (10 M), which precipitates the products. Then, the precipitate was repeatedly washed with water to remove DMSO and dried in oven at 65 ^{0}C for overnight. Finally, the required amount of FA-CS conjugate was redispersed in acidic water and is used for the synthesis of the composite NPs.

4.3.3 Synthesis of the fluorescent silver nanoclusters (Ag NCs)

Fluorescent Ag NCs were synthesized based on the previous method with slight modification.[28] For 20 mL reaction, 2 mL of bovine serum albumin (BSA 96%; 50 mg/mL) was taken in a conical flask and 400 µL of 10 mM Ag NO_3 was added into it. Then, 40 µL of a freshly prepared aqueous solution of $NaBH_4$ (10 mM) was added along with the addition of 100 µL of 0.3 M NaOH and incubated in the dark with ice (4^0C) under vigorous stirring for 12 h for complete reduction of the silver to silver nanoclusters. The yield of the formation of the NCs completely relies on the reaction environment, minute variation leads to formation of Ag NPs.

4.3.4. Synthesis of the fluorescent Ag NCs embedded folic acid-chitosan composite NPs (Ag NC –FA-CS NPs) and paracetamol dimer (PD) loaded composite NPs

0.5 mL of (0.5% w/v) FA-CS conjugated product was mixed with aforementioned BSA-Ag NCs with a ratio of 2.5:1 (w/w). Then, 0.2 mg/mL of sodium tripolyphosphate (TPP) was added drop wise for the synthesis of composite NPs (Ag NC- FA CS NPs), by using the ionotropic gelation method, originally developed by Calvo et al.[29] For the synthesis of the drug loaded composite NPs, 10 mg/mL pre-synthesized paracetamol dimer (PD)[22] were added into the reaction mixture prior to addition of the TPP (0.2 mg/mL). After the addition of TPP, the clear solution turned into milky white indicating the formation of the composite NPs, which was collected by centrifugation at 10,000 rpm for 5 min.

4.3.5. Analytical measurements

UV–vis spectra and fluorescence spectra were recorded by a Perkin–Elmer lambda 45 spectrophotometer (Perkin–Elmer, Fremont, CA) and Perkin–Elmer fluorescence spectrophotometer (model: LS 55) respectively.

4.3.6. Transmission electron microscopy (TEM)

To observe, the nanocarriers and Ag NCs under a high-resolution transmission electron microscope (TEM; JEM 2100; Jeol, Peabody, MA, USA) 10 μL of each samples were drop coated onto a carbon coated copper TEM grid followed by air drying. The voltage was fixed at 200 keV during TEM analysis. Selected area electron diffraction (SAED) and energy dispersive X-ray (EDX) spectroscopy were carried out using the same instrument and for same samples.

4.3.7. Dynamic light scattering study

The zeta potential and hydrodynamic diameter of the composite NPs and drug loaded composite NPs were measured by dynamic light scattering-based analysis (Malvern Zetasizer Nano ZS).

4.3.8. Fourier transforms infrared (FTIR) spectroscopy

Lyophilized samples were mixed with KBr to make the pellets, and characterized by FTIR spectroscopy (Perkin-Elmer) in the range 400−4000 cm^{-1}.

4.3.9. Epi fluorescence microscopy

To visualize the cells after treatment with Ag NCs and composite NPs epi fluorescence microscopy was done. 1×10^5 cells were seeded into 6 wells plate for overnight followed by addition of the Ag NCs-CS NPs. Same microscope was also used to observed acridine orange and ethidium bromide (AO/EtBr) double staining after treatment of the IC50 dose of drug loaded composite NPs for 24 h.

4.3.10. Cell culture

HeLa cells (human cervical carcinoma) and A549 cells were procured from National Center for Cell Sciences (NCCS), Pune, India, and cultivated in Dulbecco's Modified Eagle's Medium supplemented with L-glutamine (4 mM), penicillin (50 units/mL), streptomycin (50 mg/mL), and 10% (v/ v) fetal bovine serum (obtained from PAA Laboratories, Austria) in 5% CO_2 humidified incubator at 37 °C.

4.3.11. Cell viability assay

To perform MTT based cell viability assay, 1×10^4 HeLa and A549 cells/well were seeded in a 96- well microtiter plate and grown overnight by maintaining the same medium and condition as described previously. Then, different amount composite NPs and the drug loaded composite NPs were added into it and incubated for 24 h prior to addition of MTT (3-(4,5- dimethylthiazolyl-2)-2,5-diphenyltetrazolium bromide) dye to find out the number of viable cells. Viable cells reduce MTT into colour formazan which has absorbance at 550 nm. The % of cell viability was calculated as below by taking absorbance at 690 nm as background interference.

$$\% \text{ viable cells} = \frac{(A550 - A690)\ of\ NP\ treated\ cells}{(A550 - A690) of\ control\ cells} \times 100$$

4.3.12. Cell cycle analysis

Propidium iodide (PI) based cell cycle analysis was carried out in flow cytometer (FACS) which measures the DNA content of the cells at different stages of cell division. For that, 1×10^5 cells were seeded into 6 well plates and incubated for 12 h under the same conditions as mentioned above. Then, the cells were treated with drug loaded composite NPs for 24 h along with their respective controls. Cells were collected after

trypsinization and were fixed by addition of 1 mL of cold 70% ethanol, and kept it at -20 ^{0}C for 1 h. Finally, the fixed cells were collected by centrifugation and redispersed in PBS followed by RNase A (100 µg/mL) treatment at 37 ºC for 1 h. Prior to do analysis the cells were incubated in dark with PI (30 µg/mL) for 30 min and flow cytometry assay FACS Calibur (BD Biosciences, NJ) was carried out . The PI fluorescence data were collected in FL2 channel (band pass filter, 585/42 nm) which corresponds to red emission for 15,000 cells in each sample and data were analysed by the CellQuest pro.

4.3.13. ROS measurement

Reactive oxygen species (ROS) generation was determined by fluorescence activated cells sorter (FACS) using 2, 7-dichlorofluoresceindiacetate (DCFH-DA; Sigma-Aldrich, USA) staining method. For this, 1× 10^5 cells were seeded into 6 -well plates and incubated for 12 h. The cells were than treated with IC_{50} dose of drug loaded composite NPs with their respective controls for 3 hours and to this 10 µL of 1 mM DCFH-DA was added and kept at 37^{0}C for 10 min. Then, the cells were collected after trypsinization and suspended in 1 mL of DMEM before analysed in a flow cytometer (FacsCalibur, BD Biosciences, NJ). The emission of the DCF was collected in FL1-H channel (530/30 nm) which corresponds to green emission. The fluorescence data were recorded with the CellQuest program (BD Biosciences) for 15, 000 cells in each sample.

4.3.14. Caspase 3- assay

To probe apoptotic mediated cell death, FACS based caspase-3 assay was performed. For that, 1× 10^5 cells were seeded into 6 -well plates and kept for overnight incubation. Cells were treated with IC_{50} dose of drug loaded composite NPs along with their respective controls, and incubated for another 24 h. After incubation the cells were collected in PBS and were fixed with 0.1% (v/v) of formaldehyde for 15 min. The fixed cells were harvested by centrifugation at 650 rcf, followed by incubation in dark with 1 mL of membrane permealization solution (0.5% of Tween 20 in PBS) for 20 min in dark. Cells were washed twice with PBS to remove the surfactant prior to the addition of phycoerythrin (PE) conjugated Rabbit Anti –Active Caspase-3 (BD Biosciences) for 30 min in dark. The fluorescence data were recorded for 15 000 cell in FL2 channel (band pass filter, 585/42 nm) of FACS and analysed by CellQuest program (BD Biosciences).

4.4. Results and discussion

To synthesize the tumour cell specific targeted nanoparticles, folic acid was conjugated with chitosan via amide bond formation by using EDC as coupling agent. Folic acid conjugated chitosan was precipitated by increasing the pH of the solution to 9.0, and was repeatedly washed with deionized water to remove the excess folic acid and EDC. The formation of the amide bond was confirmed by the UV-vis spectroscopy, which reveals the absorption peak in the range of 280 nm. [30-32] The control i.e., chitosan did not show any peaks at that region (refer to Appendix, **Figure A4.1**). Additionally, FTIR analysis displayed the characteristic absorption peaks of amide bond along with the corresponding peaks of both CS and FA. The peaks at 1648 cm^{-1} and 1587 cm^{-1}, corresponding to stretch of amide band I (-CO-) and stretching vibrations of amide-II (NH)[30] respectively, confirmed the formation of the amide bonds between CS and FA (**Figure 4.1a**). The fluorescent silver nanoclusters (Ag NCs) were synthesised by reaction of equimolar amount of Ag NO3 and sodium borohydride along with 50 mg/mL of bovine serum albumin (BSA), which acted as a template. For the synthesis of composite NPs, previously formed folic acid linked chitosan (0.5% w/v) was mixed with the BSA-Ag NCs followed by addition of sodium tripolyphosphate (TPP).

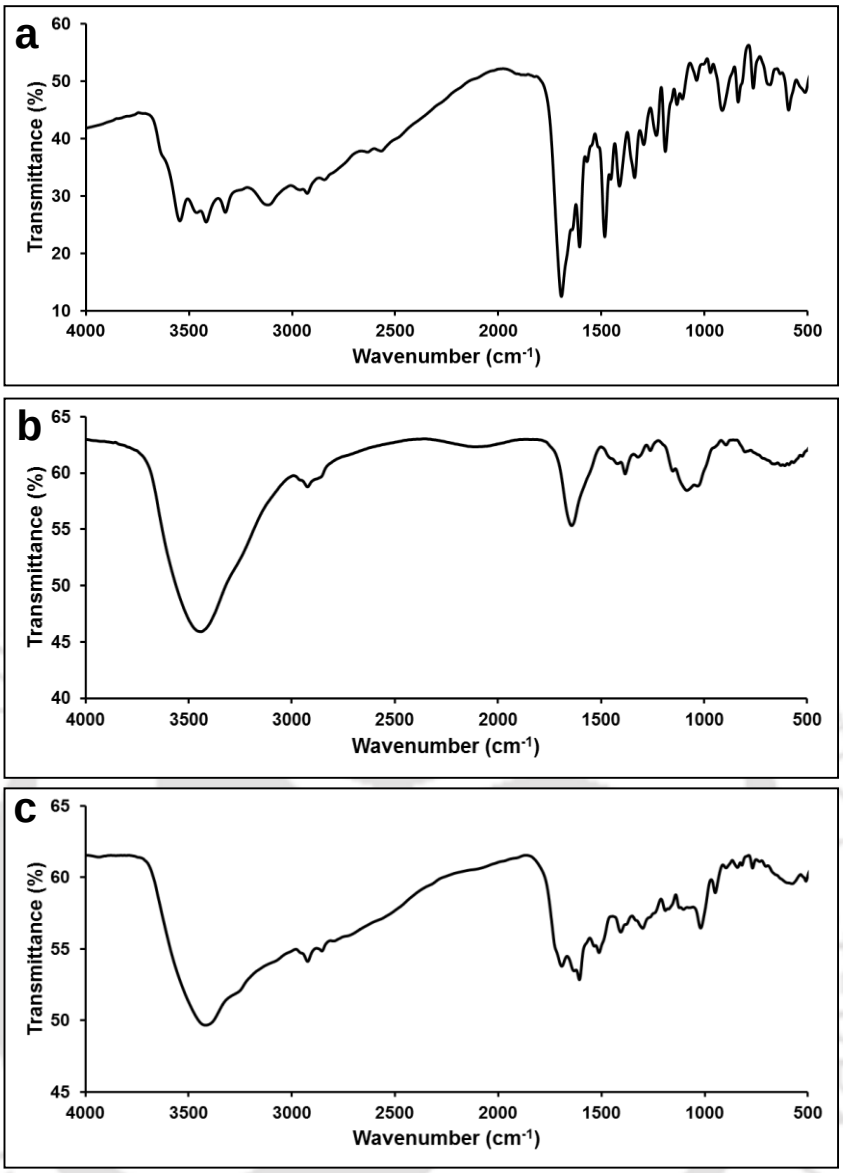

Figure 4.1 FTIR spectra of the (**a**) Folic acid (**b**) chitosan (**c**) Folic acid conjugated chitosan

The formation of composite NPs and the silver NCs was evinced by UV-vis spectroscopy study, where the characteristic plasmon peak of the Ag NP in the range of 390-450 nm was not appear (inset of **Figure 4. 2a)**. However, the composite showed strong emission peak at 690 nm and small peak at 400-430 nm when excited with the UV light of 320 nm as shown in **Figure 4.2a**. The control experiments were also performed under similar condition and no emission peak was found, indicating the formation of the fluorescent Ag NCs. Further, TEM analysis confirmed the formation of Ag NCs **(Figure 4.2b)**. The average diameter of the NCs was found to be 1.42 ± 0.33 nm. The EDX spectrum was recorded during the TEM analysis for the same sample, confirmed the presence of silver (refer to appendix, **Figure A4.2**). DLS analysis was carried out to determine the hydrodynamic diameter and the zeta potential of the composite NPs. The hydrodynamic diameter was found to be 214 nm, and the zeta potential value was 28.08 mV, which is known to be favourable for the cellular uptake **(Figure 4.2c-d).**

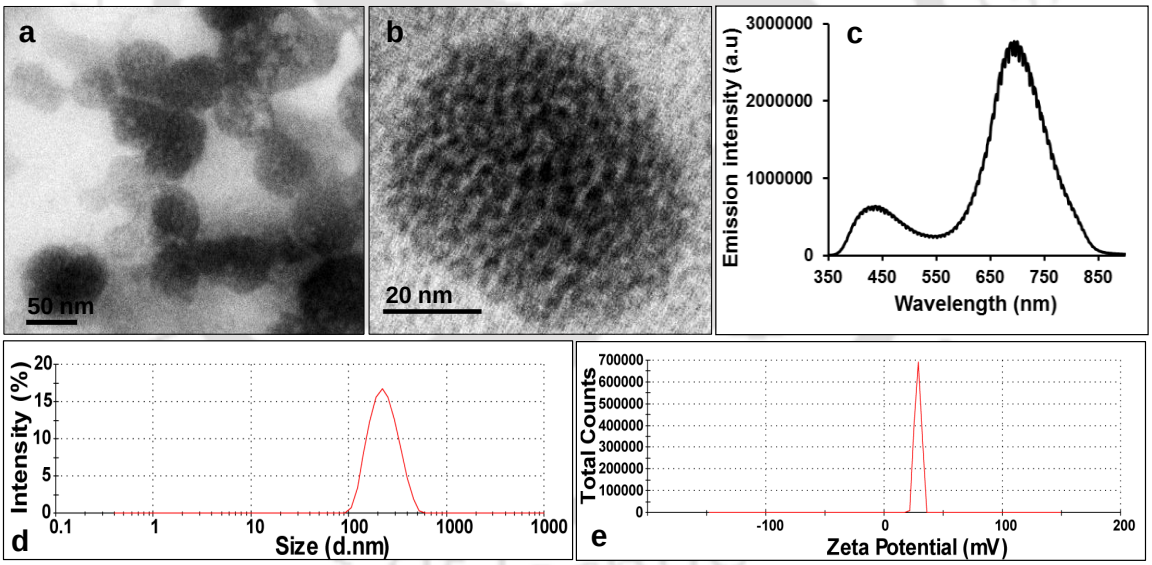

Figure 4.2 (**a**) TEM image of the composite NPs (Ag NC-CS NPs), (**b**) Magnified TEM image of the composite NPs. (**c**) Fluorescence spectrum of the composite NPs, showing emission at 670 nm when excited at 320 nm. (**d**) Dynamic light scattering showing the hydrodynamic NPs of the composite NPs (**e**) Zeta potential of the composite NPs.

As we have taken folic acid (FA) by means of a cell targeting agent, two different cancer cell lines, namely HeLa and A549 have been selected as a model system. Generally, HeLa cells overexpress the folic acid receptors (FR^+), whereas, A549 cells down regulates the folic acid receptor (FR^-). Relative expression level of folic acid receptors was confirmed prior to perform the cell based assays. For that the total RNA was extracted from two different cell lines and subsequently transformed into its cDNA by reverse transcription polymerase chain reaction (RT-PCR). The cDNA was used to examine the expression level of the FR by semi quantitative polymerase chain reaction (PCR) analysis followed by the agarose gel electrophoresis. The results demonstrated that FR expression was significantly high in case of HeLa as compare to the A549, while β-actin a house keeping gene, served as an endogenous control showed the similar expression level in both the cell lines as depicted in **Figure 4.3a**. The corresponding bar graph **(Figure 4.3b)** showed FR expression was 2.3 ± 0.10 times higher in case of the HeLa cell as compared to the A549, the results are alike with the previous studies.[33]

After studies of the expression of the FR, it's crucial to infer the interaction of the folic acid conjugated NPs between the two cell lines which were established by probing the fluorescence of Ag NCs with epi fluorescence microscopy. For that, the cells were incubated with the composite NPs for 3 h and were observed under microscope after thorough washing with PBS. Fluorescence microscopy images shows red fluorescence emission on the surface of the composite NPs treated cells when excited with UV light as showing in **Figure 4.3c-d**. The fluorescence intensity was relatively higher in HeLa cells than A549 cells. This could be due to differential expression of the folic acid receptors, which facilitated relatively higher amount of uptake in case of the HeLa cells, which eventually over expressed the folic acid receptors as compared to its counterpart.

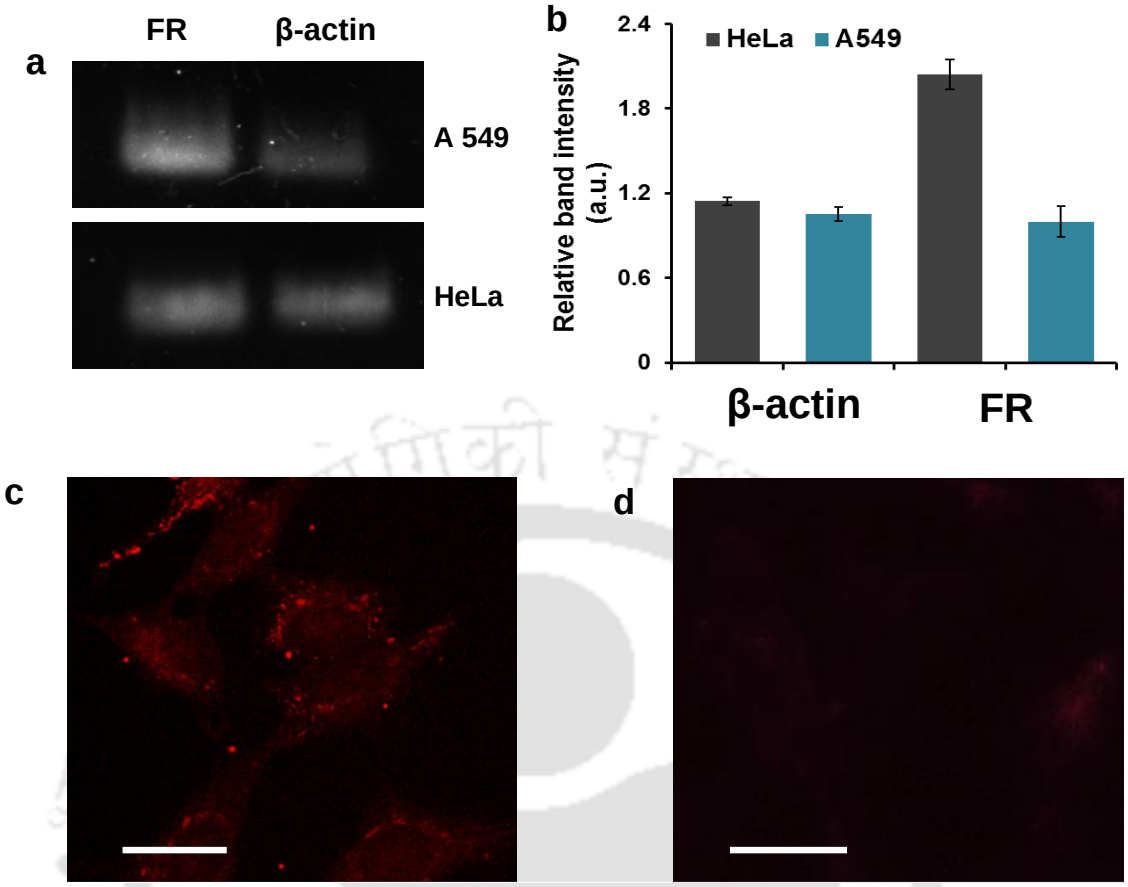

Figure 4.3 (**a**). Agarose gel showing the relative gene expression of the folic acid receptors for both HeLa and A549 cells, β-actin has taken as endogenous control. (**b**) Bar graph is showing the relative band intensity FR for both HeLa and A549. The values are represented as mean ± SD of results from three individual experiments. (**c-d**) Epi fluorescence microscopy images. (**c**) HeLa cells are showing the bright red fluorescence of the Ag NCs (**d**) A549 cells are showing weak fluorescence to due difference expression of the FR which leads to differential uptakes of the folic acid conjugated nanoparticle. Scale bar 20 µm.

To study the cell viability activity, MTT assay was carried out by adding different concentrations of the composite NPs on two different cell lines (HeLa and A549). The results demonstrated that the cell viability was gradually decreased with increasing concentration of NPs in case of the HeLa cells, but no significant cell mortality was revealed in case of A549 cells with same silver concentration. This result indicates that the folic acid conjugated NPs were more effective for the FR^+ cells as compared to its counter parts. The IC_{50} value of the composite was found to be 21.65 µg/mL with 2.65 ± 0.20 µg/mL of Ag NCs (**Figure 4.4**). It is worth mentioning here that the amount of

silver required to obtain the IC_{50} was far less than the Ag NPs, particle size typically > 2 nm.[9,] This is possibly due to the size of the NCs, which played a crucial role in reduction of silver concentration in the present case. It is also evident that by using this FA conjugated composite NPs, a significant level of selectivity could be obtained for FR^+ cells over its counter parts and offers the likelihood of the tumour 'theranostics'.

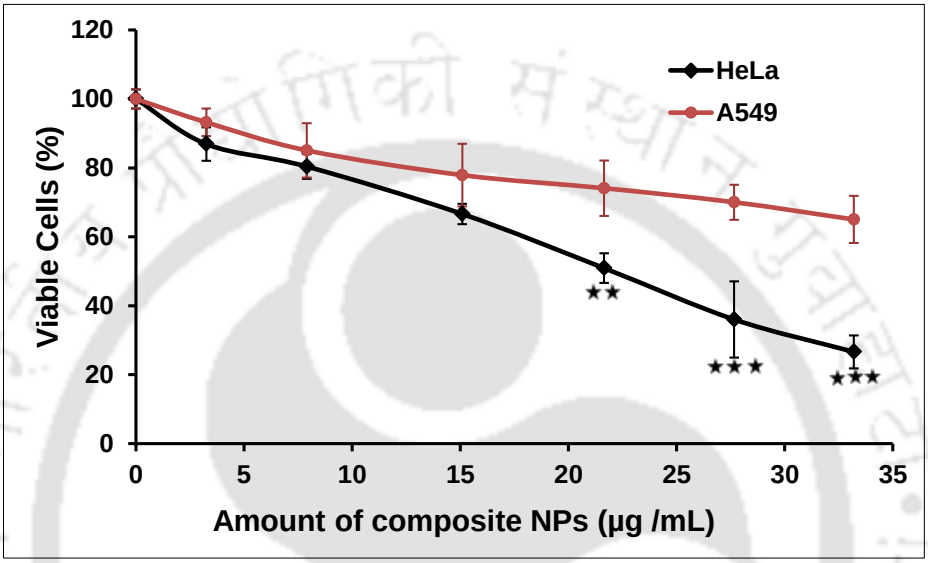

Figure 4.4 MTT assay showing the anti-cell proliferation of HeLa and A549 cells. The values are represented as mean ± SD of results from three individual experiments. The ANOVA test with pairwise comparison was carried out to find out the statistical significance for each concentration. ★($p < 0.05$), ★★($p < 0.01$) and ★★★($p < 0.001$)

Further, to use this composite NPs as a suitable drug delivery cargo, paracetamol dimer (PD) was loaded as model drug with the anticipation that the drug loaded composite NPs would eventually offer better therapeutic activity with reduced silver concentration. Moreover, transportation of the drug can be traced by probing the fluorescence of the Ag NCs. Hence, paracetamol dimer (PD) was delivered into the HeLa cells by using these composite NPs. Our previous report has demonstrated that PD can be employed as prodrug as it converts to NAPQI by ROS in case of *E.coli* and caused bacterial cell death in presence of Ag NPs.[22] It would be worth mentioning that the NAPQI is the potential topoisomerase II inhibitor in case of the mammalian cells which causes apoptosis mediated cell death.[25] However, in case of mammalian cells there is no report on the usage of PD as a prodrug to produce NAPQI with intra cellular reactive

oxygen species (ROS) generated by Ag NPs. Hence, we have loaded it into the composite NPs, the loading efficiency was found to be 45.23 ± 5.23 %. It is to be mentioned here that composite NPs is positively charged because of the protonated amine groups of chitosan whereas the PD possess negative charge owing to deprotonation of the hydroxyl groups at the physiological pH, offering the plausibility of the electrostatic interaction between duos. This was supported by the zeta potential, where the zeta potential value of NP decreased from 28.8 mV to 19 mV after interaction with the PD, whereas the hydrodynamic diameter of the PD loaded NPs were slightly increased from 214 nm to 230 nm (**Figure 4.5a-b**). Before adding the PD loaded NPs to the cancer cells, *in vitro* protein release study was performed, which revealed that about 22.94 ± 1.4 % protein was released within 48 h in PBS buffer (at pH 7.4) as shown in **Figure 4.5c**. It could be inferred from aforementioned results that release of PD was significantly low in physiological condition, which is favourable as it increases the efficiency of the intra cellular delivery of PD. Further, to visualize the PD loaded composite NPs, microscopy analysis was carried out which evidently showed the presence of the composite NPs within cells as depicted in **Figure 4.5d**.

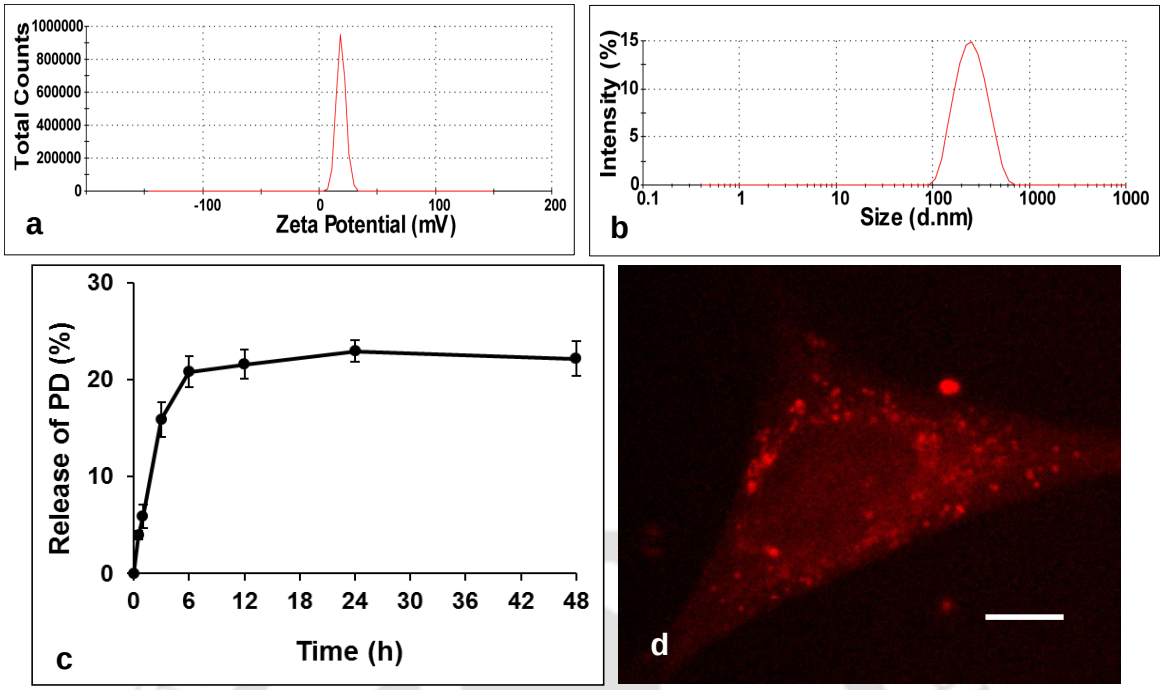

Figure 4.5 (**a**) zeta potential of the PD loaded composite NPs (**b**) Hydrodynamic diameter of the Pd loaded composite NPs.(**c**) Release study of the PD in the PBS. Data are represented as mean ± SD of results from three individual experiments. (**d**) Fluorescence microscopy image of the PD loaded composite NPs, showing the red emission of the Ag NCs. Scale bar 5 µm.

To find out the effects of PD loaded NPs over the Ag NCs, the HeLa cells were treated with different concentrations of NPs for 24 h followed by MTT assay, which showed that cell viability was significantly decreased with the increasing concentration NPs **(Figure 4.6a)**, as compared to their respective control (i.e., Ag NCs and PD). The IC_{50}, value of the Ag NCs was significantly decreased to 1.43 ± 0.12 µg/mL, as compared to only Ag NCs. The results indicated that PD augments the cytotoxic effects of the HeLa cells with addition of Ag NCs which eventually led to reduce the effective concentration of the Ag NCs also. It would be mentioned here that only PD could not offer significant effect on the cell viability unlike Ag NCs. To understand the mechanism of cell death, the HeLa cells were treated with IC_{50} dose of NPs for 3 h followed by flow cytometer (FACS) based reactive oxygen species measurement (ROS) using DCFH-DA staining method. Intra cellular ROS oxidizes DCFH to fluorescent DCF (green emission). Hence, the amount of fluoresce intensity is directly correlates with the amount of ROS production inside the cells and the fluorescent signal was collected in the FL1 channel of FACS. The FACS results conferred that there is subsequent amount of increment in the ROS level in

the PD loaded composite NPs as compared to its respective controls as shown **Figure 4.6b**.

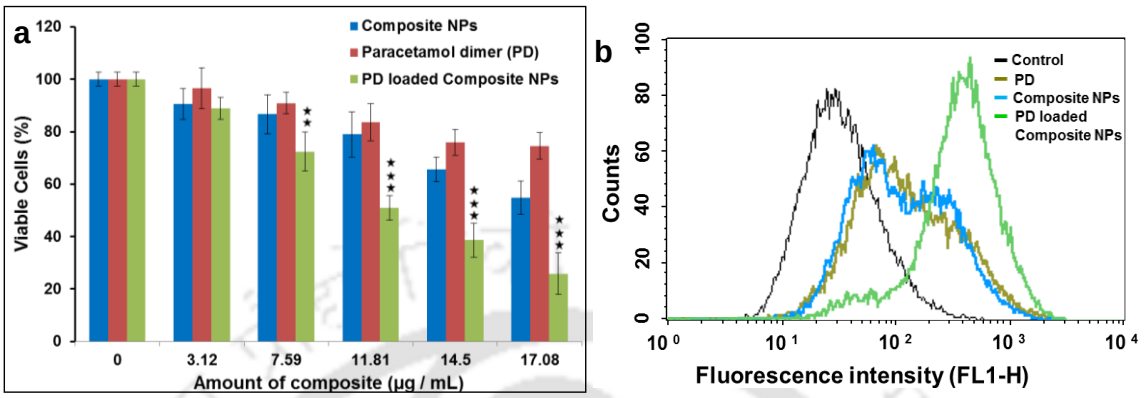

Figure 4.6 (**a**) MTT assay of the PD loaded NCs. The values are represented as mean ± SD of results from three individual experiments. The ANOVA test with pairwise comparison was done to find out the statistical significance for each concentration. ★($p < 0.05$), ★★($p < 0.01$) and ★★★($p < 0.001$) (**b**) FACS analysis of reactive oxygen species (ROS) generation in HeLa cells which is showing the PD loaded composite NPs exhibited prominent, implying higher level of ROS production. The FL1-H corresponds to the green emission of the DCF.

Further, ethidium bromide (EtBr) and acridine orange (AO) dual staining was performed as AO stains live cells nuclei and gives green emission when excited with blue light, whereas the dead cells emitted red fluorescence due to uptake of EtBr when excited with green light. Thus, merged image of the dual staining method provides distinctive view among the live and the dead cells. The results demonstrated that cell treated with IC_{50} dose of PD loaded composite showed more red cells than their respective control. In case of PD loaded composite NPs treated cells, chromatin fragmentation was prominent, which the characteristic feature of apoptotic cell death (**Figure 4.7**).

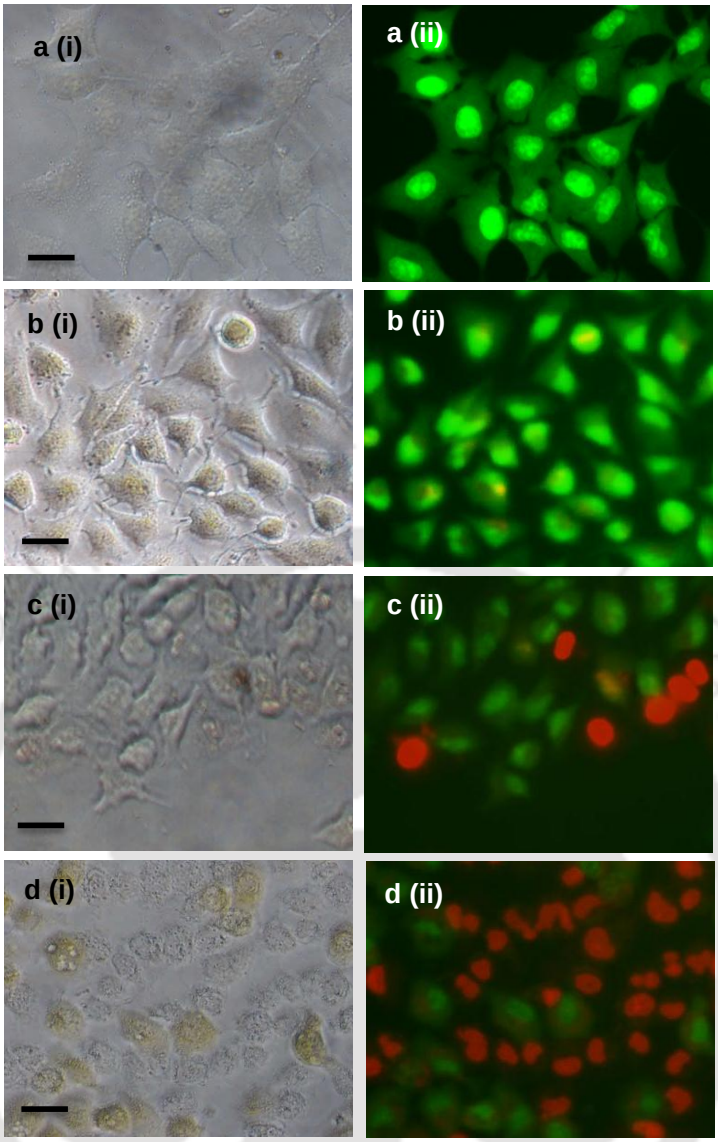

Figure 4.7 Ethidium bromide (EtBr) and acridine orange (AO) based dual staining showing the live and death cells. Dead cells show red emission by uptakes EtBr and live cells green due to uptakes of AO (**a**) Control, (**b**) PD, (**c**) composite NPs (Ag NC- FA CS NPs) and (**d**) PD loaded composite NPs treated cells respectively. (**i**) and (**ii**) indicate bright field images and merged image of EtBr/ AO respectively. Scale bar 20 μm.

To substantiate the above observation, FACS based caspase-3 assay was performed. The caspase-3 is an important cysteine protease enzyme present in cells in an inactive form; however, during the early phase of apoptosis it converts into active form by proteolysis and control several downstream pathways responsible for apoptosis. Hence, the number of caspase -3 cells directly correlates the number of apoptotic cells. For caspase-3 assay, cells were treated with the PD loaded composite NPs along with its respective controls followed by the addition of phycoerythrin (PE) conjugated rabbit anti-active-caspase-3. The PE emission was collected in FL2-H channel of the FACS, which corresponds to red emission. Cells treated with the PD loaded composite NPs showed maximum number of apoptotic cells as compared to its respective controls, i.e., around 8.3% of cells were apoptotic in caspase 3 assay after 24 h of treatment with PD loaded composite NPs as shown in **Figure 4.8 a-d**.

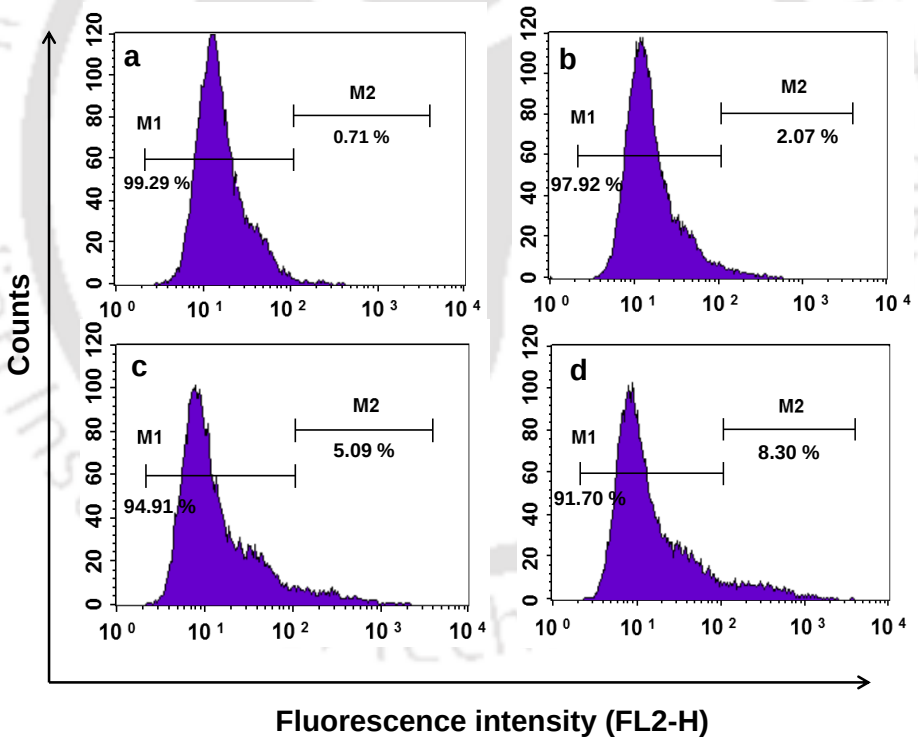

Figure 4.8 FACS based caspase 3 analysis after treatment of the PD loaded composite NPs. PE emission was collected in FL2-H channel of the FACS corresponds to red emission. (**a**), (**b**), (**c**) and (**d**) are the control, PD, composite NPs (Ag NCs) and PD loaded composite NPs, respectively. In the histogram M1 and M2 corresponds to caspase positive and caspase negative cells, respectively

Additionally, FACS based cell cycle analysis revealed that there was a significant (5.2 %) rise in the sub G0 population, which corresponds to the apoptotic population; in case of the PD loaded NPs treated cells as compared to its control such as PD and the Ag NCs as illustrated in **Figure 4.9**. The details of the same had also incorporated in the **Figure 4.9a-c** to support the afar mentioned analysis. Induction of the apoptosis further validated by FESEM analysis depicted the membrane indentation and irregularity for the composite NPs treated cells as compared to the control. This is typical signature of initiation of apoptotic bodies as shown in **Figure 4.10a-b**. Thus, the overall results demonstrated that the PD augment the therapeutic efficacy of the Ag NCs than their individual components, which leads to apoptosis mediated cells death possibly due to complementary effects.

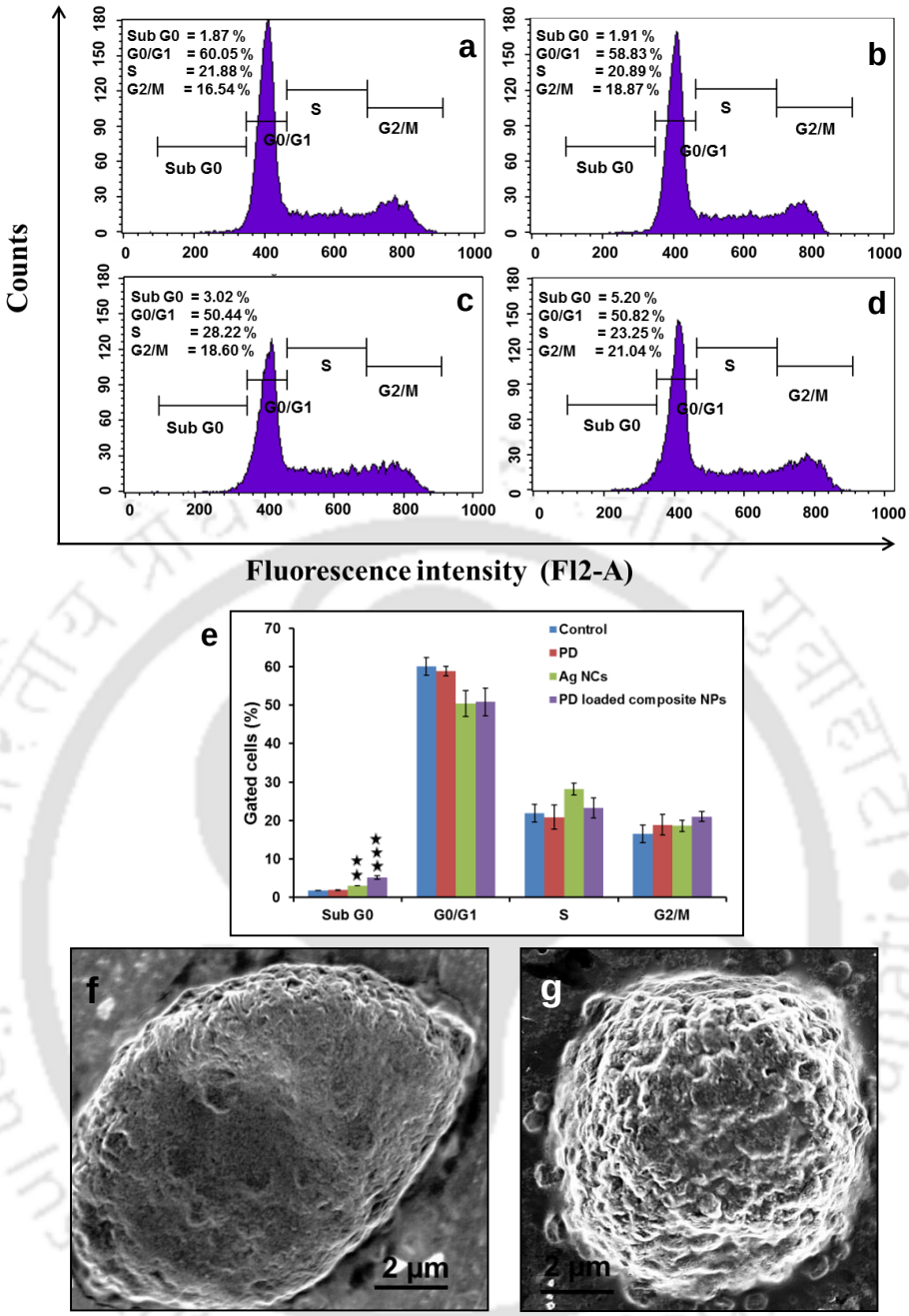

Figure 6. (a-e) Cell cycle analysis depicting different stages of the cell cycle. (**a**) Control cells, (**b**) PD treated cells (**c**) Composite NPs treated cells and (**d**) PD loaded Composite NPs treated cells. (e) Bar graph showing the increase in the sub G0 population after treatment with PD loaded composite NPs. Data is represented as mean ± SD of results from three individual experiments. The ANOVA test with pairwise comparison was performed to find out the statistical significance for each concentration. ★ ($p < 0.05$), ★★($p < 0.01$) and ★★★ ($p < 0.001$) FESEM images (**f**) Control and (**g**) treated cell showing membrane indentation after exposure of the PD loaded composite NPs. Scale bar 2 µm.

4.5. Conclusion

In brief, highly fluorescent silver nanoclusters (Ag NCs) have been synthesized and conjugated with folic acid for targeted delivery. To demonstrate the effect of the Ag NCs, two different cancer cell lines, HeLa and A549 have been opted. The results illustrated that HeLa cells were more liable than A549 for the over expression of the FA receptors, evident from the fluorescence of Ag NCs. The composite NPs were employed to deliver the paracetamol dimer (PD) into the cancer cells, which augmented apoptosis mediated cell death at very low concentration of silver. Therefore, it is to be deemed that Ag NCs embedded composite NPs offers a great deal of scope for the tumour 'theranostics'.

4.6. References

1. C. Holohan, S. Van Schaeybroeck, D. B. Longley, and P. G. Johnston, *Nat. Rev. Cancer*, 2013, **13**, 714–726.
2. T. Fojo and S. Bates, *Oncogene*, 2003, **22**, 7512–7523.
3. M. M. Gottesman, T. Fojo, and S. E. Bates, *Nat. Rev. Cancer*, 2002, **2**, 48–58.
4. J. L. Arias, *Mini. Rev. Med. Chem.*, 2011, **11**, 1–17.
5. R. Khandelia, A. Jaiswal, S. S. Ghosh, and A. Chattopadhyay, *Small*, 2013, **9**, 3494–3505.
6. S. M. Moghimi, A. C. Hunter, and J. C. Murray, *Pharmacol. Rev.*, 2001, **53**, 283–318.
7. O. C. Farokhzad and R. Langer, *ACS Nano*, 2009, **3**, 16–20.
8. D. Peer, J. M. Karp, S. Hong, O. C. Farokhzad, R. Margalit, and R. Langer, *Nat. Nanotechnol*, 2007, **2**, 751–760.
9. P. V. AshaRani, G. Low Kah Mun, M. P. Hande, and S. Valiyaveettil, *ACS Nano*, 2009, **3**, 279–290.
10. P. Sanpui, A. Chattopadhyay, and S. S. Ghosh, *ACS Appl. Mater. Interfaces*, 2011, **3**, 218–228.
11. N. Chaubey, A. K. Sahoo, A. Chattopadhyay, and S. S. Ghosh, *Biomater. Sci.*, 2014, **2**, 1080- 1089.
12. E. Locatelli, M. Naddaka, C. Uboldi, G. Loudos, E. Fragogeorgi, V. Molinari, A. Pucci, T. Tsotakos, D. Psimadas, J. Ponti, and M. C. Franchini, *Nanomedicine*, 2014, **9**, 839–849.
13. Y. Wang, B. B. Newell, and J. Irudayaraj, *J. Biomed. Nanotechnol.*, 2012, **8**, 751–759.
14. C. E. Ashley, E. C. Carnes, G. K. Phillips, D. Padilla, P. N. Durfee, P. A. Brown, T. N. Hanna, J. Liu, B. Phillips, M. B. Carter, N. J. Carroll, X. Jiang, D. R. Dunphy, C. L. Willman, D. N. Petsev, D. G. Evans, A. N. Parikh, B. Chackerian, W. Wharton, D. S. Peabody, and C. J. Brinker, *Nat. Mater.*, 2011, **10**, 389–397.
15. Z. M. Qian, H. Li, H. Sun, and K. Ho, *Pharmacol. Rev.*, 2002, **54**, 561–587.
16. A. R. Gliga, S. Skoglund, I. Odnevall Wallinder, B. Fadeel, and H. L. Karlsson, *Part. Fibre Toxicol.*, 2014, **11**, 2-17.
17. C. Carlson, S. M. Hussain, A. M. Schrand, L. K. Braydich-Stolle, K. L. Hess, R. L. Jones, and J. J. Schlager, *J. Phys. Chem. B*, 2008, **112**, 13608–13619.

18. I. Díez and R. H. A. Ras, *Nanoscale*, 2011, **3**, 1963.
19. J. Zheng, P. R. Nicovich, and R. M. Dickson, *Annu. Rev. Phys. Chem.*, 2007, **58**, 409–431.
20. J. Wang, G. Zhang, Q. Li, H. Jiang, C. Liu, C. Amatore, and X. Wang, *Sci. Rep.*, 2013, **3,** 1157
21. H. Xu and K. S. Suslick, *ACS Nano*, 2010, **4**, 3209–3214.
22. A. K. Sahoo, M. P. Sk, S. S. Ghosh, and A. Chattopadhyay, *Nanoscale*, 2011, **3**, 4226-4233.
23. A. K. Sahoo, S. Sharma, A. Chattopadhyay, and S. S. Ghosh, *Nanoscale*, 2012, **4**, 1688-1694.
24. G. V. Crichlow, J. B. Lubetsky, L. Leng, R. Bucala, and E. J. Lolis, *Biochemistry*, 2009, **48**, 132–139.
25. J. E. Deweese and N. Osheroff, *Nucleic Acids Res.*, 2009, **37**, 738–748.
26. R. P. Bender, R. H. Lindsey,, D. A. Burden, and N. Osheroff, *Biochemistry*, 2004, **43**, 3731–3739.
27. S.-J. Yang, F.-H. Lin, K.-C. Tsai, M.-F. Wei, H.-M. Tsai, J.-M. Wong, and M.-J. Shieh, *Bioconjugate Chem.*, 2010, **21**, 679–689.
28. X. Le Guével, B. Hötzer, G. Jung, K. Hollemeyer, V. Trouillet, and M. Schneider, *J. Phys. Chem. C*, 2011, **115**, 10955–10963.
29. P. Calvo, C. Remun˜a´N-Lo´Pez, J. L. Vila-Jato, And M. J. Alonso, J. Appl. Polym. Sci. 1997, **63**, 125 – 132.
30. D. Depan, J. Shah, and R. D. K. Misra, *Mater. Sci. Eng. C*, 2011, **31**, 1305–1312.
31. Y. Teow and S. Valiyaveettil, *Nanoscale*, 2010, **2**, 2607–2613.
32. A. Jaiswal, A. Chattopadhyay, and S. S. Ghosh, *Mater. Lett.*, 2012, **68**, 261–264.
33. M. García-Díaz, S. Nonell, Á. Villanueva, J. C. Stockert, M. Cañete, A. Casadó, M. Mora, and M. L. Sagristá, *Biochim. Biophys. Acta*, 2011, **1808**, 1063–1071.

Chapter 5

Simultaneous RGB Emitting Au Nanoclusters in Chitosan Nanoparticles for Anticancer Gene Theranostic

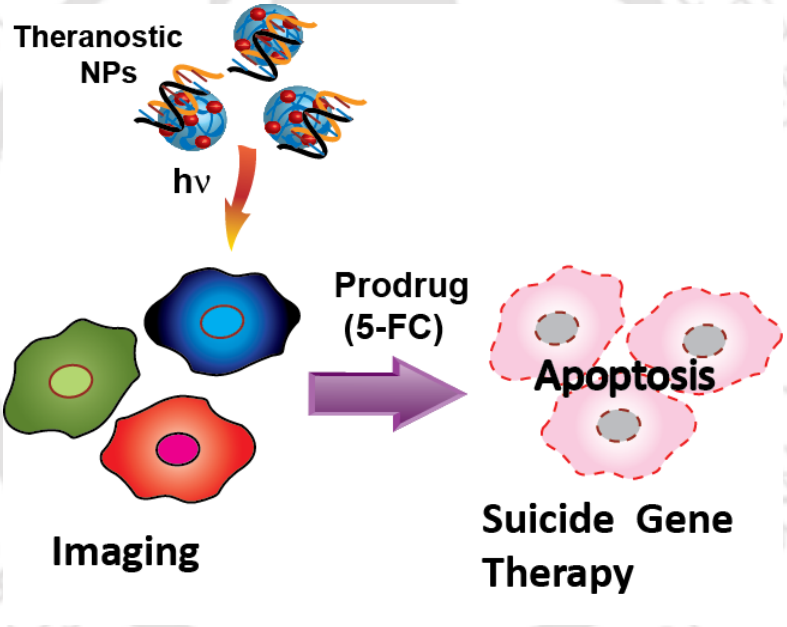

A. K. Sahoo, S. Banerjee, S. S. Ghosh and A. Chattopadhyay, **2014**. ***ACS Applied Materials & Interfaces***, 6, 712–724.

Chapter 5:

Simultaneous RGB Emitting Au Nanoclusters in Chitosan Nanoparticles for Anticancer Gene Theranostic

5.1. Introduction

The ephemeral nature of noble metal nanoclusters (NCs) in liquid medium makes stabilization as the primary challenge in their syntheses.[1] Thus, while reduction of parent salt into surface plasmon resonance (SPR) active metallic nanoparticles (NPs), in the presence of suitable stabilizing agent, has been transformed into routine exercises, the same cannot be taken for granted in the case of NCs. Here lies the need of extraordinary craftsmanship of chemistry, in the development of suitable methods for the generation of stable atomic clusters, conferred with remarkable photophysical and chemical properties. This becomes particularly important in the context of strong particle size-dependent discretization of energy levels of clusters, as their sizes approach the Fermi wavelength of electron (ca. 0.7 nm).[2-3] Given that the discretization of energy levels, in a multi-electron artificial atom model, scales with $N^{-1/3}$, where N is the number of atoms in the cluster, there seems to be an apparent fundamental disadvantage in not being able to synthesize NCs of exactly the same sizes. However, this inherent difficulty could be an advantage if one considers emission wavelength-tuneability in the case of particles with varied sizes. In other words, in the presence of a distribution of particles sizes, that the emission wavelengths could be different may be useful in probing biological systems, where the fluorescence inherent to the biomolecules - at several wavelengths - could otherwise interfere with the particular emission of the NCs. Further, the role of the stabilizing ligands in tuning the energy levels augurs well for the development of systematic chemistry in generating NCs with 'programmed' chemical and photophysical properties.[4-6]

Among the noble metals, Au NCs are attractive as they are potentially non-cytotoxic and the additional advantages of high fluorescence quantum yield, low photo-bleaching and large Stokes-shifted emission make them a preferred choice as multi-colored dye for sensitive bio-labeling and bio-imaging in-vivo as well as in vitro.[7-9]

Further, their fluorescence life time is useful in resolving their emission from cellular auto-fluorescence, which is essential in bio-imaging.[10] In addition, these small clusters have high potential for chemical and photochemical catalysis.[11-13] As a consequence of their high potential for applications, a growing number of methods are being reported in the literature, which consists primarily of their synthesis in the presence of various stabilizing agents. They involve reduction of the parent salt and stabilization of the product NCs, using species such as dendrimers, DNA, proteins, polymers, and polyelectrolytes.[14-16] Typical reaction conditions invoke prolonged incubation time (~24 h), high pH and elevated temperatures; in some cases addition of extra reducing agent is necessary.[17-20] Further, chemical etching of larger Au NPs (>3 nm) leading to the formation of NCs has been demonstrated to be a feasible option.[21-23] However, NCs produced using the reported methods are either not easily amenable to use for applications in different medium conditions or their large-scale syntheses are not viable.[24-27] In addition, the potential for applications of these novel and useful materials has not been demonstrated with clear vision, possibly because of lack of ability to maneuver the so-produced NCs. Therefore, newer methods of NC synthesis are essential, which will be convenient and produce NCs with extraordinary optical properties. Also, they should involve rather easy steps for manipulation of the products for practical applications. The favored methods ought to have the easy scale-up feasibility.

5.2. Outline of the research work

1. A convenient, fast and 'green' method of synthesis of red, green and blue light emitting Au NCs, using the biopolymer chitosan, in combination with mercapto propionic acid (MPA), as the reducing agents and the stabilizers was established.
2. The formation of the Au NCs was confirmed by fluorescence spectroscopy, MALDI-TOF and TEM analysis.
3. The composite was converted into stable powder and film without compromising the photophysical properties of NCs.
4. Further, the fluorescence emission of Au NCs was found to change reversibly by varying the pH of the medium, which offers a simple way to modify the fluorescence properties of NCs, without altering their sizes.

5. The composite was turned into chitosan nanoparticle (CS NP), favorable for cellular uptake, and which was used as theranostic device for induction of apoptosis in mammalian cancer cells, based on suicide gene therapy.
6. Composite NPs were used as a novel bioimaging agent in microscopy and flow cytometry (FACS) analysis without the use of additional dyes.
7. The NP was employed to deliver of suicide gene, corresponding to E. coli cytosine deaminase uracil phosphoribosyltransferase (CD-UPRT) enzyme, to HeLa cells, was probed using optical emission based and other biochemical methods, which showed nanocarrier mediated gene transfection (CD-UPRT), inducing apoptosis and thus killing the cancer cells.

5.3. Experimental section

5.3.1. Chemicals

Chitosan (viscosity averaged molecular weight, Mv, 672 kDa and degree of deacetylation > 75%), $HAuCl_4$ (Au, 17 wt% in dilute HCl; 99.99%), mercapto propionic acid (MPA), sodium tripolyphosphate (TPP), agarose were procured from Sigma-Aldrich and used as received. Milli-Q grade water (> 18 MΩ cm^{-1}, Millipore) was used in all experiments.

5.3.2. Synthesis of Au NCs

To synthesize the fluorescent Au NCs, chitosan solution was first prepared by dissolving 5 mg/ mL in Milli Q water containing 0.1% (v/v) acetic acid, followed by filtration to remove the residual components. The pH of the solution was then adjusted to 6.4 ± 0.2 by adding 10 M NaOH. Separately, 4 mL water was taken in a 20 mL beaker, to which 0.5 mL of the chitosan solution (as above) was added. This was followed by addition of 40 µL of 0.11 M mercaptopropionic acid (MPA) under vigorous stirring condition for 1 min. To this 75 µL of 10 mM $HAuCl_4$ was added drop-wise. Following addition of $HAuCl_4$, the solution was kept above a UV trans-illuminator (excitation wavelength 305 nm) after 1 min of constant starring, for observation of color characteristic of Au NCs, which appeared red after addition of the salt.

5.3.3. Synthesis of composite NPs

Composite NPs were synthesized by using ionotropic gelation method, developed by Calvo et al, which was slightly modified herein[30]. Briefly, aqueous solution of TPP (0.2 mg/mL) was drop-wise added, under stirring condition at room temperature, into previously prepared Au NC-chitosan composite (as above). Formation of opalescent suspension indicated the synthesis of Au NC-chitosan NPs, which was also observed using a UV-trans illuminator. The solid composite was collected by centrifugation (6000 rpm, 5 min), which was followed by redispersion in sterile PBS buffer (pH 7.4) before using in cell culture medium. Blank chitosan NPs (without Au NCs) were synthesized by using the same method and at the same chitosan concentration (without using $HAuCl_4$) for control experiments.

5.3.4. Transmission electron microscopy (TEM)

The composite and composite NPs (as-synthesized) were examined using a ultra-high resolution transmission electron microscope (TEM; JEM 2100; Jeol, Peabody, MA, USA), operating at a maximum accelerating voltage of 200 KV. For that, 8 μL of as-synthesized composite and composite NP dispersions were separately drop-coated onto carbon coated copper TEM grids, air dried for 12 h and then observed under TEM.

5.3.5. Fluorescence Measurements

Fluorescence experiments were carried out using fluorescence spectrophotometers LS55, Perkin Elmer and Fluorolog-3, Horiba Jobin Yvon, Edison, NY USA.

5.3.6. Dynamic Light scattering study

The zeta potential and hydrodynamic diameter of the composite NPs and gene-loaded composite NPs were measured by dynamic light scattering-based analysis using a Malvern Zetasizer Nano ZS.

5.3.7. Matrix-assisted laser desorption ionization time-of-flight mass spectrometry (MALDI-TOF MS) analysis

MALDI–TOF **(**Applied Biosystems 4800 Plus MALDI TOF/TOF Analyzer) was performed using R-cyano-4-hydroxycinnamic acid (CHCA) matrix.

5.3.8. Fourier transform infrared (FTIR) spectroscopy

To perform FTIR analysis, the samples were freeze-dried (Lyophilized), mixed with KBr to make the pellets and were characterized by a Perkin-Elmer Spectrum One machine in the range of 4000 - 400 cm^{-1}.

5.3.9. Field-emission scanning electron microscopy (FESEM)

FESEM measurements were performed in a Carl Zeiss, SIGMA VP, instrument. Typically, 20 µL of sample was drop-cast on a glass slide covered with aluminum foil, air dried and sputter-coated with gold film using a sputter coater (SC7620"Mini", Polaron Sputter Coater, Quorum Technologies, Newhaven, England), before analyzing under the FESEM.

5.3.10. Cell Culture

HeLa cells (human cervical carcinoma) were obtained from National Center for Cell Sciences (NCCS), Pune, India and cultured in Dulbecco's Modified Eagle's Medium supplemented with L-glutamine (4 mM), penicillin (50 units/mL), streptomycin (50 mg/mL; obtained from Sigma-Aldrich), and 10% (v/v) fetal bovine serum (obtained from PAA Laboratories, Austria) in 5% CO_2 humidified incubator at 37 ^{0}C.

5.3.11. Epi Fluorescence Microscopy

For imaging, 1× 10^4 HeLa cells were seeded into a 6-well plate and incubated for 24 h. Cells were then treated with Au NC-chitosan NPs for 4 h and were maintained under same condition and medium as described above. To observe the fluorescence of NCs inside the cells, the medium was discarded; the cells were washed with 10 mM PBS and analyzed under an epi-fluorescence microscope (Nikon ECLIPSE, TS100, and Tokyo). Different excitation band-pass filters such as UV (340-380 nm), blue (465-495 nm) and green (540/25 nm) and corresponding emission band-pass filters blue (435-485 nm), green (515-555 nm) and red (605/55 nm), respectively, were used in order to probe different colors of Au NCs present in the cell. To image the fluorescence of Au NCs, nano-composite (Au NC-chitosan) NP dispersion was drop-cast on glass slide; air dried and was observed using the same microscope as above.

5.3.12. FACS analysis

To study the uptake of Au NC-chitosan NPs by cells, 1×10^{5} HeLa cells were grown in 60 mm tissue culture dishes (BD Falcon) for overnight. Then, Au NC-chitosan NPs were added and incubated for 4 h and 8 h before harvesting them. To collect the cells, residual medium was removed, carefully washed with PBS, trypsinized and collected by centrifugation (650 rcf, 5 min). The cell pellets were redispersed into cold PBS and analysed by FACS Calibur (BD Biosciences, NJ). Fluorescence of Au NC (in the form of Au NC-chitosan NP) uptake by cells were recorded with the CellQuest pro in different fluoresce channels, including FL1 (530/30 nm), FL2 (band pass filter, 585/42 nm) and FL3 (low pass filter, 670 nm) for 15,000 cells in each sample.

5.3.13. DNA binding and DNase protection assays

In order to find out the DNA binding ability of NPs (Au NC–chitosan NPs), varying concentrations (0.0, 0.2, 0.5, 1.0, 2.0 and 3.0 μg) of NPs were incubated with pCD-UPRT (0.5 μg) at 37 ^{0}C for 1 h, followed by gel electrophoresis. The above-mentioned polyplexed of pDNA–NPs were used to carry out the DNase protection assay, in presence and absence of 1 U/mL DNase I (Promega, USA) for 15 min and at 37 °C, prior to gel electrophoresis. To perform partial digestion, the working concentration of enzyme used was less than the original concentration (10 U/mL DNase I) as described by manufacturer's protocol. The gel electrophoresis was performed in 0.8% agarose gel at 5 V/cm and was visualized in gel documentation system.

5.3.14. Cell viability assay

To quantify the cell viability due to the delivery of suicide gene, 1×10^{4} HeLa cells/well were seeded in 96-well microtiter plate and grown overnight by maintaining the same medium and condition as described previously. Before performing the gene transfection, the cells were supplemented in serum free medium and treated with the CD-UPRT gene loaded Au NC-chitosan NPs for 6 h as well by maintaining the same physiological condition described above. Then, serum free medium was removed, washed with PBS, and redispersed in serum medium and subsequently different concentrations of 5 FC were added. After 72 h, MTT (3-(4, 5-dimethylthiazolyl-2)-2, 5-diphenyltetrazolium bromide) assay was performed to find out the number of viable cells. In live cells, the respiratory mitochondria reduce MTT into color formazan. Thus, amount of formazan product (i.e. absorbance at 550 nm) is directly proportional to the number of live cells in culture. The

absorbance at 690 nm is due to background interference. The % of cell viability was calculated as.

% viable cells= [(A_{550}-A_{690}) of NP treated cells / (A_{550}-A_{690}) of control cells] ×100

5.3.15. Quantum yield measurements

Quantum yield (QY) of Au NCs was determined by using established protocol available in the literature, by taking quinine sulfate in 0.10 M H_2SO_4 solution as the standard. Absolute value of QY was calculated based on this following equation.

$$QY = QY_r \frac{m}{m_r} \frac{n^2}{n_r^2}$$

Where, m is the slope of the plot of integrated fluorescence intensity vs. absorbance, n is the refractive index and suffix r refers to the reference fluorophore (quinine sulphate solution). We used the same solutions to record the UV-Vis spectra and to measure the fluorescence emission. Absorbance value was kept less than 0.025 for fluorescence measurements. The refractive index of solvent (water) is 1.33 and quantum yield of the standard (QY_r) is 0.54.

5.3.16. Formation of thin film

For Au NC embedded chitosan film generation, the same protocol for synthesis of Au NCs was adopted; however, the reaction volume was increased. For example, 25 mL of 5 mg/mL chitosan (at pH 6.3) and 500 µL of 0.11 M mercaptopropionic acid (MPA) were mixed under vigorous stirring and 750 µL of 10 mM $HAuCl_4$ was added drop-wise into it. The starring was continued for another 10 min and the characteristic red fluorescence of Au NCs was confirmed using a UV-trans illuminator (305 nm). The pH of the resultant suspension (25 mL) was adjusted before casting into a polyethylene petri dish, which was then dried for 24 h at 42 ^{0}C in an incubator. All films were stored in a desiccator at room temperature.

5.3.17. Annexin V-PI staining

To find out the mode of death after treatment with 5FC, cells previously transfected with CD-UPRT gene, were double stained with FITC-labeled annexin-V and propidium iodide (PI); this differentiates the necrotic cells from the apoptotic ones based on the plasma membrane integrity. Loss of membrane asymmetry during apoptosis results in the

exposure of phosphatidylserine at the surface of the cells which preferentially binds with FITC-labeled annexin V thus exhibiting the green fluorescence. The necrotic cells accumulate the PI due to complete damage of the plasma membrane and show red fluorescence. The cells were treated with the 5FC for 48 h after being transfected with pCD-UPRT gene by Au NC-chitosan NPs and were then harvested by centrifugation (650 rcf, 5 min). The cells (10^7 cells/ mL) were redispersed in PBS and stained with FITC-annexin-V and PI as per manufacturer's instructions (FITC Annexin V Apoptosis Detection Kit, BD Pharmingen, NJ) and analyzed in FACS Calibur (BD Biosciences, NJ) flow cytometer. The data were collected with CellQuest Pro software for 15 000 cells in each sample.

5.3.18. Cell Cycle Analysis

Cell cycle analysis was performed in a flow cytometer, which measured the DNA content of cells in different stages of cell division of the treated and the control cells. NP mediated suicide gene transfected cells were treated with the 5-FC for 48 h along with the respective controls. Cells (1×10^6 cells /mL) were then collected by trypsinization, fixed by slowly adding 1 mL of cold 70% ethanol, and stored at -20 ^{0}C for 1 h. Then the fixed cells were collected by centrifugation followed by redispersion in PBS. The cells were incubated with PI (30 μg/mL) and RNase A (100 μg/mL) at 37 ^{0}C for 45 min in the dark prior to analysis in FACS Calibur (BD Biosciences, NJ). PI fluorescence data were collected in FL2 channel for 15,000 cells in each sample and data were analyzed by the CellQuest pro.

5.4. Results and discussion

5.4.1. Synthesis and characterization of the Au NCs

A simple, fast and 'one-step' method has been developed to synthesize highly fluorescent Au NCs in aqueous medium, by reacting 10 mM $HAuCl_4$ and 5 mg/mL chitosan (at pH 6.3), in presence of mercapto propionic acid (MPA) at room temperature. The reaction was virtually complete in about 1 min, following which probe revealed characteristic NC formation. The UV-Vis spectrum of the colorless dispersion did not exhibit any peak in the region of 400-800 nm **(Figure 5.1a)**, thus excluding the formation of SPR active Au NPs. However, the spectrum consisted of peaks at 290 nm and 340 nm (marked by arrows in the spectrum in **Figure 5.1a**). Literature reports attribute the peaks to the formation of

Au (I) - thiolate complexes, either as independent species or on the surface of clusters of Au atoms.[16-17, 31-33] Control experiment, involving recording of UV-Vis spectrum of $HAuCl_4$, indicated that the peak at 310 nm is due to the $AuCl^{4-}$ ions. Additionally, the spectrum due to a mixture of chitosan plus MPA showed no peak in the region. The disappearance of peak at 310 nm following reaction, accompanied by absence of SPR peak of Au NPs, indicated possible conversion of the salt into Au clusters. Interestingly, the UV-Vis spectrum recorded after 1, 5 and 15 min of mixing the reagents remained virtually the same, indicating that the products were possibly formed in the first 1 min of reaction and any change in the nature and amount of product might have been marginal after the first minute. Importantly, upon excitation by UV light (at 300 nm), the composite exhibited a strong emission peak at 610 nm and two comparatively weaker peaks in the region of 400-450 nm (**Figure 5.1b**). The fluorescence spectrum is indicative of the formation of Au NCs, as it is similar to characteristic spectrum of the NCs reported in the literature.[16] Excitation spectrum of the dispersion, corresponding to the emission peak at 610 nm consisted of two peaks – one at 302 nm, while the other one at 334 nm -, which are possibly due to the Au NC and Au (I) complex[17], respectively (**Figure 5.1c**). Further, fluorescence spectrum of the reaction medium (**Figure 5.1b**), recorded at several time points after addition of reactants, indicated the formation of product primarily in the first 1 min of reaction. The reaction appeared to be complete by 15 min, as there was no difference in emission intensities recorded at 15 and 30 min of reaction. The apparent minor difference in changes as a function of reaction time between UV-vis and fluorescence results could be due to surface passivation of the clusters occurred in the presence of changing chemical environment of the product NCs. Generally, synthesis of NCs requires, other than harsher reaction conditions, several hours for product formation, which has been reduced to a few minutes, making the current method rather straightforward and rapid. Additionally, fluorescence spectrum recorded over a week showed no change in product formation over the time period, indicating stable NC formation in the medium (**Figure 5.1d**). That the method does not require extra steps and time for purification of NCs, usually associated with the formation of larger NPs, provides the current way a unique advantage over earlier reported methods.[34- 39]

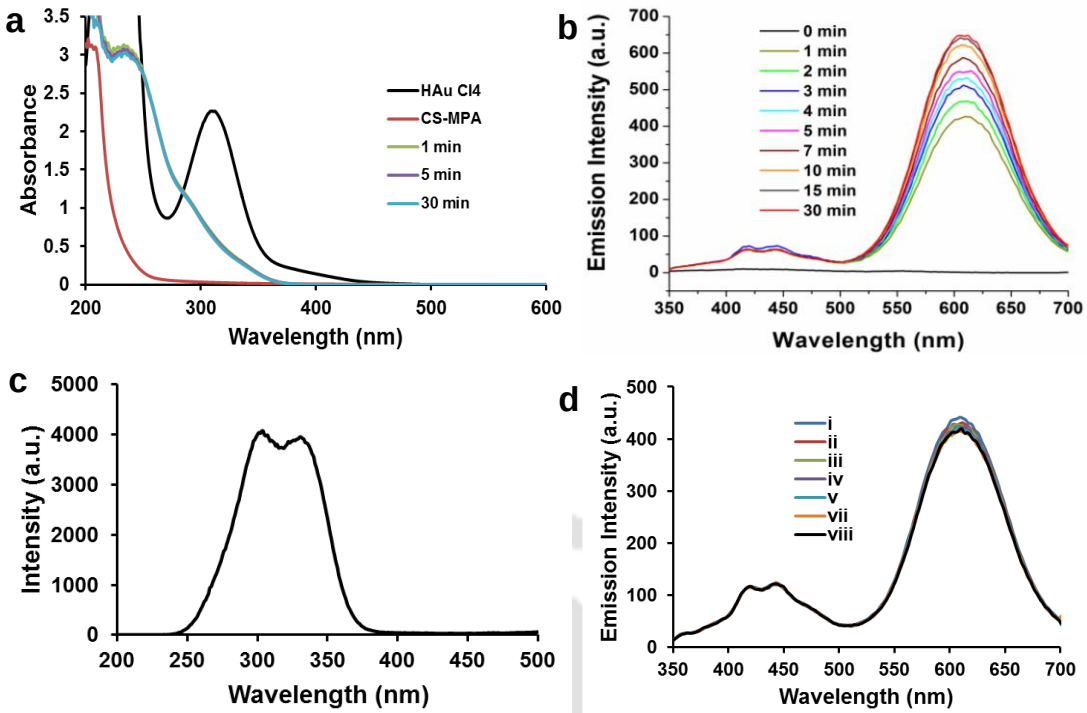

Figure 5.1 (a) UV-vis absorption spectra recorded at different times, demonstrating the formation of Au NCs from a mixture of $HAuCl_4$ and MPA in the presence of chitosan. Also, shown is the absorption spectrum of $HAuCl_4$. (**b**) Time-dependent emission spectra of the product (Au NCs) consisting of a major peak at 610 nm which was observed when excited by 300 nm light. (**c**) Excitation spectrum of the Au NCs present in the composite. The emission peak was set at 610 nm. (**d**) Time dependent fluorescence emission spectra demonstrating the stability of Au NCs in aqueous medium. The spectra in (i-vii) represent recording at 1 h and after 1, 2, 3, 7, 9 day respectively.

Further, TEM analysis of as-prepared sample revealed the formation of spherical nanoscale particles with nearly uniform size distribution (**Figure 5.2a**). The average diameter calculated from several images consisting of 100 such particles was found to be 1.12 ± 0.43 nm (**Figure 5.2b**). The HRTEM image (Inset of the **Figure 5.2a**) of the particles showed no distinct lattice spacing of single crystalline NCs. The presence of Au was further confirmed by EDX spectrum of the particles, recorded during the TEM analysis of the same sample (**Figure 5.2c**). Additionally, MALDI-TOF based mass spectrometric measurement of the sample (**Figure 5.2d**) exhibited a weak but clear peak at 5575.44 (in addition to a strong peak due to the polymer at 3690.0), which could be assigned to $[Au_{20}(MPA)_{15} + 3Na^{+} - 7H^{+}]^{4-}$, indicating the presence of NC with 20 Au

atoms as the main cluster. There are some additional peaks appeared at lower mass (2500-3500) possibly due to fragmentation or presence of smaller NCs.

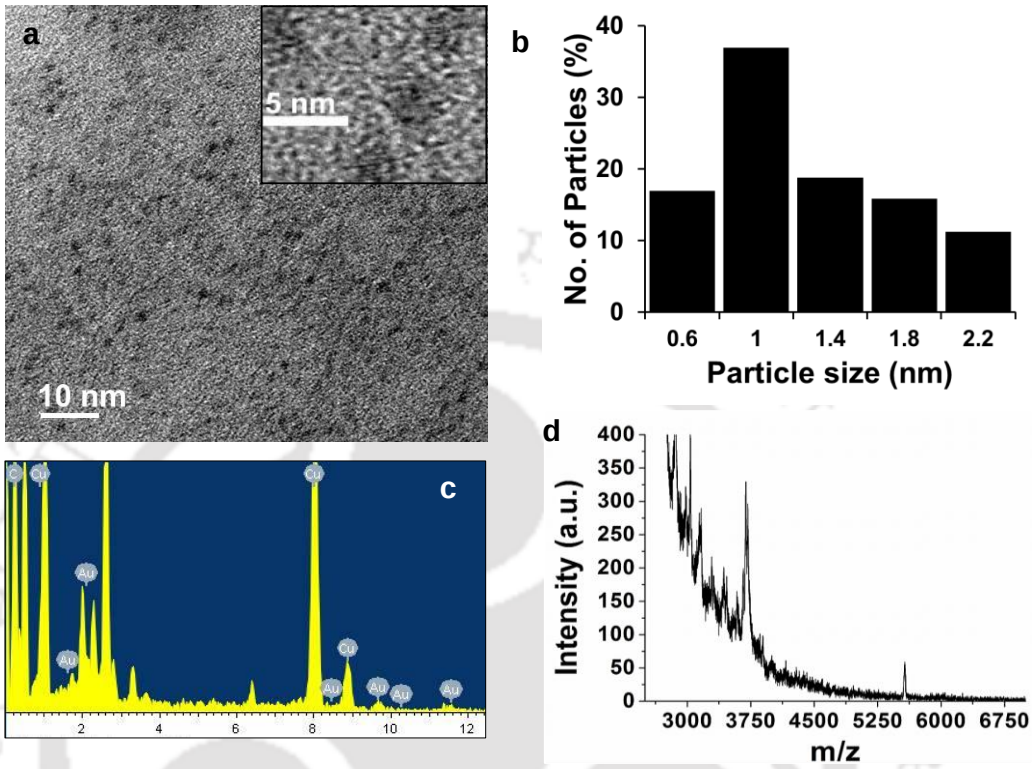

Figure 5.2 (**a**) TEM images of the NCs. Inset is the HRTEM images of a few such particle. (**b**) Particle size distribution, which was calculated based on TEM images. (**c**) EDX spectrum of the Au NCs present in chitosan. The signals due to cupper and carbon were from the TEM grid. (**d**) MALDI- TOF spectrum of the composite.

The above mentioned results indicated the formation of Au NCs as the product of the reaction and plasmonic nanoparticles (NPs) with higher average sizes were possibly not generated in the medium. Further, photoemission quantum yield of the NCs was measured to be 14.7 % (at pH 4.2), using quinine sulfate as the reference (**Figure 5.3a**). This is comparable to reported emission efficiency of Au NCs and thus indicated the generation of strongly emitting clusters.[40-41] Additionally, photo-stability study revealed that the emission intensity of the NCs remained nearly unaltered under continuous exposure of irradiation. For example, the fluorescence intensity decrease rate (F/F_0) of the NCs was 0.26 % per min, whereas in case of commonly used fluorescent dye such as rhodamine 6G, it was found to be 1.15 % per min (**Figure 5.3b**). Importantly, the

synthesized Au NCs could be stored in solid forms as powder or film, obtained after removing water by lyophilization (**Figure 5.3c-f**).

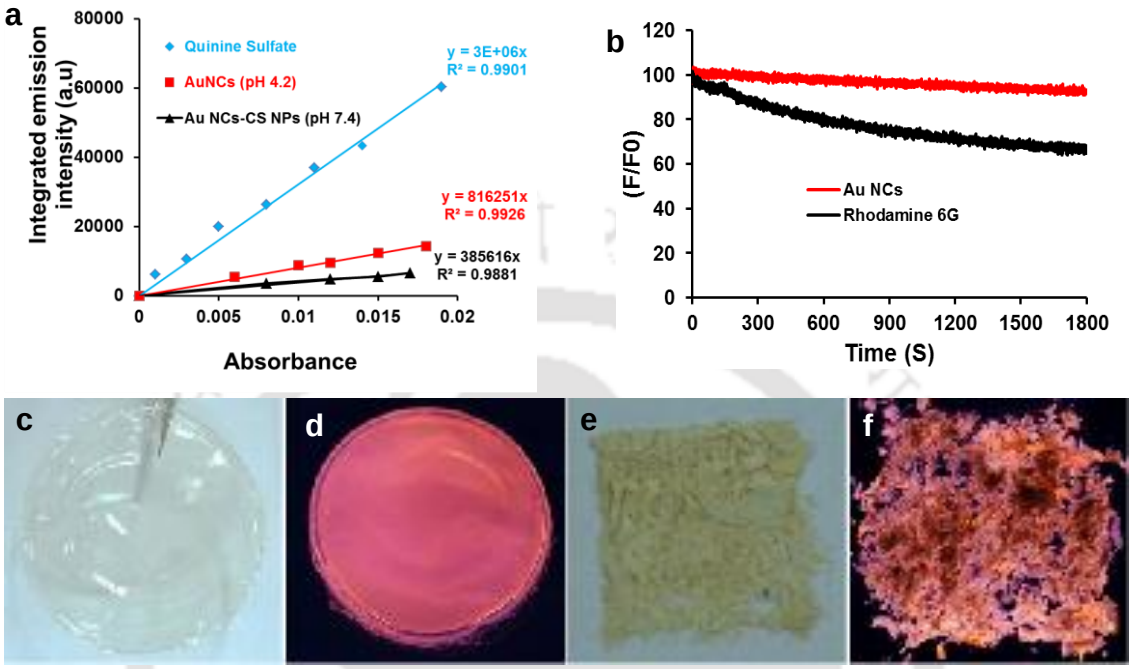

Figure 5.3 (a) Quantum yield (QY) measurements of the Au NC in chitosan and that of Au NC-chitosan NP. Quinine sulfate was used as standard. **(b)** Photo bleaching studies of the Au NC in chitosan and rhodamine 6G. The Y-axis represents the fluorescence intensity ratio at the measured time and that at the beginning. (**c-d**) photograph of the same film recorded using UV light (305 nm). The film appeared red. (**e**) and (**f**) Photographs of the lyophilized Au NC-chitosan composite recorded using visible and UV light (305 nm).

Further, the fluorescence emission of the solid film and also of the same measured by dissolving in water, after one week exhibited the same characteristic emission as of the original as-prepared solution, pointing to the stability of the NCs in solid form (**Figure 5.4a-b**). Thus the current method not only produced highly luminescent Au NCs but also those which could be stored in the solid form. That the NCs could be finally obtained in stable solid form and stored for use is new as far as literature report is concerned. In addition, chitosan is non-toxic, biodegradable and easily available derivative of natural polymer. Therefore, this fast and facile method of preparation of water-soluble highly

fluorescent Au NCs could possibly be adopted for large scale production of NCs, necessary for commercial use.

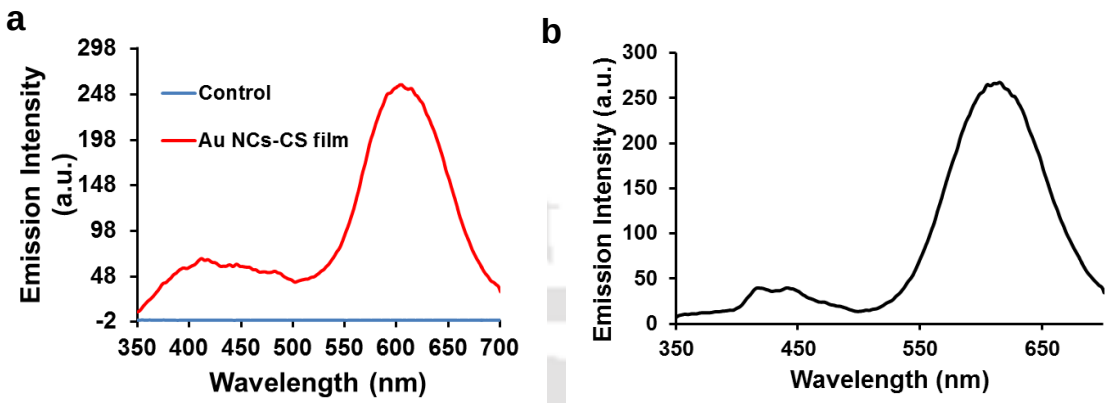

Figure 5.4 Fluorescence emission spectra of the solid samples: (**a**) film of control (chitosan only) and Au NC-chitosan. (**b**)The fluorescence spectrum of a lyophilized measured following dissolution in water (at pH 6.2).

5.4.2. pH dependent reversible change in the emission of Au NCs

Interestingly, it was observed that the luminescence of Au NCs could be reversibly tuned by altering the pH of the medium. For example, on raising the pH from 6.3 to 9.0, the emission maximum of the major peak of as-synthesized NCs gradually shifted from 612 nm to 630 nm. This was accompanied by decrease in the intensity of emission, which diminished greatly at above pH 9.0. It may be mentioned here that at higher pH chitosan is insoluble in water and thus precipitation of the composite could also contribute to reduction in intensity. However, the accompanying increase in intensity of the peak occurring in the region of 400 - 450 nm indicated the effect of pH as the primary origin of the observed changes. Further, when the pH of the solution was again made acidic by adding diluted HCl into the basic solution, the fluorescence peak reverted back to its earlier positions and on lowering the pH below 6.3, blue shift of emission peak was observed (**Figure 5.5a**). Separately, when the pH of medium was adjusted to a value of 4.5 from the original 6.3, the peak not only shifted to 580 nm but also its intensity increased substantially. However, upon further decrease of pH to a value of 2.5, the

intensity at 580 nm increased, without any change of the emission wavelength (**Figure 5.5b**). On the other hand, the positions of the smaller peaks (400-450 nm) remained unaltered but the intensity decreased with lowering of pH. The results indicated that not only was the fluorescence dependent on the pH of the medium but also was reversible with respect to change in pH of the medium over a wide range (**Figure 5.5c**). Interestingly, the thin films of the composite prepared from the medium at pH 4.0 and 7.0 emitted yellow and orange colors, respectively (**Figure 5.5d- e**). The results thus indicated not only pH tunable emission of the clusters in the medium but also in solid form. It is important to mention here that a film could not be formed at higher pH as majority of the composite settled due to insolubility of chitosan.

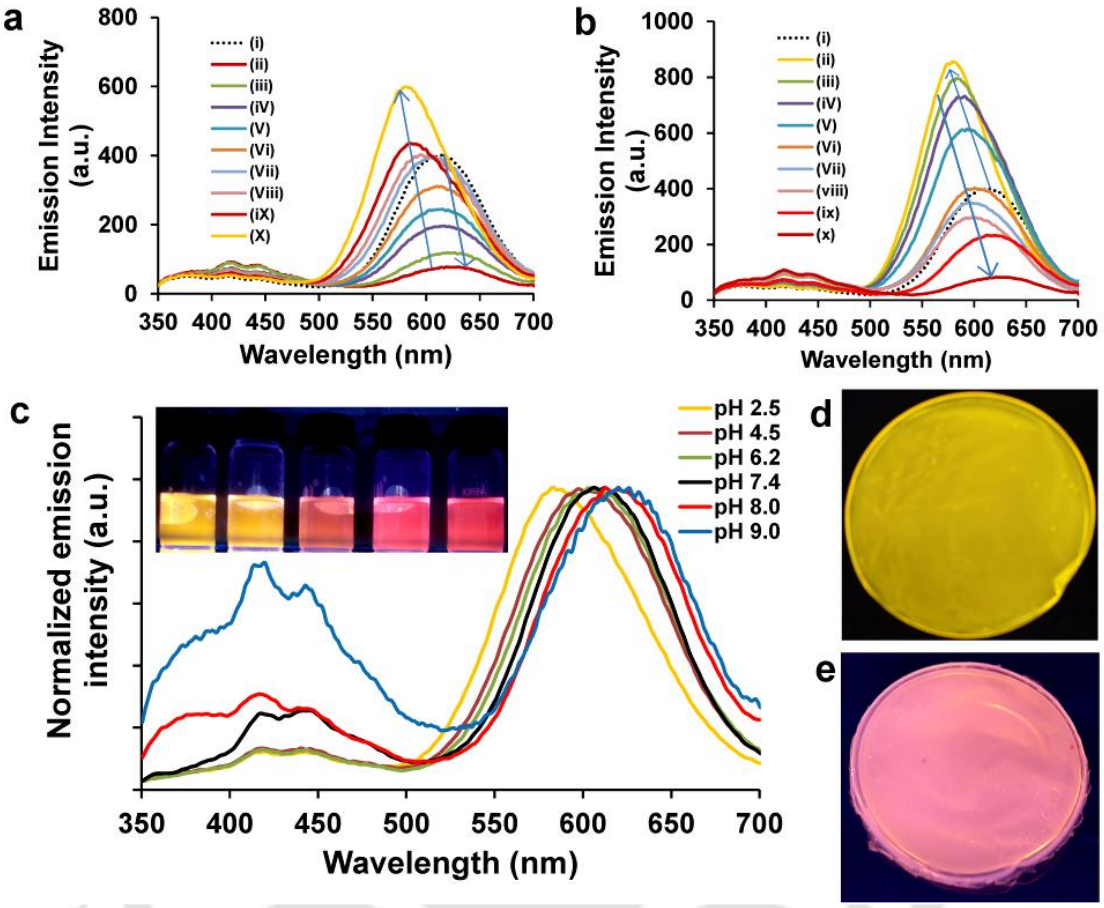

Figure 5.5 (**a-b**) In both the panels, the emission spectrum of as-synthesized NCs is marked by dotted line (i). For the spectra reported in panel (**a**) the pH of the medium of as-synthesized Au NCs was first increased by adding 0.3 M NaOH, which decreased the emission intensity with a red shift of the emission peak as in (ii). To this medium, (iii) 0.1 m M , (iv) 0.3 mM, (v) 0.5 mM , (vi) 0.7 mM, (vii) 1.0 mM (viii) 1.2 mM, (ix) 1.5 mM and (x) 2.0 mM dilute HCl was added, which resulted in the resumption of the fluorescence intensity with gradual blue shift. On the other hand, for the spectra reported in panel (**b**) the pH of the medium of as-synthesized Au NCs was dropped first by adding 0.1 M HCl, which resulted in the increase of fluorescence intensity accompanied by blue shift of the emission peak as in (ii). To this medium, (iii) 0.2 mM, (iv) 0.5 mM , (v) 0.7 mM , (vi) 1.0 mM, (vii) 1.2 mM, (viii) 1.5 mM, (ix) 2.0 mM and (x) 2.5 mM dilute NaOH was added, which resulted in the decrease of fluorescence intensity with gradual red shifting of the emission peak. (**c**) Plots of pH-dependent emissions of Au NCs with intensity normalized to the maximum. In the inset, the photographs of the solutions at different pH values, recorded using a UV light source (305 nm). (**d-e**) UV-light illuminated photographs of the composite films. The pH of the parent medium was 4.0 (**d**) and 7.0 (**e**) respectively.

It may be noted here that photoluminescence of Au NCs has been explained based on their size, free electron density surrounding the metal core and also on the interactions with the species stabilizing them.[5, 2, 40, 42] Thus, while discretization of energy bands owing to quantum confinement of electrons could primarily account for the extraordinary emission, charge transfer involving metal core, surrounding shell and surface ligands also contribute to the tuneability of energy gaps. In the present case, ligand-to-metal charge transfer (LMCT) could primarily account for the change and reversibility of fluorescence based on the pH of the surrounding medium. In that context, the structure of $[Au_n(SC_2H_4COO\text{-})_m]$ can be considered to be consisting of core-shell geometry with Au core forming -S-Au bond with the negatively charged MPA ($-SC_2H_4COO^-$). This was partly supported by FTIR spectral analysis (**Figure 5.6**). Notably, the characteristic peak due to -SH stretching of MPA at ~2594 cm^{-1} was absent in the FTIR spectrum of the sample. This could possibly be due to formation of -S-Au bond. On the other hand, the peak corresponding to –CO stretching (carboxyl group) of MPA (albeit weak) and that due to –NH stretching of chitosan appeared at 1710 cm^{-1} and at 3470 cm^{-1} respectively. The overall negative charge of the cluster helps it to be stabilized by the positively charged NH_3^+ group of chitosan. On the other hand, it could also be possible that the clusters were actually stabilized by both NH_3^+ groups of chitosan and $–COO^-$ groups of MPA. Thus at acidic pH the amine group would remain positively charged with carboxylate being neutral. On the other hand, under alkaline conditions neutral $-NH_2$ along with $–COO^-$ of MPA would remain bound to the clusters. The difference in charges and nature of the bonds would alter the emission behavior of the NCs as a function of pH of the medium. The exact energy levels of the clusters would, however, be dependent on the pK_a of the functional groups stabilizing them.

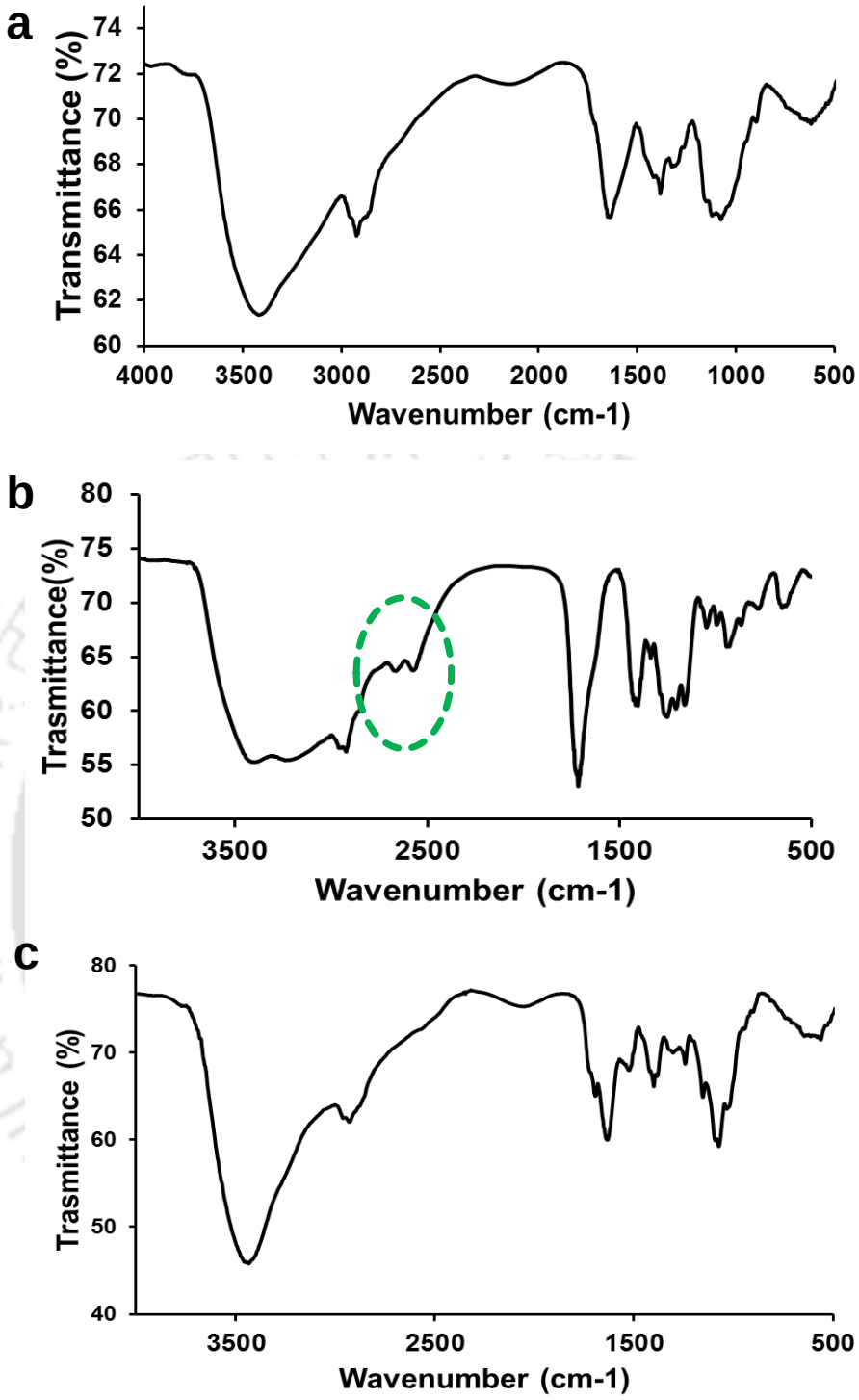

Figure 5.6 FTIR spectra of (**a**) chitosan, (**b**) MPA (-SH stretching is marked by green circle) and (**c**) Au NC –chitosan composite.

MALDI –TOF mass spectrometric analyses of the samples prepared at different pH revealed that the clusters remained unaltered in different pH. The molecular formula of the cluster remained same at different pH, although the degree of protonation varied, depending on the pH of the medium. For example, the mass spectral analysis indicated the presence of $[Au_{20}(MPA)_{15} + 3\ Na^{+} - 11\ H^{+}]^{8-}$ species at pH 8.0; on the other hand, when the pH of the medium was 7.2 and 4.8, the species present were $[Au_{20}(MPA)_{15} + 3\ Na^{+} - 7\ H^{+}]^{4-}$ and $[Au_{20}(MPA)_{15} + 3\ Na^{+} - 4\ H^{+}]^{-}$, respectively (**Figure 5.7a-d**). Further, measurements of zeta potential at different pH of the medium indicated primacy of occurrence of positive charge at acidic pH (+43.9 mV at pH 4.2), whereas that was decreased to +30.3 mV at alkaline pH (9.0). The photoluminescence quantum yield of the NCs also varied with pH. For example, the maximum yield of 14.7% was observed at pH 4.2, whereas that was reduced to 8.03 % and 2.51% at pH 7.4 and 9.0, respectively. Overall, the above results indicated that the presence of chitosan and MPA as the stabilizers not only conferred stability to the NCs but also the ability to tune the optical emission based on the charge manipulation of the species present on the surface of the clusters. Thus the material i.e. the Au NCs with their inherently superior optical properties and the control over their emission, using charges of the stabilizing species, provided a new way of tuning their optical properties, based on acid-base chemistry of the medium. This, arguably, brings in new prospects for exploring their application potential using principles of chemistry.

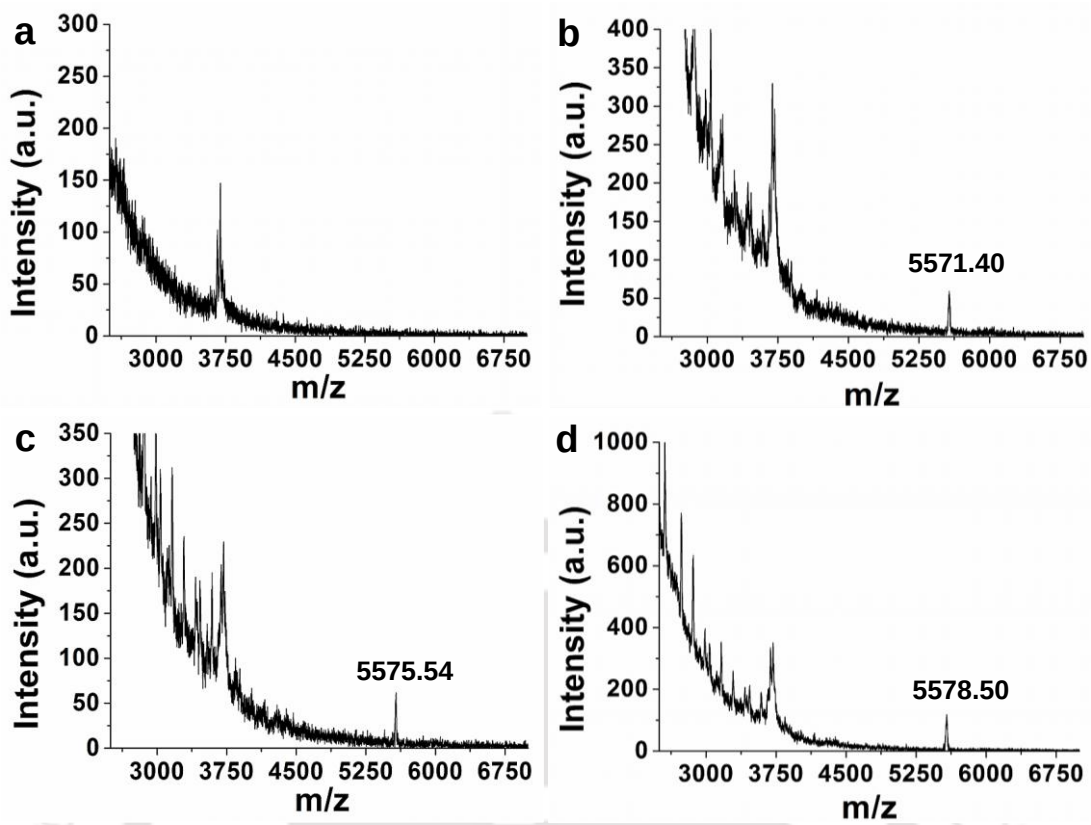

Figure 5.7 MALDI-TOF results of (**a**) chitosan plus MPA mixture. The results in (**b**), (**c**) and (**d**) are from the Au NC- chitosan composite at different pH (basic, neutral and acidic, respectively). The molecular formula can be defined as $[Au_{20}(MPA)_{15} + 3\,Na^{+} - 11\,H^{+}]^{8-}$ in basic pH (8.0) and the same at pH 7.2 and 4.8 can be written as $[Au_{20}(MPA)_{15} + 3\,Na^{+} - 7\,H^{+}]^{4-}$ and $[Au_{20}(MPA)_{15} + 3\,Na^{+} - 4\,H^{+}]^{-}$ respectively.

5.4.3. Synthesis of the Au NCs CS NPs for bioimaging

An important class of applications of the brightly fluorescent, multi-color emitting, highly photostable and potentially non-cytotoxic Au NC-chitosan composite could be in theranostics. This could involve cell imaging; this may also be delivering drug to target organ (and cells therein) with simultaneous use of the fluorescent properties for imaging. In one hand, smallness of the size of the clusters and their surface properties (if suitably modified) would allow their delivery to almost all parts of the body, including circulatory system and cells. On the other hand, size, structure or charge on the polymer- at physiological pH may - not favor their transport and delivery to organs and cells easily. This includes size-selective exclusion of the polymer from entering cell membrane. Thus it may appear to limit the application potential of the current composite. Fortunately,

chitosan polymer could be converted into NP fairly easily using the well-established ionic gelation method. It was observed that NPs of the Au NC-chitosan composite could also be formed without sacrificing the properties of the NCs. For example, the emission maximum of the composite NP was observed to be at 612 nm, when excited by 300 nm light, which was the same as that of the as-synthesized composite. In addition, the QY was measured to be 6.9 % (at pH 7.4) which was also close to the value of as-synthesized composite. Further, the Au NC-chitosan NPs exhibited a mean hydrodynamic diameter of 92.2 nm and zeta potential of +24 mV. The results indicated an ideal size regime of the composite NPs which could be utilized for cellular delivery. Additionally, TEM analysis (**Figure 5.8b- c**) indicated that the average size of the composite NP was 72.1 ± 21.8 nm, which is close to the hydrodynamic diameter measured in the liquid medium. More importantly, it was observed that the average size and shape of the Au NCs remained unaffected following conversion of chitosan into NPs i.e. the composite NPs. The observed mean size of the NCs in the composite NP was found to be 1.23 ± 0.56 nm. Thus, not only do we have a fast and convenient method of synthesis of highly fluorescent Au NCs in a biopolymer but also have a way of converting the bulk polymer into NPs, with NCs being embedded in them, along with retention of their optical properties. This fulfills an important requirement as far as use of the NCs in theranostic applications is concerned. An easy and established probe for cellular indicators - be it drug delivery or functional understanding of phenomena – is based on optical imaging. In general, organic dyes are used for this purpose; they are chosen such that their emission profiles are specific to cellular regions or events - which could then easily be distinguished. In order to check the potential of the composite NPs for imaging application, they were drop-cast from the dispersion medium onto glass slides, followed by observation under epi-fluorescence microscope. The results are shown in **Figure 5.7d-e**. As is clear from the figures, isolated particles with emission distinct from the background could be observed in all the three images. More interestingly, when excited by UV, blue and green light the same particles could easily be observed to be emitting blue, green and red light respectively. This can, arguably, be considered extraordinary as this seems to be the first report where all three basic colors are emitted by the same set of NCs. Although, there are literature reports of preparation of Au NCs emitting different colors, 40, 43 however, there are none where different colors are emitted by the same set of NCs. That the evaporated (solid) NP sample emitted color which could easily be

recorded microscopically is of potentially great advantage in applying these NC containing NPs for cellular probes.

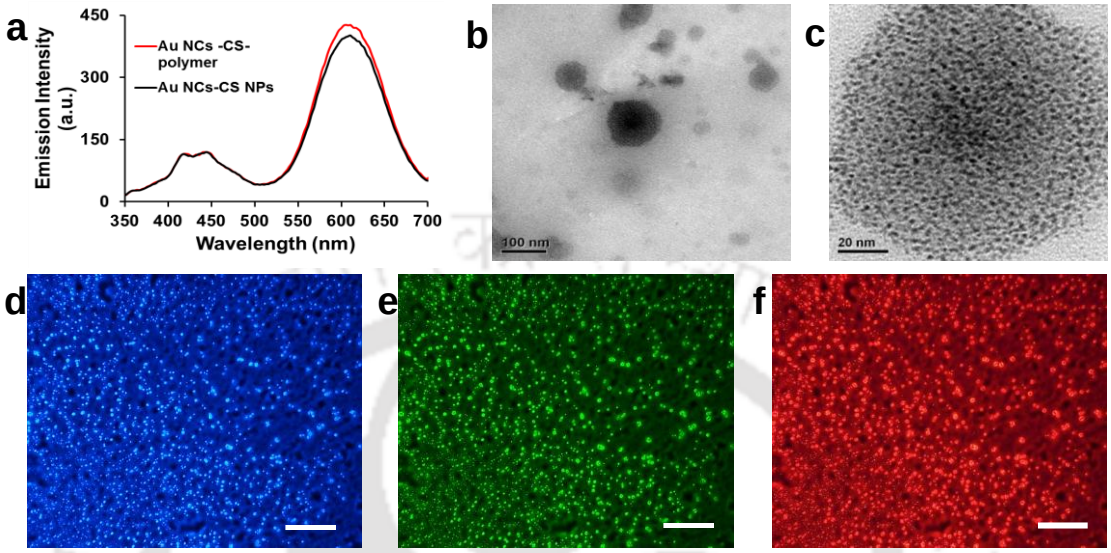

Figure 5.7 (**a**) Fluorescence spectra of the Au NCs (in chitosan) recorded before and after the formation of composite NPs. (**b**) Typical TEM inage of the composite NPs. (**c**) Magnified TEM image of a composite NP, which illustrated that Au NCs retained their sizes and shapes following the formation of the NPs. (**d-f**) Fluorescence microscopic images of the composite NPs. The composite NP-containing medium was evaporated on a glass slide in order to record the images. The three colors, namely, blue, green and red were observed when the sample was excited by UV, blue and green light respectively.Scale bar is 10 μm.

In order to test the suitability of these NPs for use as intracellular probes, human cervical cancer (HeLa) cells were incubated with 50 µg /mL of the NPs in cell culture medium for 4 h, followed by microscopic imaging. The results are shown in (**Figure 5.8a-d**). Interestingly, emissions in the form of all three basic colors, namely, blue, green and red, could be observed to be emanating from the cells. Also, the images indicated that NPs were possibly present in both the nuclei and cytoplasm giving rise to emissions from the whole cells. Control experiments with cells only indicated that these colors were indeed due to NPs (containing Au NCs) and not from any other source. It may be noted here that cellular auto-fluorescence may also give rise to emission at the selected wavelength, thereby providing a false signal or interfere with the real signal. It would thus be important to find out whether such distinction could be made in the presence of competing signals. To address this, DAPI (4',6-diamidino-2-phenylindole, dihydrochloride) , one of the widely employed nuclear staining fluorescent dyes, was used as positive control along with the introduction of fluorescent NPs to the cells. DAPI was added 4 h after addition of the NPs to the medium. Wavelength selective excitation of the cells revealed that green and red emissions could be observed in the presence of the characteristic blue emission of DAPI (**Figure 5.8e, f**). The results not only indicated that the NCs, as delivered to the cells in the form of composite NPs, gave rise to imaging with clarity but also their emission color which could easily be discerned in the presence of parallel emissions in similar wavelength range.

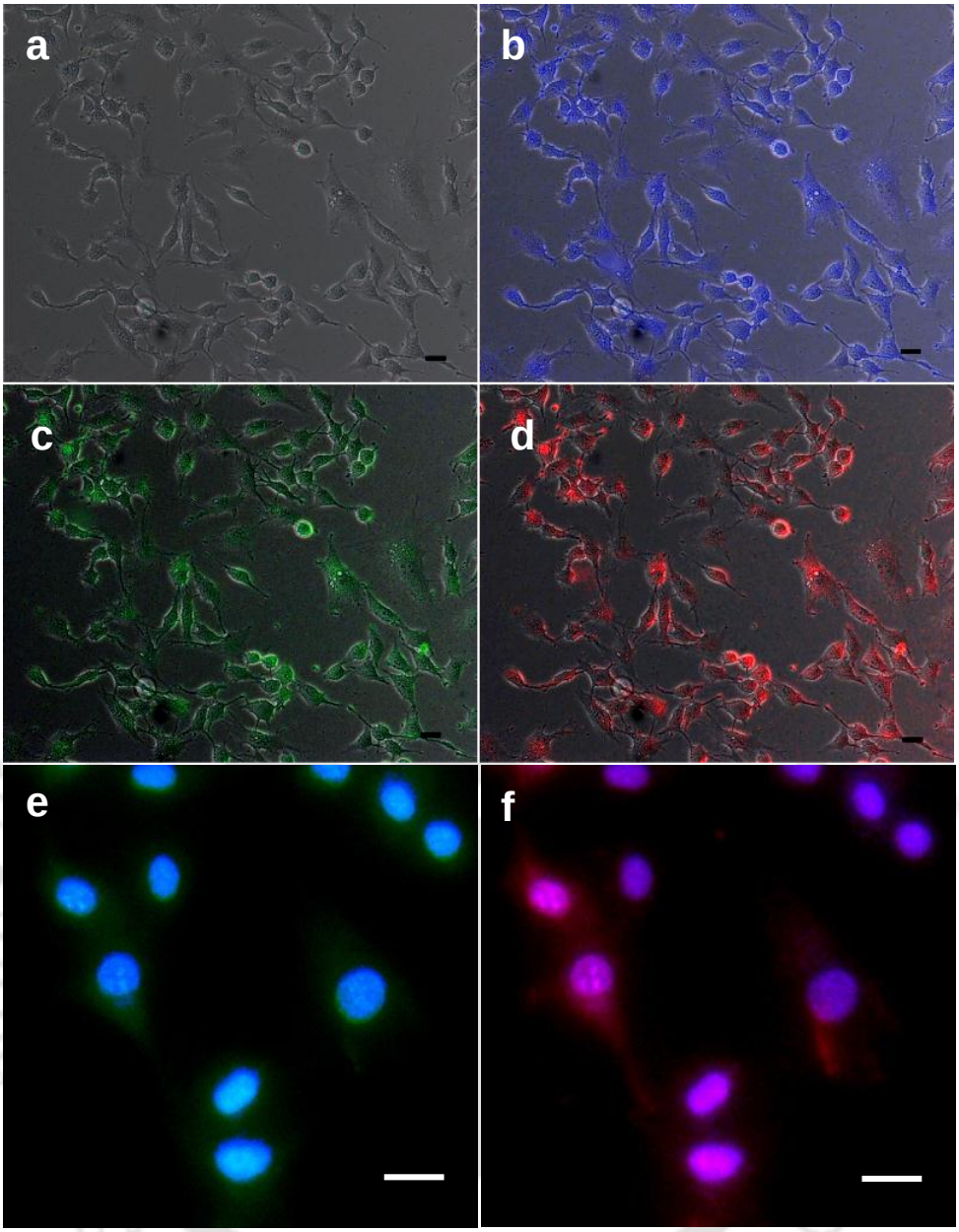

Figure 5.8 The images were recorded following treatment for 3 h. (**a**) is bright field image; (**b**),(**c**) and (**d**) are the fluorescent images merged with bright field of the same cells when excited by UV, blue and green light, respectively. (**e-f**) Magnified merged fluorescence images of same cells recorded after staining with nucleus specific dye DAPI. The blue color of the stained nuclei could be observed along with the green and red fluorescence (due to the presence of Au NCs). Scale bar: 20 µm.

An important issue that needs to be settled here is the origin of three-color emission from the same set of Au NCs present in the NPs. As mentioned earlier, TEM investigations revealed that the Au NCs present in the composite NPs had sizes of 1.23 ± 0.56 nm. This means considerable difference in sizes of the produced particles constituting the NCs. This could potentially be the origin since the energy level discretization scales with $N^{-1/3}$ (N being the number of atoms in the cluster). Thus small difference in the particle size would mean a significant difference in the energy level separations of corresponding particles, giving rise to significant difference in their emission wavelengths.[43-44] It should be noted here that control experiment indicated the presence of a weak background fluorescence in the blue region due to chitosan, which became stronger following synthesis of the NCs. This indicated the role of NCs in the emission in the blue region also.

That the three basic colors were emitted by the NCs and could be observed microscopically when present inside cells is vital to their applications in cellular imaging. However, in order for the NCs (in the composite NPs) to be useful as fluorescent probes for cellular imaging *in vivo* they must necessarily meet the criterion of non-cytotoxicity. The test for potential cytotoxicity of the NPs was performed following the well-known 3-(4, 5-dimethylthiazolyl-2)-2, 5-diphenyltetrazolium bromide (MTT) assay. The results (**Figure 5.9b**) indicated that the NC containing NPs were not cytotoxic to mammalian cells and thus could possibly be used for imaging *in vivo*. For example, at an amount of NPs (100 µg /mL) which is double of what was used for imaging, there was only about 5 % cell death, indicating sufficient viability of the cells in the presence of the composite NPs. It may be mentioned here that for the last few decades, semiconductor nanocrystals otherwise known as quantum dots (Qdots) have been widely employed as cellular and *in vivo* imaging agents, replacing the traditional fluorescent organic dyes - which themselves have poor photo-stability and tracking life time.[46-48] However, apparent cytotoxicity of majority of Qdots is limiting their large-scale use in biomedical applications.[49] On the other hand, Au NCs are not only highly fluorescent with good photo-stability but also non-cytotoxic. Thus, they can be considered as important candidates for replacement of existing imaging modalities during real time molecular tracking and *in vivo* imaging. In that regard, the composite NPs with embedded Au NCs would form model imaging agents.

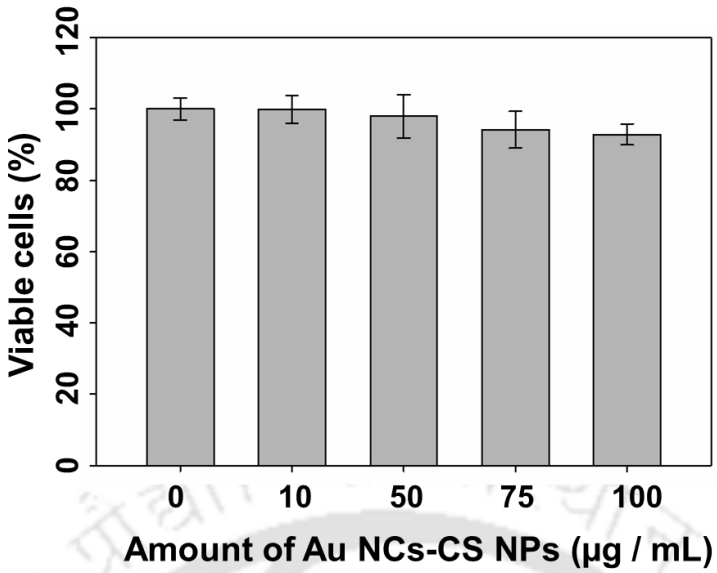

Figure 5.9 Cell viability assay (MTT assay) following treatment with the Au NC-chitosan NPs. The results indicated that the composite NPs did not result in significant cell death at both the concentrations used (50 and 75 µg/mL). The values are represented as mean ± SD of three individual experiments.

5.4.4. Suicide gene delivery to the cancer cells

Exclusive color emission of the Au NCs and favorable physicochemical properties of CS NPs prompted us to investigate the theranostic potential of the composite NPs. This was pursued by testing their ability to deliver suicide gene and kill cancer cells. Treatment of cancer continues to be a major challenge as use of conventional chemotherapeutic agents brings in unavoidable toxicity and serious side effects due to their poor pharmacokinetics and non-specificity. It has been established that tumor tissues consist of leaky angiogenic vessels and have poor lymphatic drainage.[50-52] In this regard, NP-mediated delivery of therapeutic agents has superior potential, owing to their critical size regime allowing the particles to permeate and accumulate in tumor tissues in comparison to normal tissues. This phenomenon of passive targeting is commonly referred to as 'enhanced permeability and retention (EPR)'.[53] As a test case, the current NPs were employed to deliver suicide gene, which produces bi-functional cytosine deaminase-uracil phosphoribosyltransferase (CD-UPRT) enzyme, where CD converts nontoxic prodrug 5-fluorocytosine (5-FC) to toxic drug 5-fluorouracil (5-FU). Additionally, uracil phosphoribosyltransferase (UPRT), a pyrimidine salvage enzyme converts 5-FU to other metabolites including 5-FdUMP and

5-FUTP, which inhibit DNA replication and RNA synthesis respectively. Thus, co-expression of CD-UPRT genes ultimately leads to death of transfected cells.[54-56]

An important requirement for a viable gene delivery cargo is that it should have fairly strong interaction with the genetic material for efficient delivery to the destination i.e. inside cells and for protection against exogenous DNase. Thus, before pursuing the experiments involving transfection of gene (CD-UPRT) into the cancer cells, the DNA binding and nuclease protection assay by the composite NPs were performed. In order to probe DNA binding efficacy, different amounts of the composite NPs were incubated with pDNA followed by agarose gel electrophoresis. The results (**Figure 5.10a**) revealed that the amount of pDNA migration reduced gradually with increasing concentrations of the NPs. For example, when 0.2 and 0.5 μg mL^{-1} of composite NP were added to 0.5 μg mL^{-1} pDNA, there was observable migration of DNA with lesser amount for the higher concentration of the composite (**Figure 5.10b**). On the other hand, for addition of 1.0, 2.0 and 3.0 μg mL^{-1} of the NP there was no migration at all and the DNA was localized in the wells. This indicated incorporation of pDNA in the composite NP and their stability when embedded in the composite. Thus, from the gel electrophoresis study, it was clear that more than 1.0 μg of Au NC-chitosan NPs was required to form suitable polyplex with the 0.5 μg of pDNA.

In order to further probe the stability of the pDNA in the composite NP, DNase protection assay was performed. The results of gel electrophoresis analysis, following treatment of the DNA-composite NP polyplex with DNase, are shown in **Figure 5.10b** of. The results indicated that for a fixed concentration of DNA the intensity of smeared band due to fragments of DNA, being produced following digestion by DNase, decreased with the increase the amount of NP, indicating stability of the DNA in the polyplex structure. For example, when the amounts of composite NP was 0.2, 0.5 and 1.0 μg mL^{-1}, for the same amount of pDNA (0.6 μg mL^{-1}), there was smearing of band but the same decreased with increased NP concentration. On the other hand, for the NP concentration of 2.0 and 3.0 μg mL^{-1} there was no smearing. The DNA was observed to have been retained in the well, indicating protection against cleavage by the enzyme. Thus, the results demonstrated that pDNA formed stable polyplex with composite NPs and was not susceptible to degradation by exogenous DNase.

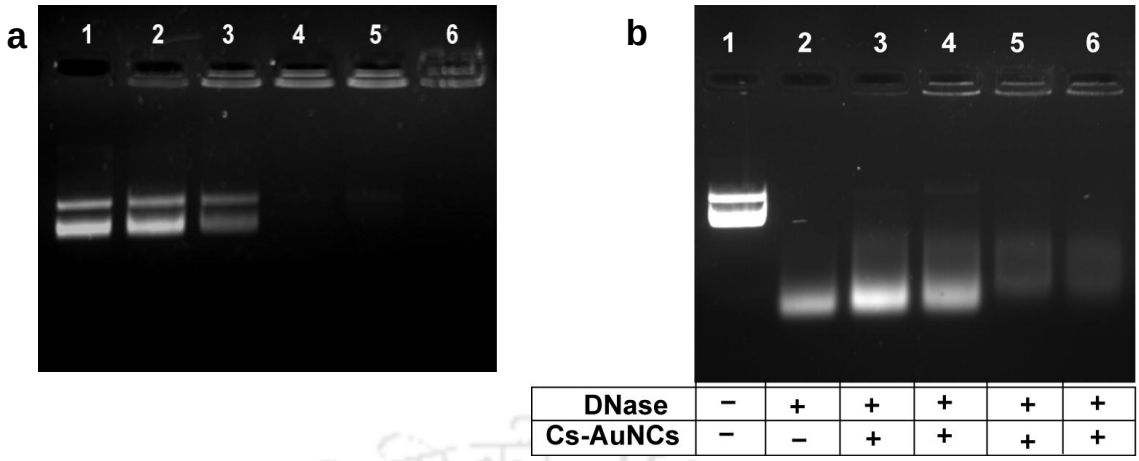

Figure 5.10 (a) DNA binding Assay. Lane 1: control DNA. Lanes 1-6 : pCD-UPRT (0.5 µg) incubated with varying concentration of Au NCs chitosan NPs (0.2, 0.5, 1.0, 2.0 and 3.0 µg respectively). The gel microgram revealed that migration of pDNA was gradually hindered with increasing concentrations of Au NCs chitosan NPs, and pDNA was completely blocked into the well at the highest concentration of Au NCs chitosan NPs. (**b**) DNAse protection assay. The polyplexed of pDNA and chitosan NPs were used to carry out the DNAse protection assay. Lane 1: control DNA. Lanes 2-6: different concentrations of Au NCs chitosan NPs (0.2, 0.5, 1.0, 2.0 and 3.0 µg respectively) and pDNA (0.6 µg) incubated with DNAse enzyme. It is clear from the gel microgram that in the Lanes: 2-3, due to inadequate amount of Au NCs chitosan NPs, most of the DNA remained free, which were degraded by exogenous DNase and formed smear in their corresponding lanes, whereas with the gradual increase of the amount of Au NCs chitosan NPs and by keeping the amount of DNA fixed, the DNA remained protected from DNase and was observed in the respective wells (lanes: 4-6).

Interestingly, following treatment with pDNA, the average hydrodynamic diameter of the Au NC-chitosan composite NP was found to have been increased from 92.2 nm to 159.3 nm (**Figure 5.11a**). The increase in diameter indicated interaction between the DNA and NP. Further, zeta potential was measured to have decreased from +24 mV to +20 mV (**Figure 5.11b**). This possibly means an electrostatic interaction between the NP and the DNA. Chitosan is positively charged under physiological pH owing to abundance of $-NH_2^+$ moiety in its structure. On the other hand, the overall negative charge of pDNA would lead to polyplex formation due to electrostatic interaction between the two species.[57 -58] This would lead to reduction in the zeta potential value of chitosan. The stability of the complex against DNase enzymatic action indicated its potential for DNA

delivery. It may be mentioned here that although viral vectors are used as efficient gene delivery vehicles, there are still concerns of their usage owing to immunogenicity and other biosafety issues. There are thus requirements of alternative methods of delivery of genes to affected tissues. In this context, use of chitosan and Au NCs in the form of composite NPs could be considered important, as they meet the criteria of size of the final complex, protection of DNA against digestion by nuclease, and possibly retaining structural integrity of the DNA. That the overall size of the polyplex was measured to be about 159 nm indicated their potential in gene delivery to cancer tissues preferentially to healthy ones. [59-60] this, however, needed to be tested.

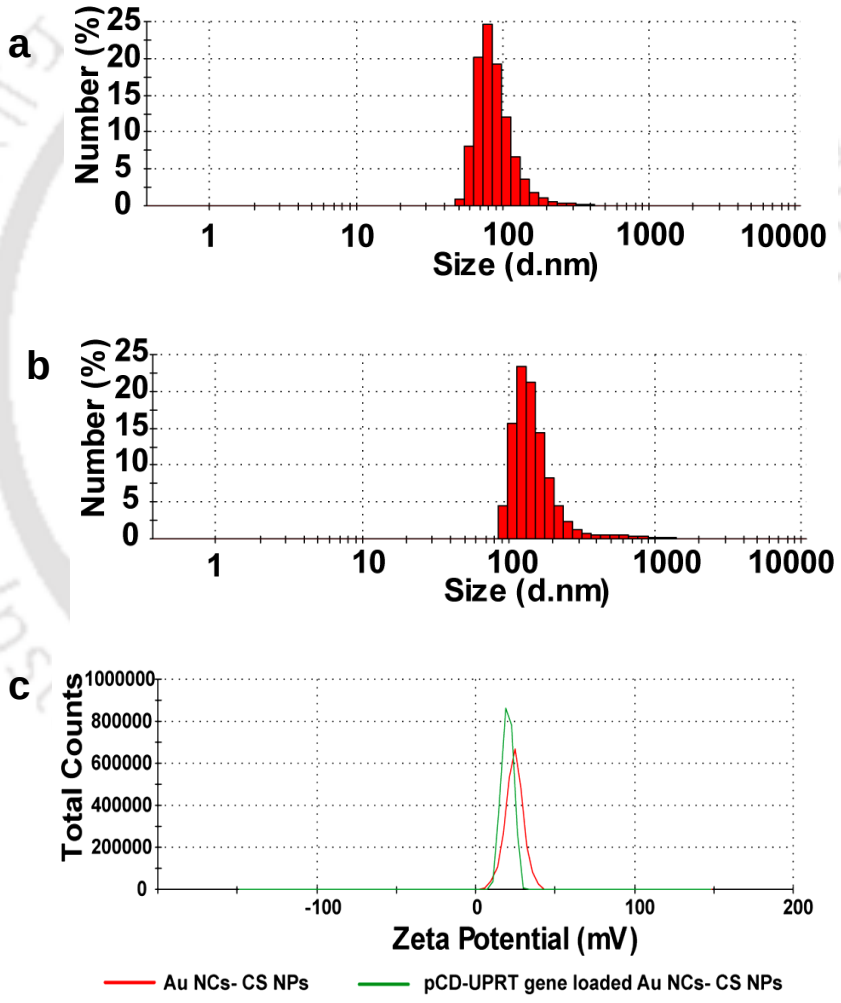

Figure 5.11 Particle size analyses results of (a) Au NC-chitosan NPs and (b) gene-loaded Au NC-chitosan NPs. Zeta potential measurement results of Au NC-chitosan NPs before and after loading of gene.

The test for potential of the composite NPs for gene delivery was carried out with *in vitro* delivery of the suicide gene (CD-UPRT) to human cervical cancer (HeLa) cells. In gene therapy, the emergence of cellular imaging by fluorescent probe is convenient for real-time evaluation of the therapeutic approaches and their optimization.[61] As discussed before, the specificity of properties of the Au NCs make their choice ideal for probe, especially when embedded in a drug delivery vehicle. They also represent important replacement of conventional organic dyes, especially due to their photostability and high quantum yield. This was observed to be all the more interesting as their multi-color emission allowed probe of cellular delivery of the composite NPs using flow cytometry. Thus the delivery of gene loaded composite NPs to the cancer cells could be probed by using FACS (fluorescence activated cell sorter), without the use of traditional dyes. When the cells were incubated with different amount of gene-loaded Au NC-chitosan NPs for 4 h, a prominent shift of fluorescence intensity in FL3-H (low pass / 670 nm) channels, which correspond to red fluorescence, was observed in comparison to signals of controls such as those of cells treated with only chitosan NPs and only gene-loaded chitosan NPs (i.e. without Au NCs) and cells in absence of any treatment**.** It should be noted here that, the shift of fluorescence intensity was maximum in the FL3-H channel which was comparatively less in FL1-H channel (band pass 530/30 nm) and much less in FL2-H (band pass 585/42 nm) channel. This was possibly due to large Stokes shift of the metallic Au NC emission, as blue laser (available in FACSCalibur, Ex. 488 nm) was used for excitation of the Au NCs. Further, two different doses of gene-loaded Au NC-chitosan NPs were used (50 μg mL^{-1} and 75 μg mL^{-1}) for FACS analysis, upon which a gradual shift of fluorescence intensity in FL3-H channel occurred, confirming the interaction of NPs with the cells (**Figure 5.12a**). Next, time-dependent FACS analysis revealed that fluorescence due to NCs could be followed for 8 h (**Figure 5.12b**). This suggests that Au NCs being delivered to the cells in the form of composite NP were stable in the complex cell culture medium and the cellular environment. Thus, the NCs could indeed be used for probing mammalian cells and can compete with organic dyes as a new generation of robust cellular tracking agents.

The NP-mediated gene uptake was further supported by TEM analysis, where incorporation of the composite NPs with NCs in the cell was clearly observed (**Figure 5.12f-i**). The average size of the NC matched with the as-synthesized NCs, confirming not only the uptake of the particles but also retention of their structural integrity, which is essential for their role as support for theranostic devices. Interaction of gene-loaded NPs with cancer cells was further validated by microscopic studies. For that, HeLa cells were treated with gene loaded fluorescent composite NPs for 8 h followed by observation under epi-fluorescence microscope, which (Figure 5c-e) showed the characteristic three color emissions of blue, green and red due to Au NCs, when excited by UV, blue and green light, respectively. Therefore, TEM, FACS and optical microscopy experiments clearly demonstrated the delivery of composite NPs to cancer cells with retention of size and properties of the constituent NCs.

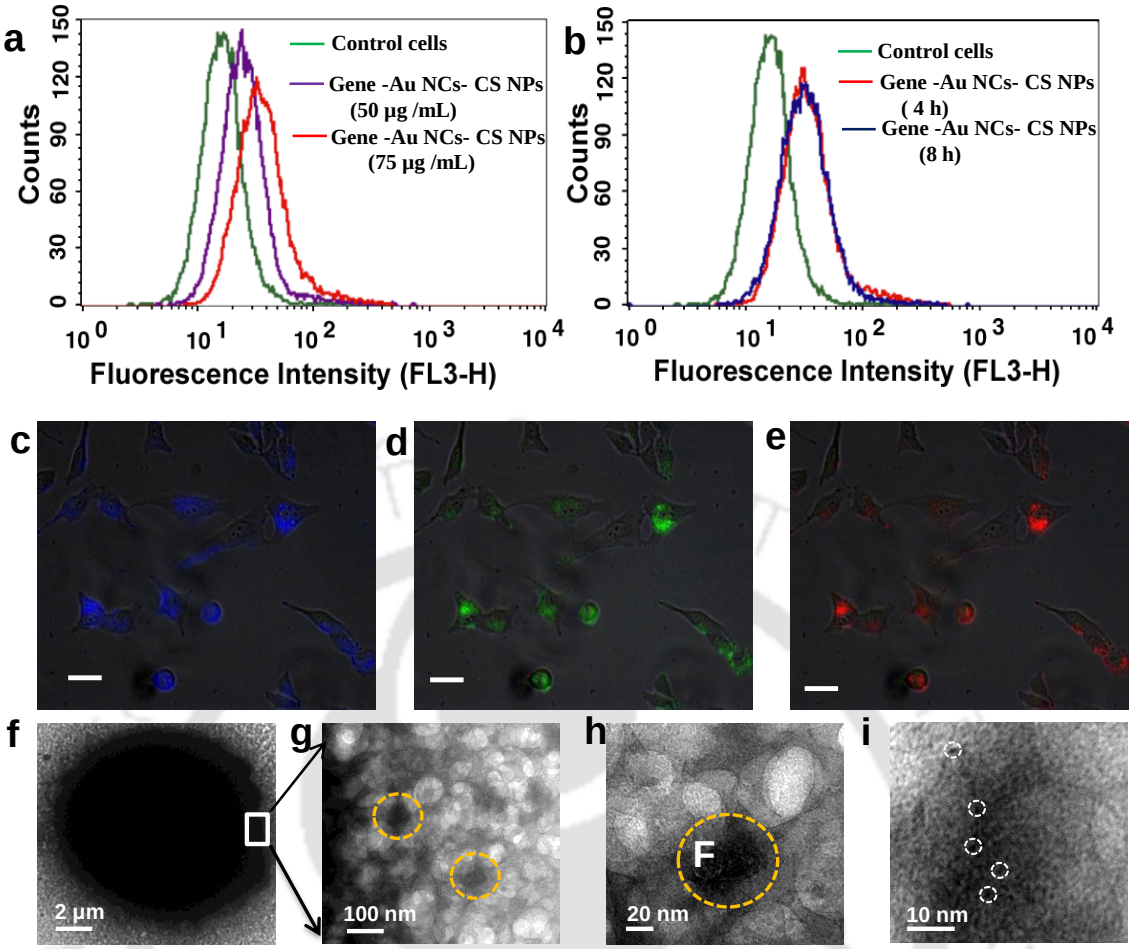

Figure 5.12 (**a**) FACS analysis of HeLa cells was carried out (4 h) after transfection with different amount of suicide gene loaded Au NC-chitosan NPs. The concentrations of the composite NPs were kept at 50 µg/mL and 75 µg/mL. The results indicated dose-dependent change of fluorescence intensity in FL3-H. It may be noted here that additional dye was not used and the fluorescence from Au NCs was used for the probe. (**b**) For the same cells, time-dependent FACS data revealed that the fluorescence due to Au NCs present in the cells remained stable up to 8 h. (**c-e**) Fluorescence microscopy images merged with bright field of suicide gene loaded Au NC –chitosan NP treated cells, which showed the same three colors due to Au NCs after transfection of suicide gene in the HeLa cells. Scale bar: 20 µm. The images were recorded at 8 h following treatment of the cells. (**f-i**) The TEM image of the cells treated with gene-loaded NPs for 8 h. (**g**) and (**h**) Magnified images of cells showed presence of composite NPs (of similar dimensions as those of as-prepared NPs) in the cells, some of which are marked with yellow circles. (**i**) Magnified image of one of the composite NPs showed the presence of Au NCs, some of which are marked with white circle.

Considering that FACS experiments suggested transfection of HeLa cells, by NC and gene carrying composite NPs, it was deemed important to probe cell viability in order to appreciate the potential of gene therapy. This was pursued by addition of different doses of prodrug 5-FC to the transfected cells followed by incubation for 72 h. Subsequently, 3-(4, 5-dimethylthiazolyl-2)-2, 5-diphenyltetrazolium bromide (MTT) assay of the cells was performed. The assay revealed that the viability of the cells decreased gradually with increasing concentration of 5-FC as compared to control cells (**Figure 5.12a**). It is known that in the cells successfully transfected with CD-UPRT plasmid non-toxic prodrug 5-FC gets converted into toxic 5-FU by CD enzyme expressed by the plasmid. The toxic drug (5-FU) eventually kills the cell. That the cells were systematically annihilated upon treatment with the produg following NP delivery clearly established the merit of drug delivery system. Further, the IC_{50} value of 5-FC (at which 50% of cells died) was found to be 14 ± 2.0 μg mL^{-1} 5-FC. This is consistent with previously reported value, thus clearly supporting the validity of the approach.[55, 62-63]

5.4.5. Apoptosis mediated cell death

It would be worth mentioning here that apoptosis or 'programmed cell death' is a common mechanism for exclusion of unwanted cells from the body and is generally a preferred mode of cell death pursued by treatment of any therapeutic agent, whereas necrosis is the sudden death of cells. In order to have an idea of the mechanism of cell death involved in the present case, cell cycle analysis by propidium iodide (PI) staining was performed, which showed that the cell populations in different phases of cell cycle (G0/G1, S, and G2/M) remained unaffected (**Figure 5.12b**), after treatment with suicide gene (as was present in the composite NP), as compared to their respective controls. However, significant increase in sub-G0/G1 population (relating to the apoptotic population) was observed in cells treated with suicide genes (7.1 ± 1.6 %), which was the primary signature of the apoptosis as the mode of cell death (further details are available in **Figure S16c-e**).

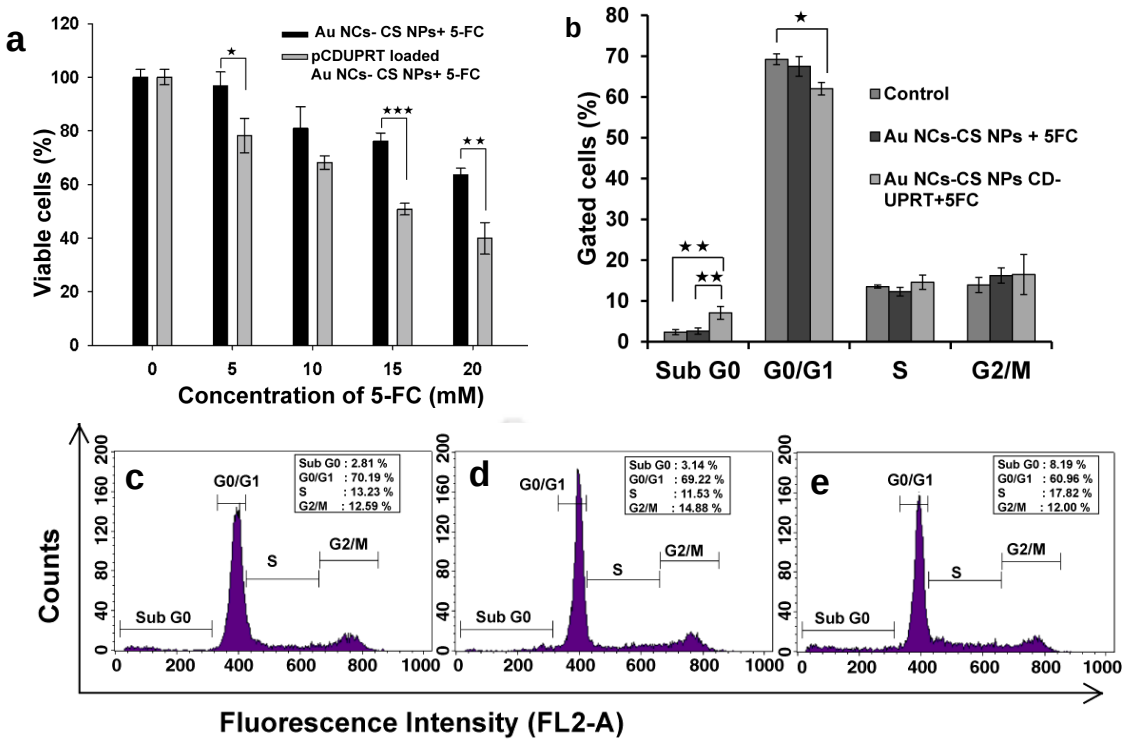

Figure 5.12 (**a**) Cell viability, followed using MTT assay, of cells treated with 5-FC only and Au NC-chitosan NP meditated suicide gene (CD-UPRT) transfected cells following treatment with 5-FC . The values are represented as mean ± SD of results from three individual experiments. Student's-t test was carried out to find out the statistical significance for each concentration between Au NC-chitosan NPs (blank NPs) and suicide gene (CD-UPRT) loaded Au NC-chitosan NPs after treatment with the 5-FC. The statistical significance is denoted by ★($p < 0.05$), ★★($p < 0.005$), and ★★★ ($p < 0.001$). (**b-e**) Cell cycle analysis by FACS. The data represents mean ± SD of three individual experiments. The statistical significance was found out by comparing the control with the different type of treated cells such as treated with blank NPs and suicide gene loaded NPs. The p values represent the same level of significance as described above.

Treated cells were further examined under (FESEM), which (**Figure 5.13a-b**) substantiated the formation of apoptotic bodies. Another important point needed to be addressed is that the mode of cell death was primarily due to apoptosis not necrosis. For this, FITC conjugated annexin-V –PI double staining experiment was performed and was probed by using FACS (**Figure 5.12c-e**). The FACS results illustrated that in the present case, due to functional expression of suicide genes, there was a substantial number of cell population in early (3.7 ± 0.8 %) and late apoptotic (5.5 ± 0.9 %) stages, as compared to the necrotic population (2.1 ± 0.1 %). Moreover, the total apoptotic cells in the early and late stages were found to be~ 9.2%, which was similar to the sub G0/G population observed in PI staining. Overall, the experiments revealed that use of NC containing NPs in suicide gene delivery to cancer cells was effective in carrying out 'programmed cell death'. These results in conjunction with the results from the Au NC based fluorescence microscopy and FACS studies clearly indicated the competitive edge of the use of fluorescent Au NCs over organic dyes in probing the effects of gene prodrug delivery to cancer cells. Also, the current method of synthesis of Au NCs being embedded in chitosan, which can easily be converted into nanocarriers, creates a new concept in theranostics and brings in new ideas in cancer therapy.

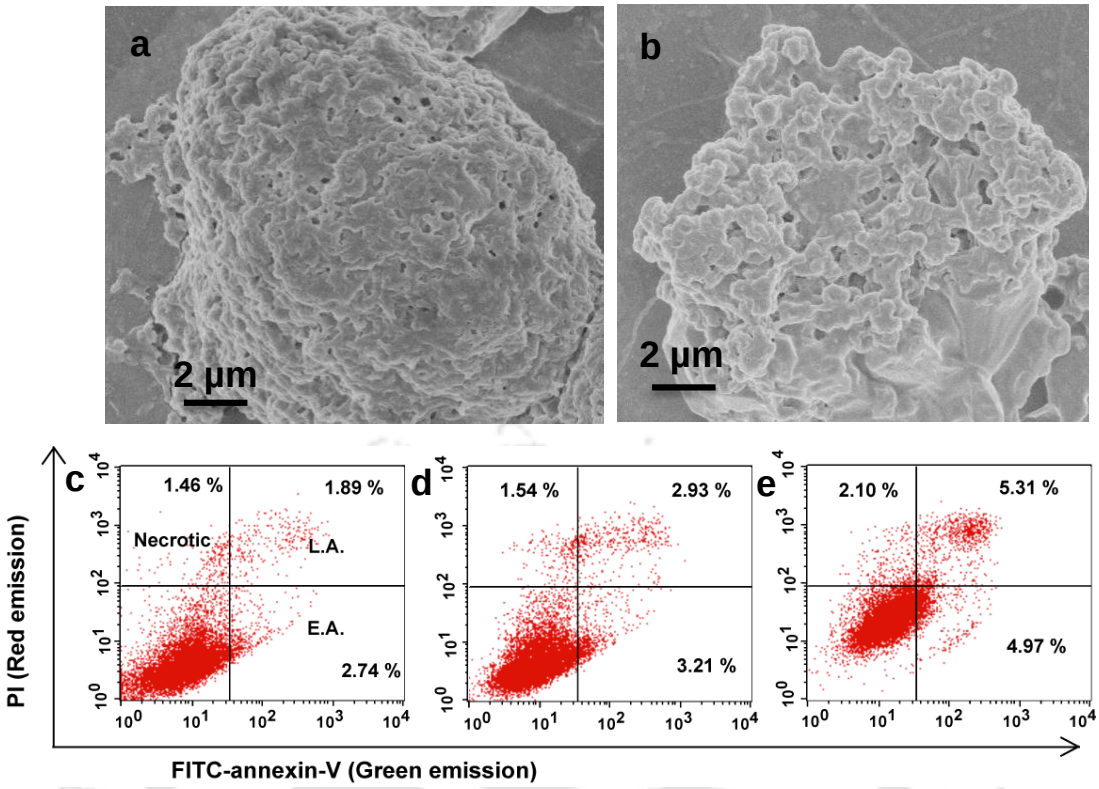

Figure 5.13 (**a-b**) FESEM images of a control cell and a cell treated with suicide gene loaded NPs (followed by treatment with 5-FC). The formation of the apoptotic bodies in case of the treated cells was observed from the FESEM image. (**c-e**) Flow cytometric analyses via FITC conjugated annexin-V-propidium iodide (PI) staining in order to find out the apoptotic and necrotic populations (%). Here (**e**)**,** (**f**) and (**g**) represent the control cells, cells treated with blank NPs and 5-FC and cells treated with suicide gene loaded NPs and 5-FC, respectively. In the dot plots, 1st, 2 nd and 3rd quadrants denote the live, early apoptotic (E.A.) and late apoptotic (L.A.) population of cells, respectively.

5.5. Conclusion

In a nutshell, we have developed a fast and easy aqueous method of synthesis of highly fluorescent, RGB emitting Au NCs, by using chitosan (in combination with MPA) as reducing and stabilizing agents. The Au NCs in chitosan were stable in aqueous phase as well as in solid powder. Results also indicated that surface property or ligand, other than size of the NC, was important in the origin and reversible tuning of fluoresce at different pH of the medium. The use of chitosan helped in the facile formation of composite NPs, which was useful for drug delivery to cancer cells in conjunction with easy imaging. Further, the advantage of emission of three basic colors (RGB) was useful in imaging cells while therapy was being pursued. Additionally, they helped in FACS analysis without the use of additional dyes. Chitosan NPs have been widely employed as suitable gene carriers; however, in the present case the fluorescent property of the delivery vehicle helped in direct evaluation of suicide gene delivery, by performing either FACS or microscopy study. This current method of formation of fluorescent NCs and their use in theranostic application bring in a new approach in modern nanotechnology-based drug delivery. This is expected to augment as well as alter conventional approaches in gene therapy and other drug-based therapeutics.

5.6. References

1. Zheng, J.; Nicovich, P. R.; Dickson, R. M. *Annu. Rev. Phys. Chem.***2007**, *58*, 409–431.
2. Shang, L.; Dong, S.; Nienhaus, G. U. *Nano Today* **2011**, *6*, 401–418.
3. Varnavski, O.; Ramakrishna, G.; Kim, J.; Lee, D.; Goodson, T. *J. Am. Chem. Soc.* **2010**, *132*, 16–17.
4. Shibu, E. S.; Muhammed, M. A. H.; Tsukuda, T.; Pradeep, T. *J. Phys. Chem. C* **2008**, *112*, 12168–12176.
5. Wu, Z.; Jin, R. *Nano Letters* **2010**, *10*, 2568–2573.
6. Hong, S.; Shafai, G.; Bertino, M.; Rahman, T. S. *J. Phys. Chem. C* **2011**, *115*, 14478–14487.
7. Wang, H.-H.; Lin, C.-A. J.; Lee, C.-H.; Lin, Y.-C.; Tseng, Y.-M.; Hsieh, C.-L.; Chen, C.-H.; Tsai, C.-H.; Hsieh, C.-T.; Shen, J.-L.; *et al. ACS Nano* **2011**, *5*, 4337–4344.
8. Tian, D.; Qian, Z.; Xia, Y.; Zhu, C. *Langmuir* **2012**, *28*, 3945–3951.
9. Retnakumari, A.; Setua, S.; Menon, D.; Ravindran, P.; Muhammed, H.; Pradeep, T.; Nair, S.; Koyakutty, M. *Nanotechnology* **2010**, *21*, 055103.
10. Zhang, J.; Fu, Y.; Conroy, C. V.; Tang, Z.; Li, G.; Zhao, R. Y.; Wang, G. *J. Phys. Chem. C* **2012**, *116*, 26561–26569.
11. Valden, M.; Lai, X.; Goldman, D. W. *Science* **1998**, *281*, 1647-1650.
12. Turner, M.; et. al. *Nature* **2008**, *454*, 981-983.
13. Gao, Y.; Shao, N.; Pei, Y.; Zeng, X. C. *Nano Letters* **2010**, *10*, 1055–1062.
14. O'Neill, P. R.; Young, K.; Schiffels, D.; Fygenson, D. K. *Nano Letters* **2012**, *12*, 5464–5469.
15. Wen, X.; Yu, P.; Toh, Y.-R.; Hsu, A.-C.; Lee, Y.-C.; Tang, *J. Phys. Chem. C* **2012**, *116*, 19032–19038.
16. Guével, X. Le; Hötzer, B.; Jung, G.; Hollemeyer, K.; Trouillet, V.; Schneider, M. *J. Phys. Chem. C* **2011**, *115*, 10955–10963.
17. Xie, J.; Zheng, Y.; Ying, J. Y. *J. Am. Chem. Soc.***2009**, *131*, 888–889.

18. Schaeffer, N.; Tan, B.; Dickinson, C.; Rosseinsky, M. J.; Laromaine, A.; McComb, D. W.; Stevens, M. M.; Wang, Y.; Petit, L.; Barentin, C.; *et al. Chem. Commun.* **2008**, 3986-3988.
19. Wei, H.; Wang, Z.; Yang, L.; Tian, S.; Hou, C.; Lu, Y. *The Analyst* **2010**, *135*, 1406-1410.
20. Liu, G.; Shao, Y.; Ma, K.; Cui, Q.; Wu, F.; Xu, S. *Gold Bulletin* **2012**, *45*, 69–74.
21. Pettibone, J. M.; Hudgens, J. W. *ACS Nano* **2011**, *5*, 2989–3002.
22. Duan, H.; Nie, S. *J. Am. Chem. Soc.***2007**, *129*, 2412–2413.
23. Lin, C.-A. J.; Yang, T.-Y.; Lee, C.-H.; Huang, S. H.; Sperling, R. A.; Zanella, M.; Li, J. K.; Shen, J.-L.; Wang, H.-H.; Yeh, H.-I.; *et al. ACS Nano* **2009**, *3*, 395–401.
24. Wu, Z.; Suhan, J.; Jin, R. *J. Mater. Chem.* **2009**, *19*, 622–626.
25. Zhang, H.; Huang, X.; Li, L.; Zhang, G.; Hussain, I.; Li, Z.; Tan, B. *Chem. Commun.* **2012**, *48*, 567-569.
26. Qian, H.; Jin, R. *Chem. Mater.* **2011**, *23*, 2209–2217.
27. Schaaff, T. G.; Whetten, R. L. *J. Phys. Chem. B* **1999**, *103*, 9394–9396.
28. Sanpui, P.; Chattopadhyay, A.; Ghosh, S. S. *ACS Appl. Mater. Interfaces* **2011**, *3*, 218–228.
29. Vassaux, G.; Martin-Duque, P. *Expert Opin. Biol. Ther.* **2004**, *4*, 519–530.
30. Calvo, P.; Remunan-Lopez, C.; Vila-Jato, J.L.; Alonso, M.J. J. Appl. Polym. Sci. **1997**, *63*, 125-132.
31. Negishi, Y.; Tsukuda, T. *Chem. Phys. Lett.* **2004**, *383*, 161–165.
32. Lebedkin, S.; Langetepe, T.; Sevillano, P.; Fenske, D.; Kappes, M. M. *J. Phys. Chem. B* **2002**, *106*, 9019–9026.
33. Luo, Z.; Yuan, X.; Yu, Y.; Zhang, Q.; Leong, D. T.; Lee, J. Y.; Xie, J. *J. Am. Chem. Soc.* **2012**, *134*, 16662–16670.
34. Yuan, X.; Luo, Z.; Zhang, Q.; Zhang, X.; Zheng, Y.; Lee, J. Y.; Xie, J. *ACS Nano* **2011**, *5*, 8800–8808.
35. Qian, H.; Zhu, Y.; Jin, R. *ACS Nano* **2009**, *3***,** 3795–3803.
36. Yu, Y.; Luo, Z.; Yu, Y.; Lee, J. Y.; Xie, J. *ACS Nano* **2012**, *6***,** 7920–7927.
37. Jhaveri, S. D.; Foos, E. E.; Lowy, D. A.; Chang, E. L.; Snow, A. W.; Ancona, M. G. *Nano Letters* **2004**, *4*, 737–740.
38. Murayama, H.; Narushima, T.; Negishi, Y.; Tsukuda, T. *J. Phys. Chem. B* **2004**, *108*, 3496–3503.

39. Schaaff, T. G.; Knight, G.; Shafigullin, M. N.; Borkman, R. F.; Whetten, R. L. *J. Phys. Chem. B* **1998**, *102*, 10643–10646.
40. Zheng, J.; Zhang*, C.; Dickson, R. Phys. Rev. Lett.**2004**, 93,* 077402-1, 077402-4.
41. Guével, X. Le; Trouillet, V.; Spies, C.; Li, K.; Laaksonen, T.; Auerbach, D.; Jung, G.; Schneider, M. *Nanoscale* **2012**, *4*, 7624-7631.
42. Xavier, P. L.; Chaudhari, K.; Baksi, A.; Pradeep, T. *Nano Reviews* **2012**, *3,*14767.
43. Xu, H.; Suslick, K. S. *ACS Nano* **2010**, *4*, 3209–3214.
44. Shen, Z.; Duan, H. W.; Frey, H. *Adv. Mater.***2007**, *19*, 349–352.
45. Shang, L.; Dong, S. J. *Chem. Commun.***2008**, *9*, 1088–1090.
46. Medintz, I. L.; Uyeda, H. T.; Goldman, E. R.; Mattoussi, H. *Nat. Mater.***2005**, *4*, 435–446.
47. Stürzenbaum, S. R.; Höckner, M.; Panneerselvam, A.; Levitt, J.; Bouillard, J.-S.; Taniguchi, S.; Dailey, L.-A.; Khanbeigi, R. A.; Rosca, E. V.; Thanou, M.; *et al. Nat. Nanotechnol.* **2013**, *8*, 57–60.
48. Chang, Y.-P.; Pinaud, F.; Antelman, J.; Weiss, S. *J. Biophotonics* **2008**, *1*, 287–298.
49. Chan, W.; Shiao, N. *Acta Pharmacol. Sin.***2008**, *29*, 259–266.
50. Peer, D.; Karp, J. M.; Hong, S.; Farokhzad, O. C.; Margalit, R.; Langer, R. *Nat. Nanotechnol.* **2007**, *2*, 751–760.
51. Kamaly, N.; Xiao, Z.; Valencia, P. M.; Radovic-Moreno, A. F.; Farokhzad, O. C. *Chem. Soc. Rev.* **2012**, *41*, 2971-3010.
52. Davis, M. E.; Chen, Z. (Georgia); Shin, D. M. *Nat. Rev. Drug Discovery* **2008**, *7*, 771–782.
53. Ruoslahti, E.; Bhatia, S. N.; Sailor, M. J. *J. Cell Biol.* **2010**, *188*, 759–768.
54. Kaliberov, S. A.; Chiz, S.; Kaliberova, L. N.; Krendelchtchikova, V.; Della Manna, D.; Zhou, T.; Buchsbaum, D. J. *Cancer Gene Ther.***2006**, *13*, 203–214.
55. Gopinath, P.; Ghosh, S. S. *Biotechnol. Lett* **2008**, *30*, 1913–1921.
56. Huang, Y.H. et. al. *Cancer Res.* **2009**, *69*, 6184–6191.
57. Han, L.; Zhao, J.; Zhang, X.; Cao, W.; Hu, X.; Zou, G.; Duan, X.; Liang, X.-J. *ACS Nano* **2012**, *6*, 7340–7351.
58. Lee, D.; Mohapatra, S. S. *Methods Mol. Biol.* **2008,** *433*,127–140.
59. Lu, F.; Wu, S.-H.; Hung, Y.; Mou, C.-Y. *Small* **2009**, *5*, 1408–1413.

60. Kim, J.-H.; Kim, Y.-S.; Park, K.; Lee, S.; Nam, H. Y.; Min, K. H.; Jo, H. G.; Park, J. H.; Choi, K.; Jeong, S. Y.; *et al. J. Controlled Release* **2008**, *127*, 41–49.
61. Bogdanov Jr, A.; Weissleder, R. *Trends Biotechnol.* **2002**, *20*, S11–S18.
62. Gopinath, P.; Ghosh, S. S. *Mol. Biotechnol.***2008**, *39*, 39–48.
63. Kawamura, K. *et. al. Cancer Gene Ther.***2000**, *7*, 637–643.

Chapter 6

Single Cycle PCR Based Synthesis of Highly Fluorescent Au Nanoclusters for Gene Expression

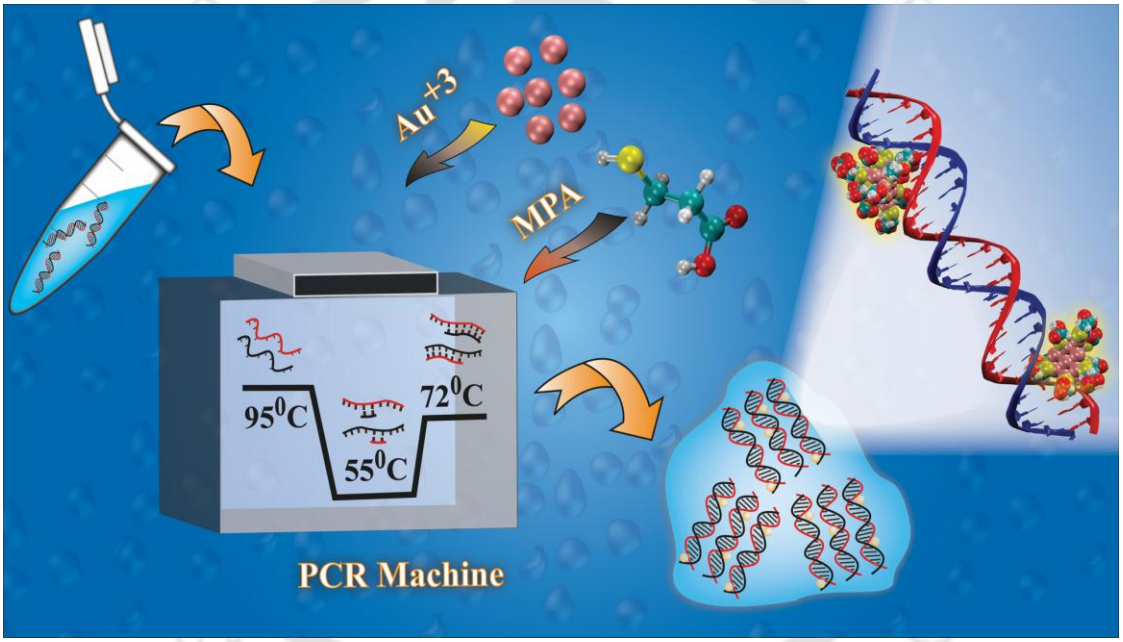

Chapter 6:

Single Cycle PCR Based Synthesis of Highly Fluorescent Au Nanoclusters for Gene Expression

6.1. Introduction

Cellular events occur with high degree of precision depending on the gene expression; – any incongruity of this 'programmed' event imparts severe discrepancies in downstream signaling pathway, leading to several diseases including cancer.[1-3] Hence, it is vital to quantitatively acquire the gene expression (i.e. amount of DNA) in ultra-small scales, which eventually acts as an important diagnostic tool to identify the root causes and further study the progress of diseases to decipher the mystery of several cellular events.[4] Traditionally, the target specific DNA amplification and quantification are done by real time polymerase chain reaction (PCR).[5] In principle, it relies on monitoring of fluorescence signal of the probing organic fluorophore. However, there lies issues with the traditional PCR implementation, which includes the poor photo-stability and toxicity of the organic fluorophore molecule making the system costly and unfavourable for frequent usage.[6] Material science renders significant opportunities to address the issue. Recent progress in the field of 'nanophotonics' has led to a few atomic fluorescent nanoclusters which exhibit excellent photo-physical properties and could be an option for fluorophore.[7] This strong size tunable fluorescent nanostructures not only possess high photo-stability and low photo-blinking but, importantly, being biocompatible[8-9] can form an alternative to the conventional fluorophore for DNA quantification, provided they possess a strong relationship with the intrinsic properties of DNA. Previous reports had demonstrated the synthesis of NCs based on DNA and their various applications like bioimaging,[8] hybridization,[10] sensing,[11] and even study of the single base pair polymorphisms.[12] The methods adopted were cumbersome and time consuming and further a rapid quantification is not carried out, which makes them unfavourable for real time DNA analysis.

DNA serves as excellent scaffold to anchor nanostructures due to its chemical specificity and programmed self-assembly.[13-14] Temperature stability of DNA further

offers flexibility to function at different thermal zones and gives a possibility to modulate the interactions of the scaffold with the nanostructures. Engineering of NPs on the double stranded DNA (ds DNA) or even complex form of DNA such as super coiled DNA (sc DNA) based on specific binding-interactions along with the parallel synthesis of NPs remains one of the major challenges so far.[15] However, an even challenging task would be to engineer and develop nanostructures at the atomic regime marking the simultaneous growth of scaffold in a way to quantify the growth process of scaffold.[16-17] This is achieved and reported herein with fluorescent metal clusters in the resolution of nanometer scale which gets synthesized with the growing scaffold i.e., DNA and simultaneously the output fluorescence is used to quantify the amount of DNA. This simple method of DNA engineering with nanoclusters not only offers a great deal of scope in replacing the expensive toxic organic dyes conventionally used in PCR but also paves a way towards designing of the futuristic devices to identify and monitor the most prominent cellular activities responsible for various diseases. Moreover, previous reports have demonstrated that Au NPs (>10 nm) increases the PCR yield and sensitivity by facilitating the heat transfer rate.[18-19] Thus, depiction of the role of fluorescent Au NCs (<2 nm) in the PCR and exploring its remarkable photophysical properties offers great deal of scope in order to develop fluorescent cluster based PCR.

6.2. Outline of the research work

1. A simple method of synthesis of highly fluorescent gold nanoclusters (Au NCs) was developed by using PCR. The formation of the Au NCs was confirmed by fluorescence spectroscopy, TEM, XPS, MALDI-TOP analysis.
2. Quantum yield and photostability of NCs were also carried out along with the circular dichroism (CD) analysis in order to find out conformation change of DNA after formation of NCs.
3. The results demonstrated that critical size and the surface charge of the synthesized NCs possibly allowed them to bind into major grooves and assembled periodically as a linear array on the DNA.
4. Precursor concentrations were varied to see the alteration in critical size of NCs and to explore relative spacing between Au NCs. Based on the precursor concentration and spacing of Au NCs, empirical relations were established which is ultimately linked to the intrinsic properties of DNA.

5. To explore its real life application, the method was employed to determine the relative gene expression level of cancer cells based on the relative fluorescence intensity of the NCs without using any additional fluorescent dye.
6. This development can be considered as particularly important as the dyes (e.g. ethidium bromide, propidium iodide) commonly used to visualize the DNA are highly carcinogenic[20], which is a huge concerns for users and even affects the environment when discarded without proper precautions.

6.3. Experimental section

6.3.1. Synthesis of composite Au NCs

Palm cycler PCR was used, for 20 µL of reaction, 3 µL of 1 mM $HAuCl_4$ and 0.01M mercapto propionic acid (MPA) mixed properly with 2 µL of DNA. Then, it was heated for 1.5 min at 95 ^{0}C. The heating was also carried out by using standard PCR condition such as denaturation at 95°C for 30 s, followed by annealing at 55°C for 30 s and amplification at 72 °C for 35 s. Various other temperature combinations have also tried for synthesis of Au NCs.

6.3.2. Fluorescence measurements

Fluorescence experiments were performed using Fluorolog-3, Horiba Jobin Yvon, Edison, NY USA

6.3.3. Transmission electron microscopy (TEM)

The DNA-Au NCs were observed under ultra-high resolution transmission electron microscope (TEM; JEM 2100; Jeol, Peabody, MA, USA), which was operated at a maximum accelerating voltage of 200 KV. For that, 7 µL of as-synthesized samples were drop-coated onto carbon coated copper TEM grids, air dried overnight and then analyzed under TEM.

6.3.4. Circular Dichroism (CD)

The conformation change of the DNA after formation of the NCs –if any - was pursued by circular dichroism (using a Jasco J-815 CD spectrophotometer). Spectra were recorded using 1 mm cuvette, with 1.0-nm bandwidth and 50 nm/min scan speed at 20 °C by comparing with reference (blank). Four independent scans were documented in the range of 190 - 400 nm wavelength to get the final spectra.

6.3.5. Matrix-assisted laser desorption ionization time-of-flight mass spectrometry (MALDI-TOF MS) analysis

MALDI–TOF **(**Applied Biosystems 4800 Plus MALDI TOF/TOF Analyzer) analysis of the as synthesized Au NC-DNA was carried out by using R-cyano-4-hydroxycinnamic acid (CHCA) matrix in negative mid-mass mode.

6.3.6. Cell culture

HeLa cells (Human cervical adenocarcinoma cells), U87 MG cells (Human glioblastoma cells) and A549 (Human lung carcinoma cells) were procured from National Center for Cell Sciences (NCCS), Pune, India and grown in Dulbecco's Modified Eagle's Medium supplemented with L-glutamine (4 mM), penicillin (50 units/mL), streptomycin (50 mg/mL) (from Sigma), and 10% (v/v) fetal bovine serum (from PAA Laboratories, Austria) in 5% CO_2 humidified incubator at 37 ^{0}C.

6.3.7. Reverse transcriptase polymerase chain reaction (PCR) for preparation of cDNA

Primers for β-Actin gene, Forward: 5'-CTGTCTGGCGGCACCACCAT-3' and Reverse: 5'-GCAACTAAGTCATAGTCCGC-3', p53 gene, Forward: 5'-TGGCCCCTCCTCAGCATCTTAT-3' and Reverse: 5'-GTTGGGCAGTGCTCGCTTAGTG-3', folate receptor (FR) gene, Forward primer- 5'-GATTGCATGGGCCAGGACTGAGC-3' and Reverse primer- 3'-TGCCAGTTGCTCTTGCAGGTGTAGG-5'. The cDNA containg the gene of interest was synthesized from total mRNA which was extracted from the U87MG cells, by reverse transcriptase reaction before doing the gene(s) amplification by PCR. For the cDNA synthesis, mRNA (1 µg) and random hexamer primer were taken in the nuclease free water and incubated at 65°C for 5 min in PCR machine. Then, the reaction tubes

were chilled on ice for few minutes followed by addition of the reaction buffer, RNase inhibitor, dNTPs and reverse transcriptase as per manufacturer protocol. It was kept for 5 min at 25°C followed by 60 min at 42°C. Finally, the reaction was terminated by heating at 70°C for 5 min.

6.3.8. PCR for amplification of gene

For the reaction of Palm cycler machine with following PCR condition- initial denaturation at 95 °C for 3 min, followed by a 3 stage PCR cycle with denaturation at 95 °C for 30 s, annealing at 55 °C for 30 s and amplification at 72 °C for 35 s for 30 cycles. Then final extension was given at 72 °C for 5 min. The PCR samples were analysed at 1.0 % agarose gel stained with ethidium bromide (EtBr).

6.3. 9. Agarose gel electrophoresis

Migration pattern of DNA and DNA-Au NCs were analyzed using 0.8% and 1.0 % agarose at 5 v/cm and was visualized under UV transilluminator (excitation at 305 nm).

6.4. Results and discussion

For the synthesis of fluorescent Au NCs, normal PCR reaction conditions were followed, i.e., denaturation, primer annealing and primer extension. This can be achieved either outside or using the PCR machine itself. PCR machine facilitates uniform heating for lower volumes and offers fast heat transfer. The NC precursors $HAuCl_4$ and mercapto propionic acid (MPA) were added into the reaction vessel containing the scaffold, i.e., DNA. The mixture was then subjected to one PCR cycle. Though denaturisation, primer annealing and primer extension are involved in PCR, it is found that only denaturisation followed by hybridization was sufficient to carry out the synthesis with maximum photoluminescence emission intensity of the clusters (**Figure 6.1a and b**). Results of other temperature combinations tried are shown in **Figure 6.1a** and **b**. It is anticipated that mercapto propionic acid (MPA) served as stabilizing agent for the NCs with the DNA as the scaffold. The UV-Vis spectrum of the colourless solution did not show any peak in the region of 500-800 nm depicted in **Figure 6.1c**. The so synthesized NCs showed the characteristic fluorescence emission at 585 nm upon excitation at 320 nm. The control experiments carried out in the similar condition did not show any fluorescence, as shown in **Figure 6.1d**.

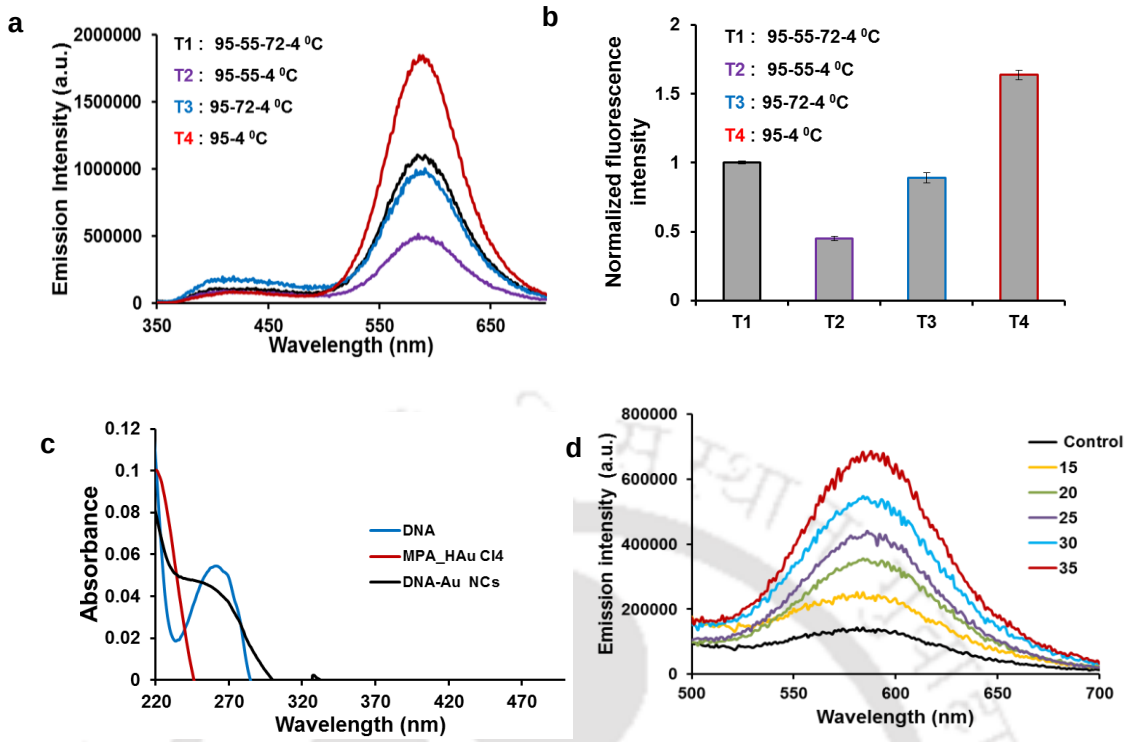

Figure 6.1 (**a**) Various PCR temperature combination used for synthesis of Au NCs and their fluoresce intensity. (**b**) Bar graph represents normalised fluorescence intensity of Au NCs obtained by varying temperature of PCR. (c) UV-Vis spectra of the DNA-Au NC along with the others control, none of which showed SPR peak due to Au NPs. (**d**) Fluorescence spectra showing the relative fluorescence intensity of Au NC's. The legend indicates different PCR cycle after which Au NC synthesis was performed.

The as synthesized fluorescent clusters with the scaffold DNA can be viewed under the fluorescent microscope, as shown in **Figure 6.2a**. The TEM images showed the so formed clusters from plasmid DNA were of size less than 2 nm as depicted in **Figure 6.2b** and the EDX confirmed that NCs contained gold (**Figure 6.2c)**. The X-ray photoelectron spectroscopy (XPS) of as synthesized DNA-Au NCs showed peaks at 84.0 and 87.6 eV corresponding to metallic Au ($^4f_{5/2}$, $^4f_{7/2}$) which was bonded to thiol group (corresponding to the peak of $2p_{3/2}$ at 161.2 eV) as shown in **Figure 6.2d**.[20] Also, circular dichroism (CD) experiments revealed typical signature of characteristic bands of B-DNA such as positive band (peak) at about 270 nm and a negative band (deep) around 235 nm; however, native DNA conformation was slightly changed after formation of the NCs as peak was shifted to longer wavelength i.e., from 270 nm to 274 nm, as shown in the

Figure 6.2e.[21] The MALDI-TOF analysis revealed peak (m/z) maxima at 4828.12 which can be assigned to the structure $[Au_{18}\ MPA_{12} + Na^{+} - H^{+}]^{-}$, following comparison with the mass spectrum of the control as shown in **Figure 6.2f**.

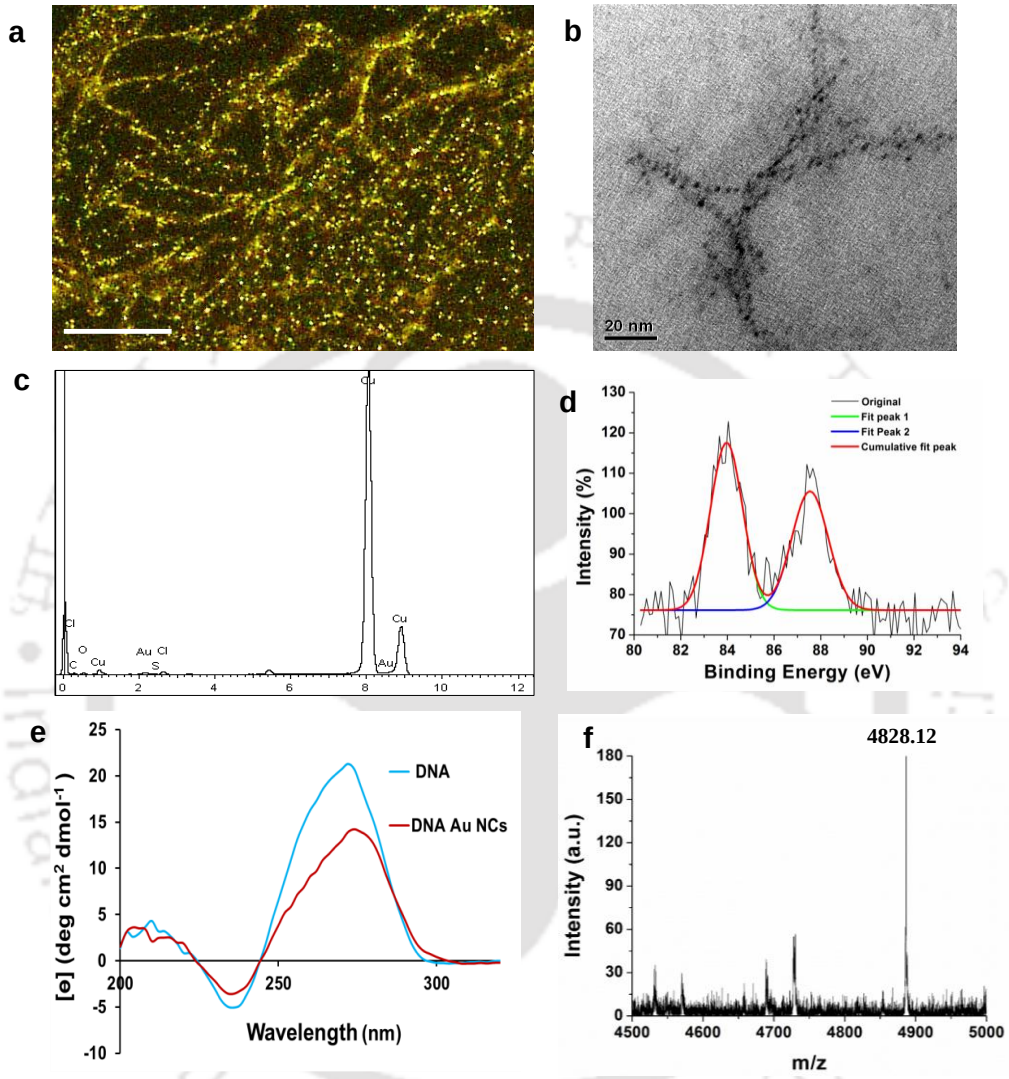

Figure 6.2 (a) Fluorescence microscopy image of DNA- Au NCs, showing the strong characteristic yellow coloured fluorescence of Au NCs, when excited with UV light. Scale 10 µm. (**b**) TEM image of the gold clusters formed with plasmid DNA. (**c**) EDX spectrum of DNA- NCs indicating the presence of Au (0), copper signal is due to copper grid. (d**)** XPS analysis of the synthesized DNA-Au NCs which showed peaks at 84.0 and 87.6 eV, corresponding to metallic Au ($^{4}f_{5/2}$, $^{4}f_{7/2}$). (**e)** Circular dichromic spectra of the DNA before and after formation of the Au NCs. (**f**) MALDI-TOF spectrum revealing the peak at 4828.12, which corresponds to $[Au_{18}\ MPA_{12}+Na^{+}-H^{+}]^{-}$.

Importantly, it was found that NCs arrayed on to the DNA showed difference in spatial arrangement, with varying concentrations of the NC precursor or the concentration of the scaffold. The average spacing between clusters gave an indication that they may be attached to both the groves (minor and major) of the DNA, depending on their dimensions. In order to establish a relationship, a statistical study was carried out in two ways from various TEM images. Firstly, the formation of cluster for various concentrations of precursor $HAuCl_4$, with fixed concentration of DNA, was examined with transmission electron microscopy. The results showed a pattern where the formed clusters depicted the resemblance of 'beads on a string' with the DNA backbone as shown in **Figure 6.3.** It can be anticipated that the clusters were formed within the groves of the DNA and are ultimately responsible for the fluorescence of the whole composite. The statistical analysis of multiple sets of data revealed interesting results linking various parameters of clusters and intrinsic properties of DNA.

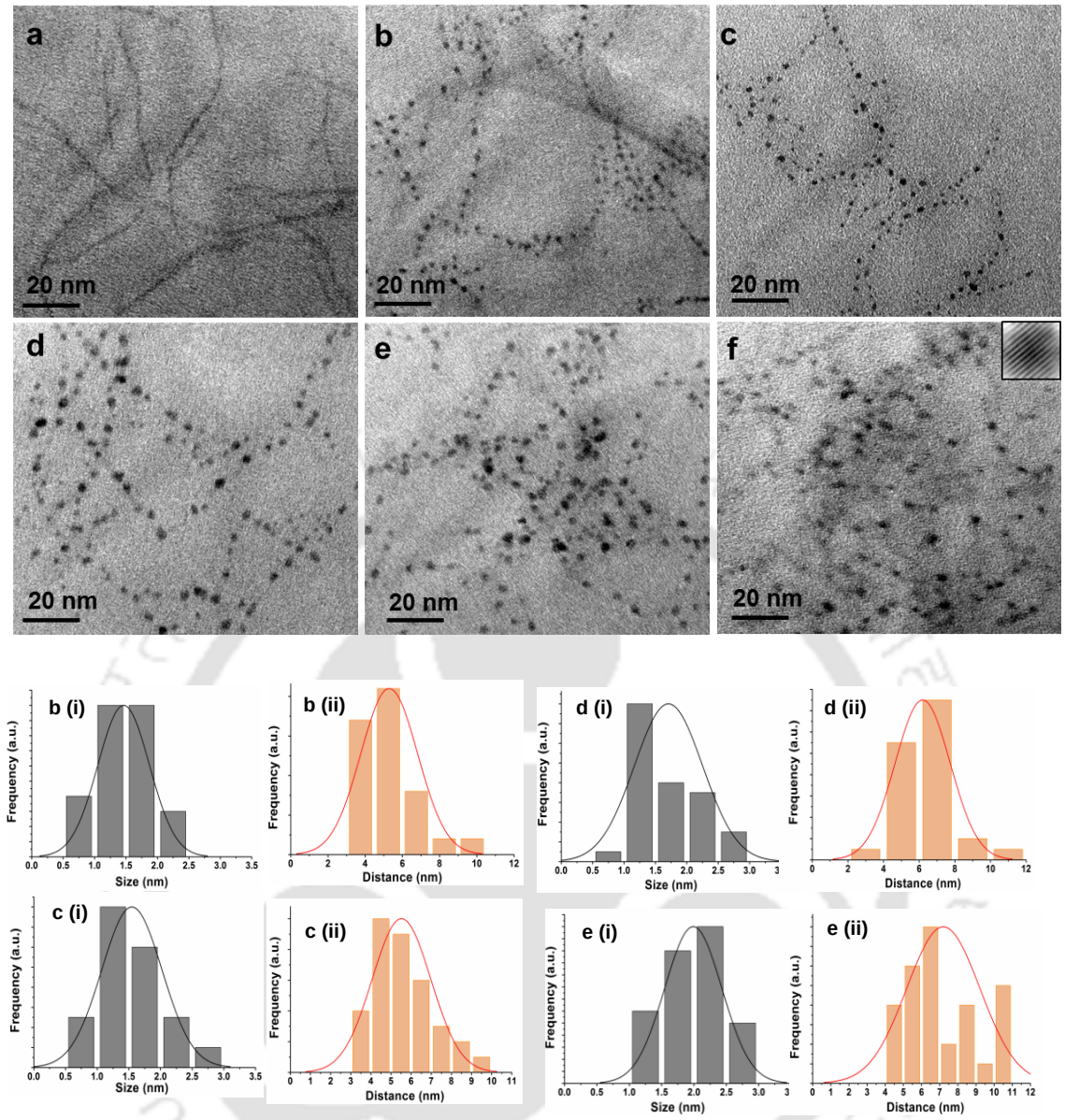

Figure 6.3 The formation of gold clusters/nanoparticles on the fixed concentration of DNA is examined from the TEM images. The concentrations of the precursors gold salt shown in the figure (**a - f**) are 0.03, 0.05, 0.08, 0.1, 1.2 and 1.5 µg/µL, respectively, with the fixed concentration of DNA. Bar graph represents the variation in size and distance between clusters. (**i**) and (**ii**) represent size (**d**) and distance (**D**) plot respectively. The concentrations of the gold (**a-d**) are 0.03, 0.05, 0.08 and 0.1 µg/µL, respectively.

The parameters, distance between adjacent clusters (**D**), diameter of the clusters (**d**) were found to follow a linear relationship with the precursor's concentration with the [DNA] fixed. However, an interesting relationship is achieved connecting the parameters **(D-d)** and **[Au]/[DNA]** as indicated in **equation 1.** Further, the relationship can be approximated to the intrinsic properties of DNA as shown in **equation 2**.

$$\left.\mathbf{(D-d)} = 3.4317 \cdot \frac{\mathbf{[Au]}}{\mathbf{[DNA]}} + 2.9759\right\} \text{ for } 0.1875 \leq \frac{\mathbf{[Au]}}{\mathbf{[DNA]}} \leq 0.625 \qquad (1)$$

$$\left.\mathbf{(D-d)} = \text{dmm} \cdot \left(\frac{\mathbf{[Au]}}{\mathbf{[DNA]}} + 0.9 \right) \right\} \text{for } 0.1875 \leq \frac{\mathbf{[Au]}}{\mathbf{[DNA]}} \leq 0.625 \qquad (2)$$

where, dmm = pitch of the B-DNA (3.4nm)

A set of studies showed that the increase in concentrations of gold, with identical other experimental conditions, resulted in the decrease of the amount of nanoclusters and finally resulted in the formation of nanoparticles. Hence, it was found necessary to maintain a range for the concentration of precursor for achievement of effective fluorescence and formation of nanoclusters. However, one can eventually either tune the system to be in quantum or plasmonic domain by just varying the precursor's concentration. The 3D plot relating to these two parameter i.e., size and distance is also shown in **Figure 6. 4b**.

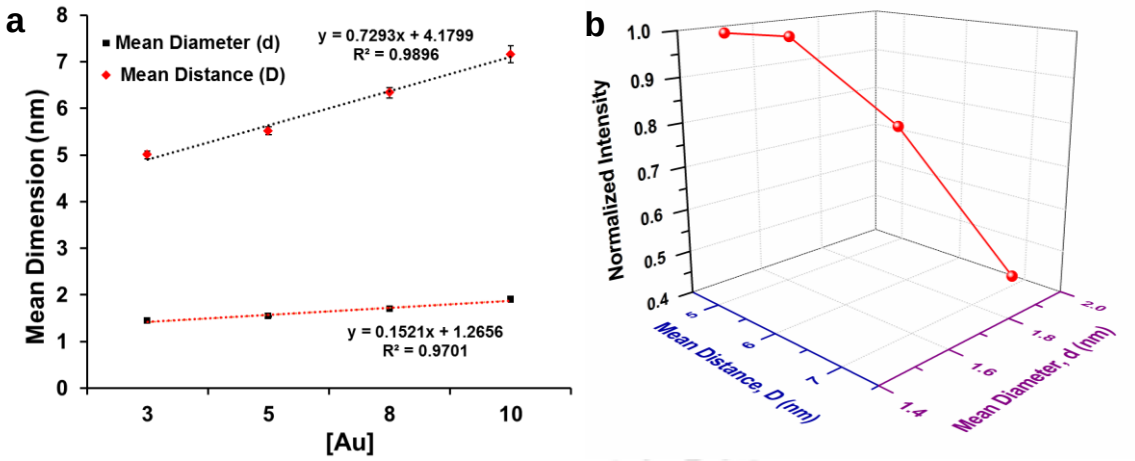

Figure 6.4 (**a**) The graph illustrates that the size of the clusters (**d**) and the distance (**D**) between them increase linearly with the increasing concentration of gold. The distance is measured from one centre to other centre of the gold nanocluster/nanoparticle. (**b**) 3D plot of size, distance and fluorescence intensity.

It can also be deduced from equation 1 that, there exists a linear relationship between D, and d. With the increase in the size (d) of the formed nanoclusters/nanoparticles, the spacing between adjacent particles (D) increased. This can be attributed to the preferential binding to major grove over the minor grove of DNA or formation of nanoparticle at random suitable sites. Evidently, the concentration of gold ultimately influences the output fluorescence intensity, $\mathbf{I_r}$, for a fixed concentration of DNA. A relationship can be arrived at from the experimental data as shown in **Figure 6.5** and can be written as,

$$\mathbf{I}_r = -4.4963 \cdot \left(\frac{\mathbf{[Au]}}{\mathbf{[DNA]}} \right)^2 + 2.24287 \frac{\mathbf{[Au]}}{\mathbf{[DNA]}} + 0.6942 \Bigg\} \text{ for } 0.1875 \leq \frac{\mathbf{[Au]}}{\mathbf{[DNA]}} \leq 0.625 \quad (3)$$

As inferred from **equation 3** and **Figure 6.5**, the intensity of the clusters dips down with the increase in the concentrations of gold. When the concentration of the precursor for the formation of nanoparticle was reached, the fluorescence completely ceased.

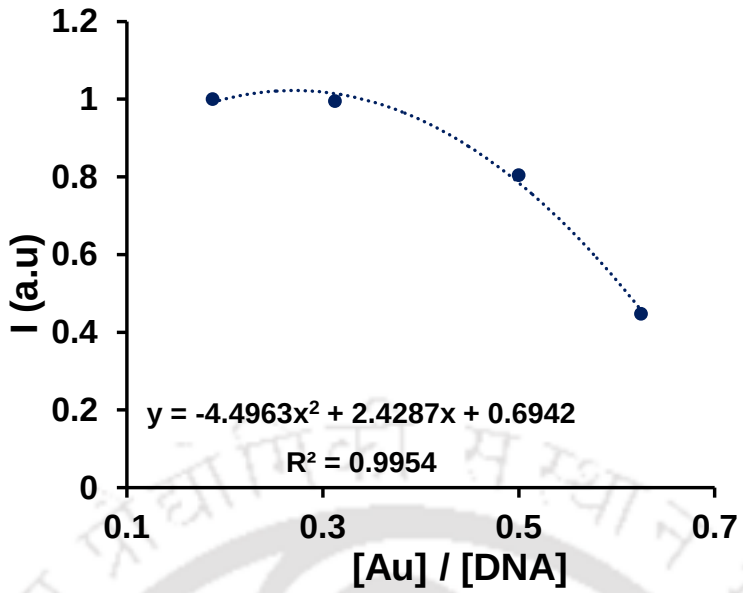

Figure 6.5 Plot of concentration of gold and fluorescence intensity. Decrease of fluorescent intensity of the gold clusters (at 585 nm), when excited at 320 nm, is significant at the low concentration of the precursor gold.

However, in order to quantify DNA, it is necessary to know the possible interactions of the fluorophore with the unit length of the DNA. To address this, a relationship must be achieved linking the intensity of the fluorophore (NCs) to its size (**d**) and the frequency of its existence per pitch (**n**) of the double helical DNA. The variation of the intensity of the fluorophore with the size (**d**) and the frequency per pitch **(n)** is shown in the **Figure 6.6** and can be mathematically expressed as,

$$\mathbf{I} = -2.6106\cdot(\mathbf{nd})^2 + 12.241\cdot(\mathbf{nd}) - 13.339 \Big\} \text{ for } 0.1875 \le \frac{\mathbf{[Au]}}{\mathbf{[DNA]}} \le 0.625 \quad (4)$$

The above equation indicates that the higher the frequency of the clusters of small sizes, the higher is the intensity of fluorescence. Since, the nanoclusters are responsible for the fluorescence properties, the range of concentration of gold had to be maintained at those values. **Figure 6.5b** is representing the 3D plot of the same.

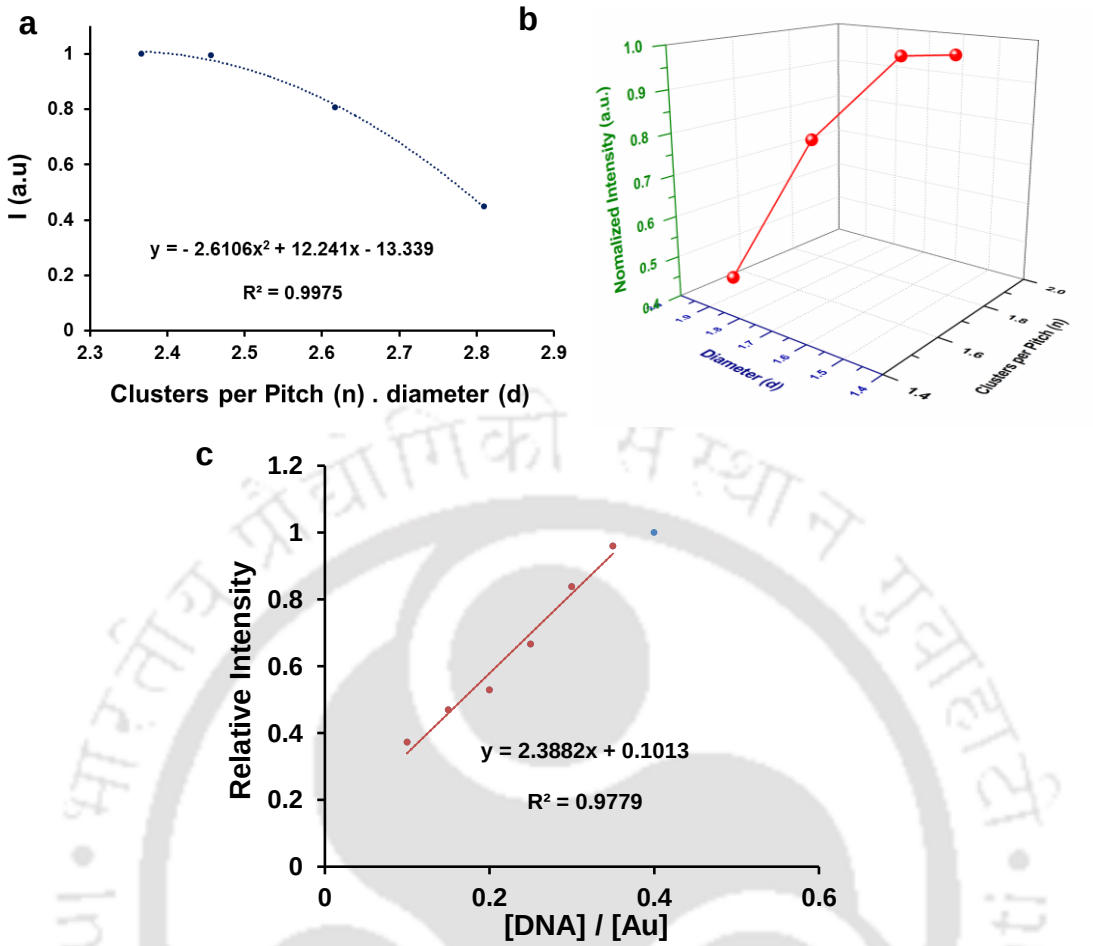

Figure 6.6 (**a**) The fluorescence intensity of the gold clusters increased with the increase in the number of clusters per pitch of DNA. The overall influence of the intensity for the variation in frequency of cluster per pitch (**n**) and size (**d**) is shown in the figure. (**b**) The 3D illustration shows the variation of intensity with the size and frequency of clusters per pitch. As the size of the clusters/nanoparticles increases, the frequency of the clusters per pitch of DNA decreases. The larger sized particles results in the diminishing pattern of fluorescence and decreased frequency of clusters per pitch as evident from the graph. (**c**) The graph illustrates that the florescence intensity increases with the increasing amplification of the DNA for a fixed concentration of precursor gold. However, after the certain amplification of the DNA, since the complete precursor gold is utilized, the fluorescence intensity saturates.

In the second process, DNA concentration was varied, keeping the gold concentration fixed. The gold concentration was suitably chosen for the formation of cluster. We observed that the fluorescence increased with the increase in concentration of DNA for a range and then there was no change observed, as shown in **Figure 6.7**. In that particular

concentration range, there is a linear relationship of intensity with the concentration of DNA. The saturation is possibly indicates complete utilization of NC precursor.

The DNA-Au NC composite has photoluminescence quantum yield of 4.6% as measured based on the reference dye quinine sulphate (**Figure 6.8a**). More importantly, the Au NCs were found to be highly photostable, with fluorescence intensity decrease rate (F/F_0) of the NCs 0.016 % per min, while in case of commonly used fluorescent dye rhodamine 6G it was observed to be 0.27% per min (**Figure 6.8b**). To check its functionality in quantification of DNA following PCR application, we had carried out the single cycle synthetic method after different amplifications (different cycles) for three genes, namely, p53, β-act and gene of folic acid receptors (FR). Synthesis of the NCs was done after different number of PCR cycles (15, 20, 25, 30 and 35), which corresponds to the increase in amount of respective gene.

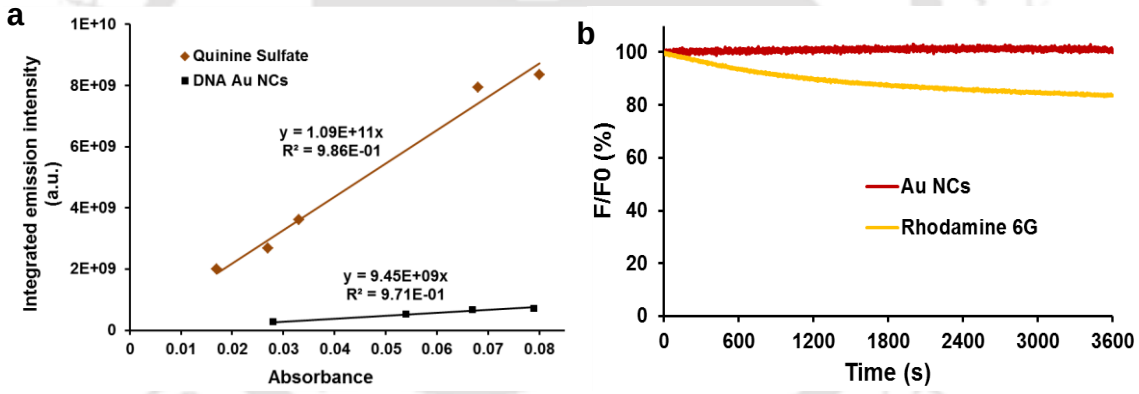

Figure 6.8 (a) Quantum yield (QY)**,** calculated based on quinine sulphate as standard. (**b**) Photo bleaching of Au NCs.

The fluorescence results were then compared with the agarose gel stained with ethidium bromide **Figure 6.8 a-c**. We found that the formation of clusters is directly linked with the amount of scaffold present (after amplification) which was essentially leading to exponential increase in fluorescence intensity of Au NCs. Thus this was related to PCR amplification, which follows exponential amplification of the amount of DNA with progress of number of PCR cycles. Therefore, this method could be used to quantitate the amount of gene amplification.

Cancer cells are known to over-express several genes in comparison to the healthy cells. Hence, it is important to measure the relative gene expression of the cell. For example, folic acid receptor gene (FR) over-expresses in various cancer cell lines as compared to healthy cells. Hence, the relative quantification of a folic acid receptor gene (FR gene) would help in detection as well as targeted therapy of cancer. In an objective to achieve the relative gene expression of the cancer cell to normal cell with this system, we had distinguished their expression using the fluorescence of the gold NCs. Two different cell lines, HeLa cells (human cervical adenocarcinoma cells) and A549 cells (human lung carcinoma cells) were taken and folic acid receptor gene was targeted in the process. We had observed that HeLa cells over-expressed folic acid receptor gene by 2.3 times in comparison to the A549 cells, which is comparable with the results from standard method of gel electrophoresis, through ethidium bromide (EtBr) staining, as depicted in **Figure 6.9**.

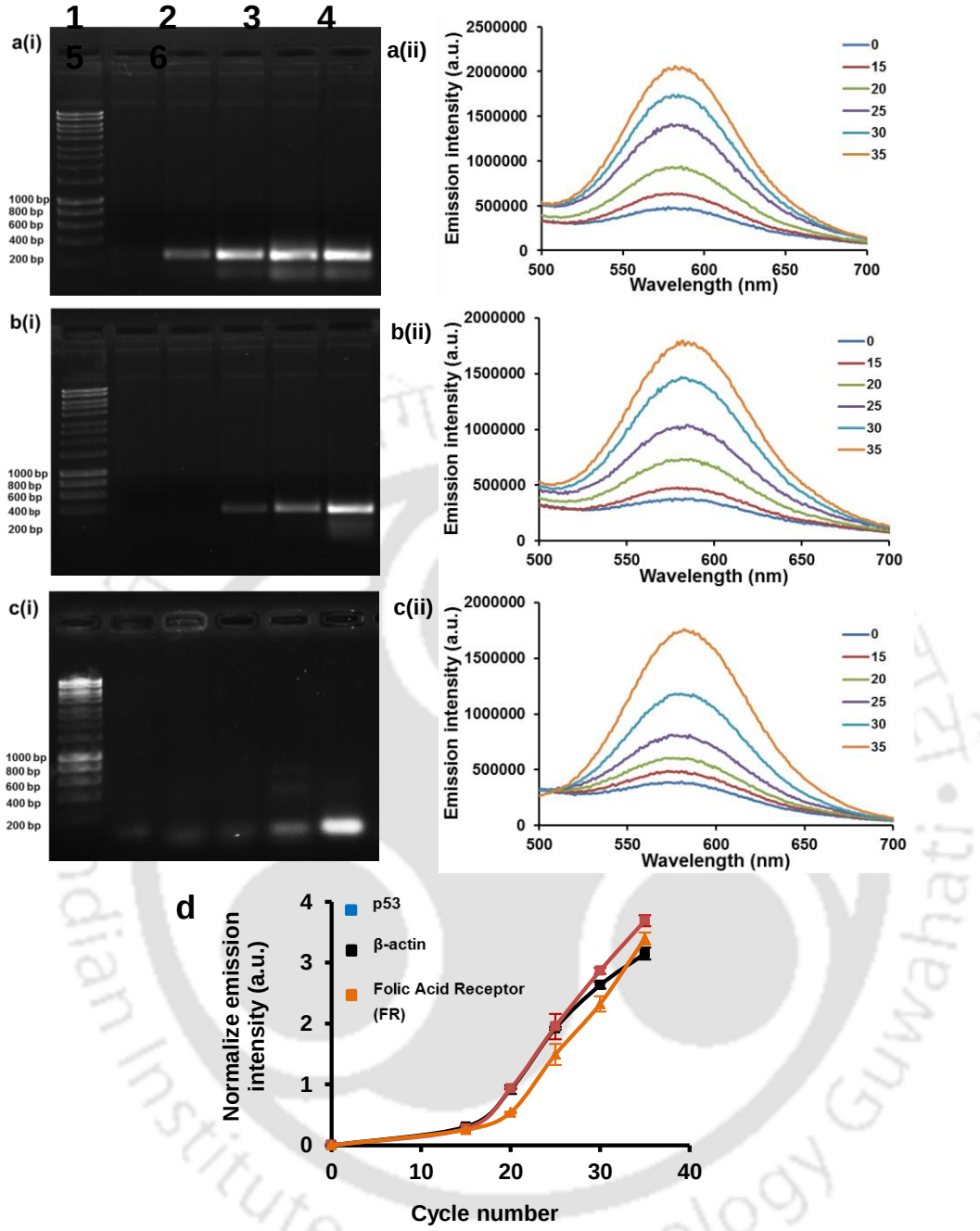

Figure 6.8 Gene amplification study by the relative fluorescence intensity of the Au NCs, which was synthesised after respective PCR cycles (15, 20, 25, 30 and 35) based on the amplified DNA. (**a-c**) are β-act, p53 and FR gene respectively. (**i**) and (**ii**) are same results obtained from gel electrophoresis stained with ethidium bromide and corresponding fluorescence spectra of Au NCs. In agarose gel microgram, Lane 1: marker, Lane 2: 15 cycles, Lane 3: 20 cycles, Lane 4: 25 cycles, Lane 5: 30 cycles and Lane 6: 35 cycles. (**d**) Relative expression of the three genes, as measured based of fluorescence of Au NCs.

It would be mentioned here that β-act, a housekeeping gene, was taken as endogenous control. It was observed that its relative expression remained almost similar in both the cell lines. Hence, this method consisting gold NCs can be utilized for the detection of disease causing factors, eventually leading to point of care diagnostics and prognosis.

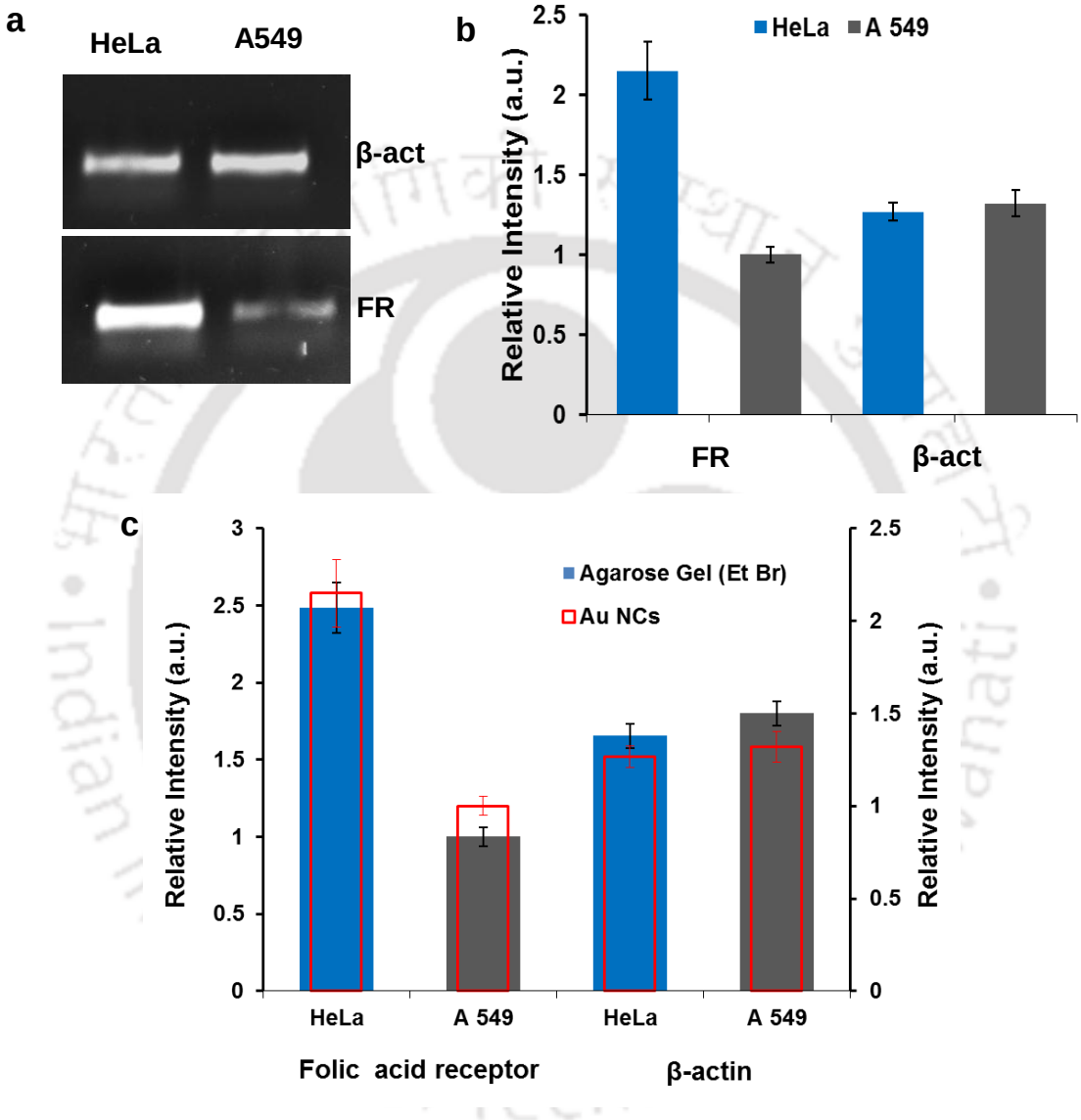

Figure 6.9 Relative gene expression of folic acid receptors of HeLa and A 549 cell lines measured by (**a**) agarose gel electrophoresis and (**b**) based on the fluorescence of Au NCs. (**d**) Bar graph represents the combined results of the study using the two different methods.

6.5. Conclusion

In short, a novel bio friendly method of synthesis procedure of gold NCs on DNA has been developed. Also, the method provided an option to quantify DNA through the photoluminescence of the synthesized NCs. Considering carcinogenic conventional dyes; this marks an effective option and even can be implemented without sophisticated machinery using minimum laboratory equipment. As it is a green method of synthesis, it reduces the risk on human health and the environment. Quantification of the gene amplification and relative expression were achieved, utilizing this simple method to detect the modulations in various cell lines including cancer. Eventually, simple portable low cost equipment can be built using the principles demonstrated through this work in a way towards replacing the golden era of bulky PCR machines.

6.6. References

1. . T. Ross, U. Scherf, M. B. Eisen, C. M. Perou, C. Rees, P. Spellman, V. Iyer, S. S. Jeffrey, M. Van de Rijn, M. Waltham, A. Pergamenschikov, J. C. F. Lee, D. Lashkari, D. Shalon, T. G. Myers, J. N. Weinstein, D. Botstein, and P. O. Brown, *Nature Genetics*, 2000, **24**, 227–235.
2. C. Sotiriou and M. J. Piccart, *Nature Reviews Cancer*, 2007, **7**, 545–553.
3. L. J. van 't Veer, H. Dai, M. J. van de Vijver, Y. D. He, A. A. M. Hart, M. Mao, H. L. Peterse, K. van der Kooy, M. J. Marton, A. T. Witteveen, G. J. Schreiber, R. M. Kerkhoven, C. Roberts, P. S. Linsley, R. Bernards, and S. H. Friend, *Nature*, 2002, **415**, 530–536.
4. V. Emilsson, G. Thorleifsson, B. Zhang, A. S. Leonardson, F. Zink, J. Zhu, S. Carlson, A. Helgason, G. B. Walters, S. Gunnarsdottir, M. Mouy, V. Steinthorsdottir, G. H. Eiriksdottir, G. Bjornsdottir, I. Reynisdottir, D. Gudbjartsson, A. Helgadottir, A. Jonasdottir, A. Jonasdottir, U. Styrkarsdottir, S. Gretarsdottir, K. P. Magnusson, H. Stefansson, R. Fossdal, K. Kristjansson, H. G. Gislason, T. Stefansson, B. G. Leifsson, U. Thorsteinsdottir, J. R. Lamb, J. R. Gulcher, M. L. Reitman, A. Kong, E. E. Schadt, and K. Stefansson, *Nature*, 2008, **452**, 423–428.
5. C. A. Heid, J. Stevens, K. J. Livak, and P. M. Williams, *Genome Research*, 1996, **6**, 986–994.
6. P. Mouritzen, M. Noerholm, P. S. Nielsen, N. Jacobsen, C. Lomholt, H. M. Pfundheller, and N. Tolstrup, *Nature Methods*, 2005, **2**, 313–316.
7. S. Bustin, Journal of Molecular Endocrinology, 2002, **29**, 23–39.
8. J. Zhang, Y. Fu, C. V. Conroy, Z. Tang, G. Li, R. Y. Zhao, and G. Wang, *The Journal of Physical Chemistry C*, 2012, **116**, 26561–26569.
9. S. Pal, R. Varghese, Z. Deng, Z. Zhao, A. Kumar, H. Yan, and Y. Liu, *Angewandte Chemie International Edition*, 2011, **50**, 4176–4179.
10. H.-C. Yeh, J. Sharma, J. J. Han, J. S. Martinez, and J. H. Werner, *Nano Letters*, 2010, **10**, 3106–3110.
11. Y. Zhang, Y. Cai, Z. Qi, L. Lu, and Y. Qian, *Analytical Chemistry*, 2013, **85**, 8455–8461.
12. X. Jia, J. Li, L. Han, J. Ren, X. Yang, and E. Wang, *ACS Nano*, 2012, **6**, 3311–3317.

13. R. J. Macfarlane, B. Lee, M. R. Jones, N. Harris, G. C. Schatz, and C. A. Mirkin, *Science*, 2011, **334**, 204–208.
14. P. W. K. Rothemund, *Nature*, 2006, **440**, 297–302.
15. J. G. Railsback, A. Singh, R. C. Pearce, T. E. McKnight, R. Collazo, Z. Sitar, Y. G. Yingling, and A. V. Melechko, *Advanced Materials*, 2012, **24**, 4261–4265.
16. P. R. O'Neill, K. Young, D. Schiffels, and D. K. Fygenson, *Nano Letters*, 2012, **12**, 5464–5469.
17. L. Feng, Z. Huang, J. Ren, and X. Qu, *Nucleic Acids Research*, 2012, **40**, e122–e122.
18. H. Li, J. Huang, J. Lv, H. An, X. Zhang, Z. Zhang, C. Fan, and J. Hu, *Angewandte Chemie International Edition*, 2005, **44**, 5100–5103.
19. M. Li, *Nucleic Acids Research*, 2005, **33**, e184–e184.
20. N. von Wurmb-Schwark, L. Cavelier, and G. A. Cortopassi, *Mutat. Res.*, 2006, **596**, 57–63.
21. X. Le Guével, B. Hötzer, G. Jung, K. Hollemeyer, V. Trouillet, and M. Schneider, *The Journal of Physical Chemistry C*, 2011, **115**, 10955–10963.
22. M. Endo and T. Majima, *Chemical Communications*, 2004, 1308-1309.

Chapter 7

Conclusion and Future Outlook

Chapter 7:

Conclusion and Future Outlook

7.1. Summary of the Present Work

The present dissertation primarily aimed to synthesize nanoparticles and its composites suitable for 'theranostic' applications. In initial study attention has been directed to address one of the most common challenges of bacterial infections which are posing a huge threat due to the emergence of the drug resistant species. To identify the bacterial infection, a simple, fast method of detection of the bacteria was developed by using fluorescent Au NPs-paracetamol dimer (PD) composite which was synthesized from the conventional drug paracetamol. The method was sensitive and can be useful for employment in general contamination test for both Gram positive and Gram negative bacteria with a sensitivity of 100 CFU/mL.

After achieving this feat in the subsequent study, the attention was directed to kill those bacterial species by synthesizing novel bactericidal agent. For this, Ag NPs composite was synthesized by following the similar synthesis protocol of Au NPs. The nanocomposite (Ag NPs-PD)–with minimum concentration of silver showed strong bactericidal effects against both Gram positive and Gram negative bacteria .Essentially, it was revealed that PD acted as prodrug accompanied with ROS which generated NAPQI, leading to linearization of the plasmid DNA by inhibiting the DNA gyrase enzyme and thus resulting in bacterial death. This result prompted to employ the PD in cancer therapy with potent ROS generator like Ag NPs. The size of the Ag NPs plays crucial role in their activity, as smaller sizes (typically, less than 10 nm in diameter) offer better activity for the cell death. Therefore, Ag NCs was synthesized from BSA due to its small size (<2 nm) and remarkable photophysical properties. This was served as potent ROS generator while delivered with PD by using chitosan NPs (CS). Moreover, for the targeted delivery of PD-Ag NCs, folic acid (FA) was conjugated with the CS nanocarriers prior to deliver into the cancer cells. The results demonstrated that PD is equally effective as cancer therapeutics along with Ag NCs. Hence, it is to be deemed that the use of PD along with

some conventional anti-cancer drug would serve as ROS generator and can be used for the cancer therapy in future.

Next, to reduce the time for synthesis of nanoclusters simple fast and aqueous synthesis of Au NCs was developed in chitosan matrix which was further converted into polymeric nanoparticles which can be used as effective bioimaging agent suitable for microscopy and the flow cytometer analysis. To show the theranostic application of this composite nanoparticle the suicide gene corresponds to cytosine deaminase uracil phosphoribosyltransferase (CD-UPRT) was loaded and delivered into cervical cancer cells (HeLa). The CD-UPRT enzyme converts nontoxic prodrug 5- fluorocytosine (5-FC) to 5-fluorouracil (5-FU) and other toxic metabolites which kill transfected cancer cells. Cell viability assay displayed the ability of these composite NPs to deliver the suicide gene, alongside induced apoptosis upon addition of its substrate 5-FC. This suicide gene loaded theranostic NPs has huge promises in the future for *in vivo* study. Importantly, this has broadened the scope of personalized medicine for new generation and could be tested in a better way as an effective alternative of conventional chemo and radio therapy to cure diseases like cancers.

Finally, by exploring polymerase chain reaction (PCR) machine Au NCs was synthesized based on the amplified DNA as scaffold and fluorescence intensity of the Au NCs employed to measure quantitative gene expression. Three different genes such as β-actin, p53 and folic acid receptor (FR) were employed to establish the study. Further, it was found that the method can be employed to measure the relative gene expression in the cancer cells. As the Au NCs was found to be non-cytotoxic, therefore, the method offers exceptional promises in order to synthesize the highly fluorescent Au NCs and concurrently estimate the DNA amplification which can be applicable for designing the future devices to explore the molecular events without using carcinogenic dyes.

7.2. Future Outlook

In this light, the aim and domain of the present findings can be expanded even further for more innovative applications that will contribute to resolve issues of healthcare in a better way in future.

- ✓ The Au NPs-PD composite based method of the bacterial detection can be tested for the real life sample.

- ✓ With the conjugation of the suitable ligand with Au NPs, significant level of specificity can be obtained for the selection of the bacterial strain which would be preferred choice for the detection bacterial contamination in specific case.
- ✓ In order to kill drug resistant bacterial strain, different drugs/antibiotics can be used along with the Ag NPs for the combination therapy to reduce the concentration of the silver in killing the resistant bacterial strains which would eventually reduce the chances of side effects to the human health and environment.
- ✓ The mechanism of the bacterial cells by formation of the NAPQI from the PD in conjecture with ROS can tested to the efficacy for other diseases such as tuberculosis (TB).
- ✓ The cancer cells therapy by targeted delivery of the Ag NCs and the PD can be promoted for the *in-vivo* model for better batter understanding and applications.
- ✓ Solid chitosan film formed with highly fluorescent Au NCs can be used for the various application of formation of the bio and chemo sensors.
- ✓ The pH dependent reversible change of the fluorescence intensity of the Au NCs can be used for the various logical implementation required for the molecular computing.
- ✓ PCR based synthesis of the Au NCs can be used for real-time synthesis of the NCs which would resolve several issues RT-PCR and will offer immense possibility of generating 'Atomic cluster- RT- PCR'.

Publications and presentations

Journal Publications

1. Subhojit Das, **Amaresh Kumar Sahoo**, Siddhartha Sankar Ghosh and Arun Chattopadhyay, **2010**. Plasmonic Signatures in the Composite Crystals of Gold Nanoparticles and p - Hydroxyacetanilide (Paracetamol). ***Langmuir,*** 26, 15714–15717.

2. **Amaresh Kumar Sahoo**, Md Palashuddin Sk, Siddhartha Sankar Ghosh and Arun Chattopadhyay, **2011**. Plasmid DNA linearization in the antibacterial action of a new fluorescent Ag nanoparticle–paracetamol dimer composite. ***Nanoscale,*** 3, 4226-4233.

3. **Amaresh Kumar Sahoo**, Shilpa Sharma, Arun Chattopadhyay and Siddhartha Sankar Ghosh, **2012**. Quick and simple estimation of bacteria using a fluorescent paracetamol dimer–Au nanoparticle composite. ***Nanoscale,*** 4, 1688-1694.

4. Subhamoy Banerjee, **Amaresh Kumar Sahoo**, Arun Chattopadhyay and Siddhartha Sankar Ghosh, **2013**. Hydrogel nanocarrier encapsulated recombinant IκBα as a novel anticancer protein therapeutics. ***RSC Advances,*** 3, 14123-14131.

5. Raihana Begum, **Amaresh Kumar Sahoo**, Siddhartha Sankar Ghosh and Arun Chattopadhyay**, 2014**. Recovering Hidden Quanta of Cu^{2+}-doped ZnS Quantum Dots in Reductive Cellular Environment. ***Nanoscale,*** 6, 953-961.

6. **Amaresh Kumar Sahoo**, Subhamoy Banerjee, Siddhartha Sankar Ghosh and Arun Chattopadhyay, **2014**. Simultaneous RGB Emitting Au Nanoclusters in Chitosan Nanoparticles for Anticancer Gene Theranostic. ***ACS Applied Materials & Interfaces,*** 6, 712-724.

7. Nidhi Chaubey, **Amaresh Kumar Sahoo**, Arun Chattopadhyay and Siddhartha Sankar Ghosh, **2014**. Silver nanoparticle loaded PLGA composite nanoparticles for improving therapeutic efficacy of recombinant IFNγ by targeting cell surface. ***Biomaterials Science***, 2, 1080-1089.

8. Rama Ghosh**, Amaresh Kumar Sahoo**, Siddhartha Sankar Ghosh, Anumita Paul and Arun Chattopadhyay, **2014.** Blue emitting copper nanoclusters synthesized in the presence of Lysozyme as candidates for cell labelling. ***ACS Applied Materials & Interfaces,*** 6, 3822-3828.

9. Subhamoy Banerjee, **Amaresh Kumar Sahoo**, Arun Chattopadhyay, Siddhartha Sankar Ghosh, **2014**. Recombinant IκBα loaded curcumin nanoparticles for improved cancer therapeutics. ***Nanotechnology,*** 25, 345102 (11p).

10. Sunil Kumar Sailapu, **Amaresh Kumar Sahoo**, Siddhartha Sankar Ghosh and Arun Chattopadhyay, **2014**. Hierarchical Logic Structures Based on Responsive Fluorescent Gold Nanoclusters. ***Small***, DOI: 10.1002/smll.201401421.

11. Subhamoy Banerjee, **Amaresh Kumar Sahoo**, Arun Chattopadhyay, Siddhartha Sankar Ghosh, **2014**. Chemosensitization of IκBα overexpressing glioblastoma towards anti-cancer agents. ***RSC Advances***, 4, 39257-39267**.**

12. **Amaresh Kumar Sahoo**, Subhamoy Banerjee, Siddhartha Sankar Ghosh and Arun Chattopadhyay, **2014**. Single cycle PCR based synthesis of highly fluorescent Au nanoclusters for determination of the gene expression. (**Communicated**)

13. Devendra Kumar Maravi, **Amaresh Kumar Sahoo**, Upashi Goswami, Doolthi Shambu Prasad , Siddhartha Sankar Ghosh and Lingaraj Sahoo, Phytogenic 'green synthesis' of silver NPs with enhanced antibacterial activity (**Communicated**).

14. **Amaresh Kumar Sahoo**, Upashi Goswami, Siddhartha Sankar Ghosh and Arun Chattopadhyay, Fluorescent Ag nanoclusters embedded folic acid–chitosan nanocarriers for targeted drug delivery into the cancer cells (**Communicated**).

15. Upashi Goswami, **Amaresh Kumar Sahoo**, Siddhartha Sankar Ghosh and Arun Chattopadhyay, Fast and facile synthesis of Au NCs on bacterial cells to estimate the number of bacteria (**Communicated**).

Conference presentations

1. Subhojit Das, **Amaresh Kumar Sahoo**, Siddhartha Sankar Ghosh, and Arun Chattopadhyay, Plasmonic Properties of Gold Nanoparticles in their Composite Crystals with p-Hydroxyacetanilide, Poster Presentation, **International Symposium on Advances in Nanomaterials (ANM 2010),** December 6-7, 2010, Central Glass and Ceramic Research Institute (CGCRI), Kolkata, India.

2. **Amaresh Kumar Sahoo**, Md Palashuddin Sk, Siddhartha Sankar Ghosh and Arun Chattopadhyay; New Fluorescent Silver Nanoparticle-Paracetamol Dimer Composite Causing Linearization of Plasmid DNA in Antibacterial Action ,Poster Presentation, 2nd **International Conference on Advanced Nanomaterials and Nanotechnology**, **ICANN 2011**, December 8-10, 2011, IIT Guwahati, India.

3. **Amaresh Kumar Sahoo**, Md Palashuddin Sk, Siddhartha Sankar Ghosh and Arun Chattopadhyay; Novel Antibacterial Ag Nanoparticles-Paracetamol dimer Composite Causing Linearization in Plasmid DNA, Poster Presentation, **India-Australia International Workshop on Nanotechnology In Materials and Energy Application, IAWNT 2011**, December 29- 31, 2011, Jadavpur University, Kolkata, India.

4. Subhamoy Banerjee, **Amaresh Kumar Sahoo** and Siddhartha Sankar Ghosh; pH sensitive biodegradable hydrogel nanoparticles for functional delivery of GST-tagged IκBα as therapeutic agent, Poster Presentation, **World Congress on Biotechnology-2012,** May 4-6 , 2012, Hyderabad, Andhra Pradesh, India.

5. Subhamoy Banerjee**, Amaresh Kumar Sahoo**, Arun Chattopadhyay and Siddhartha Sankar Ghosh; A novel protein therapeutic approach using recombinant IκBα loaded hydrogel nanocarrier in cancer therapy, Poster Presentation, **Frontiers in Chemical Science (FICS-2012),** December 2-3, 2012, Department of Chemistry, IIT Guwahati, India.

6. Nidhi Chaubey, **Amaresh Kumar Sahoo** and Siddhartha Sankar Ghosh; Recombinant IFNγ encapsulated polymeric nanoparticles in cancer therapy, Poster Presentation, **Frontiers in Chemical Science (FICS-2012)**, December 2-3, 2012, Department of Chemistry, IIT Guwahati, India.

7. **Amaresh Kumar Sahoo**, Arun Chattopadhyay and Siddhartha Sankar Ghosh; Metal Nanoparticle Based Nanocomposites for Sensing and Therapeutic Applications, Oral Presentation, **Young Scientists Colloquium-2013. Material Research Society of India (MRSI) - Kolkata chapter.** August 28, 2013, Jadavpur University, Kolkata. India.

8. Devendra Kumar Maravi, **Amaresh Kumar Sahoo**, Upashi Goswami, Doolthi Shambu Prasad, Siddhartha Sankar Ghosh and Lingaraj Sahoo; Phytogenic 'green synthesis' of silver NPs with enhanced antibacterial activity, Poster presentation, **International Conference on Harnessing natural Resources for Sustainable Development- Global Trend.** January 29-31, 2014, Cotton College, Guwahati, India.

9. Rama Ghosh, **Amaresh Kumar Sahoo**, Siddhartha Sankar Ghosh, Arun Chattopadhyay and Anumita Paul; Metal Nanoclusters and their Biological Applications, Poster presentation, **Internal Conference On Nanoscience and Technology** (**ICONSAT 2014**), March 3 – 5, 2014, INST, Chandigarh, India.

Appendix

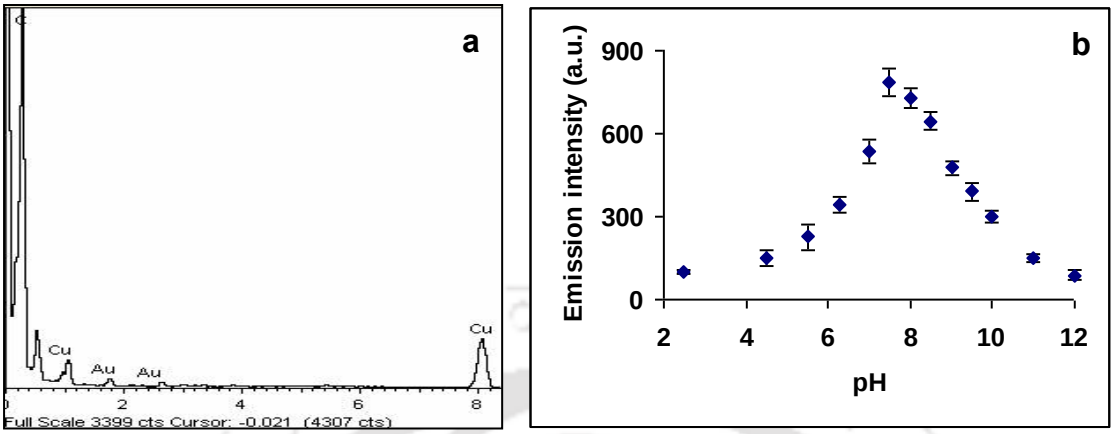

Figure A2.1 (a) EDX spectrum of the Au NPs-PD composite, showing the presence of gold (Au). (**b**) pH responsive emission change of Au NPs-PD composite.

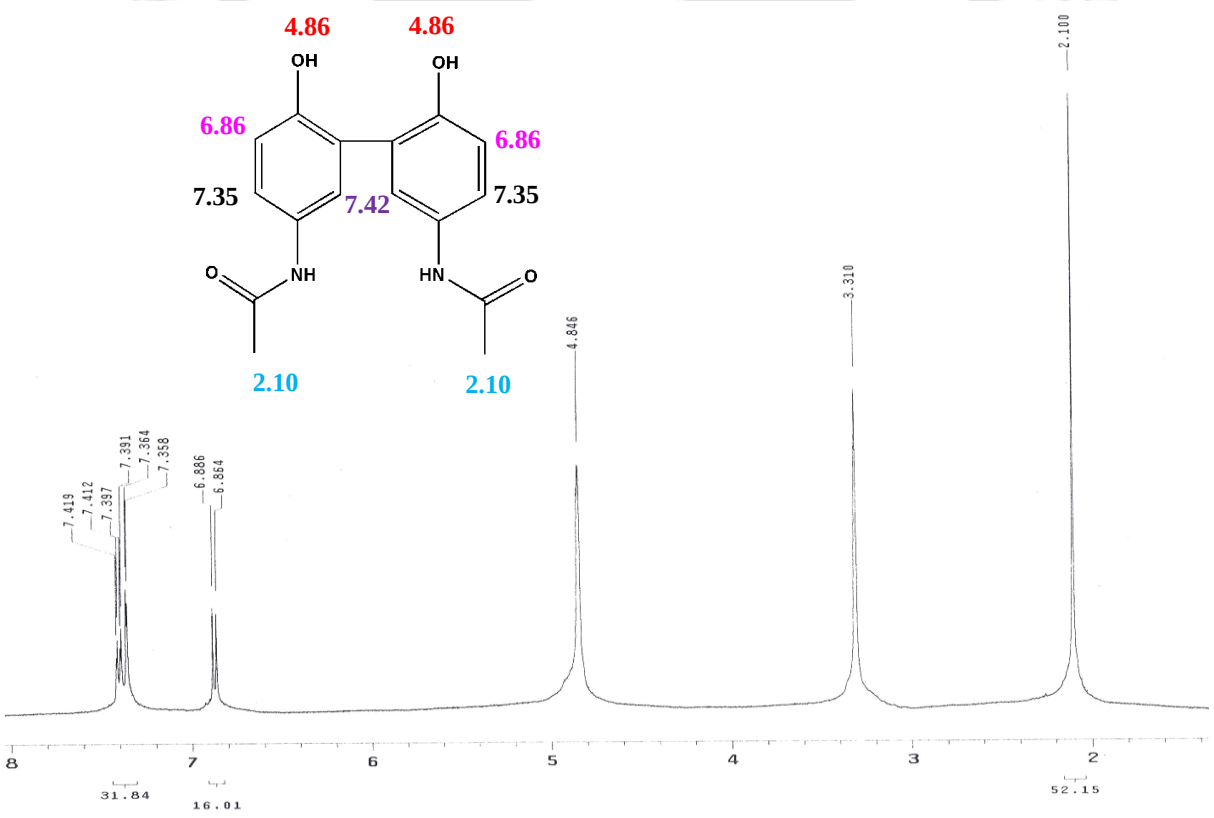

Figure A3.1 (**a**) ^{1}H NMR (400 MHz, MeOD-d_4)

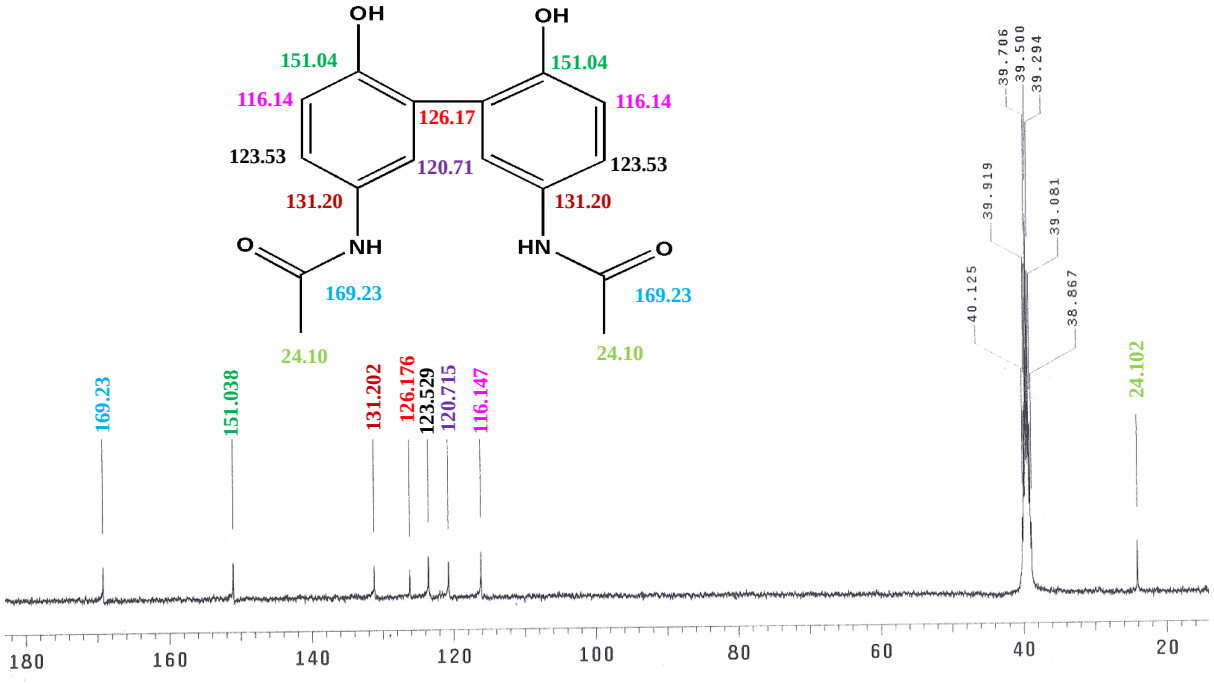

Figure A3.1 (b) ^{13}C NMR (100 MHz, DMSO-d_6)

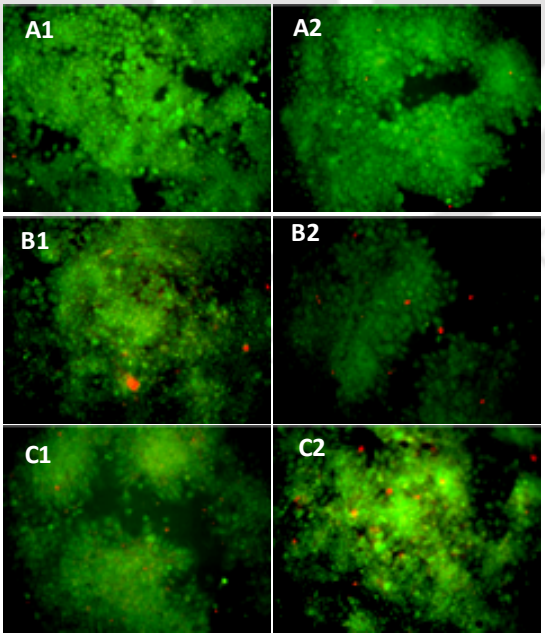

Figure A3.2 Fluorescence microscopy images (20X) of HT29 cells double stained with acridine orange and ethidium bromide. **A** refers to the control sample; **B** and **C** are the treated cells at MIC and

MBC (used for *E. Coli*) respectively; whereas 1 and 2 indicate corresponding cell images at 24 h and 48 h, respectively.

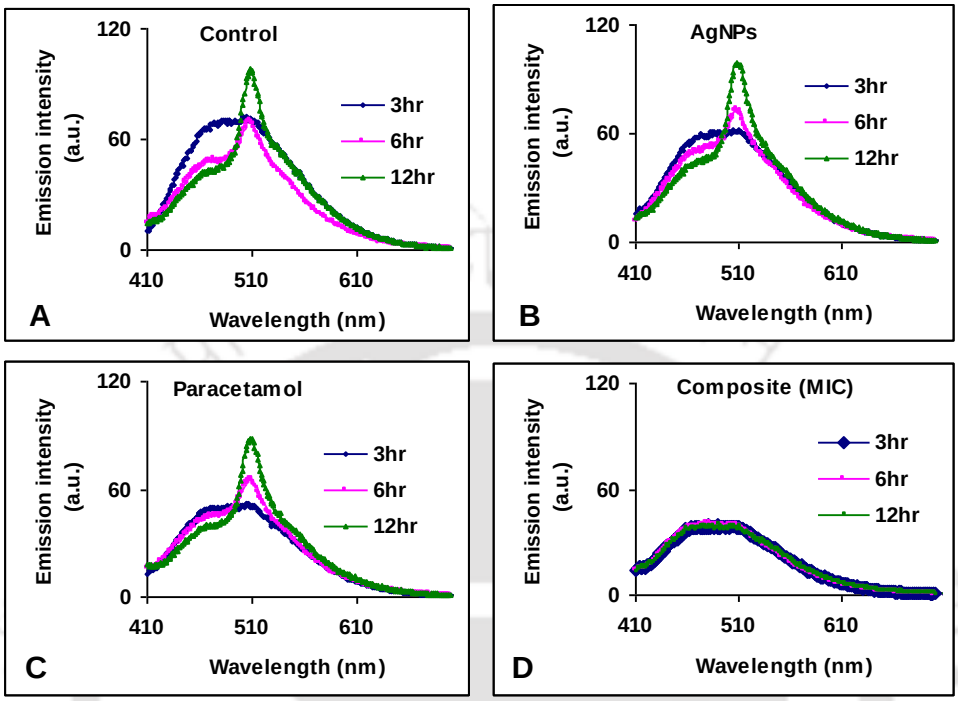

Figure A3.3 Fluorescence spectra of the GFP expressing E.coli bacteria (**A**) in the absence of composite or other agent i.e. Control; (**B**) in the presence of Ag NPs only; (**C**) in the presence of pHA and (**D**) in the presence of the PD-Ag NP composite (at MIC).

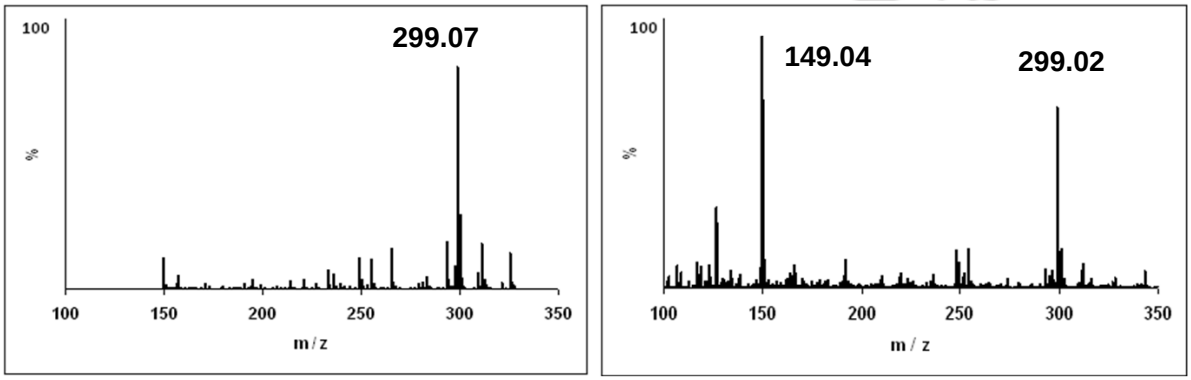

Figure A3.4 ESI (-) Mass spectrum of the isolated PD before (upper) and after (lower) H2O2¬-treatment.

Title: Simultaneous RGB Emitting Au Nanoclusters in Chitosan Nanoparticles for Anticancer Gene Theranostics

Author: Amaresh Kumar Sahoo, Subhamoy Banerjee, Siddhartha Sankar Ghosh, and Arun Chattopadhyay

Publication: Applied Materials

Publisher: American Chemical Society

Date: Jan 1, 2014

PERMISSION/LICENSE IS GRANTED FOR YOUR ORDER AT NO CHARGE

This type of permission/license, instead of the standard Terms & Conditions, is sent to you because no fee is being charged for your order. Please note the following:

- Permission is granted for your request in both print and electronic formats, and translations.
- If figures and/or tables were requested, they may be adapted or used in part.
- Please print this page for your records and send a copy of it to your publisher/graduate school.
- Appropriate credit for the requested material should be given as follows: "Reprinted (adapted) with permission from (COMPLETE REFERENCE CITATION). Copyright (YEAR) American Chemical Society." Insert appropriate information in place of the capitalized words.
- One-time permission is granted only for the use specified in your request. No additional uses are granted (such as derivative works or other editions). For any other uses, please submit a new request.

If credit is given to another source for the material you requested, permission must be obtained from that source.

Copyright Clearance Center

1 PAYMENT 2 REVIEW 3 CONFIRMATION

Step 3: Order Confirmation

Thank you for your order! A confirmation for your order will be sent to your account email address. If you have questions about your order, you can call us at +1.855.239.3415 Toll Free, M-F between 3:00 AM and 6:00 PM (Eastern), or write to us at info@copyright.com. This is not an invoice.

Confirmation Number: 11222650
Order Date: 06/14/2014

If you paid by credit card, your order will be finalized and your card will be charged within 24 hours. If you choose to be invoiced, you can change or cancel your order until the invoice is generated.

Payment Information

AMARESH SAHOO
asahoo@iitg.ernet.in
+91 9401228412
Payment Method: n/a

Order Details

Trends in biotechnology

Order detail ID:	65166593
Order License Id:	3407490811199
Article Title:	Nanosilver as a new generation of nanoproduct in biomedical applications
Author(s):	Chaloupka, Karla ; Malam, Yogeshkumar ; Seifalian, Alexander M.
DOI:	10.1016/J.TIBTECH.2010.07.006
Date:	Nov 01, 2010
ISSN:	0167-7799
Publication Type:	Journal
Volume:	28
Issue:	11
Start page:	580
Publisher:	ELSEVIER LTD.

Permission Status:	**Granted**
Permission type:	Republish or display content
Type of use:	reuse in a thesis/dissertation
Number of pages	9
Portion	figures/tables/illustrations
Number of figures/tables /illustrations	2
Format	both print and electronic
Are you the author of this Elsevier article?	No
Will you be translating?	No
Title of your thesis/dissertation	Drug Based Nanocomposites in Biological Applications
Expected completion date	Aug 2014
Estimated size (number of pages)	200
Elsevier VAT number	GB 494 6272 12

Note: This item will be invoiced or charged separately through CCC's **RightsLink** service. More info **$ 0.00**

TH-1344_09615301

This is not an invoice.

Total order items: 1

Order Total: $ 0.00

Confirmation Number: 11222650

Special Rightsholder Terms & Conditions

The following terms & conditions apply to the specific publication under which they are listed

Trends in biotechnology
Permission type: Republish or display content
Type of use: reuse in a thesis/dissertation

INTRODUCTION

1. The publisher for this copyrighted material is Elsevier. By clicking "accept" in connection with completing this licensing transaction, you agree that the following terms and conditions apply to this transaction (along with the Billing and Payment terms and conditions established by Copyright Clearance Center, Inc. ("CCC"), at the time that you opened your Rightslink account and that are available at any time at http://myaccount.copyright.com).

GENERAL TERMS

2. Elsevier hereby grants you permission to reproduce the aforementioned material subject to the terms and conditions indicated.

3. Acknowledgement: If any part of the material to be used (for example, figures) has appeared in our publication with credit or acknowledgement to another source, permission must also be sought from that source. If such permission is not obtained then that material may not be included in your publication/copies. Suitable acknowledgement to the source must be made, either as a footnote or in a reference list at the end of your publication, as follows:

"Reprinted from Publication title, Vol /edition number, Author(s), Title of article / title of chapter, Pages No., Copyright (Year), with permission from Elsevier [OR APPLICABLE SOCIETY COPYRIGHT OWNER]." Also Lancet special credit - "Reprinted from The Lancet, Vol. number, Author(s), Title of article, Pages No., Copyright (Year), with permission from Elsevier."

4. Reproduction of this material is confined to the purpose and/or media for which permission is hereby given.

5. Altering/Modifying Material: Not Permitted. However figures and illustrations may be altered/adapted minimally to serve your work. Any other abbreviations, additions, deletions and/or any other alterations shall be made only with prior written authorization of Elsevier Ltd. (Please contact Elsevier at permissions@elsevier.com)

6. If the permission fee for the requested use of our material is waived in this instance, please be advised that your future requests for Elsevier materials may attract a fee.

7. Reservation of Rights: Publisher reserves all rights not specifically granted in the combination of (i) the license details provided by you and accepted in the course of this licensing transaction, (ii) these terms and conditions and (iii) CCC's Billing and Payment terms and conditions.

8. License Contingent Upon Payment: While you may exercise the rights licensed immediately upon issuance of the license at the end of the licensing process for the transaction, provided that you have disclosed complete and accurate details of your proposed use, no license is finally effective unless and until full payment is received from you (either by publisher or by CCC) as provided in CCC's Billing and Payment terms and conditions. If full payment is not received on a timely basis, then any license preliminarily granted shall be deemed automatically revoked and shall be void as if never granted. Further, in the event that you breach any of these terms and conditions or any of CCC's Billing and Payment terms and conditions, the license is automatically revoked and shall be void as if never granted. Use of materials as described in a revoked license, as well as any use of the materials beyond the scope of an unrevoked license, may constitute copyright infringement and publisher reserves the right to take any and all action to protect its copyright in the materials.

9. Warranties: Publisher makes no representations or warranties with respect to the licensed material.

10. Indemnity: You hereby indemnify and agree to hold harmless publisher and CCC, and their respective officers, directors, employees and agents, from and against any and all claims arising out of your use of the licensed material other than as specifically authorized pursuant to this license.

11. No Transfer of License: This license is personal to you and may not be sublicensed, assigned, or transferred by you to any other person without publisher's written permission.

12. No Amendment Except in Writing: This license may not be amended except in a writing signed by both parties (or, in the case of publisher, by CCC on publisher's behalf).

13. Objection to Contrary Terms: Publisher hereby objects to any terms contained in any purchase order, acknowledgment, check endorsement or other writing prepared by you, which terms are inconsistent with these terms and conditions or CCC's Billing and Payment terms and conditions. These terms and conditions, together with CCC's Billing and Payment terms and conditions (which are incorporated herein), comprise the entire agreement between you and publisher (and CCC) concerning this licensing transaction. In the event of any conflict between your obligations established by these terms and conditions and those established by CCC's Billing and Payment terms and conditions, these terms and conditions shall control.

14. Revocation: Elsevier or Copyright Clearance Center may deny the permissions described in this License at their sole discretion, for any reason or no reason, with a full refund payable to you. Notice of such denial will be made using the contact information provided by you. Failure to receive such notice will not alter or invalidate the denial. In no event will

TH-1344_09615301

Elsevier or Copyright Clearance Center be responsible or liable for any costs, expenses or damage incurred by you as a result of a denial of your permission request, other than a refund of the amount(s) paid by you to Elsevier and/or Copyright Clearance Center for denied permissions.

LIMITED LICENSE

The following terms and conditions apply only to specific license types:

15. **Translation**: This permission is granted for non-exclusive world **English** rights only unless your license was granted for translation rights. If you licensed translation rights you may only translate this content into the languages you requested. A professional translator must perform all translations and reproduce the content word for word preserving the integrity of the article. If this license is to re-use 1 or 2 figures then permission is granted for non-exclusive world rights in all languages.

16. **Posting licensed content on any Website**: The following terms and conditions apply as follows: Licensing material from an Elsevier journal: All content posted to the web site must maintain the copyright information line on the bottom of each image; A hyper-text must be included to the Homepage of the journal from which you are licensing at http://www.sciencedirect.com/science/journal/xxxxx or the Elsevier homepage for books at http://www.elsevier.com; Central Storage: This license does not include permission for a scanned version of the material to be stored in a central repository such as that provided by Heron/XanEdu.

Licensing material from an Elsevier book: A hyper-text link must be included to the Elsevier homepage at http://www.elsevier.com . All content posted to the web site must maintain the copyright information line on the bottom of each image.

Posting licensed content on Electronic reserve: In addition to the above the following clauses are applicable: The web site must be password-protected and made available only to bona fide students registered on a relevant course. This permission is granted for 1 year only. You may obtain a new license for future website posting.

For journal authors: the following clauses are applicable in addition to the above: Permission granted is limited to the author accepted manuscript version* of your paper.

***Accepted Author Manuscript (AAM) Definition:** An accepted author manuscript (AAM) is the author's version of the manuscript of an article that has been accepted for publication and which may include any author-incorporated changes suggested through the processes of submission processing, peer review, and editor-author communications. AAMs do not include other publisher value-added contributions such as copy-editing, formatting, technical enhancements and (if relevant) pagination.

You are not allowed to download and post the published journal article (whether PDF or HTML, proof or final version), nor may you scan the printed edition to create an electronic version. A hyper-text must be included to the Homepage of the journal from which you are licensing at http://www.sciencedirect.com/science/journal/xxxxx. As part of our normal production process, you will receive an e-mail notice when your article appears on Elsevier's online service ScienceDirect (www.sciencedirect.com). That e-mail will include the article's Digital Object Identifier (DOI). This number provides the electronic link to the published article and should be included in the posting of your personal version. We ask that you wait until you receive this e-mail and have the DOI to do any posting.

Posting to a repository: Authors may post their AAM immediately to their employer's institutional repository for internal use only and may make their manuscript publically available after the journal-specific embargo period has ended.

Please also refer to Elsevier's Article Posting Policy for further information.

18. **For book authors** the following clauses are applicable in addition to the above: Authors are permitted to place a brief summary of their work online only.. You are not allowed to download and post the published electronic version of your chapter, nor may you scan the printed edition to create an electronic version. **Posting to a repository:** Authors are permitted to post a summary of their chapter only in their institution's repository.

20. **Thesis/Dissertation**: If your license is for use in a thesis/dissertation your thesis may be submitted to your institution in either print or electronic form. Should your thesis be published commercially, please reapply for permission. These requirements include permission for the Library and Archives of Canada to supply single copies, on demand, of the complete thesis and include permission for UMI to supply single copies, on demand, of the complete thesis. Should your thesis be published commercially, please reapply for permission.

Elsevier Open Access Terms and Conditions

Elsevier publishes Open Access articles in both its Open Access journals and via its Open Access articles option in subscription journals.

Authors publishing in an Open Access journal or who choose to make their article Open Access in an Elsevier subscription journal select one of the following Creative Commons user licenses, which define how a reader may reuse their work: Creative Commons Attribution License (CC BY), Creative Commons Attribution – Non Commercial - ShareAlike (CC BY NC SA) and Creative Commons Attribution – Non Commercial – No Derivatives (CC BY NC ND)

Terms & Conditions applicable to all Elsevier Open Access articles:

Any reuse of the article must not represent the author as endorsing the adaptation of the article nor should the article be modified in such a way as to damage the author's honour or reputation.

The author(s) must be appropriately credited.

If any part of the material to be used (for example, figures) has appeared in our publication with credit or acknowledgement to another source it is the responsibility of the user to ensure their reuse complies with the terms and

conditions determined by the rights holder.

Additional Terms & Conditions applicable to each Creative Commons user license:

CC BY: You may distribute and copy the article, create extracts, abstracts, and other revised versions, adaptations or derivative works of or from an article (such as a translation), to include in a collective work (such as an anthology), to text or data mine the article, including for commercial purposes without permission from Elsevier

CC BY NC SA: For non-commercial purposes you may distribute and copy the article, create extracts, abstracts and other revised versions, adaptations or derivative works of or from an article (such as a translation), to include in a collective work (such as an anthology), to text and data mine the article and license new adaptations or creations under identical terms without permission from Elsevier

CC BY NC ND: For non-commercial purposes you may distribute and copy the article and include it in a collective work (such as an anthology), provided you do not alter or modify the article, without permission from Elsevier

Any commercial reuse of Open Access articles published with a CC BY NC SA or CC BY NC ND license requires permission from Elsevier and will be subject to a fee.

Commercial reuse includes:

- Promotional purposes (advertising or marketing)
- Commercial exploitation (e.g. a product for sale or loan)
- Systematic distribution (for a fee or free of charge)

Please refer to Elsevier's Open Access Policy for further information.

21. **Other Conditions**:

v1.7

Close

Confirmation Number: 11222650

Citation Information

Order Detail ID: 65166593

Trends in biotechnology by ELSEVIER LTD.. Reproduced with permission of ELSEVIER LTD. in the format reuse in a thesis/dissertation via Copyright Clearance Center.

Close

Copyright Clearance Center RightsLink®

Home | Account Info | Help

ACS Publications
MOST TRUSTED. MOST CITED. MOST READ.

Title: Negligible Particle-Specific Antibacterial Activity of Silver Nanoparticles

Author: Zong-ming Xiu, Qing-bo Zhang, Hema L. Puppala, Vicki L. Colvin, and Pedro J. J. Alvarez

Publication: Nano Letters

Publisher: American Chemical Society

Date: Aug 1, 2012

Logged in as:
Amaresh Kumar Sahoo
Account #:
3000788127

LOGOUT

PERMISSION/LICENSE IS GRANTED FOR YOUR ORDER AT NO CHARGE

This type of permission/license, instead of the standard Terms & Conditions, is sent to you because no fee is being charged for your order. Please note the following:

- Permission is granted for your request in both print and electronic formats, and translations.
- If figures and/or tables were requested, they may be adapted or used in part.
- Please print this page for your records and send a copy of it to your publisher/graduate school.
- Appropriate credit for the requested material should be given as follows: "Reprinted (adapted) with permission from (COMPLETE REFERENCE CITATION). Copyright (YEAR) American Chemical Society." Insert appropriate information in place of the capitalized words.
- One-time permission is granted only for the use specified in your request. No additional uses are granted (such as derivative works or other editions). For any other uses, please submit a new request.

If credit is given to another source for the material you requested, permission must be obtained from that source.

BACK CLOSE WINDOW

TH-1344_09615301